Large-Scale Laboratory Testing of Timber Tie-Lateral Resistance in Two Ballast Materials

by

Courtney E. Mulhall

A thesis submitted in partial fulfillment of the requirements for the degree of

Master of Science

in

Geotechnical Engineering

Department of Civil and Environmental Engineering

University of Alberta

ABSTRACT

For railway track geometry to meet regulatory requirements under normal operating conditions, railway ballast must provide sufficient lateral resistance to control track deformations. This implies that on tangent tracks the lateral resistance of the ballast must be sufficient to resist thermal rail expansion forces during hot summer months and contraction forces during cold winter months. The ballast must also resist lateral deformations associated with loaded trains traversing curves at the maximum allowable speed. Thus, when considering the suitability of a material to be used as ballast the ability of the material to resist lateral track deformations must be evaluated.

For this research, the tie-lateral resistance provided by two ballast materials, the McAbee Ballast and Gravel Ballast, was evaluated through material characterization and tie-lateral resistance tests. The McAbee Ballast consists of particles with rough, angular to sub-angular faces (blasted and crushed faces) and is an important source of ballast material in Western Canada. The Gravel Ballast consists of particles with smooth, rounded faces (uncrushed faces) and/or rough, angular to sub-angular faces (crushed faces) and is being evaluated for use on branch-lines.

Material characterization tests were completed on the McAbee Ballast and Gravel Ballast, including sieve analysis to determine particle size distribution, photogrammetry analysis to determine shape parameters (e.g., form and angularity indices), flakiness index tests to determine flakiness index, and Los Angeles Abrasion and Micro-Deval tests to assess durability. Based on the material characterization tests results, the McAbee Ballast was expected to provide

more tie-lateral resistance than the Gravel Ballast because it was rougher, more angular, and contained less flaky-particles.

A large-scale ballast box (1.52 m long, 1.27 m wide, 0.51 m high, and 0.005 m thick) was designed to complete tie-lateral resistance tests for a wide range of test conditions and to determine the contribution of each component of tie-lateral resistance (i.e., the base friction, crib friction, and shoulder resistance that develops at the tie-ballast interface) to overall tie-lateral resistance. The research methodology considers three test configurations to determine the three components of tie-lateral resistance, respectively. For each test, the ballast box is filled with ballast, and a single timber tie is placed on or in the ballast and pushed laterally up to 40 mm at a loading rate of 0.5 mm/sec. The test is then repeated under several normal loads, ranging from 5 kN (the estimated weight of the track superstructure) up to 160 kN (the maximum potential in-service ballast load). The test results are used to determine the peak-lateral resistance per tie, and the relationship between lateral load and normal load for each material and test configuration.

From the tie-lateral resistance tests, it was determined that the Gravel Ballast provides 15% less tie-lateral resistance than the McAbee Ballast. It was also determined that the base friction, crib friction, and shoulder resistance contribute 65% to 70%, 10% to 15%, and 15% to 20%, respectively, under a normal load of 10 kN; and 98%, less than 1%, and less than 2%, respectively, under a normal load of 160 kN. These results are based on the peak-lateral resistance of a single timber tie in dry, clean, freshly-tamped ballast under normal loads ranging from 5 kN to 160 kN; and may vary for other test or in-service conditions.

PREFACE

Dr. Saleh Balideh from the University of Alberta (U of A) completed the material characterization tests presented in Chapter 3. The testing apparatus and methodology discussed in Chapter 4 was developed by myself, Dr. Saleh Balideh, Dr. Renato Macciotta, Dr. Derek Martin, and Dr. Michael Hendry from the U of A. Jakob Brandl from the U of A designed the stiffeners on the ballast box; Brian Horvath from Black Arrow Machine & Welding Inc. fabricated the ballast box; and Greg Miller and Cameron West from the U of A provided technical support in the laboratory. The tie-lateral resistance tests presented in Chapter 5 were completed by myself and Dr. Saleh Balideh, with the assistance of Greg Miller and Cameron West. The analysis of the material characterization and tie-lateral resistance test results, and the writing of this thesis and the publications listed below are my original work.

Portions of this thesis were published as:

- Mulhall, C., Balideh, S., Macciotta, R., Hendry, M., Martin, D., and Edwards, T. 2016. “Large-Scale Testing of Tie Lateral Resistance in Two Ballast Materials”. *In* Proceedings of the Third International Conference on Railway Technology: Research, Development and Maintenance Cagliari, Sardinia, Italy, 5-8 April 2016. Civil-Comp Press, Stirlingshire, UK, Paper 4.

- Mulhall, C., Balideh, S., Macciotta, R., Hendry, M., Martin, D., and Edwards, T. 2016. “Large-scale Laboratory Testing of the Lateral Resistance of a Timber Tie”. *In* Proceedings of the Symposium of Railroad Ballast Testing and Properties, Sheraton New Orleans, New Orleans, Louisiana, USA, 24 January 2018. American Society for Testing and Materials (ASTM) International, West Conshohocken, Pennsylvania, USA, Manuscript STP-2017-0030.R1 (in press).

In the publications, a brief overview of the research is provided with the details of the testing apparatus and methodology. The 2016 paper also presents the preliminary Phase 1 base test results in both materials, and the 2018 manuscript presents the Phase 1 base, Phase 2 crib, and Phase 3 shoulder test results in the McAbee Ballast.

ACKNOWLEDGEMENTS

This research was made possible by the Canadian Rail Research Laboratory (CaRRL) (www.carrl.ca), which is funded by the Natural Sciences and Engineering Research Council of Canada (NSERC), Canadian Pacific Railway, Canadian National Railway, the Association of American Railways – Transportation Technology Center Inc., the National Research Council of Canada, Transport Canada and Alberta Innovates – Technology Futures.

I would like to extend my sincere gratitude to Dr. Derek Martin, Dr. Michael Hendry, and Dr. Renato Macciotta from the University of Alberta (U of A) for their supervision and guidance throughout this research. Your immense knowledge, pragmatism, and dedication to your students has made my time at the university thoroughly enjoyable. I am grateful for everything you have taught me, and everything you continue to do for the university.

I would like to give special thanks to the following individuals and establishments who assisted with this research:

- Tom Edwards from Canadian National Railway who sponsored this research;
- Dr. Saleh Balideh from the U of A who completed the material characterization tests and assisted with the tie-lateral resistance tests;
- Jakob Brandl from the U of A who completed a stress analysis on the ballast box and designed the ballast box stiffeners;
- Brian Horvath from Black Arrow Machine & Welding Inc. who fabricated the ballast box;
- Greg Miller and Cameron West from the U of A Morrison Structures Laboratory who provided technical support during the tie-lateral resistance tests; and

- the numerous other faculty and staff members at the U of A who provide continuous support to the students conducting research at the university, particularly Annette Busenius, Vivian Giang, and Sally Petaske.

To my family and friends, thank-you for your continuous support and encouragement, it has empowered me to pursue my dreams. To my partner, Jordan Baker, you have been a pillar of strength and love throughout this journey. I am immensely gratefully for everything that you do, including your (sometimes unappreciated) wittiness and subtle words of encouragement. I love all of you.

Finally, thank-you to my colleagues at the university for their leadership, companionship, and laughter; collaborating with you gave me the motivation to succeed. You also helped me empty and fill the ballast box, which I am eternally grateful for.

TABLE OF CONTENTS

LIST OF TABLES

LIST OF FIGURES

CHAPTER 1.0 INTRODUCTION

1.1 Background Information

Canadian National Railway's (CN Rail's) primary source of ballast material in Western Canada is blasted and crushed diorite produced at CN Rail's McAbee Pit located in the Province of British Columbia. The cost of this material is proportional to the distance between the McAbee Pit and the section of track being constructed or maintained. As transportation and manufacturing costs continue to increase; additional, less-expensive sources of ballast can help optimize track construction and maintenance costs. CN Rail has thus proposed using locally sourced and produced crushed gravel from the neighboring Province of Alberta for some of their branch-lines. The main difference between the two materials is that the McAbee Ballast consists of particles with rough, angular to sub-angular faces (blasted and crushed faces), while the Gravel Ballast consists of particles with smooth, rounded faces (uncrushed faces) and/or rough, angular to sub-angular faces (crushed faces). The objective of this research is to evaluate the suitability of the gravel to be used as ballast material relative to the currently used McAbee Ballast.

1.2 Research Scope and Methodology

In-service railway track safety and reliability is dependent on the ability of the track structure (e.g., the tie-ballast interface) to resist lateral track deformations, which are pronounced when trains are traversing curves, but can also be significant on tangent tracks when thermal rail expansion and contraction forces cause track buckling. Thus, when considering the suitability of a material to be used as ballast the ability of the material to resist lateral track deformation must be evaluated. The ability of a material to resist lateral track deformations is dependent on the ultimate frictional resistance and stiffness of the ballast, and the mechanical performance and durability of the ballast particles. As part of this research, the ability of the Gravel Ballast to resist lateral track deformations is evaluated relative to the currently used McAbee Ballast through material characterization tests (Chapter 3) and tie-lateral resistance tests (Chapters 4 through 6).

1.2.1 Material Characterization Tests

Previous research has shown that particle angularity and surface roughness influence the frictional resistance of granular materials. Generally, this resistance increases as the material becomes rougher and more angular (Selig and Waters 1994). Therefore, material characterization tests were completed on the McAbee Ballast and Gravel Ballast, including sieve analysis to determine particle size distribution, photogrammetry analysis to determine shape parameters (e.g., form and angularity indices), flakiness index testing to determine flakiness index, and Los Angeles Abrasion tests and Micro-Deval tests to assess durability. The results of these material characterization tests were then compared to the performance and behavior of each material during the tie-lateral resistance tests.

1.2.2 Tie-Lateral Resistance Tests

The components of a ballasted track structure can be grouped into two main categories: the superstructure (e.g., rails, fastening system, and ties) and the substructure (e.g., ballast, subballast, and subgrade). The superstructure guides the train and transfers concentrated train wheel loads to the underlying substructure, which in turn stabilizes and supports the superstructure. The superstructure and substructure are separated by the tie-ballast interface, which resists lateral track deformations through the development of base friction, crib (side) friction, and shoulder (end) resistance at the contact between the tie and the base ballast, crib ballast, and shoulder ballast, respectively.

The contribution of each component of tie-lateral resistance (i.e., the base friction, crib friction, and shoulder resistance) to overall tie-lateral resistance is poorly understood; and although tie- and track-lateral resistance tests have been carried out, they are rarely reported in the literature. Moreover, much of the literature does not explicitly present the testing details (e.g., ballast type, geometry, and condition; loading conditions or rate), or include test results for tests conducted in different ballast materials or under a range of normal loads. Therefore, a large-scale ballast box (1.52 m long, 1.27 m wide, 0.51 m high, and 0.005 m thick) was designed to complete tie-lateral resistance tests for a wide range of test conditions and to determine the contribution of each component of tie-lateral resistance to overall tie-lateral resistance.

The research methodology considers three test configurations to determine the tie-ballast base friction, crib friction, and shoulder resistance, respectively. For each test, the ballast box is filled with ballast, and a single timber tie is placed on or in the ballast and pushed laterally up to 40 mm at a loading rate of 0.05 mm/sec. The test is repeated under several normal loads, ranging from 5 kN (the estimated weight of the track superstructure) up to 160 kN (the maximum potential in service ballast load). The test results are used to determine the peak-lateral resistance per tie, and the relationship between lateral load and normal load for each material and test configuration.

1.3 Research Objectives

The research objects are as follows:

(1) Complete material characterization tests to determine the particle size distribution, shape parameters (e.g., form and angularity indices), flakiness index, and durability of each material. Compare the results with CN Rail's ballast specifications for main-line track (CN Rail 2003).

(2) Determine the maximum potential in-service train load transferred to a single timber tie (i.e., the maximum potential in-service ballast load).

(3) Develop a test to quantify the three components of tie-lateral resistance for the expected range of in-service ballast loads;

(4) Conduct tie-lateral resistance tests in the McAbee Ballast and Gravel Ballast under the expected range of in-service ballast loads, then:

    (a) relate the performance and behavior of each material during the tie-lateral resistance tests to the results of the material characterization tests;

    (b) compare the tie-lateral resistance provided by the McAbee Ballast and Gravel Ballast; and

(c) determine the percent contribution of each component of tie-lateral resistance to overall tie-lateral resistance.

1.4 Thesis Organization

This thesis is organized into seven chapters:

- **Chapter 1** introduces the research topic, objectives, and methodology.
- **Chapter 2** presents the literature review findings, including background information on ballasted track structures, previous in-situ and laboratory tie-lateral resistance tests, and relevant ballast specifications.
- **Chapter 3** presents and discusses the material characterization test methods and results.
- **Chapter 4** details the tie-lateral resistance tests, including the estimation of the maximum potential in-service ballast load, ballast box design, test configurations, equipment characteristics, testing methodology, and testing program.
- **Chapter 5** presents and discusses the tie-lateral resistance test results.
- **Chapter 6** provides a comparison of the tie-lateral resistance provided by the McAbee Ballast and Gravel Ballast, the percent contribution of each component of tie-lateral resistance to overall tie-lateral resistance, and a comparison of the results with the literature review findings.
- **Chapter 7** presents the key observations, findings, and conclusions of this research.

CHAPTER 2.0 REVIEW OF BALLAST MATERIAL AND PREVIOUS TIE-LATERAL RESISTANCE TESTS

2.1 Review of a Ballasted Track Structure

2.1.1 Components of a Ballasted Track Structure

The components of a ballasted track structure can be grouped into two main categories: the superstructure and the substructure. The superstructure consists of the rails, a fastening system, and the sleeper supports or railway ties; while the substructure consists of the ballast, the sub-ballast, and the subgrade. The superstructure and substructure are separated by the tie-ballast interface. A cross-section orientated perpendicular to the rails of a ballasted track structure is illustrated in Figure 2.1A and a longitudinal cross-section is illustrated in Figure 2.1B.

The Superstructure and Ties

The superstructure consists of two parallel rails, a fastening system, and ties that are evenly spaced along the length of rail. The two parallel rails guide the train wheels, the fastening system anchors the rails to the ties, and the ties hold the fastening system. Fundamentally, the fastening system and the ties secure the rail and maintain track gauge by preventing rail movement and overturning. Ties also resist vertical, lateral, and longitudinal movements of the track (i.e., the ties maintain track alignment) by anchoring the superstructure to the substructure; and distributing concentrated train wheel loads, received from the rails and the fastening system, to the substructure at an acceptable bearing pressure (AREMA 2014, Indraratna et al. 2011, and Selig and Waters 1994).

Rails consist of longitudinal steel members that are either bolted or welded together and ties consist of timber (wood) or (pre-stressed, reinforced) concrete blocks. The fastening system can include tie plates and an assortment of spring clips, (electrical) insulators, shoulder/inserts, railseat pads, spikes and rail anchors, cap screws and rail clips, bolts, washers, and nuts (AREMA 2014, Indraratna et al. 2011, and Selig and Waters 1994).

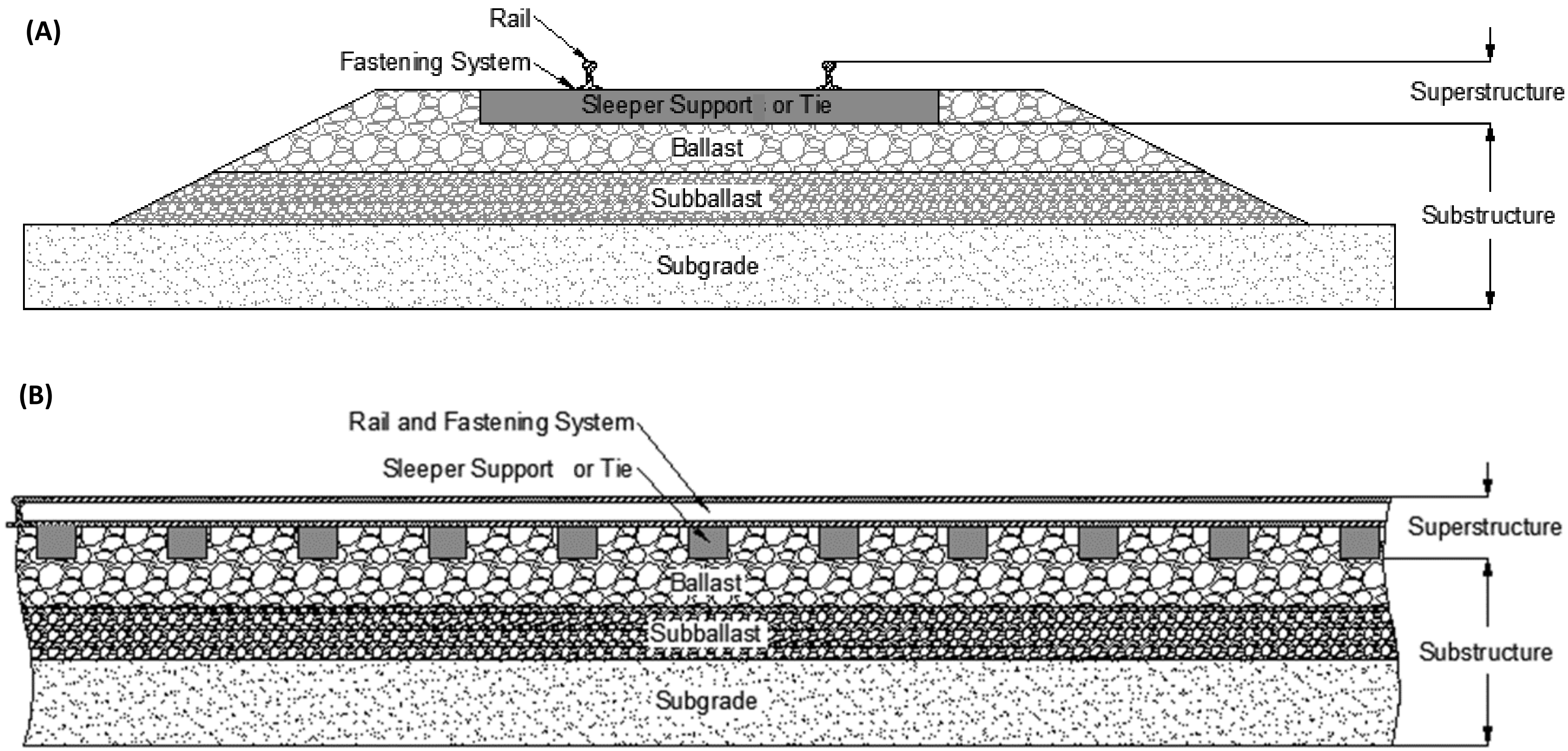

Figure 2.1: (A) Perpendicular cross-section and (B) longitudinal cross-section of a ballasted track structure

The Substructure and Ballast

The substructure supports the superstructure and consists of (AREMA 2014, Indraratna et al. 2011, and Selig and Waters 1994):

- **Ballast** – the upper strata of granular material, which typically consists of uniformly-graded coarse-grained rock that is free of fine-grained material.
- **Subballast** – the lower strata of granular material, which typically consists of well-graded rock or a sandy gravel mixture.
- **Subgrade** – the underlying foundation material, which typically consists of natural formation and/or placed fill.

Within a ballasted track structure, the ballast and the subballast (AREMA 2014, Hay 1982, Indraratna et al. 2011, and Selig and Waters 1994):

- stabilize the tie against lateral, longitudinal, and vertical movements;
- support the track superstructure by providing a stable foundation;
- distribute concentrated wheel loads received from the ties to the subgrade at an acceptable bearing pressure;
- facilitate track maintenance and adjustments to the track geometry (e.g., alignment, grade, and cross level);
- provide dynamic resiliency and energy absorption for the track;
- provide storage for fouling material;
- provide drainage (e.g., they intercept water falling on the track and direct it away from the subgrade, and provide drainage for subsurface water flowing up from the subgrade;

- inhibit vegetation growth; and
- shield the subgrade from degradation, weathering, and climatic forces (e.g., they alleviate frost heaving and swelling in the subgrade by providing an insulating layer).

Subballast also functions as a filter and a separating layer by preventing (Indraratna et al. 2011 and Selig and Waters 1994):

- coarse-grained ballast aggregates from penetrating into finer-grained subgrade materials; and
- the upward migration of subgrade material into the ballast, which in the presence of water, can lead to the formation of a slurry and track pumping as the ballast becomes fouled with slurry.

There are three types of ballast within a ballasted track structure, as shown in Figure 2.1: (1) base ballast below the ties, (2) crib ballast between the ties, and (3) shoulder ballast at the end of the ties. The base ballast primarily distributes concentrated wheel loads received from the superstructure to the underlying subballast and subgrade, the crib ballast primarily confines the base ballast and resists longitudinal track movements, and the shoulder ballast primarily resists lateral track movements (Le Pen 2008).

The Tie-Ballast Interface

The tie-ballast interface anchors the superstructure to the substructure; distributes concentrated train wheel loads to the substructure at a suitable bearing pressure; and maintains track alignment by resisting vertical, lateral, and longitudinal forces in the track structure. Of particular interest is the lateral resistance provided by the tie-ballast interface (i.e., tie-lateral resistance). Specifically, the base friction, crib friction, and shoulder resistance that develops at the contact between the tie and base ballast, crib (side) ballast, and shoulder (end) ballast, respectively (Selig and Waters 1994). The three components of tie-lateral resistance in a ballasted track structure are illustrated in Figure 2.2.

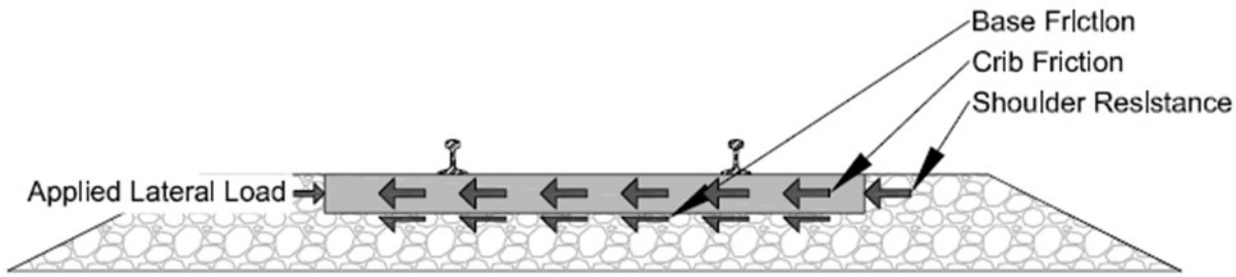

Figure 2.2: The three components of tie-lateral resistance in a ballasted track structure

2.1.2 Forces Generated within a Ballasted Track Structure

Normal Forces

Normal forces act perpendicular to the track structure and consist of:

- **Train wheel forces** – these forces occur when a static load is applied by a train, and/or a dynamic load is applied at the contact between the train wheel and rail by wheel and rail irregularities (e.g., wheel impact forces from wheel flats or track joints), and/or cross-winds (Indraratna et al. 2011, and Selig and Waters 1994). The dynamic load is difficult to quantify, so the total normal load is typically calculated by multiplying the static load by an 'impact factor' or a 'dynamic amplification factor' that accounts for dynamic track effects (AREMA 2014 and Indraratna et al. 2011).

- **Uplift forces** – these forces occur when the rail lifts-up ahead of the train wheel. If the uplift force exceeds the force applied by the weight of the superstructure and the frictional resistance between the tie and crib ballast, the tie will lift, creating a pumping action (i.e., rail wave action) (Selig and Waters 1994).

Normal forces transferred to the tie-ballast interface are not uniformly distributed across the bottoms of the ties. Their distribution is dependent on the tie properties, tie dimensions, tie spacing, reaction of the ballast and subgrade, and stiffness of the rail and the fastening system. The average pressure at the bottom of the tie, or ballast pressure, is equal to the axle load, modified by distribution and impact factors, divided by the bearing area of the tie (AREMA 2014). There are various methods for estimating and measuring the bearing area. For example, the

American Railway Engineering and Maintenance-of-Way Association (AREMA) assumes a value equal to two-thirds the tie footprint (AREMA 2014), and Abadi et al. (2015) uses pressure paper and McHenry (2013) use surface sensors to measure the bearing area. In this research, a ballast load is used instead of a ballast pressure to avoid having to determine the tie bearing area; which varies test to test and continuously changes as the ballast particles re-arranged under the moving tie. Not accounting for bearing area will likely lead to a greater scatter in the results (e.g., two tests may show different peak-lateral loads, but they may provide the same peak-lateral resistance per unit tie length if their bearing areas were accounted for), but not so much that it will impact the major conclusions of this research. Moreover, this addresses the different ballast particle arrangements that may be encountered in in-service track.

In section 4.1, the maximum potential static ballast load is estimated to be 16 000 Kg (35 000 lb) or 160 kN, which is similar to values reported by Selig and Waters (1994), Le Pen (2008), Clark et al. (2011), and Read et al. (2011).

Longitudinal Forces

Longitudinal forces act parallel to the rails and are caused by train acceleration and deacceleration, thermal rail expansion and contraction, shrinkage from track welding, rail wave action, and track creep (Indraratna et al. 2011 and Selig and Waters 1994). These forces are resisted by the fastening system, which anchors the rails to the tie, and the crib ballast (AREMA 2014). These forces are not considered in detail in this research, but it should be noted that longitudinal forces can increase the crib friction component of tie-lateral resistance by providing a confining pressure within the crib ballast.

Lateral Forces

Lateral forces act perpendicular to the rails and consist of:

- **Lateral wheel forces** – these forces occur when friction develops at the contact between the train wheel and rail, and/or a lateral load is applied by the trail wheel to the rail. The lateral load applied by the train wheel to the rail are influenced by wheel and rail irregularities, track geometry (e.g., straight versus curved track with centrifugal forces), and cross-winds (Selig and Waters 1994).

- **Lateral buckling forces** – these forces occur when the rail buckles under compressive forces induced by thermal rail expansion and contraction – this has become more prevalent with the increased use of Continuous Welded Rail (CWR) (Kish and Samavedam 2013) – and can include: radial breathing of the track in curves, and the buckling of straight track as discussed in Kish and Samavedam (1993). Samavedam and Kish (2013) reports that the amplitude of the buckling deflection can be on the order of 0.15 m to 0.76 m, and the wavelength on the order of 12 m to 18 m.

Lateral forces within a ballasted track structure are resisted by the rail, the fastening system, and the tie-ballast interface. The lateral (bending) stiffness of the rail distributes the lateral loads to the fastening system, while the lateral (torsional) stiffness of the fastening system distributes the lateral loads to the ties. The tie-ballast interface then resists the lateral track movements through the development of base friction, crib friction, and shoulder resistance. Tie-lateral resistance is influenced by: tie type, weight, dimensions and spacing; ballast type and condition (e.g., fouled, wet, or frozen); ballast geometry (e.g., shoulder width and crib depth); the frictional resistance of the tie-ballast interface; train loads and uplift forces; and track consolidation (e.g., lightly-consolidated to well consolidated) and maintenance (AREMA 2014, Kish 2011, Selig and Waters 1994).

The base friction component of tie-lateral resistance is predominately influenced by the frictional resistance of the tie-ballast interface and the applied load. In the presence of uplift forces, the base friction component can be reduced or eliminated as the tie bottom loses contact with the base ballast (Sussmann et al. 2014). In the presence of concentrated train wheel loads, the base friction component can be increased as the ballast near the base of the tie becomes confined. The frictional resistance of the tie-ballast interface can be represented as a unitless friction coefficient defined as the ratio of the measured base friction to applied normal load (Samavedam and Kish 1993) or a friction angle defined as the inverse tangent of the friction coefficient.

The crib friction component of tie-lateral resistance is predominately influenced by the depth and compaction of the crib ballast, and the shoulder resistance component by the geometry and compaction of the shoulder ballast (Kish 2011, and Sussmann et al. 2014). In other words, the crib friction and shoulder resistance are related to the internal friction of the ballast and the volume of particles being mobilized during horizontal tie movements (De Iorio 2016).

2.2 Concepts of Tie-lateral Resistance in the Literature

Tie-lateral resistance typically exhibits one of the characteristic load-horizontal displacement curves presented in Figure 2.3**,** where F_p is the peak resistance, F_L is the limit resistance, W_P is the displacement at F_p, and W_L is the displacement at F_L (Samavedam et al. 1993 and 1995, and Kish and Samavedam 2013). 'Strong' (i.e., well-maintained or consolidated) ballast exhibits a strain-softening response with the resistance reaching a peak value at a small displacement, typically on the order of 6 mm to 13 mm, followed by a 'softening' to a limiting value at a limiting displacement, typically on the order of 76 mm and 127 mm. Samavedam et al. (1995) attributes this behavior to the breakdown of the bond at the tie-ballast interface as ballast particles displace under the moving tie creating voids and/or a reduction in ballast consolidation. 'Weak' (i.e., freshly-tamped or lightly-consolidated) ballast or track exhibits an elastic-plastic response where F_P is equal to F_L (Samavedam et al. 1993 and 1995, and Kish and Samavedam 2013).

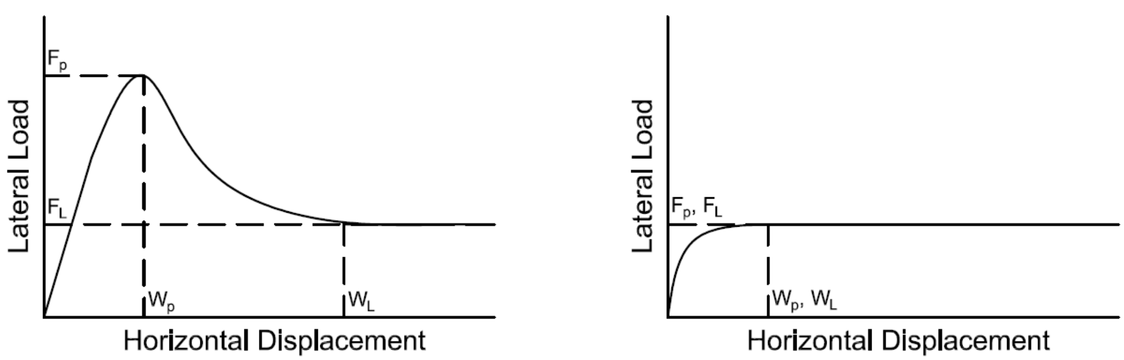

(A) Consolidated ballast

(B) Freshly-tamped or lightly-consolidated ballast

Figure 2.3: Typical load-horizontal displacement curves for tie-lateral resistance tests (modified from Le Pen 2008, Kish 2011, Kish and Samavedam 2013)

Kish (2011) suggests the peak-lateral resistance per tie is less than 6.2 kN for weak ballast; between 6.2 kN and 8.9 kN for marginal conditions, where consolidation is occurring; between 8.9 kN to 12 kN for average conditions; and above 12 kN for strong ballast. Clark et al. (2011) considers values greater than 13 kN typical of strong ballast. While, Samavedam et al. (1993) suggests a value of 8 N/m for weak ballast and a value of 26 N/m for strong ballast, and Kish and Samavedam (2013) suggests a value of 8 N/m for weak ballast and a value of 53 N/m for strong ballast. According to Prud'homme and Weber (1973), the lateral load is limited by the Prud'homme relation given by (W/3) + 10 where W is the axle load in kilonewtons (kN). So, for a maximum potential in-service train load of 160 kN (see Section 4.1) the lateral load would be limited to 63 kN.

Kish and Samavedam (2013) suggest the peak-lateral resistance is a function of tamped resistance, and an incremental increase due to compaction and traffic consolidation. Testing completed by Samavedam et al. (1995 and 1999), Clark et al. (2011), Read et al. (2011), and Sussmann et al. (2014) suggest that immediately after track maintenance and re-surfacing operations (e.g., lining, levelling, and tamping) the tie-lateral resistance drops significantly and the behavior changes from that of strong ballast to weak ballast. Then after stabilization (e.g., after the use of dynamic track stabilizer) and consolidation (e.g., after trains have traversed the track, which is typically measured in millions of traffic tonnage [MGT]) the tie-lateral resistance increases and the behavior changes from that of weak ballast to strong ballast. This research only considers the tamped resistance under static train loading, so the incremental increase due to compaction and traffic consolidation will not be discussed further.

Determining the limiting tie-lateral resistance and displacement typically involves displacing a tie at least 75 mm, which can be quite destructive to in-service track. Samavedam et al. (1995) presents a series of empirical formulas derived from test data to determine the limiting tie-lateral resistance and displacement from the peak-lateral resistance and displacement data. Whereas, Samavedam et al. (1993) and Jeong (2013) suggest a series of mathematical curve-fitting formulas (e.g., one for constant lateral resistance, one for softening lateral resistance, and one for full non-linear lateral resistance) to determine the limiting tie-lateral resistance and displacement from the peak lateral-resistance and displacement data. In this research, the limiting tie-lateral resistance is measured because it is difficult to determine the input parameters required for these calculations.

2.3 Review of Previous Tie-Lateral Resistance Tests

As discussed in Section 1.2.2, the contribution of each component of tie-lateral resistance to overall lateral resistance is poorly understood; and although tests have been carried out, they are rarely reported in the literature (De Iorio 2016 and Le Pen 2008). Of the reported tests, many measure overall tie-lateral resistance through single tie push tests (STPTs) or track-lateral resistance through cut or uncut panel pull tests (CPPTs or UPPTs). These tests generally aim to better understand the effects of track maintenance on lateral resistance, the effects of temperature on CWR, and to determine input parameters for programs that model CWR buckling (e.g., CWR-Buckle and CWERRI).

In this chapter, previous in-situ and laboratory tie-lateral resistance tests conducted and published by Clark, De Iorio, Esmaeili, Estaire, Moraal, Le Pen, Powrie, Kish, Read, Samavedam, Sussmann, van't Zand and their associates are summarized. Other publication by Hayano et al. (2014), Jeong (2013), and litchtberger (2007) were also used as a reference for this research, but are not summarized herein.

2.3.1 Types of Tests Used to Determine Tie-lateral Resistance

Commonly, three types of in-situ tests are used to determine tie- and track-lateral resistance (Kish 2011):

(1) *Single tie push tests (STPTs*), which involve pushing an unfastened tie laterally through the ballast to measure the tie-lateral resistance offered by a single tie without train loading.

(2) *Cut-panel pull tests (CPPTs)*, which involve detaching a section of track and pulling it laterally through the ballast to measure the non-uniform tie-lateral resistance offered by several ties.

(3) *Uncut-panel pull tests (UPPTs)*, which involve pulling an attached section of track through the ballast to measure track-lateral resistance.

These tests are illustrated in Figure 2.4. In general, STPTs are the preferred method for determining tie-lateral resistance because they directly measure the lateral resistance provided by a single tie; the test equipment is portable and easy to use; and the test is minimally destructive compared to panel pull tests (PPTs), which require the cutting or displacement of large portions of track (Samavedam et al. 1995). However, individual STPTs show wide ranges of values and multiple tests are necessary to characterize the tie-lateral resistance of a given tie-ballast arrangement (Le Pen 2008). Samavedam et al. 1995 recommends at least three tests to determine the statistical variation. While these field tests appear simple to conduct they require track time which is often not available on in-service track. These field tests also lack normal loading and the quality control that can be achieved with laboratory tests.

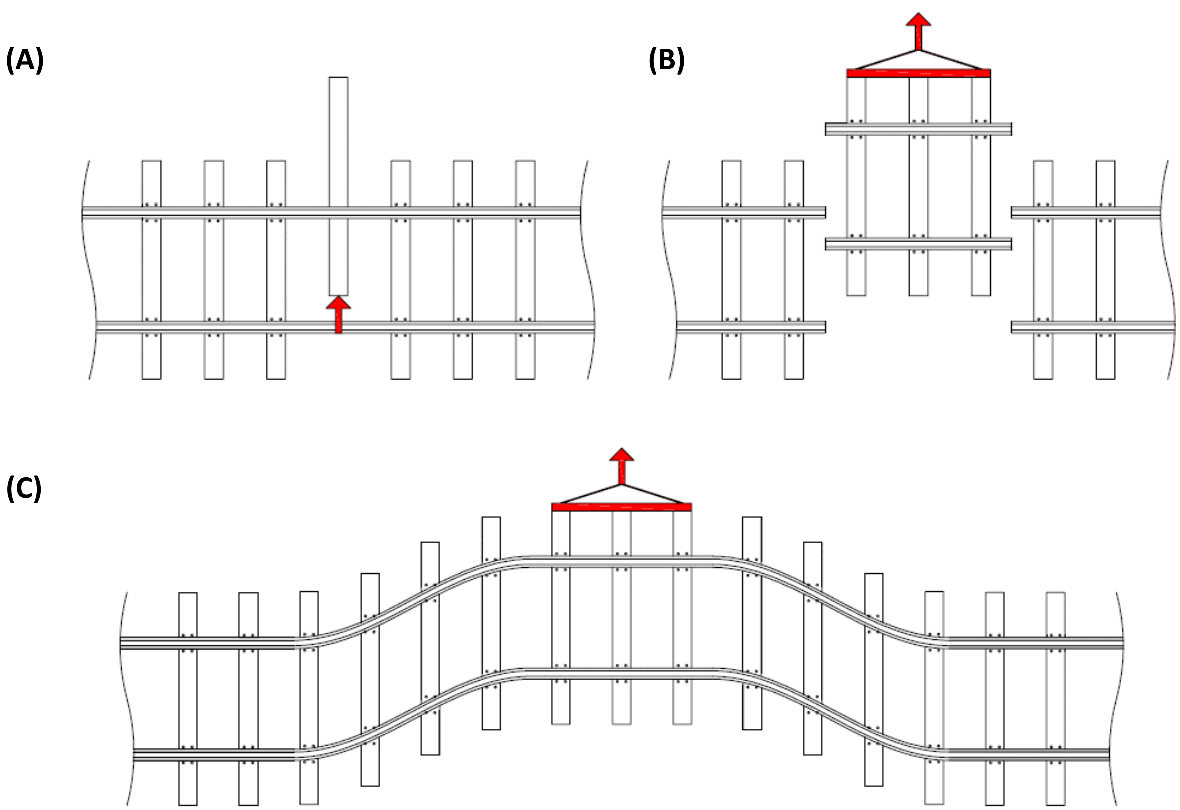

Figure 2.4: Typical in-situ tests of tie- and track-lateral resistance (a) single tie push test (STPT), (b) cut panel pull test (CPPT), and (c) uncut panel pull test (UPPT)

There are no standards for completing STPTs; however, AREMA (2014) and Sussmann et al. (2014) suggest the following procedure:

(1) Select a section of track with at least several consecutive ties of similar condition. AREMA (2014) suggests at least three ties.

(2) Fasten a hydraulic piston to the middle tie and a reaction bracket to the rail, so the hydraulic piston can push-off the reaction bracket during the test (see Figure 2.5).

(3) Fasten reaction blocks to each tie adjacent to the test tie to stabilize the rail.

(4) Remove the fastenings from several ties on either side of the test tie, then raise the track away from the test tie so that it can move freely.

(5) Attach a measuring device to monitor the horizontal tie displacement (e.g., a string potentiometer or linear variable differential transformer [LVDT]).

(6) Push the unfastened tie lateralyl using the hydraulic piston until the peak-lateral resistance is recorded. AREMA (2014) suggests displacing the tie at least 50 mm.

(7) Push the tie back into place and re-assembly the track superstructure.

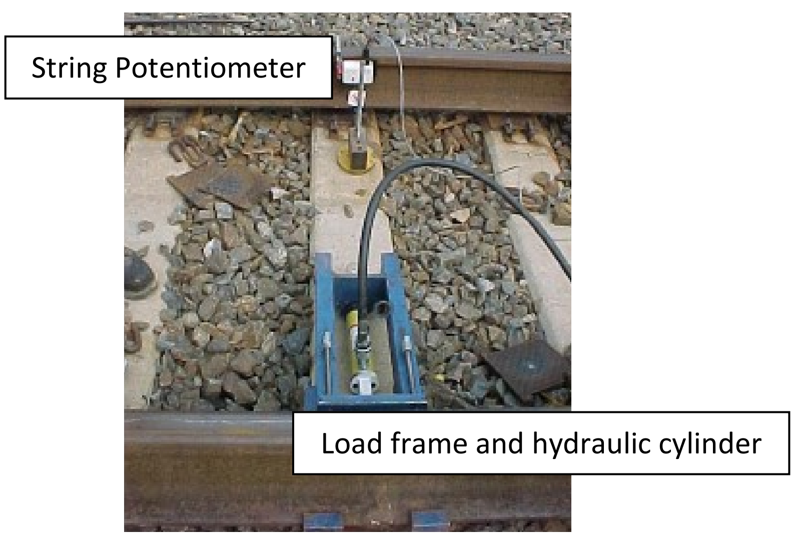

Figure 2.5: Typical STPT equipment and testing configuration (after Sussmann et al. 2003)

2.3.2 Previous In-Situ Tie-lateral Resistance Tests

Samavedam et al. (1995)

Samavedam et al. (1995) conducted STPTs and PPTs to quantify the effects of track consolidation, the influence of different ballast types on lateral resistance, and the contribution of each component tie-lateral resistance to overall lateral resistance. In total, they considered 12 test configurations on timber ties with varying ballast configurations (full crib and shoulder ballast – test type 'PR', no shoulder ballast – test type 'BBC1', and no crib or shoulder ballast – test type 'BBC2'), track curvatures (5° curve and tangent track), materials (slag and granite), and ballast consolidations (from 0 MGT up to 100 MGT). Configurations 1 through 6 investigate the factors affecting tie-lateral resistance and determine the contribution of each component of tie-lateral resistance to overall lateral resistance. The remaining tests configurations investigate factors affecting track-lateral resistance and will not be discussed herein.

The peak-lateral resistance obtained by Samavedam et al. (1995) is summarized in Table 2.1; and typical load-horizontal displacement curves and average characteristic load-horizontal displacement curves obtained by Samavedam et al. (1995) are presented in Figures 2.6 and 2.7, respectively.

The results obtained by Samavedam et al. (1995) indicate there is an approximate 15% to 45% reduction in average peak-lateral resistance, with a median of 21%, when the crib ballast is removed; and an approximate 85% to 90% reduction in average peak-lateral resistance, with a median of 85%, when the crib and shoulder ballast is removed, regardless of track curvature, ballast type, and ballast consolidation. The results show a significant amount of scatter with the standard deviation ranging from approximately 10% to 30% of the peak-lateral resistance, with a median of 17%. Samavedam et al. (1995) concludes that the base friction, crib friction, and shoulder resistance contribute 25% to 35%, 65% to 45%, and 10% to 25%, respectively, to overall lateral resistance; and that the contribution from the crib is the most important because it confines the base ballast, while also resisting lateral tie movements. It is noted that the tests did not consider an applied normal load.

It is observed from Figures 2.6 and 2.7, that for low consolidation levels (i.e., 0.1 MGT) the track exhibits weak track behavior and for high consolidation levels (e.g., 100 MGT) the track exhibits strong track behavior, and that the peak-lateral resistance typically occurs at approximately 7.5 mm (0.3 in) of horizontal displacement.

Table 2.1: Summary of peak-lateral resistance obtained by Samavedam et al. (1995)

Configuration		Track Curvature	Material	Consolidation (MGT)	Peak-Lateral Resistance (lb)				Average Displacement at Peak (inches)	Number of Tests
					Max.	Min.	Ave.	S.D.		
1	PR	5° curve	Slag	0	2300	940	1469	258	0.27 ± 0.12	89
1	BCC1			0	1500	850	1129	172	0.40 ± 0.25	29
1	BCC2			0	325	150	227	50	0.13 ± 0.08	15
2	PR	5° curve	Granite	25	3030	1175	1993	397	0.19 ± 0.10	91
2	BCC1			25	1500	800	1078	177	0.21 ± 0.12	30
2	BCC2			25	285	125	209	44	0.25 ± 0.20	13
3	PR	5° curve	Slag	25	3320	1550	2374	351	0.29 ± 0.12	88
3	BCC1			25	2200	1075	1504	245	0.26 ± 0.11	29
3	BCC2			25	300	100	202	64	0.28 ± 0.28	15
4	PR	tangent	Slag	0	1500	700	1038	148	0.70 ± 0.30	71
4	BCC1			0	1200	650	849	128	0.55 ± 0.31	30
4	BCC2			0	250	100	167	36	0.28 ± 0.24	15
5	PR	tangent	Slag	100	4300	1900	3176	560	0.31 ± 0.10	85
5	BCC1			100	4225	1875	2666	466	0.37 ± 0.17	31
5	BCC2			100	575	350	468	62	0.08 ± 0.04	14
6	PR	tangent	Granite	25	3390	1250	2206	411	0.26 ± 0.14	78
6	BCC1			25	2265	1520	1790	226	0.18 ± 0.06	14
6	BCC2			25	575	155	324	126	0.10 ± 0.08	14

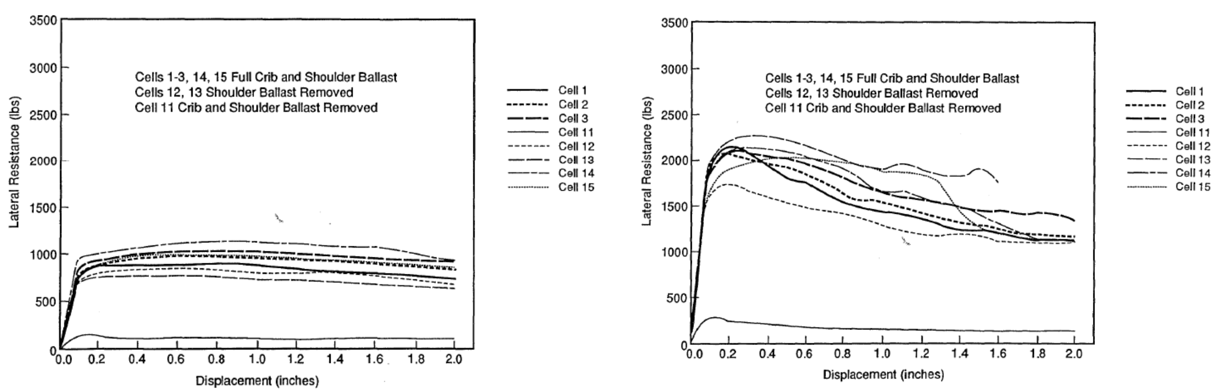

(A) Configuration 4 – tangent, slag, 0.1 MGT **(B) Configuration 5 – tangent, slag, 100 MGT**

Figure 2.6: Typical load-horizontal displacement curves obtained by Samavedam et al. (1995)

Samavedam et al. (1999)

Samavedam et al. (1999) conducted STPTs on a section of in-service track to quantify the effects of track maintenance and re-surfacing operations on the lateral resistance of concrete ties. Specifically, Samavedam et al. (1999) considers the tie-lateral resistance provided by pre-surfaced, post-surfaced, and post-stabilized ballast.

The peak-lateral resistance obtained by Samavedam et al. (1999) is summarized in Table 2.2; and the average load-horizontal displacement curves obtained Samavedam et al. (1999) is presented in Figure 2.8 for each ballast condition. The pre-surfaced ballast exhibits strong ballast behavior with an average peak-lateral resistance of 3438 lbs (15.3 kN) per tie, and the post-surfaced and post-stabilized track exhibits weak ballast behavior with an average peak-lateral resistance of 1869 lbs (8.3 kN) per tie and 1938 lbs (8.6 kN) per tie, respectively. Indicating, pre-surfacing reduces the average peak-lateral resistance by 46%, and stabilization by a dynamic track stabilizer increases it by 4%. The results also show a significant amount of scatter with the standard deviation ranging from approximately 8% to 15% of the peak-lateral resistance. The peak-lateral resistance typically occurrs at 2.5 mm (0.1 in) of horizontal displacement as show in Figure 2.8.

Table 2.2: Summary of peak-lateral resistance obtained by Samavedam et al. (1999)

Pre-Surfacing		Post-Surfacing		Post-Stabilization	
Test and Tie Number	Peak-lateral Resistance (lb)	Test and Tie Number	Peak-lateral Resistance (lb)	Test and Tie Number	Peak-lateral Resistance (lb)
1 – 83	3000	1 – 17	2200	9 – 67	1800
2 – 622	3200	6 – 235	2025	10 – 336	2100
3 – 756	3650	7 – 454	1675	11 – 521	1800
4 – 890	3900	8 – 689	1575	12 – 840	2050
Ave.	3438	Ave.	1869	Ave.	1938
S.D.	411	S.D.	293	S.D.	160

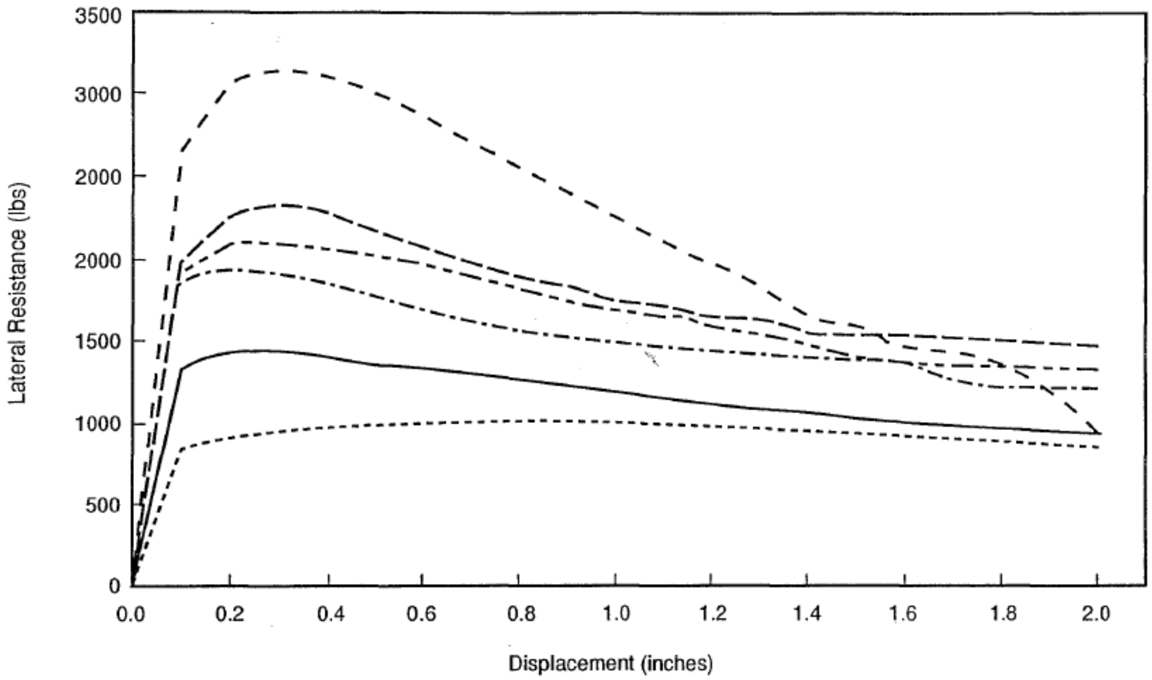

Figure 2.7: Average load-horizontal displacement curves obtained by Samavedam et al. (1995)

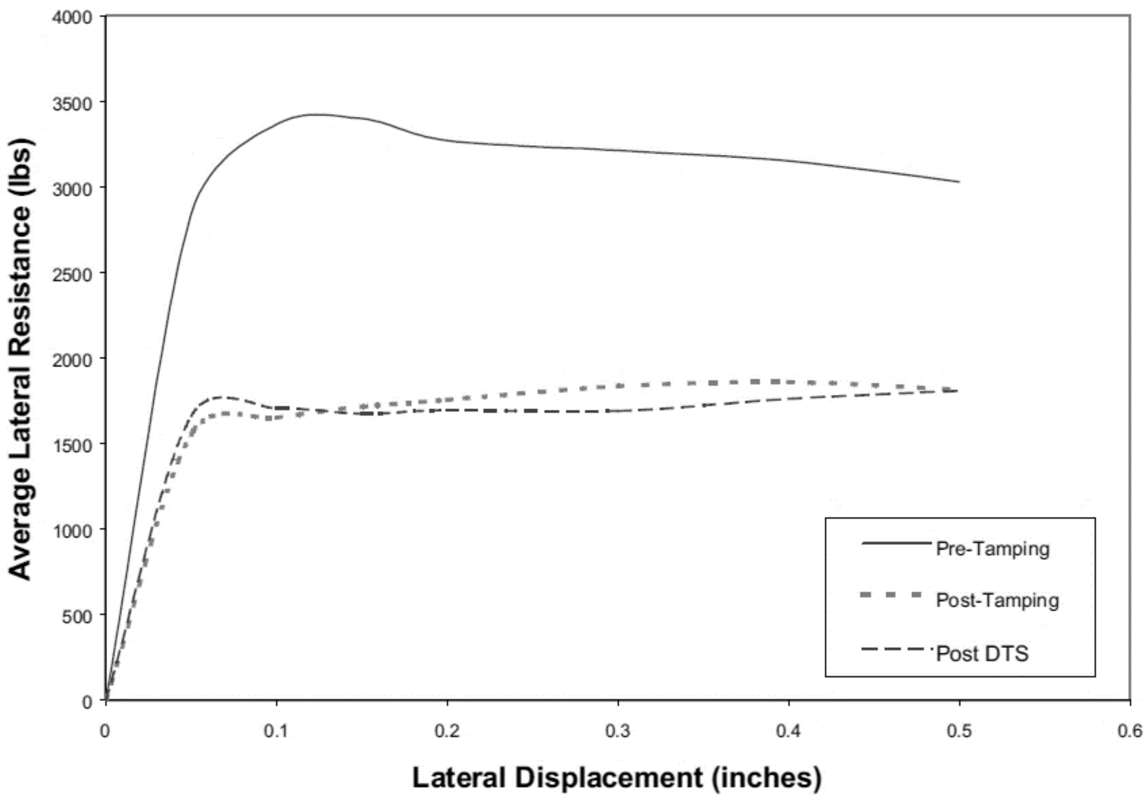

Figure 2.8: Average load-horizontal displacement curves obtained by Samavedam et al. (1999)

Sussmann et al. (2003)

Sussmann et al. (2003) conducted STPTs on a section of in-service track to quantify the effects of track maintenance and re-surfacing operations on the lateral resistance of concrete ties with 0.3 m to 0.45 m of shoulder ballast. Specifically, Sussmann et al. (2003) considers the tie-lateral resistance provided by pre-surfaced, post-surfaced, post-stabilized, and post-trafficked ballast.

The peak-lateral resistance obtained by Sussmann et al. (2003) is summarized in Table 2.3 for each test configuration with select load-horizontal displacement curves presented in Figure 2.9. The pre-surfaced ballast exhibits strong ballast behavior with an average peak-lateral resistance of 15.1 kN per tie. While, the post-surfaced, post-stabilized, and post-consolidated ballast exhibits weak ballast behavior with average peak-lateral resistances of 8.6 kN, 11.2 kN, and 9.6 kN per tie, respectively. Indicating pre-surfacing reduces the average peak-lateral resistance by 43%, and stabilization by a dynamic track stabilizer and consolidation by 0.004 MGT of train traffic increases it by 30% and 12%, respectively. The results also show a significant amount of scatter with the standard deviation ranging from approximately 7% to 10% of the peak-lateral resistance.

Sussmann et al. (2003) concludes that well-compacted or strong ballast provides between 13 kN to 22 kN of lateral resistance per tie, and freshly-tamped or weak ballast provides between 6.2 kN to 10.7 kN of lateral resistance per tie, with the peak-lateral resistance typically occurring within 25 mm (1 in) of displacement.

Table 2.3: Summary of peak-lateral resistance obtained by Sussmann et al. (2003)

Ballast Condition	Number of tests	Peak-lateral Resistance (kN)	
		Range of Averages	Overall Average ± S.D.
Pre-surfacing	37	13.5 to 16.1	15.1 ± 9.7% of average
Post-surfacing	42	8.4 to 8.9	8.6 ± 7.1% of average
Post-stabilization	35	10.5 to 11.6	11.2 ± 9.5% of average
Post-traffic	10	Not provided	9.6 ± 9.7% of average

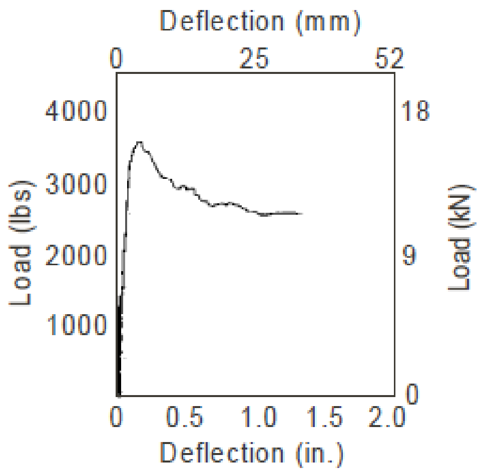

(A) Pre-surfacing test

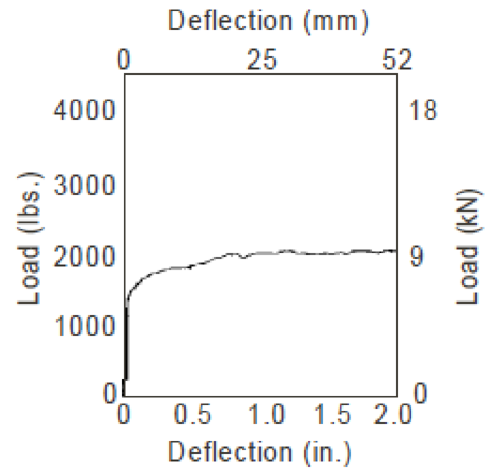

(B) Post-surfacing test

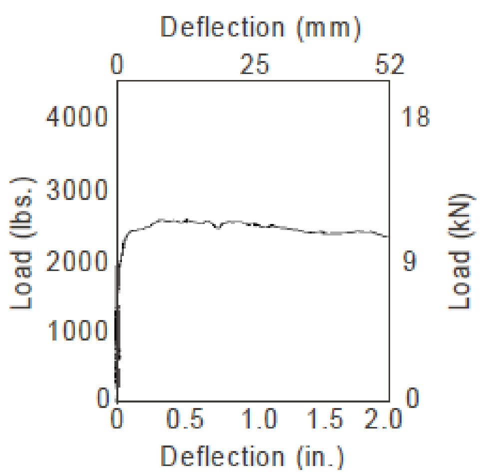

(C) Post-stabilization test

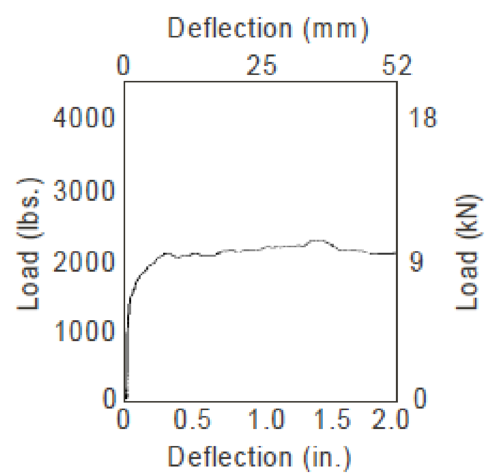

(D) Post-traffic test

Figure 2.9: Typical load-horizontal displacement curves obtained by Sussmann et al. (2014)

Clark et al. (2011) and Read et al. (2011)

Clark et al. (2011) and Read et al. (2011) conducted PPTs and STPTs on a section of in-service track to quantify the effects of reduced shoulder widths, and track maintenance and re-surfacing operations on the lateral resistance of concrete ties. During the PPTs a normal force of 89 kN was applied to each rail, while a lateral load was incrementally applied up to a maximum of 178 kN. During the STPT tests no normal load was applied.

In Clark et al. (2011) and Read et al. (2011), the average peak-lateral resistance was determined to be 40.4 kN, 32.7 kN, and 16.5 kN per tie for pre-surfaced track with an 0.45 m, 0.3 m, and 0.2 m wide shoulder of ballast, respectively. Indicating, a reduction in shoulder width from 0.45 m to 0.3 m has a marginal impact (20% reduction) on tie-lateral resistance and a further reduction from 0.3 m to 0.2 m has a significant impact (60% reduction).

For tests completed with a 0.45 m wide shoulder, Clark et al. (2011) and Read et al. (2011) show that re-surfacing the ballast reduces the peak-lateral resistance from 40.4 kN to 8.2 kN per tie. Subsequently, stabilizing the track using a dynamic track stabilizer increases the peak-lateral resistance to 13.6 kN per tie, consolidating the track with 0.09 MGT of train traffic increases it to 12.2 kN per tie, and both stabilizing and consolidating the track increases it to 12.1 kN per tie. These results indicate that maintenance and re-surfacing operations reduce tie-lateral resistance and change the behavior of the ballast from strong to weak, while stabilization and consolidation of the track increase tie-lateral resistance and change the behavior of the ballast from weak to strong.

Esmaeili et al. (2015)

Emaeili et al. (2015) conducted single tie pull tests (STLT) to quantify the lateral resistance of concrete ties in two different ballast materials: crushed limestone (LB) and crushed steel slag (SB). The tests considered several thicknesses of base ballast (0.3 m, 0.4 m, and 0.5 m), full crib ballast, and several widths of shoulder ballast (0.3 m and 0.4 m) at a side slope of one to one. Each test was conducted three times with the tie being displacement 2 mm in each test.

Typical load-horizontal displacement curves obtained by Emaeili et al. (2015) are presented in Figure 2.10 for tests completed with a 0.3 m and 0.5 m thick layer of ballast below the tie. It appears the tests were stopped before the peak-lateral resistance was reached, as shown in Figure 2.10, and it is expected that the lateral resistance would have continued to increase with displacement until it reached a limiting value at a high displacement.

In Figure 2.11, a summary of peak-lateral resistance is presented for each test configuration and material. From this figure, it can be seen that increasing the base ballast thickness from 0.3 m to 0.4 m increased the tie-lateral resistance by more than 20%. While, a further increase from 0.4 m to 0.5 m marginally decreased the tie-lateral resistance by less than 20%. Emaeili et al. (2015) did not provide an explanation for the decrease, but attributed the overall increase to more ballast being mobilized and less interaction occurring between the ballast and underlying materials, as the ballast thickness was increased. Emaeili et al. (2015) also observed an increase in tie-lateral resistance when they increased the shoulder width from 0.3 m to 0.4 m, which is expected based on work completed by Le Pen (2008), Le Pen and Powrie (2011), and Samavedam et al. (1995).

Emaeili et al. (2015) concludes the steel slag ballast provides 27% more tie-lateral resistance then the limestone ballast, but the reported difference was not evident in all of the test configurations. For a base ballast thickness of 0.3 m the results were similar for both materials and shoulder configurations (approximately 6 kN). While, for a base ballast thickness of 0.4 m and 0.5 m it became more evident that the steel slag ballast provided more tie-lateral resistance than the limestone ballast.

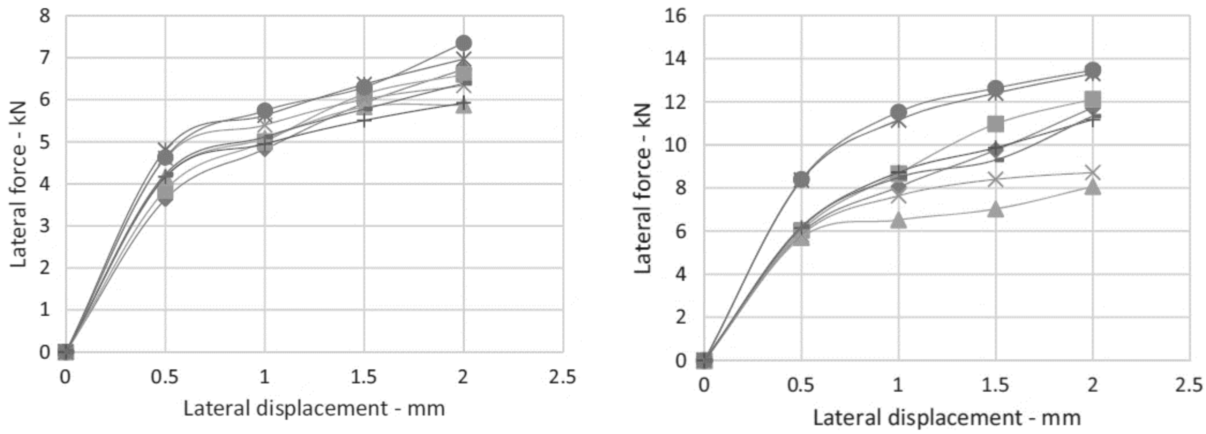

(A) Tests with 0.3 m of base ballast **(B) Tests with 0.5 m of base ballast**

Figure 2.10: Typical load-horizontal displacement curves obtained by Emaeili et al. (2015)

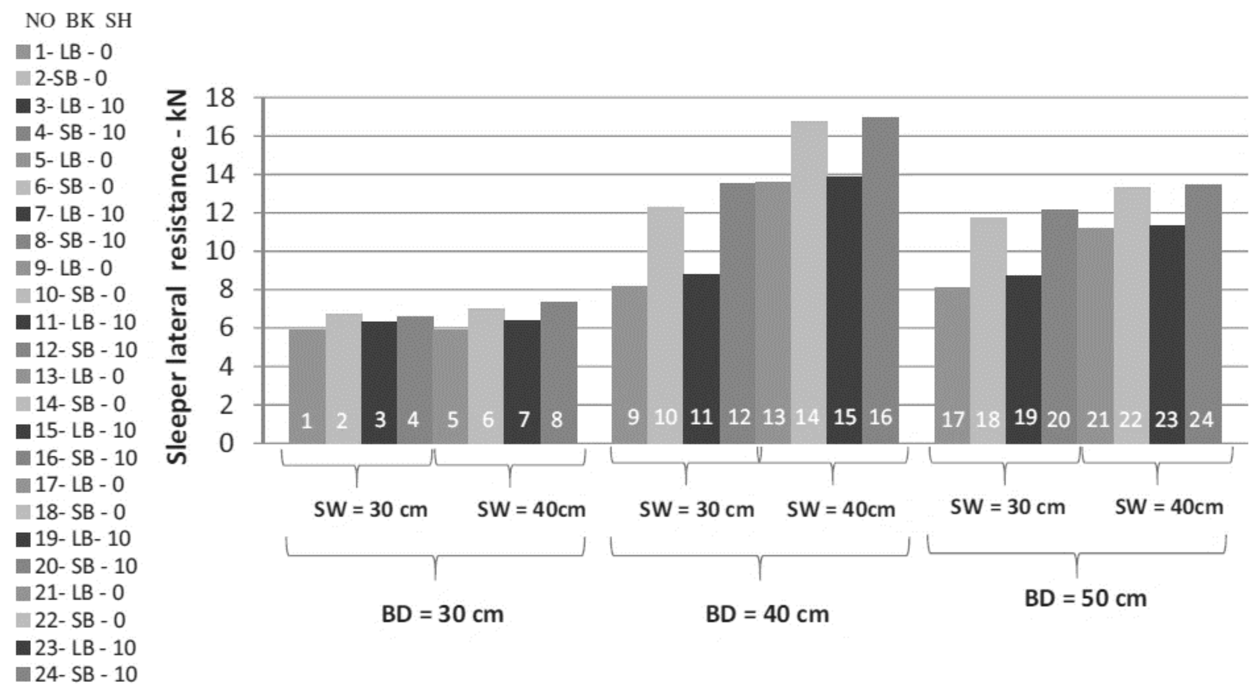

Figure 2.11: Summary of peak-lateral resistance obtained by Emaeili et al. (2015)

De Iorio et al. (2016)

De Iorio et al. (2016) conducted CPPTs on a section of tangent track to quantify the contribution of each component of tie-lateral resistance to overall lateral resistance. Four test configurations, as shown in Figure 2.12**,** were considered: one with four concrete sleepers and full ballast (BBB tests), one with four concrete sleepers and the crib ballast removed (BCB tests), one with four concrete sleepers and the shoulder ballast removed (BBU tests), and one with four concrete sleepers and the crib and shoulder ballast removed (BCU tests). The base ballast was 0.4 m thick, and the shoulder ballast, when present, was 0.6 m wide. Each panel of track was displaced at least 80 mm.

Characteristic load-horizontal displacement curves and the peak-lateral resistance obtained by De Iorio et al. (2016) are presented and tabulated in Figure 2.13 for each tie and test configuration. It is unclear why the BBB and BBU tests, which contain crib ballast, exhibit strong ballast behavior, but it is evident that the addition of crib ballast (and shoulder ballast) significantly increases peak-lateral resistance. De Iorio et al. (2016) concludes the average contribution of base friction, crib friction, and shoulder resistance to overall lateral resistance is 27%, 47%, and 26%, respectively; with the value dependent on the calculation method used. As shown in Table 2.4, they calculated the base friction contribution as the difference between the BBB and BCU results; the crib friction contribution as difference between the BBB and BCB tests, and the BBU and BCU tests; and the shoulder resistance contribution as the difference between the BBB and BBU tests, and the BCB and BCU tests with the percent contribution varying depending on the calculation method. These results suggest the different component of tie-lateral resistance do not act independently, but are dependent on each other. For example, the addition of crib friction may confine the base ballast resulting in an increase in base friction.

De Iorio et al. (2016) also calculated a limiting ratio of base friction to normal load (taken to be equal to dead load of the superstructure, which was estimated to be 3.1 kN per tie) of 0.51, which is similar to the value of 0.56 reported by Le Pen (2008), and Len Pen and Powrie (2008).

(A) BBB tests (full ballast)

(B) BCB tests (no crib ballast)

(C) BBU tests (no shoulder ballast)

(A) BCU tests (no crib or shoulder ballast)

Figure 2.12: Photographs of De Iorio et al.'s (2016) testing configurations

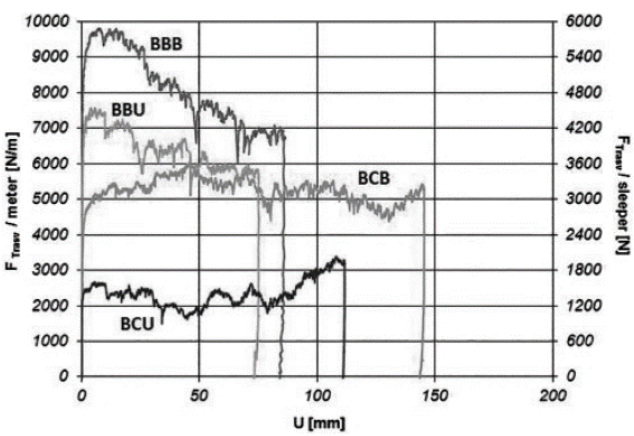

Peak-lateral Resistance per Tie	
BBB tests (full Ballast):	5879.7 N
BCB tests (no crib ballast):	3271.2 N
BBU tests (no shoulder ballast):	4541.4 N
BCU tests (no crib or shoulder ballast):	1599.3 N

Figure 2.13: Characteristic load-horizontal displacement curves obtained by De Iorio et al. (2016)

Table 2.4: Percent contribution of each component of tie-lateral resistance to overall lateral resistance as reported by De Iorio et al. (2016)

Component of Tie-lateral Resistance	Calculation Method	Peak-lateral Resistance per Tie (N)	Contribution to Overall Lateral Resistance (%)	
			-	Average
Base Friction	BBB-BCU	1599.3	27.2	27.2
Crib Friction	BBB-BCB	2608.5	44.4	47.2
	BBU-BCU	2942.1	50.0	
Shoulder Resistance	BBB-BBU	1338.3	22.8	25.6
	BCB-BCU	1672.0	28.4	

2.3.3 Previous Laboratory Tie-lateral Resistance Tests

van't Zand and Moraal (1997)

van't Zand and Moraal (1997) conducted CPPTs in a full-sized laboratory test to determine the track-lateral resistance of concrete ties with 0.3 m of base ballast, and full crib and shoulder ballast. In the construction of their testing apparatus van't Zand and Moraal (1997) emphasized the importance of the ballast box, which confines the ballast during testing, being large enough to prevent confining boundary effects; and the initial compaction state of the ballast being similar at the start of each test, which they achieved by re-tamping the ballast between tests. They used crushed stone as ballast, and installed an elastic mat underneath the ballast to represent a slightly compressible subgrade.

The peak-lateral resistance failure envelopes obtained by van't Zand and Moraal (1997) are presented in Figure 2.13 for normal loads ranging from -5 kN (uplift forces) to 35 kN. The relationship between peak-lateral resistance and normal load was observed to be near linear for the range of applied loads; with an intercept of about 5 kN, which is indicative of the lateral resistance offered by the rails and fastening system.

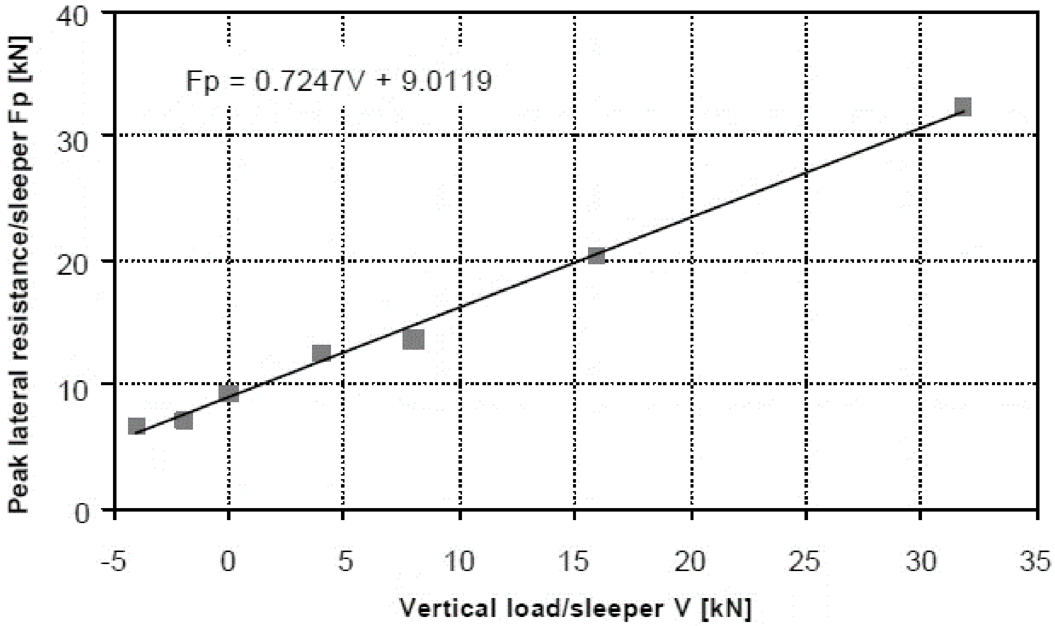

Figure 2.14: The failure envelope obtained by van't Zand and Moraal (1997)

Le Pen (2008), Le Pen and Powrie (2008) and Le Pen and Powrie (2011)

Le Pen (2008) and Le Pen and Powrie (2008 and 2011) conducted STPTs in a large-scale laboratory test to study the behavior of the tie-ballast interface under high speed tilting trains, and to quantify the tie-lateral resistance available to resist track buckling. They constructed a 5 m long, 0.65 m wide (equal to one sleeper spacing), and 0.65 m high steel ballast box with pressure plates on the walls to measured confining stresses in the ballast, a double layer of plastic sheeting on the walls to minimized low friction boundary conditions between the ballast and the ballast box, and a double layer of 20 mm wooden softboard at the base to represented a slightly compressible subgrade and to provide a compressible surface the ballast could embed into. The ballast box was filled with 0.3 m of crushed granite ballast, which was re-tamped between tests to a bulk density of 15 kN/m^3 and levelled to provide even support, before a concrete tie was placed on top, and, if applicable, the shoulder and crib ballast were constructed to the proper dimensions. A loading beam was then placed across the railheads, and two hydraulic rams, one vertical and one horizontal, were connected as shown in Figure 2.15. Linear Variable Differential Transformers (LVDTs) were connected to measure vertical and horizontal tie displacements.

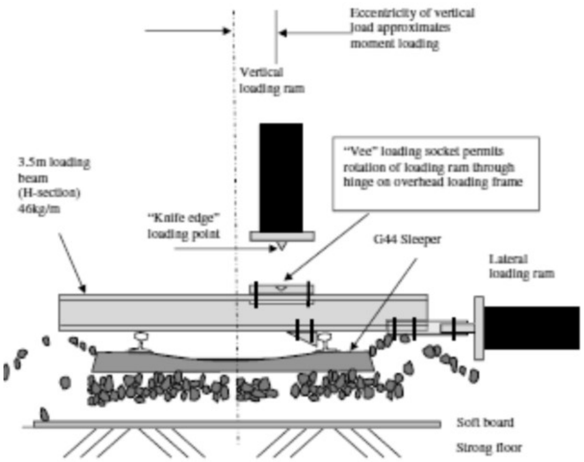

(A) A schematic of the laboratory set-up

(B) A photograph of the laboratory set-up

Figure 2.15: Le Pen (2008) and Le Pen and Powrie (2008 and 2011) laboratory set-up

After each test was set-up, Le Pen (2008) and Le Pen and Powrie (2008 and 2011) would cycle a normal load from 5 kN to 75 kN for a hundred cycles to stabilize the tie onto the ballast, which they maintained did not consolidate the ballast. Then they would cycle a horizontal load from 0 kN to one-third the normal load for a minimum of ten cycles to ensure the contact between the tie and ballast was stable. Once, the tie and ballast were stable they would conduct a single tie pull test at a rate of 0.25 mm/sec or 0.5 mm/sec, depending on the configuration of the ballast, over a distance of at least 80 mm while the normal load was maintained. Vertical and horizontal loads and displacements were recorded at 10 Hz or approximately every 0.05 mm of deflection.

In total, Le Pen (2008) and Le Pen and Powrie (2008) conducted 23 tests, as summarized in Table 2.5, including 5 tests to verify the testing method and to make improvements to the apparatus; 7 tests to study the tie-ballast interface in the presence of base ballast, including 3 under vertical and lateral loading (Type A tests) and 3 under moment loading (Type B tests); 9 tests to study the tie-ballast interface in the presence of base ballast and different dimensions of shoulder ballast (Type C tests); and 2 tests to study the tie-ballast interface in the presence of base and full crib ballast (Type D tests). Only tests 1C through 4C, 7C and 8C will discussed herein.

Table 2.5: Le Pen (2008) and Le Pen and Powries' (2008 and 2011) testing program

Test	Crib Ballast	Shoulder Width (mm)	Shoulder Height Above Tie (mm)	Measured Slope (°)	Normal Load (kN)	Position of Normal Load
1A	-	-	-	-	75	Central
2A	-	-	-	-	45	Central
3A	-	-	-	-	15	Central
1B	-	-	-	-	75	0.5 m offset
2B	-	-	-	-	15	0.5 m offset
3B	-	-	-	-	30	0.5 m offset
1C	-	400	0	41.5	15	Central
2C	-	200	0	45.0	15	Central
3C	-	200	0	42.8	45	Central
4C	-	600	0	42.8	15	Central
5C	-	400	125	45.9	15	Central
6C	-	400	62.5	40.9	30	Central
7C	-	400	0	43.9	15	Central
8C	-	300	0	41.4	15	Central
9C	-	400	125	37.6	15	Central
1D	Full	-	-	-	15	Central
2D	Full	-	-	-	15	Central

The results of the base resistance tests completed by Le Pen (2008) and Le Pen and Powrie (2008) are summarized in Table 2.6, including the tie-lateral resistance as several horizontal displacements; the mean lateral resistance from 2 mm to 20 mm, and 20 mm to 90 mm; and the peak-lateral resistance up to 10 mm, and between 2 mm and 90 mm of horizontal displacement. Tests 1A, 1B, and 1C were conducted under a centrally placed and maintained normal load (i.e., normal loading), and tests 2A, 2B, and 2C were conducted under an eccentrically placed and maintained normal load (i.e., moment loading). They also estimated an additional eccentricity of 0.4 m or moment load in all the tests due to the lateral load being applied to the railheads, but concluded the tie-lateral resistance is insensitive to the eccentricity of the normal load for the range of applied normal loads.

Table 2.6: Summary of Le Pen (2008) and Le Pen and Powries' (2008) base test results

Test	Normal Load (kN)	Horizontal displacement (mm)								
		0.5	1	2	3	5	Mean 2 to 20	Mean 20 to 90	Peak up to 10	Peak 2 to 90
Lateral Resistance per Tie (kN)										
1A	75	21.5	26.6	30.4	31.9	34.7	36.5	39.4	37.3	43.0
2A	45	12.0	17.5	21.7	21.9	23.7	24.7	25.4	25.4	27.6
3A	15	5.7	6.2	6.4	6.5	7.0	7.1	7.2	7.4	7.8
1B	75	13.8	17.8	21.2	22.6	23.9	25.5	26.1	25.0	28.2
2B	15	6.1	6.8	7.3	7.5	7.5	7.1	8.9	7.8	10.2
3B	30	9.2	11.2	12.4	12.7	13.6	15.6	17.0	15.5	18.8
Ratio of Lateral Resistance per Tie to Normal Load										
Mean		0.33	0.40	0.45	0.46	0.49	0.51	0.55	-	0.61
Median		0.31	0.39	0.45	0.46	0.48	0.50	0.57	-	0.62
Maximum		0.41	0.46	0.49	0.50	0.53	0.57	0.59	-	0.68
Minimum		0.27	0.35	0.41	0.42	0.45	0.47	0.48	-	0.52

Typical load-horizontal displacement curves for the base resistance tests completed by Le Pen (2008) and Le Pen and Powrie (2008) are presented in Figure 2.16. Overall, the ballast exhibits weak behavior and reaches a limiting resistance at approximately 20 mm of horizontal displacement; which when normalized to normal load, as shown in Figure 2.17, equals about 0.56. At horizontal displacements greater than 2 mm, the lateral load was observed to randomly drop followed by a rapid return to the previous load value, which Le Pen (2008) and Le Pen and Powrie (2008) attribute to ballast breakage and rearrangement events (e.g., fracturing, crushing, rolling, or sliding of the ballast). Whereas, at horizontal displacement less than 2 mm, the curves are relatively smooth because there has been minimal slippage at the tie-ballast interface and most of the movement is still recoverable. According to Le Pen (2008) and Le Pen and Powrie (2008), failure begins at the first evidence of ballast breakage and rearrangement; i.e., a displacement beyond which all further displacement is non-recoverable, which typically corresponds to a lateral to normal load ratio of about 0.45 in their research. They also noted the 'pre-failure zone'; i.e., the zone before the first evidence of ballast breakage or re-arrangement, and magnitude of recoverable horizontal displacement increases with normal load as shown in Figure 2.16B.

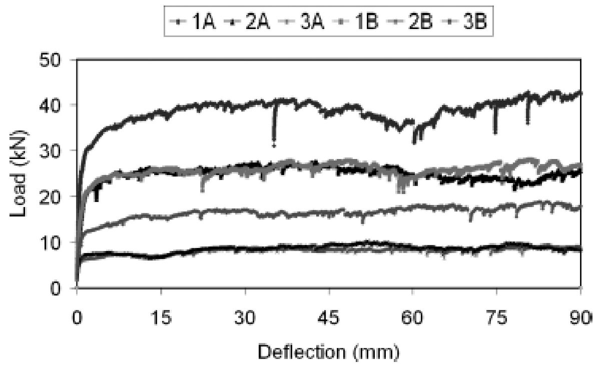

(A) Typical lateral load-horizontal displacement curves

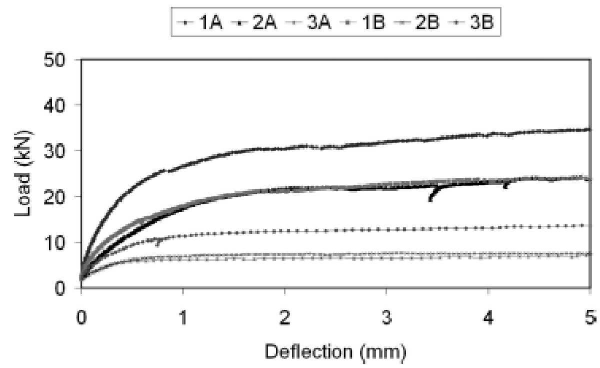

(B) Typical lateral load-horizontal displacement curves up to 5 mm

Figure 2.16: Typical load-horizontal displacement curves obtained by Le Pen (2008) and Le Pen and Powrie (2008)

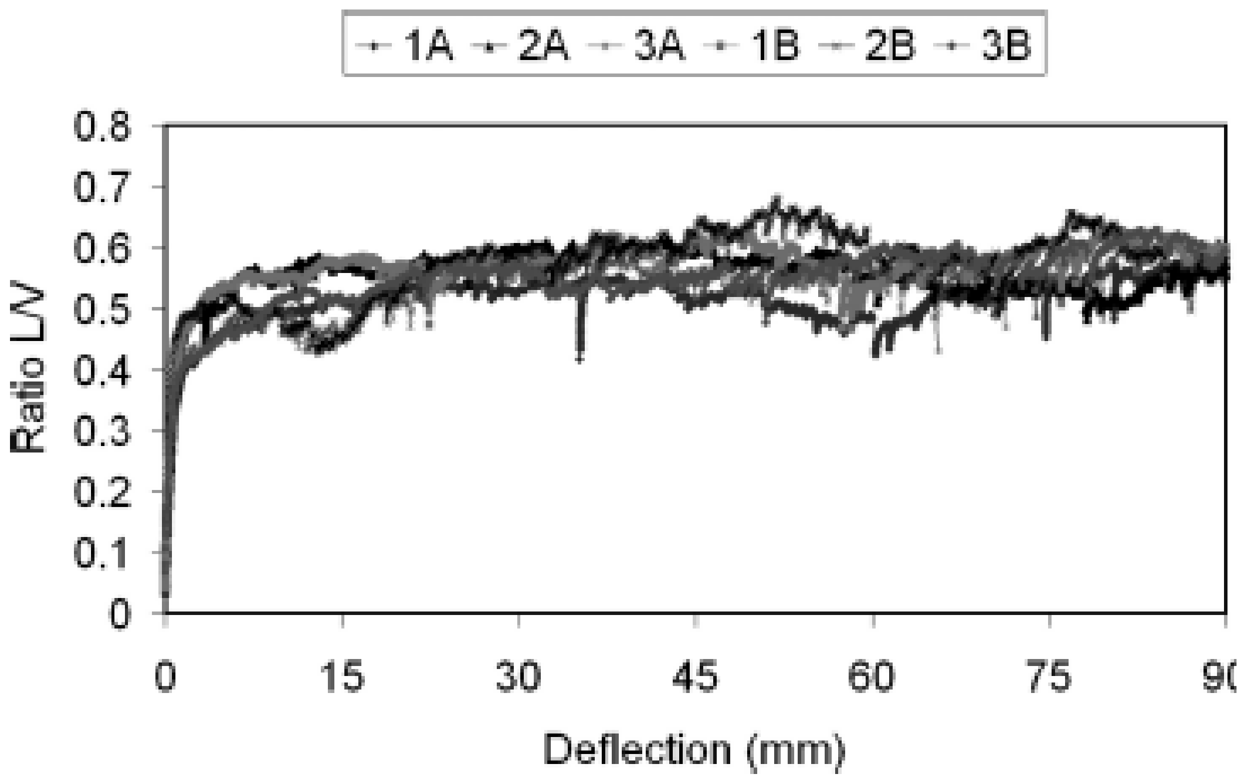

Figure 2.17: Normalized load-horizontal displacement curves obtained by Le Pen (2008) and Le Pen and Powrie (2008)

The results of the crib and shoulder resistance tests completed by Le Pen (2008) and Le Pen and Powrie (2011) are summarized in Table 2.7 and presented in Figure 2.18, including the mean increase in tie-lateral resistance due to the presence of shoulder and crib ballast. The mean increase was determined by estimating the mean ratio of lateral to normal load for the base resistance tests between 2 mm and 20 mm of horizontal displacement and subtracting the results from the mean ratio of lateral to normal load obtained during the shoulder and crib resistance tests between 2 mm and 20 mm of horizontal displacement to eliminate the contribution from the base ballast. The remaining ratio is then multiplied by the normal load for each test to estimate the contribution from the shoulder and crib ballast, respectively.

Table 2.7: Summary of Le Pen (2008) and Le Pen and Powries' (2008) shoulder and crib test results

Ballast Configuration	Test	Shoulder Width (mm)	Horizontal displacement (mm)							
			Mean 2 to 20	5	10	15	20	30	50	80
			Increase in resistance (kN)							
Shoulder Resistance Tests	2C and 3C	200	0.9	0.1	0.6	1.7	0.4	0.3	-0.05	-1.6
	8C	300	2.2	2.5	2.1	1.7	0.8	-7	0.5	2.0
	1C and 7C	400	2.0	2.1	2.0	2.0	2.0	1.3	16.7	1.6
	4C	600	2.3	2.6	2.3	2.4	1.7	1.5	1.9	2.3
Crib Resistance Tests	1D	-	2.3	2.6	2.2	1.9	1.7	1.3	-0.3	2.5
	2D	-	3.5	3.7	3.8	3.7	2.7	1833	2.2	2.9

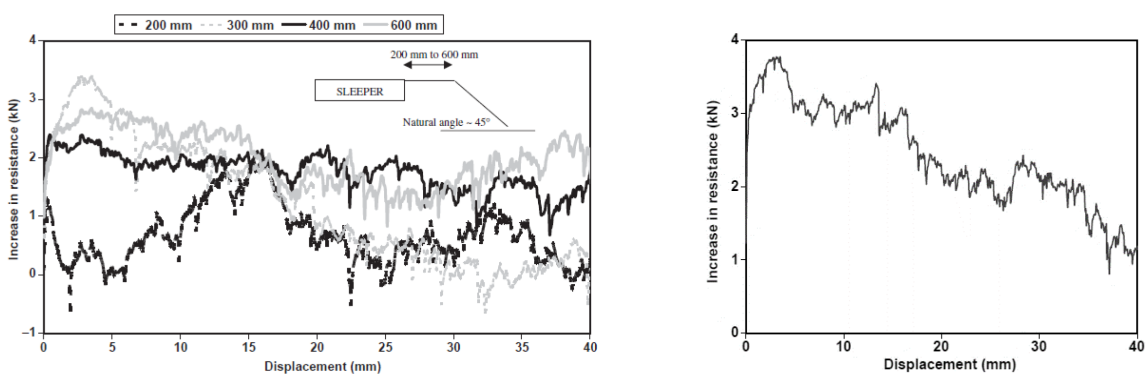

(A) Mean increase in tie-lateral resistance with different widths of shoulder ballast

(B) Mean increase in tie-lateral resistance with crib ballast

Figure 2.18: Mean increase in tie-lateral resistance obtained by Le Pen (2008) and Le Pen (2011)

Le Pen (2009) and Le Pen and Powrie (2011) found that increasing the shoulder width of 0.2 m to 0.3 m, 0.4 m, and 0.6 m increases tie-lateral resistance by approximately 0.9 kN, 2 kN, and 2.3 kN, respectively. Le Pen and Powrie (2014) concludes that a further increase in shoulder width beyond 0.6 m, which was observed to contain the entire failure wedge, will not increase the tie-lateral resistance because the critical failure mechanism is not being affected.

During the crib resistance tests, Le Pen (2008) and Le Pen and Powrie (2011) identified two potential modes of failure within the crib ballast: a slip surface developing at the contact between the tie and crib ballast, or a slip surface developing within the crib ballast. Photographs taken during the tests indicate the slip surface develops at the contact between the tie and crib ballast. In Figure 2.18B, the contribution from the crib ballast was observed to decrease with increasing sleeper movement. Le Pen (2008) and Le Pen and Powrie (2011) attribute this to the gradual loosening and loss of resistance as the ballast dilates.

Le Pen and Powrie (2011) conclude the base contributes 28% to 35%, the shoulder 15% to 32%, and the crib 41% to 50% to the overall lateral resistance of a concrete tie, as shown in Table 2.8. This calculation only considers the base friction provided under a normal load equal to the weight of the track superstructure, which was taken to be 2.0 kN.

Table 2.8: Percent contribution of each component of tie-lateral resistance as obtained by Le Pen and Powrie (2011) for no normal loading

Shoulder Size	Total (N)	Contribution					
		Base Friction		Shoulder Resistance		Crib Friction	
		(N)	% of total	(N)	% of total	(N)	% of total
200	5900	2065	35	899	15	2935	50
300	7151	2065	29	2150	30	2935	41
400	6974	2065	30	1973	28	2935	41
600	7318	2065	28	2317	32	2935	50

2.3.4 Relevance of this Research

In Table 2.9, the details of the tie-lateral resistances tests presented in Sections 2.3.2 and 2.3.3 are summarized, including the peak-lateral resistance, the contribution of each component of tie-lateral resistance to overall tie-lateral resistance; and, if provided, the test conditions (e.g., test type; tie type; ballast type, geometry, and conditions; loading conditions; loading rate). From this table, it can be seen that much of the reported literature and information on tie-lateral resistance involves the measurement of overall tie- and track-lateral resistance through STPTs and PPTs, respectively. Furthermore, much of the literature does not explicitly present the testing conditions (e.g., ballast type, geometry, and condition; loading conditions or rate), or include test results for tests conducted in different ballast materials or under a range of normal loads.

Le Pen (2008) and Le Pen and Powrie (2011) made a similar observation, when they noted most of the available data on tie-lateral resistance is unpublished and rarely presented in a way that allows the reader to identify the contribution of each component of tie-lateral resistance to overall lateral resistance. De Iorio et al. (2016) expresses a need for more experimental investigation, integrated with previous technical literature, to further our understanding of the present scientific background on ballast failure mechanisms. Particularly, De Iorio et al. (2016) expresses the need for testing programs to characterize the ballast behavior in a wide range of track configurations and service conditions, and to determine the contribution of each component of tie-lateral resistance to overall lateral stability.

This research presents a testing methodology for completing tie-lateral resistance tests for a wide range of test conditions (e.g., different tie and ballast types; consolidation, fouling, and moisture conditions; and normal loads), and for determining the contribution of each component of tie-lateral resistance to overall tie-lateral resistance. The proposed test is not meant to replace STPTs, but to supplement them. The idea of large-scale laboratory tests is to isolate particular characteristics of a system and reduce the number of variables that would otherwise obscure detail analyses. In this regard, the test can readily be used by operators to aid in their evaluation of the suitability of ballast sources, fouling conditions, and moisture contents without the need for track time or the construction of test track. Furthermore, the test allows the user to investigate the complete behavior of the tie-ballast interface over a range of applied normal loads. Even though unloaded track is more prone to buckling, understanding the complete behavior and strength characteristics of the tie-ballast interface requires analysis of its behavior under increasing strains and loads. For example, strength characteristics can be determined through evaluation of the failure envelope which is defined as the ratio of lateral load to normal load (see Section 5.2).

Table 2.9: Summary of tie-lateral resistance test results presented in the literature

Reference	Average Peak-Lateral Load		Percent Contribution of Each Component of Tie-lateral Resistance			Test Type	Tie Type	Ballast Type	Ballast Geometry			Ballast Condition	Normal Load	Loading Rate
	‘Weak’ Track	‘Strong’ Track	Base	Crib	Shoulder				Base	Crib	Shoulder			
Bakhtiary et al. (2015)	11 kN for timber ties, 13 kN for steel ties and 20 kN for concrete ties		-	-	-	STPT	Timber, steel, and concrete	Crushed rock	✓	X	X	Post-surfaced	No	-
Clark et al. (2011) and Read et al. (2011)	8.2 kN to 13.6 kN	40.4 kN	-	-	-	STPT	Concrete	-	✓	X	✓	Pre-surfaced, post-surfaced, post-stabilized, and post-traffic	-	-
De Iorio et al. (2014)			42%	42%	16%	-	-	-	-	-	-	-	-	-
	Between 4 kN and 10 kN		-	-	-	PPT	Concrete	Siliceous	✓	✓	✓	Various levels of compaction	No	0.2 mm/sec
De Iorio et al. (2016)	Approximately 5.8 kN		25%	50%	25%	CPPT	Concrete	-	✓	✓	✓	-	Yes, track superstructure, taken to be 3.1 kN	80 mm displacement
Esmaeili et al. (2015)	Between 6 kN and 17 kN		-	-	-	STPT	Concrete	Limestone and steel slag	✓	✓	✓	-	-	2 mm displacement
Kish (2011)	< 6.2 kN	> 12 kN	35% to 40%	30% to 35%	20% to 25%	-	-	-	-	-	-	-	-	-
Kish and Samavedam (2013)	8 N/m	53 N/m	40% to 55%	20% to 27%	40% to 18%	-	Timber	-	✓	✓	✓	-	Yes, track superstructure, taken to be 20 lb/in	
Le Pen (2008) and Le Pen and Powrie (2008 and 2011)	5.9 kN to 7.3 kN	-	28% to 35%	41% to 50%	15% to 32%	STLT	Concrete	Crushed granite	✓	✓	✓	Freshly-tamped	Yes, 2 kN seating load plus an applied load up to 75 kN	0.25 mm/sec to 0.5 mm/sec.
Lichtberger (2007)	-	-	45% to 50%	10% to 15%	35% to 40%	-	-	-	-	-	-	-	-	-
Samavedam et al. (1995)	-	-	25% to 35%	65% to 55%	10% to 20%	TLPT	Timber	Granite and slag	✓	✓	✓	Pre-surfaced, post-surfaced, post-stabilized, and post-traffic	-	0.3 mm/sec to 25.4 mm/sec
Samavedam et al. (1999)	8 kN	15 kN	-	-	-	STPT	Concrete	-	-	-	-	Pre-surfaced, post-surfaced, and post-stabilized	-	-
Selig and Waters (1994)	-	-	50% to 60%	10% to 20%	30% to 40%	-	-	-	-	-	-	-	No	-
	-	-	95% to 100%	0% to 5%	0% to 5%	-	-	-	-	-	-	-	Yes	-
Sussmann et al. (2003)	6.2 kN to 10.7 kN	13 kN to 22 kN	-	-	-	STPT	Concrete	-	✓	-	✓	✓	No	-
van’t Zand and Moraal (1997)	5.3 kN to 34.4 kN		-	-	-	PPT	Concrete	-	-	-	-	-	Yes, -5 kN to 35 kN	-

Note:

(1) ‘-’ denotes the information was unavailable.

(2) Pre-surfaced track refers to track that has not undergone track maintenance and/or surfacing operations (e.g., lining, levelling, and tamping); post-surfaced track refers to track after maintenance and surfacing operations; post-stabilized track refers to track that has been compacted (e.g., compacted by a dynamic track stabilizer); and post-traffic track refers to track that has been consolidated by train traffic (e.g., 15 MGTs of train traffic).

2.4 Relevant Ballast Specifications

CN Rail's (2003) and AREMA's (2014) ballast specifications are summarized in Table 2.10 with the technical standards (e.g., American Society for Testing and Materials [ASTM], and the British Standard Institute [BSI]) they suggest for conducting various material characterization tests.

A copy of CN Rail's ballast specifications for crushed rock ballast material on main-line track is included in Appendix I (CN Rail 2003).

Table 2.10: Ballast requirements and testing methods

Parameter	CN Rail (2003)		AREMA (2014)	
	Description/Criteria	Test Method	Description/Criteria	Test Method
Description	'Hard, strong and durable particles, clean and free from clay and shale and from an excess of dust or elongate particles.'	-	'Hard, dense, of an angular particle structure providing sharp corners and cubical fragments and free of deleterious materials. Ballast materials should provide high resistance to temperature changes, chemical attack, have high electrical resistance, low absorption properties and be free of cementing characteristics.'	-
Sample Preparation	Minimize abrasion of particles and segregation of sizes	-	-	ASTM D 75 and ASTM C 702
Maximum Particle Size	63 mm (2½ in)	ASTM C 136	50 mm (2 in) to 76 mm (3 in)	ASTM C 136
Mass Passing 0.75 mm (No. 200) sieve	Less than 1% by mass		Less than 1% by mass	
Grading	-		Uniformly-graded	
Percent Fractured Faces	75% of the particles by mass with two or more fractured faces and at least 98% of the particles by mass with one fractured face for each sieve size coarser than 19 mm (3/4 inch)	-	-	-
Percent flat or elongated particles (Flakiness Index)	Less than 30% by mass	BS 812	Less than 5% by mass	ASTM C 4791
Durability	less than 20% for ballast used primarily on mainline track, and less than 30% for ballast for use only on other than main line track.	ASTM C 535 'Grading 2'	Less than 35% for granite, 25% for quartzite, and 30% limestone	ASTM C 535
Minimum Depth	-	-	300 mm (12 in)	-

CHAPTER 3.0 CHARACTERIZATION OF THE MCABEE BALLAST AND THE GRAVEL BALLAST

Material characterization tests were completed on the McAbee Ballast and Gravel Ballast, including sieve analysis to determine particle size distribution, photogrammetry analysis to determine shape parameters (e.g., form and angularity indices), flakiness index testing to determine flakiness index, and Los Angeles Abrasion tests and Micro-Deval tests to assess durability. The methodology and results for each test type is presented in the following subsections. Supporting tables and figures for this chapter are included in Appendix II.

The material characterization tests were completed by Saleh Balideh. However, the analysis of the results and the writing of this chapter are my original work.

3.1 Material characterization Tests – Testing Methodology

3.1.1 Obtaining Representative Samples

In total, 3 m^3 of the McAbee Ballast and Gravel Ballast were stockpiled. Representative samples of each material were taken from these stockpiles in accordance with the following technical standards, which were suggested in CN Rail (2003) and AREMA (2014):

- **ASTM D75/D75M-14**, *Standard Practice for Sampling Aggregates* (ASTM 2014a); and
- **ASTM C702/C702M-11**, *Standard Practice for Reducing Samples of Aggregate to Testing Size* (ASTM 2011a).

Details on how representative samples were prepared for each test are provided in the succeeding subsections.

3.1.2 Sieve Analysis

The particle size distribution (PSD) of each material was determined through sieve analysis in accordance with the following technical standards, which were suggested in CN Rail (2003) and AREMA (2014):

- **MNL32-5th-EB**, *Manual on Test Sieving Methods: Guidelines for Establishing Sieve Analysis Procedures* (Smith 2014); and
- **ASTM C136/C136M-14**, *Standard Test Method for Sieve Analysis of Fine and Coarse Aggregates* (ASTM 2014b).

The sieve analysis test preparations were as follows (ASTM 2011a, ASTM 2014a, ASTM 2014b and Smith 2014,):

(1) The nominal maximum size (i.e., the smallest sieve opening through which the entire amount of aggregate is permitted to pass) of each material was estimated to be 63 mm (2.5 in).

(2) The minimal required sample size of each material was determined to be 140 kg – Test Method C136/C136M recommended 140 kg and Practice D75/D75M recommended 125 kg for aggregate with a nominal maximum size of 63 mm.

(3) Twelve separate portions of aggregate, weighing between 14 kg and 24 kg, were arbitrarily gathered from each stockpile in accordance with Practice D75/D75M. In total, 210.56 kg of the McAbee Ballast and 251.98 kg of the Gravel Ballast was collected, exceeding the minimum required sample size of 140 kg.

(4) Each portion was sieved individually in accordance with Test Method C136/C136M, so that the mass retained on each sieve did not exceed the maximum allowable quantity given in Test Method C136/C136M. The sum of all twelve was then taken for each sieve to form the 'bulk sample'.

(5) The (unwashed) bulk sample was then reduced to a 'representative sample' using a mechanical splitter in accordance with Practice C702/C702M; i.e., the twelve portions were reduced to six (i.e., six retained and six discarded), the six portions into three, the three portions into one, and the one portion into a smaller one. The final representative sample of McAbee Ballast had a mass of 12.66 kg and the final representative sample of Gravel Ballast had a mass of 14.54 kg.

(6) The representative samples were sieved using a mechanical sieve shaker in accordance with Test Method C136/C136M. Eight screen-tray sieving frames with square openings were used in the sieve shaker; they were nested, from top to bottom, in the following order of sieve opening size: 63 mm, 50 mm, 37.5 mm, 25 mm, 19 mm, 12.5 mm, 9.5 mm, and 4.75 mm. The mass retained on each sieve after 10 minutes of continuous sieving was recorded to the nearest 0.1%.

3.1.3 Photogrammetry Analysis

Photogrammetry analysis is an image processing technique used to evaluate the particle geometry, which can be described using three parameters: (1) form, which expresses the overall particle shape (e.g., circular or ellipsoid), (2) angularity, which expresses the sharpness of the particle apexes, and (3) texture, which expresses the surface roughness of the particle.

The form index is a dimensionless parameter ranging from zero for circular particles and increasing for elliptical particles, while the angularity index is a dimensionless parameter ranging from zero for rounded particles and increasing for angular particles. The average two-dimensional (2D) form and angularity indices in the x-, y-, and z-directions were determined using Equations 3.1 and 3.2, respectively; and the average three-dimensional (3D) form and angularity indices using Equations 3.3 and 3.4, respectively:

$$Form\ Index_{2D} = FI_{2D} = \sum_{\theta=0^\circ}^{\theta=360^\circ-\Delta\theta} \frac{|R_{\theta+\Delta\theta} - R_\theta|}{R_\theta} \quad \text{Equation 3.1}$$

$$Angularity\ Index_{2D} = AI_{2D} = \sum_{\theta=0^\circ}^{\theta=360^\circ-\Delta\theta} \frac{|R_\theta - R_{EE\theta}|}{R_{EE\theta}} \quad \text{Equation 3.2}$$

$$Form\ Index_{3D} = FI_{3D} = \frac{FI_{2D,x}A_x + FI_{2D,y}A_y + FI_{2D,z}A_z}{A_x + A_y + A_z} \qquad \text{Equation 3.3}$$

$$Angularity\ Index_{3D} = AI_{3D} = \frac{AI_{2D,x}A_x + AI_{2D,y}A_y + AI_{2D,z}A_z}{A_x + A_y + A_z} \qquad \text{Equation 3.4}$$

Equations 3.1 and 3.2 use incremental changes in the particle radius, R_θ (i.e., the length between the particle's geometric center and surface/boundary) at a given directional angle, θ to calculate the 2D form and angularity indices. Equation 3.2 also uses the radius of an equivalent ellipsoid, $R_{EE\theta}$ at a given θ to calculate the 2D angularity index. The equivalent ellipsoid has the same area, as well as the same first and second-degree moments of the particle. An example of an equivalent ellipsoid calculated for a particle of McAbee Ballast is provided in Figure 3.1. Equations 3.3 and 3.4 use the weighted average of the 2D form and angularity indices and the particle area, A in the x-, y-, and z -directions to calculate the 3D form and angularity indices

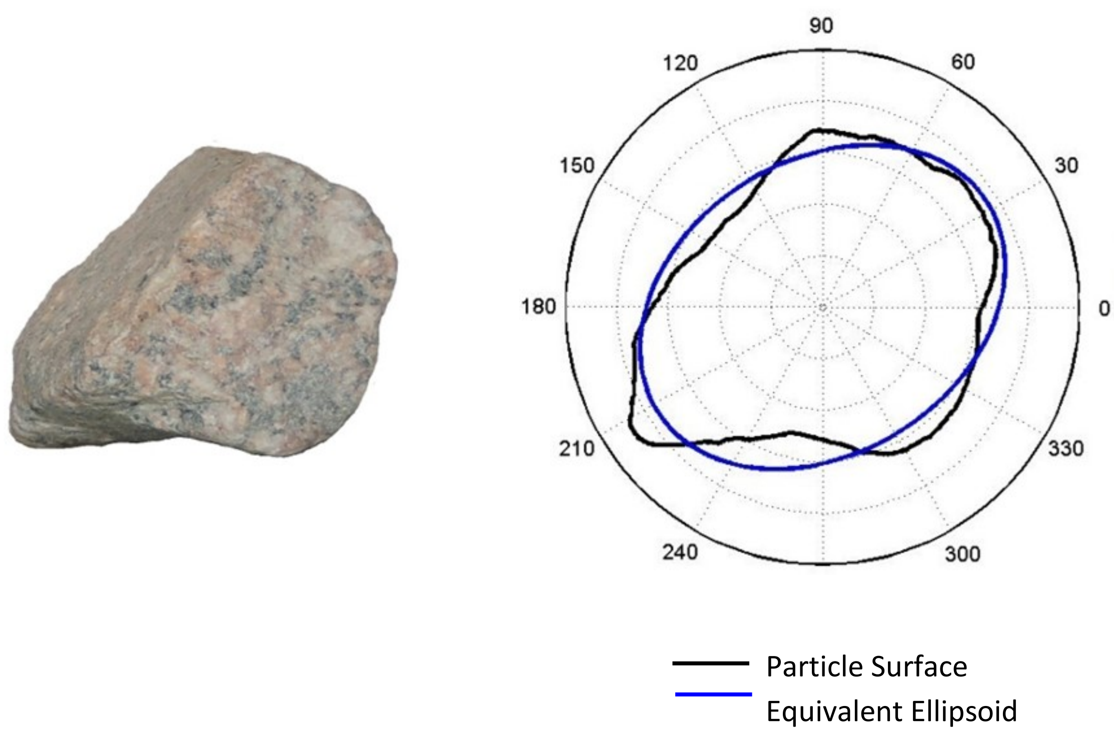

Figure 3.1: Equivalent ellipsoid for a particle of McAbee Ballast

There are no technical standards available for photogrammetry analysis, but work published by Balideh (2015), Little (2003), Masad (2001 and 2007), and Al-Rousan (2004 and 2007) was used as a guideline. The photogrammetry analysis test preparations were as follows (ASTM 2011a, ASTM 2014b, and Balideh 2015):

(1) The representative samples from the sieve analysis were sieved in accordance with Test Method C136/C136M into seven size fractions, as shown in Table 3.1.

Table 3.1: Size Fractions for photogrammetry analysis

Size Fraction	Particle Size (mm)	Retained Mass (Kg)	
		McAbee Ballast	Gravel Ballast
1	63.0 to 50.0	0.11	0.98
2	50.0 to 37.5	1.01	4.27
3	37.5 to 25.0	6.07	5.60
4	25.0 to 19.0	3.67	1.56
5	19.0 to 12.5	1.63	1.21
6	12.5 to 9.5	0.13	0.24
7	9.5 to 4.75	0.04	0.19
	Total Mass (Kg)	12.66	14.54

(2) A sixth of each size fraction was selected using the quartering method in accordance with Practice C702/C702M to reduce the quantity of aggregate in each size fraction to a manageable quantity for testing.

(3) Each particle was placed in an illuminated box and photographed from three perpendicular directions, labelled the X-, Y-, and Z-direction.

(4) MATLAB code developed by Saleh Balideh (2015) was used to analyze each photograph and calculate the 2D form and angularity indices of each particle in the x-, y-, and z -directions (see Equation 3.1 and 3.2) and then an average 3D value for each size fraction (see Equation 3.3 and 3.4).

3.1.4 Flakiness Index Tests

A particle is classified as flaky when its thickness is less than 0.6 of its mean sieve size (BSI 1989). The flakiness index, the ratio of flaky particles to total mass, of each material was determined using flakiness index tests in accordance with the following technical standards, which were suggested in CN Rail (2003):

- **BS 812:Section 105.1**, *British Standard Testing aggregates, Part 105. Methods for determination of particle shape, Section 105.1 Flakiness index* (BSI 1989).

The flakiness index test preparations were as follows (ASTM 2014a, ASTM 2014b and BSI 1989):

(1) The minimal required sample size of each material was determined to be 35 Kg – Test Method 812:Section 105.1 recommended 35 Kg for an aggregate with a nominal maximum size of 50 mm or greater.

(2) Samples were arbitrarily gathered from each stockpile in accordance with Practice D75/D75M. In total, 37.8 kg of the McAbee Ballast and 42.6 kg of the Gravel Ballast was collected, exceeding the minimum required sample size of 35 kg.

(3) The samples were sieved in accordance with Test Method C136/C136M into four size fractions, as shown in Table 3.2. Aggregate retained on the 63-mm sieve, and material passing the 20-mm sieve were removed from the sample.

Table 3.2: Size Fractions for flakiness index testing

Size Fraction	Particle Size (mm)	Mass of Representative Sample (g)	
		McAbee Ballast	Gravel Ballast
1	63.0 to 50.0	-	3246.0
2	50.0 to 37.5	4884.5	11789.0
3	37.5 to 28.0	12917.3	11092.1
4	28.0 to 20.0	13619.5	8260.1
	Total Mass (Kg)	31421.4	31141.3

(4) A flakiness gauge was used in accordance with Test Method 812:Section 105.1 to separate the flaky particles from the non-flaky particles. The total mass of flaky

particles in each size fraction was recorded and the flakiness index calculated to the nearest whole number.

3.1.5 Los Angeles Abrasion and Micro-Deval Tests

The resistance to degradation or durability of each material was determined using Los Angeles Abrasion tests and Micro-Deval tests in accordance with the following technical standards, which were suggested in CN Rail and AREMA (CN Rail 2003, and AREMA 2014):

- **ASTM C535-16**, *Standard Test Method for Resistance to Degradation of Large-Size Coarse Aggregate by Abrasion and Impact in the Los Angeles Machine* (ASTM 2016);
- **ASTM C131/C131M-14**, *Standard Test Method for Resistance to Degradation of Small-Size Coarse Aggregate by Abrasion and Impact in the Lose Angeles Machine* (ASTM 2014c); and
- **ASTM D6928-10,** *Standard Test Method for Resistance of Coarse Aggregate to Degradation by Abrasion in the Micro-Deval Apparatus* (ASTM 2010).

ASTM (2016) describes the Los Angeles Abrasion test as a test that measures the "degradation of mineral aggregates of standard grading resulting from a combination of actions including abrasion or attrition, impact, and grinding in a rotating steel drum containing twelve steel spheres". While, ASTM (2010) describes the Micro-Deval test as a test that measures the "abrasion resistance and durability of mineral aggregates resulting from a combination of actions including abrasion and grinding with steel balls in the presence of water".

Los Angeles Abrasion testing

The Los Angeles Abrasion test preparations were as follows (ASTM 2014a, ASTM 2014b, ASTM 2014c and ASTM 2016):

(1) Samples were arbitrarily gathered from each stockpile in accordance with Practice D75/D75M.

(2) The samples were washed, dried, and sieved in accordance with Test Method C136/C136M into three size fractions: 50 mm to 37.5 mm (i.e., size fraction 1), 37.5 mm to 25 mm (i.e., size fraction 2), and 25 mm to 19 mm (i.e., size fraction 3). Aggregate retained on the 50-mm sieve and passing the 19-mm sieve were removed from the sample.

(3) The size fractions for each material were recombined in accordance with Test Method C535. In total, one 'Grading 2' sample (i.e., 5 Kg of size fraction 1 combined with 5 Kg of size fraction 2) and four 'Grading 3' samples (i.e., 5 Kg of size fraction 2 combined with 5 Kg of size fraction 3) were prepared for the McAbee Ballast; and four 'Grading 2' samples were prepared for the Gravel Ballast.

(4) Each sample and twelve steel spheres were placed in the Los Angeles Abrasion machine for a 1000 revolution at 30 rpm to 33 rpm, in accordance with Test Method C535.

(5) The samples were removed from the Los Angeles Abrasion machine and sieved in accordance with Test Method C136/C136M and dried.

(6) The final mass retained on the 1.70-mm sieve was recorded and the percent loss (i.e., the difference between the original and final mass expressed as a percentage of the original mass) calculated to the nearest 1% by mass. The fourth sample of McAbee and the Gravel Ballast was sieved after 200, 400, 600, 800, and 1000 rotations to determine the percent loss as a function of the number of rotations.

Photographs of a typical McAbee Ballast and Gravel Ballast sample before, during, and after Los Angeles Abrasion tests are provided in Figure 3.2.

McAbee Ballast | **Gravel Ballast**

(A) Grading 3 sample before testing

(B) Grading 2 sample before testing

(C) Grading 3 sample after testing

(D) Grading 2 sample after testing

(E) Grading 3 sample after testing

(F) Grading 2 sample after testing

Figure 3.2: Photographs of the Los Angeles Abrasion Test samples

Micro-Deval testing

The Micro-Deval test preparations were as follows (ASTM 2010, ASTM 2014a and ASTM 2014b):

(1) Samples were arbitrarily gather from each stockpile in accordance with Practice D75/D75M.

(2) The samples were washed, dried, and sieved in accordance with Test Method D6928 into three size fractions: 19 mm to 16 mm (i.e., size fraction 1), 16 mm to 12.5 mm (i.e., size fraction 2), and 12.5 mm to 9.5 mm (i.e., size fraction 3). Aggregate retained on the 19-mm sieve and passing the 9.5-mm sieve were removed from the sample.

(3) The size fractions for each material were recombined in accordance with Test Method D6928. In total, three samples were prepared for each material by combining 375 g of size fraction 1, 375 g of size fraction 2, and 750 g of size fraction 3.

(4) The samples were immersed in water at a temperature of 20°C for at least one hour.

(5) Each sample, in accordance with Test Method D6928, was placed in the Micro-Deval machine with water and 5000 g of steel balls, and subjected to a combination of abrasion and grinding in the rotating steel jar for two hours at 102 rpm.

(6) The samples were removed from the Micro-Deval machine, sieved, and dried.

(7) The steel balls were removed from the sample using a magnet.

(8) The mass passing the 1.18 mm sieve was recorded and the percent loss (i.e., the final mass passing the 1.18 mm sieve expressed as percentage of the original mass) calculated to the nearest 0.1%.

Photographs of a typical McAbee Ballast and Gravel Ballast sample before, during, and after Micro-Deval tests are provided in Figure 3.3.

McAbee Ballast | **Gravel Ballast**

(A) Sample before testing

(B) Sample before testing

(C) Sample after testing

(D) Sample after testing

(E) Sample after testing

(F) sample after testing

Figure 3.3: Photographs of the Micro-Deval Test samples

3.2 Material characterization Tests – Results and Analysis

3.2.1 Sieve Analysis

The results of the sieve analyses tests are summarized in ; and the PSD plots obtained for each sample are presented in , with CN Rail's ballast specifications for main-line track (CN Rail 2003). The data and PSD plot for each individual test is included in Appendix II.

Table 3.3: Summary of sieve analysis test results for the McAbee Ballast and Gravel Ballast samples

Parameter			McAbee Ballast Samples		Gravel Ballast Samples		CN Rail's Ballast Requirements (2003) for main-lines
			Bulk	Representative	Bulk	Representative	
Mass of Sample (Kg)			251.98	14.54	210.56	12.66	-
Percent Passing (%)	63.0 mm	2½ in	99.8	100.0	100.0	100.0	100
	50.0 mm	2 in	93.1	91.3	99.1	97.9	70-90
	37.5 mm	1½ in	63.8	64.4	91.2	87.8	40-70
	25.0 mm	1 in	25.3	24.2	43.7	41.0	0-25
	19.0 mm	¾ in	14.6	12.2	15.0	12.2	0-3
	12.5 mm	½ in	6.3	2.9	2.2	1.8	-
	9.5 mm	No. 4	4.6	1.5	1.1	0.7	-
	4.75 mm	No. 200	3.3	0.3	0.9	0.4	0-1
D_{60}			36.0	36.0	28.8	29.1	Approximately 25 mm
D_{30}			26.9	26.9	22.5	23.1	Approximately 30 mm
D_{10}			15.9	17.9	17.5	18.6	Approximately 35 mm
C_u			2.27	2.02	1.64	1.57	Approximately 1.40
C_c			1.26	1.12	1.01	0.99	Approximately 1.02
USCS Grading Classification			GP	GP	GP	GP	GP

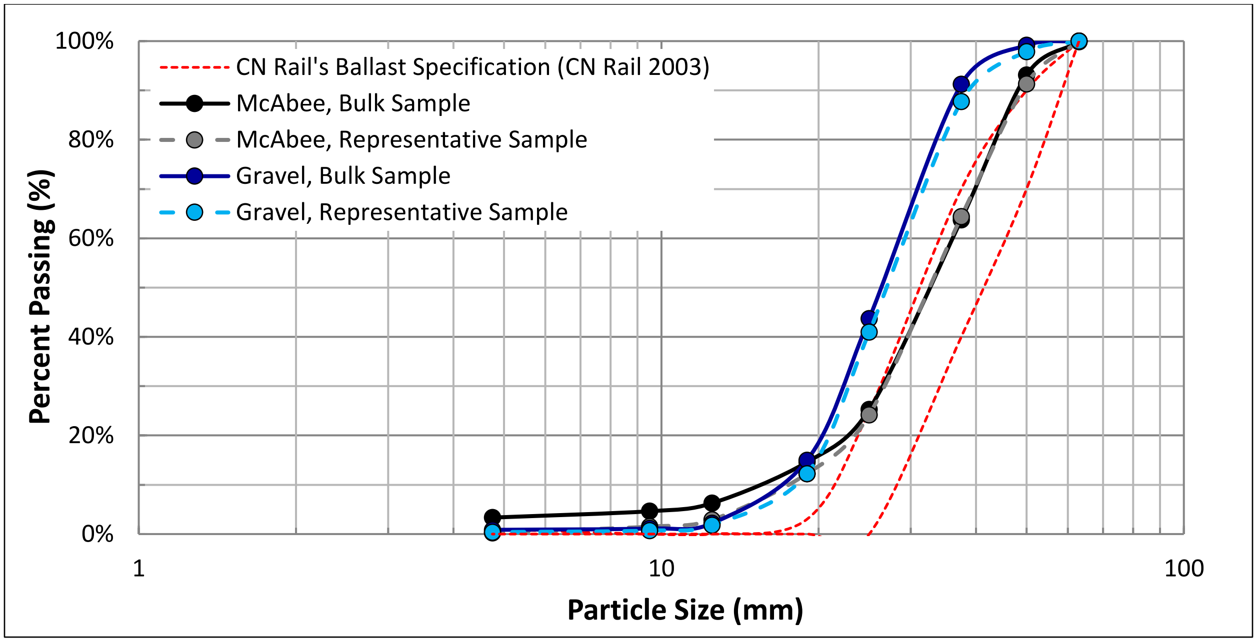

Figure 3.4: Particle Size Distribution of the bulk and representative McAbee Ballast and Gravel Ballast samples, with CN Rail's ballast specifications for main-lines (CN Rail 2003)

The particles sizes corresponding to 60%, 30%, and 10% passing (i.e., D_{60}, D_{30}, and D_{10}) were determined for each material and used to calculate the Coefficient of Uniformity, C_u and the Coefficient of Curvature, C_c, which can be expressed using the following equations, respectively (ASTM 2011b):

$$C_c = D_{60}/D_{10} \qquad \text{Equation 3.5}$$

$$C_c = \frac{(D_{30})^2}{D_{10} \times D_{60}} \qquad \text{Equation 3.6}$$

A coarse-grained aggregate is classified as well-graded (GW) in the Unified Soil Classification System (USCS) if it has a C_u greater than 4.0 and a C_c between 1.0 and 3.0; otherwise it is classified as poorly or uniformly-graded (GP), if it is not gap-graded (ASTM 2011b). The representative McAbee Ballast sample had a C_u and C_c of 2.02 and 1.12, respectively, and the representative Gravel Ballast sample had a C_u and C_c of 1.57 and 0.99, respectively, indicating both the McAbee and Gravel Ballast samples are uniformly-graded. For comparison, CN Rail's ballast specifications for main-line track (CN Rail 2003) specify a uniformly-graded material with an approximate C_u and C_c of 1.40 and 1.02, respectively.

Overall, the McAbee Ballast sample contains too many particles finer than 25 mm to satisfy CN Rail's ballast specifications for main-line track (CN Rail 2003), while the Gravel Ballast sample is too fine at all percent passing to satisfy the requirements. However, unlike the McAbee Ballast samples, the Gravel Ballast samples do have an acceptable C_u and C_c. This is evident in , where the Gravel Ballast PSD is shown to have a near parallel distribution with the CN Rail's ballast specifications for main-line track (CN Rail 2003). It is noted that these materials are being considered for use on branch-lines, which have different specifications than main-line track; and that the gradation of each material can easily be adjusted during production to meet CN Rail's ballast specifications.

Since, the McAbee Ballast and Gravel Ballast samples are uniformly-graded with a minimal quantity of fines (less than 5%) both samples are expected to compact adequately, and provide uniform support and shear strength, while reducing track deformations, resisting ballast breakage and particle segregating, and providing the necessary elasticity and void space for drainage and the storage of fouling material (AREMA 2014, Indraratna et al. 2011, and Selig and Waters 1994).

3.2.2 Photogrammetry Analysis

Typical photographs of the McAbee Ballast and Gravel Ballast taken during the photogrammetry analysis are shown in Figure 3.5. The remaining photographs of each sample particle are included in Appendix III. It is evident from the photographs that the McAbee Ballast consists of particles with rough, angular to sub-angular faces (blasted and crushed faces), while the Gravel Ballast consists of particles with smooth, rounded faces (uncrushed faces) and/or rough, angular to sub-angular faces (crushed faces).

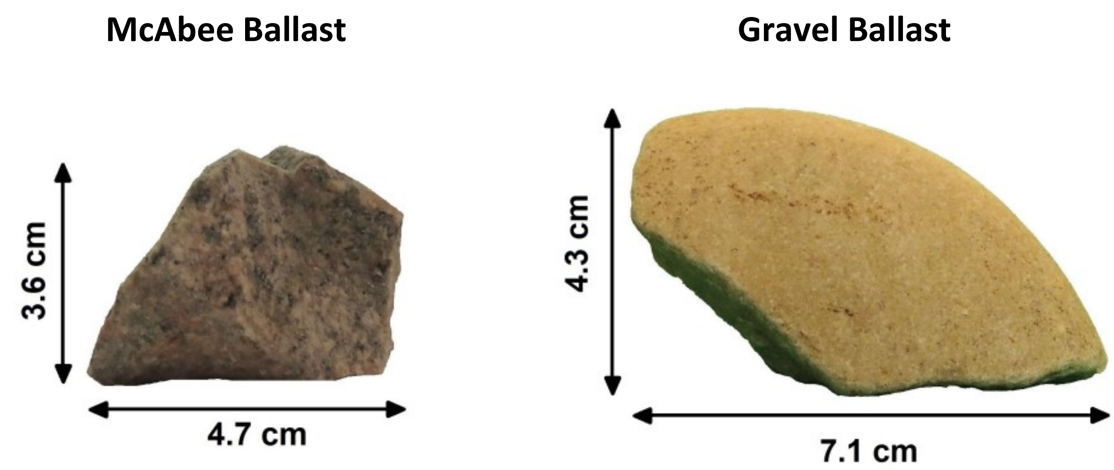

Figure 3.5: Photographs of a typical particle of McAbee Ballast and Gravel Ballast

MATLAB code was used to analyze each photograph and to calculate the 2D and 3D form and angularity indices for each material and size fraction (Balideh 2014). The 2D and 3D form and angularity indices for each material and size fraction are tabulated in Table 3.4, and plotted in Figures 3.6 and 3.7 and Appendix II. The McAbee Ballast had an average 3D form index of 2.8 and an average 3D angularity index of 32.1, while the Gravel Ballast had an average form 3D form index of 2.4 and an average 3D angularity index of 26.2. These results indicate the Gravel Ballast has more circularity and less angularity than the McAbee Ballast.

Table 3.4: Summary of photogrammetry analysis test results for the McAbee Ballast sample

Size Fraction	Particle Size (mm)	Weight in Sample (Kg)	Percentage in Sample (%)	Form Index				Angularity Index			
				2D			3D	2D			3D
				X	Y	Z		X	Y	Z	
McAbee Ballast											
1	63.0 to 50.0	0.11	0.9	3.2	2.5	2.6	2.8	32.3	40.1	30.4	33.4
2	50.0 to 37.5	1.01	8.0	2.8	2.4	2.9	2.7	29.6	28.0	30.9	29.2
3	37.5 to 25.0	6.07	47.9	2.8	2.7	2.8	2.7	35.4	35.0	32.2	33.8
4	25.0 to 19.0	3.67	29.0	2.8	3.1	2.3	2.6	30.5	35.0	24.9	29.2
5	19.0 to 12.5	1.63	12.9	3.0	3.4	2.6	2.9	30.5	38.4	30.9	32.5
6	12.5 to 9.5	0.13	1.1	3.2	2.5	2.9	3.0	40.0	40.1	33.7	37.8
7	9.5 to 4.75	0.04	0.3	3.3	2.7	3.2	3.1	33.1	30.9	25.1	28.9
Average				3.0	2.7	2.8	2.8	33.0	35.4	29.7	32.1
Standard Deviation				0.2	0.4	0.3	0.2	3.6	4.6	3.4	3.3

Table 3.5: Summary of photogrammetry analysis test results for the Gravel Ballast sample

Size Fraction	Particle Size (mm)	Weight in Sample (Kg)	Percentage in Sample (%)	Form Index				Angularity Index			
				2D			3D	2D			3D
				X	Y	Z		X	Y	Z	
1	63.0 to 50.0	0.98	6.7	2.2	2.7	1.7	2.2	23.5	16.6	12.3	16.2
2	50.0 to 37.5	4.27	29.3	2.4	2.7	2.0	2.2	33.9	29.3	21.0	27.5
3	37.5 to 25.0	5.60	38.5	3.0	2.7	2.3	2.5	32.3	29.9	25.2	28.6
4	25.0 to 19.0	1.56	10.7	3.0	3.1	2.6	2.8	32.6	33.4	24.2	29.8
5	19.0 to 12.5	1.21	8.3	2.5	2.5	2.4	2.4	29.7	28.9	20.7	25.6
6	12.5 to 9.5	0.24	1.6	2.6	2.5	2.3	2.5	31.8	35.0	21.7	28.2
7	9.5 to 4.75	0.19	1.3	2.7	2.6	2.3	2.5	29.8	32.4	22.1	27.8
Average				2.6	2.7	2.2	2.4	30.5	29.4	21.0	26.2
Standard Deviation				0.3	0.2	0.3	0.2	3.4	6.1	4.2	4.6

Surface roughness and particle angularity influence the frictional resistance (and shear strength) of granular materials. Generally, this resistance increases as the material becomes rougher and more angular because there is more granular interlock and internal friction, and a larger dilation requirement before slippage can occur (Indraratna et al. 2011, and Selig and Waters 1994). Overall, the McAbee Ballast is expected to provide more lateral resistance than the Gravel Ballast. However, this is also dependent on the ability of the materials to withstand abrasion (e.g., internal attrition and the breakage of sharp corners) which deteriorate surface roughness and angularity, and subsequently the frictional resistance of granular materials (Indraratna et al. 2011).

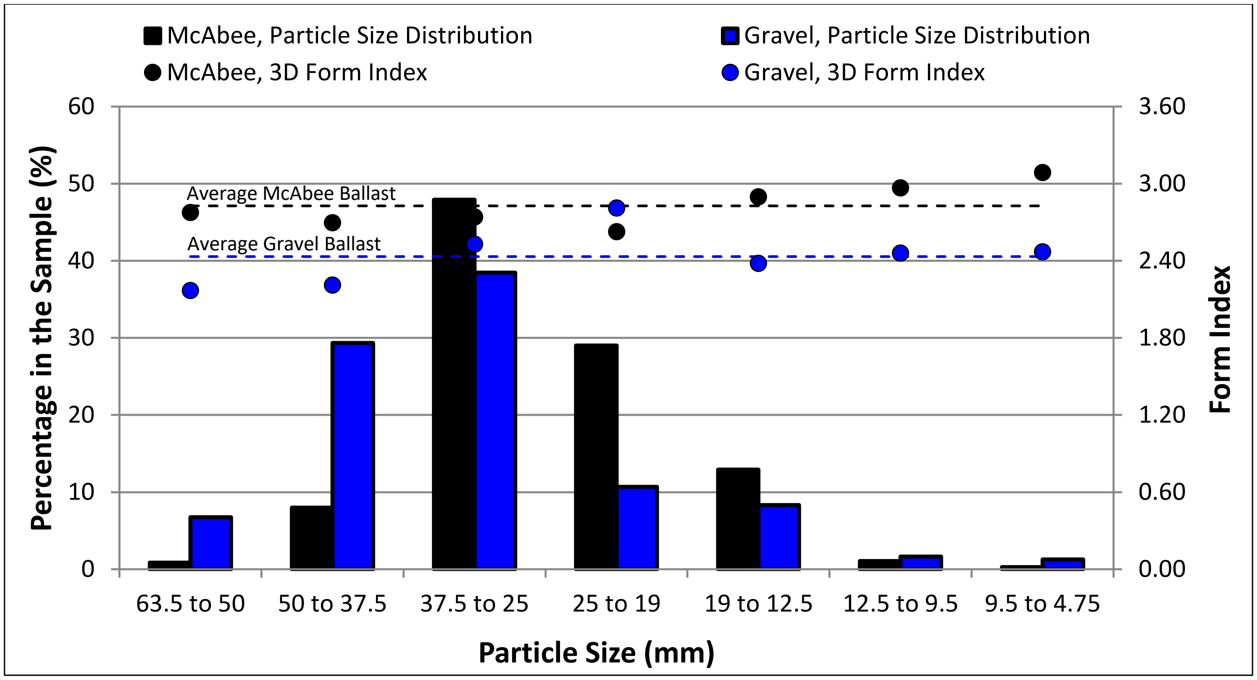

Figure 3.6: 3D form index for the McAbee Ballast and Gravel Ballast samples

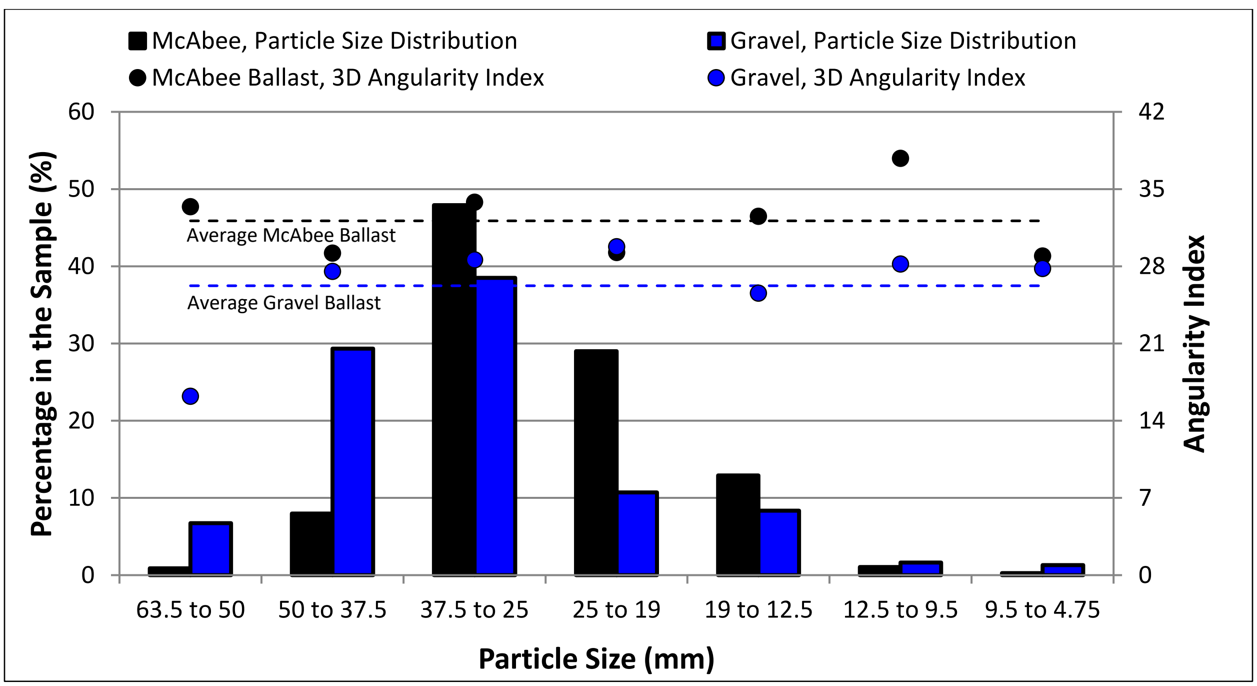

Figure 3.7: 3D angularity index for the McAbee Ballast and Gravel Ballast samples

3.2.3 Flakiness Index Tests

The presence of flaky particles in granular materials can increase abrasion and breakage; increase permanent strains under repeated loading; decrease stiffness; and, if the flaky particles were to align and form a plane of weakness, reduce the shear strength (Indraratna et al. 2011, and Selig and Waters 1994). Aligned flaky particles can also prevent drainage and the movement of fines through the ballast.

The results of the flakiness index testing on the McAbee Ballast and Gravel Ballast are summarized in Table 3.6. The McAbee Ballast and Gravel Ballast had an average flakiness index of 12% and 15%, respectively. CN Rail's ballast specifications for main-line track (CN Rail 2003) specify ballast should contain less than 30% by mass of flaky (or flat) particles. The results indicate both the McAbee Ballast and Gravel Ballast samples should compact and develop adequate shear strength, while permitting drainage and the movement of fines through the ballast.

Table 3.6: Summary of flakiness index test results for the McAbee Ballast and Gravel Ballast samples

Size Fraction	Particle Size (mm)	McAbee Ballast				Gravel Ballast			
		Total Mass (g)	Mass Passing Flakiness Gauge (g)	Flakiness-Index (%) By Particle Size	Flakiness-Index (%) Overall	Total Mass (g)	Mass Passing Flakiness Gauge (g)	Flakiness-Index (%) By Particle Size	Flakiness-Index (%) Overall
1	63 to 50	-	-	-	12	3245.97	764.84	23.6	15
2	50 to 37.5	4884.50	554.50	11.4		11789.03	1492.29	12.7	
3	37.5 to 28	12917.32	1769.90	13.7		11092.09	1194.67	10.8	
4	28 to 20	13619.54	1533.77	11.3		8260.14	1803.36	21.8	

3.2.4 Los Angeles Abrasion and Micro-Deval Tests

The results of The Los Angeles Abrasion test and Micro-Deval test results are summarized in Table 3.7. The complete data set is included in Appendix II.

In total, nine Los Angeles Abrasion tests were prepared, one Grading 2 and four Grading 3 samples for the McAbee Ballast, and four Grading 2 tests for the Gravel Ballast. The Grading 2 sample for the McAbee Ballast was prepared based on CN Rail's ballast specifications for main-line track (CN Rail 2003), but after further testing it was determined that Grading 3 samples were more appropriate for the McAbee samples. ASTM (2016) also recommends Grading 3 samples for the McAbee Ballast based on its PSD, and Clifton Associates (1991) prepared Grading 3 samples for their McAbee Ballast samples.

Table 3.7: Summary of the Los Angeles Abrasion Test and Micro-Deval test results for the McAbee Ballast and Gravel Ballast samples

Test	Material Type	Grading	Percent Loss (%)				
			Sample				Average
			1	2	3	4	
Los Angeles Abrasion	McAbee Ballast	2	12.7	-	-	-	12.7
		3	16.5	16.2	16.7	17.0	16.6
	Gravel Ballast	2	17.1	18.4	17.6	16.2	17.3
Micro-Deval	McAbee Ballast	N.A.	4.0	3.8	3.8	-	3.9
	Gravel Ballast	N.A.	4.0	5.0	4.3	-	4.4

The McAbee Ballast and Gravel Ballast had an average Los Angeles Abrasion parameter, or percent loss of 16.6% and 17.3%, respectively. CN Rail's ballast specifications for main-line track (CN Rail 2003) specify ballast should not have a Los Angeles Abrasion parameter, or percent loss greater than 20% for class 1 ballast or 30% for class 2 ballast. Clifton Associates (1991) and CN Rail (1990) reported values ranging from 14.7% to 17.5%, and 18% to 25%, respectively, for the McAbee Ballast. The McAbee Ballast and Gravel Ballast also had a Micro-Deval parameter, or percent loss of 3.9% and 4.4%, respectively. Overall, both the Los Angeles Abrasion and Micro-Deval test results indicate the McAbee Ballast and Gravel Ballast samples are of similar durability and should provide a similar amount of support without ballast breakage occurring.

The results of the Los Angeles Abrasion samples that was sieved after 200, 400, 600, 800, and 1000 rotations are summarized in Table 3.8, and the percent loss is plotted in Figure 3.8 as a function of the number of rotations. Since, both the McAbee and Gravel Ballast samples show a similar amount of degradation with the number of rotations, they are expected to degrade similarly with time. The ratio of the percent loss after 200 rotations to the percent loss after 1000 rotations was determined to be 0.21 and 0.26 for the McAbee Ballast and Gravel Ballast, respectively. Test Method C535 (ASTM 2016) specifies that the ratio of percent loss after 200 rotations to percent loss after 1000 rotations should not greatly exceed 0.20 for a uniformly hard material. These results indicate that the Gravel Ballast may not be uniformly hard.

Table 3.8: Percent loss versus number of rotations in the Los Angeles Abrasion Machine

Numbers of Rotations	McAbee Ballast			Gravel Ballast		
	Sample Mass (Kg)		Percent Loss (%)	Sample Mass (Kg)		Percent Loss (%)
	Initial	Final		Initial	Final	
200	10001.4	9639.9	3.6	10002.6	9586.6	4.2
400		9312.3	6.9		9268.2	7.3
600		8985.2	10.2		8992.6	10.1
800		8658.1	13.4		8676.5	13.3
1000		8303.9	17.0		8383.5	16.2

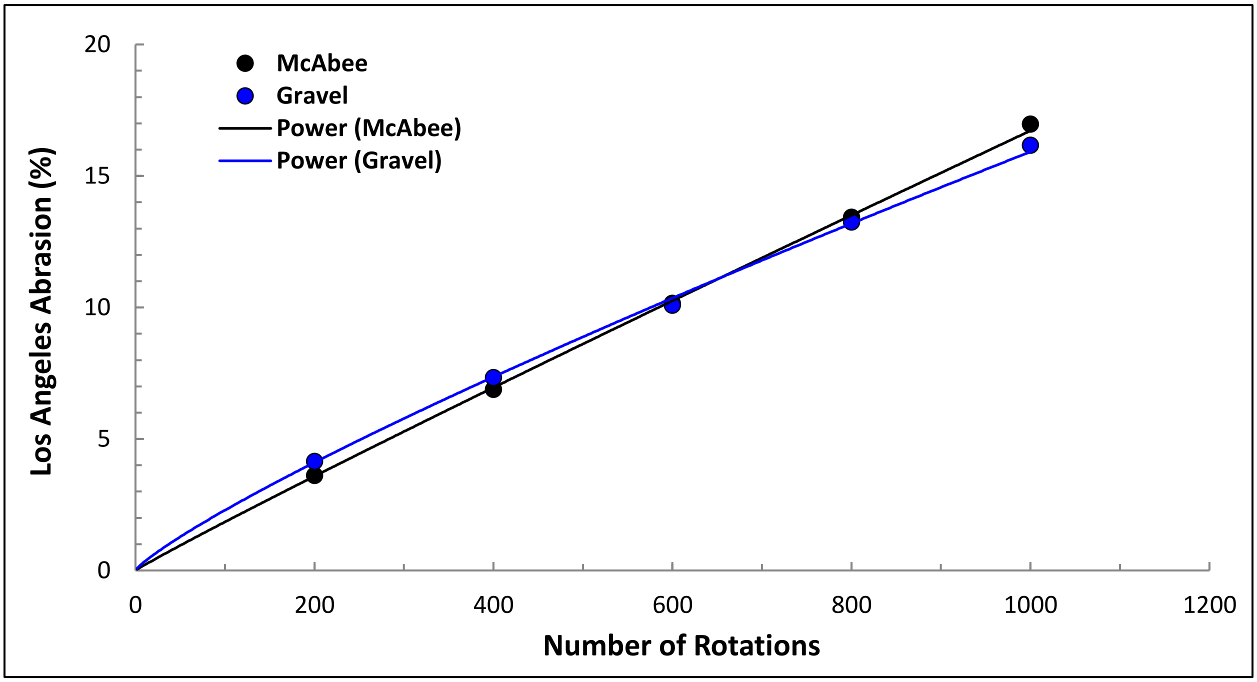

Figure 3.8: Percent loss versus number of rotations in the Los Angeles Abrasion Machine

3.3 Discussion and Conclusions

In summary, the key findings and conclusions from the material characterization tests are:

- The McAbee Ballast and Gravel Ballast samples are uniformly-graded with a minimal quantity of fines, and are expected to compact adequately, and provide uniform support and shear strength, while reducing track deformations, resisting ballast breakage and particle segregating, and providing the necessary elasticity and void space for drainage and the storage of fouling material.

- The McAbee Ballast consists of particles with rough, angular to sub-angular faces, while the Gravel Ballast consists of particles with smooth, rounded faces and/or rough, angular to sub-angular faces.

- The McAbee Ballast and Gravel Ballast samples had an average flakiness index of 12% and 15%, respectively. These results indicate both samples should compact and develop adequate shear strength, while permitting drainage and the movement of fines through the ballast.

- The McAbee Ballast and Gravel Ballast sample had an average Los Angeles Abrasion parameter of 16.6% and 17.3%, respectively, and a Micro-Deval parameter of 3.9% and 4.4%, respectively. Overall, both test methods indicate the samples are of similar durability and should provide a similar amount of support without ballast breakage occurring.

Overall, the McAbee Ballast is expected to provide more tie-lateral resistance than the Gravel Ballast because it is rougher, more angular, and contains less flaky-particles.

CHAPTER 4.0 TIE-LATERAL RESISTANCE TESTS – TESTING APPARATUS AND METHODOLOGY

A large-scale ballast box was designed to quantify the base friction, crib friction, and shoulder resistance component of tie-lateral resistance to overall tie-lateral resistance. The ballast box was used to complete tie-lateral resistance tests in the McAbee Ballast and Gravel Ballast under the expected range in-service ballast loads. The details of the tie-lateral resistance testing apparatus, methodology, and program is presented in the following subsections.

4.1 In-service Ballast Load Estimation

CN Rail is considering increasing the maximum freight car mass on its North American branch-lines from 122, 000 Kg (268, 000 lb) to 130, 000 Kg (286, 000 lb) per four axles. Thus, the maximum potential in-service static train load for CN Rail could be 32, 500 Kg per axle (71, 500 lb per axle) and the maximum potential ballast load (i.e., the static load transferred from an in-service train to the ballast) could be 16, 000 Kg (35, 000 lb) or 160 kN. Selig and Waters (1994) suggest the ballast load for heavy North American haul train is 174 kN, Clark et al. (2011) and Read et al. (2011) suggest 178 kN, and Le Pen (2008) suggests 150 kN.

The maximum potential ballast load of 160 kN was calculated using Equation 4.1 (AREMA 2014), assuming an impact factor of zero percent and a distribution factor of fifty percent:

$$Ballast\ Load = Axle\ Load\left(1 + \frac{Impact\ Factor}{100}\right)\left(\frac{Distribution\ Factor}{100}\right) \qquad \text{Equation 4.1}$$

The impact factor is the percentage increase over static normal loading and it is intended to estimate the dynamic effects of wheel and rail irregularities. While, the distribution factor is the percentage of axial load transferred to and carried by an individual tie. The assumed distribution factor of fifty percent is an upper bound assumption derived from AREMA (2014) for a single timber tie; it considers tie properties, tie spacing, ballast reaction, subgrade reaction, rail fastening system and the rail stiffness. The selected distribution factor is similar to the distribution factor (33% to 55%) reported by Le Pen (2008).

Several ballast loads, which are representative of the expected range of in-service train loads, were considered in this research (in addition to an initial setting load of 3.6 kN): 5 kN, 10 kN, 20 kN, 40 kN, 80 kN, and 160 kN. The applied setting load of 3.6 kN, which includes the weight of the loading beam, the roller supports, and the tie, was applied to represent the dead load applied by the track superstructure. Le Pen (2008), aLe Pen and Powrie (2011), and De Iorio et al. (2016) estimated the dead load of the track superstructure to be 5 kN, 2.1 kN, and 3.1 kN per tie, respectively. The ballast load was applied as a static normal load using a vertical hydraulic actuator, or vertical ram, fixed to an overhead loading frame. Roller supports were installed between the tie and the loading beam to simulate the rail locations, distribute the normal load to the tie, and permit displacement of the tie across the ballast.

The test can accommodate rollers spaced up to the standard 1.40 m track gauge (AREAM 2014), but a center-to-center spacing of 0.97 m was selected because suitable roller supports were unavailable (i.e., the available rollers were too long and could not be contained within the ballast box footprint). An analysis was completed to assess the impact of reducing the roller spacing. The analysis, which considered a beam on an elastic foundation analysis, showed a vertical deflection of less than 1 mm for the range of applied normal loads. This suggests the reduced spacing has a minimal impact on the pressure being distributed to the ballast and by extension a negligible impact on the development of tie-lateral resistance. The details of the roller spacing analysis are not presented herein.

The primary focus of this research is to provide a comparison between the McAbee Ballast and the Gravel Ballast. Therefore, this research considers the applied loading conditions, which are reasonably representative of in-service loading conditions, while providing testing flexibility, acceptable because all the tie-lateral resistance tests were conducted under similar conditions.

4.2 Testing Apparatus and Test Equipment

4.2.1 Ballast Box Design and Construction

A 1.52 m (60 in) long, 1.27 m (50 in) wide, 0.51 m (20 in) high, and 0.005 m (0.19 in) thick reinforced-steel box, or ballast box, was designed to confine the ballast during the tie-lateral resistance tests, as shown in Figure 4.1. The ballast box dimensions were selected based on recommendations in AREMA (2014) and the available laboratory space. The 1.52 m length accommodates a standard track gauge up to 1.40 m (55 in), while allowing the tie to over-hang the ballast box. The over-hang makes for easy handling and positioning of the tie; and it prevents the accumulation of ballast at the end of the tie, and subsequently, the generation of shoulder resistance during the Phase 1 base and Phase 2 crib tests. The 1.27 m width is representative of a 1.27 m center-to-center tie spacing, which is greater than the typical tie spacing of 0.45 m to 0.76 m discussed in AREMA (2014). The 0.51 m height accommodates 0.45 m of ballast below the tie, which is greater than the minimum ballast depth of 0.30 m recommended in AREMA (2014). The larger tie spacing and ballast thickness were selected to minimize confining boundary effects at the rigid interfaces between the ballast, the ballast box, and the floor (Zand and Moraal 1997, and Esmaeili 2006). Guide openings on the ballast box confine the ballast surrounding the tie, prevent the tie from resting on the ballast box frame, and guide the tie during testing.

During fabrication, the fabricator, Black Arrow Machine & Welding Inc., divided the ballast box into four wall panels and four floor panels so that it could be disassembled and stored. The following features were also added by the fabricator to increase the sturdiness and functionality of the ballast box: brackets to secure the wall and floor panels together, handles on each panel to facilitate lifting and storage, pre-drilled holes to bolt/anchor the base panel to the floor, ten vertical flanges to support the wall panels, and two stiffeners below the opening guides to support the end panels. The stiffeners were designed based on a stress analysis completed by Jakob Brandl at the U of A, the results of which are not presented herein.

Once, the ballast box was fabricated and assembled, it was lined with 0.25 in orientated strand board (OSB) to eliminate low friction boundary conditions between the ballast and the ballast box, and to provide a compressible surface the ballast could embed into; i.e., to represent a slightly compressible subgrade material (Le Pen 2008, Le Pen and Powrie 2008 and 2011, and van't Zand and Moraal 1997). The OSB was replaced with studier 0.5 in plywood during the

Phase 2 base and Phase 3 shoulder tests to extend the ballast box walls, which were too short to accommodate the crib ballast.

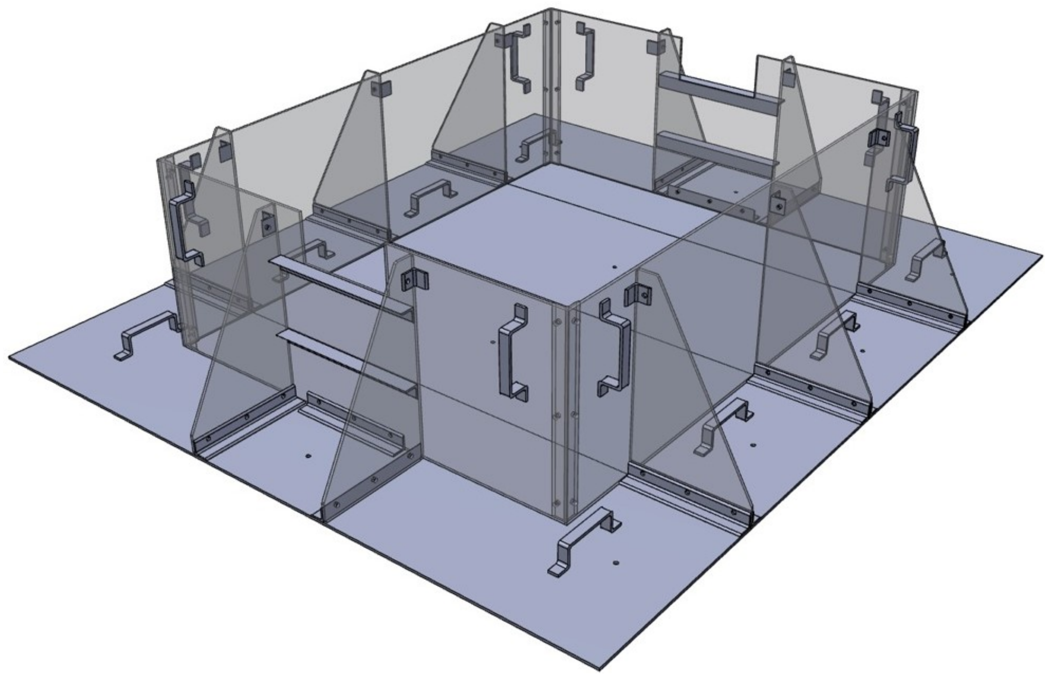

Figure 4.1: Ballast box design for the tie-lateral resistance tests

4.2.2 Other Materials and Equipment

The section details the materials and equipment used, in addition to the ballast box and ballast, to complete the tie-lateral resistance tests:

- 0.25 in thick orientated strand board (OSB) to line the ballast box during the Phase 1 base tests, and 0.5 in thick plywood to line and extend the ballast box during the Phase 2 crib and Phase 3 shoulder tests.
- A 10 in steel tamper and rubber mallet to tamp the ballast before each test.
- An 8 ft-6 in long, 9 in wide, and 7.5 in high timber tie.
- A steel plate screwed to one end of the timber tie to distribute the applied lateral load to the entire tie cross-section of the tie.
- A levelling scale to level the tie and the dead load before each test.

- An automated vertical hydraulic actuator, or vertical ram, fixed to an overhead loading frame to apply the normal loads.
- An automated horizontal hydraulic actuator, or horizontal ram, fixed to a loading column to apply the lateral loads. An automated servo valve in the horizontal ram fixed the loading rate at either a constant slow rate of 0.05 mm/sec or a fast rate of 0.5 mm/sec.
- Load cells on each ram to measure the applied loads.
- Two LVDTs, one between the vertical ram and the dead load and one between the tie end and the ballast box frame, to measure the vertical and horizontal displacement of the tie, respectively.
- A loading beam to provide an initial setting load and represent the dead load applied by the track superstructure (rails and fastening system).
- Two roller supports or rollers at the base of the loading beam to simulate the rail locations, distribute the normal load to the tie, and permit lateral displacement of the tie across the ballast.
- Two 0.45 m high support pedestals to support the tie during Phase 3 testing. Each pedestal consists of a load cell to measure the normal load transferred to each pedestal and a roller to allow the pedestal to displace across the floor.
- A bracing column to resist horizontal movements of the ballast box.

4.3 Testing Methodology

The Phase 1 base, Phase 2 crib, and Phase 3 shoulder resistance test preparation are outlined in the following subsections. The Phase 1 base and Phase 2 crib test configuration is illustrated in Figure 4.2 and the Phase 3 shoulder test configuration is illustrated in Figure 4.3.

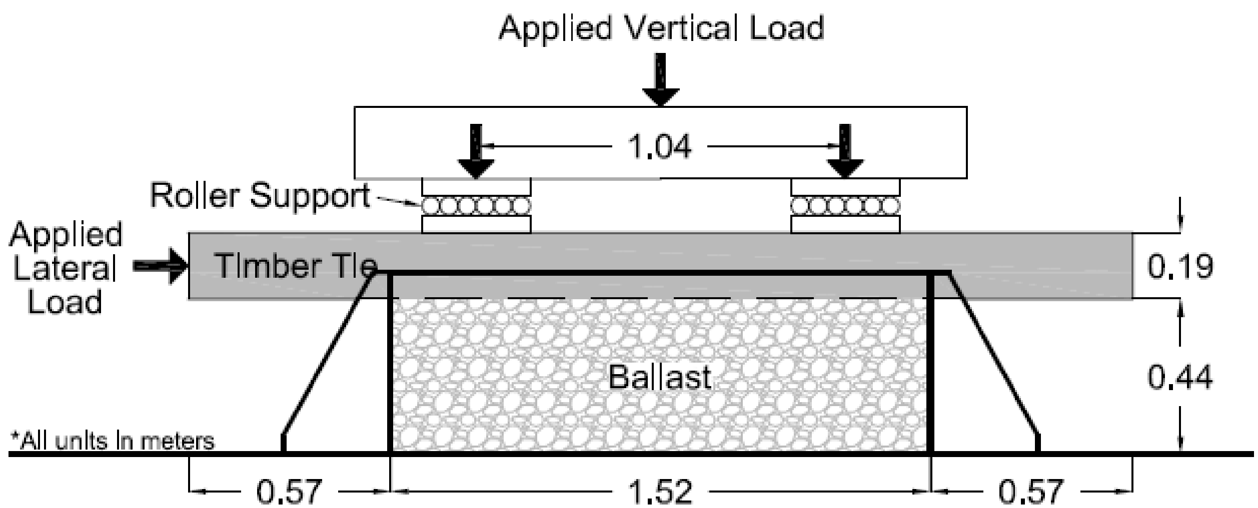

Figure 4.2: Phase 1 base and Phase 2 crib test configuration

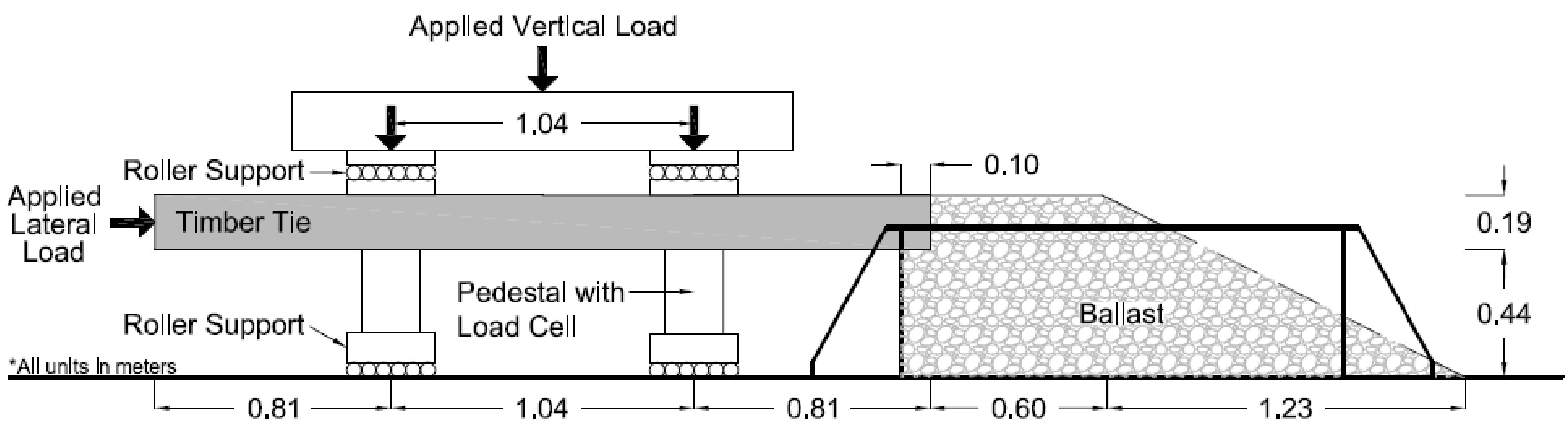

Figure 4.3: Phase 3 shoulder test configuration

4.3.1 Phase 1 Base and Phase 2 Crib Tests

The Phase 1 base and Phase 2 crib tests were completed to quantify the base friction and the crib friction, respectively. See Section 5.2 for how the base friction and crib friction were calculated from the Phase 1 base and Phase 2 crib test results.

The ballast box was assembled and aligned below the vertical ram. Two supporting columns were installed on either side of the ballast box: a bracing column to resist lateral movements of the ballast box along the floor and a loading column to provide a reaction force for the horizontal ram. The ballast box was lined with 0.25 in OSB during the Phase 1 base tests, and 0.5 in thick plywood during the Phase 2 crib tests. The plywood in the Phase 2 crib test was also used to extend the height of the ballast box, so that it could accommodate the crib ballast. Ballast was placed in the ballast box and hand tamped in three 0.15 m lifts (0.45 m total) with a 10 in steel tamper and rubber mallet. The tamped ballast had a bulk density of 15.5 kN/m^3 to 16.0 kN/m^3, which is consistent with a state of freshly-tamped or lightly-consolidated ballast (Le Pen 2008, and Le Pen and Powrie 2008 and 2011). The ballast was re-surfaced between tests back to a bulk density of 15.5 kN/m^3 to 16.0 kN/m^3 and levelled to provide even support. If applicable, an additional fourth 0.19 m thick layer of ballast was added and tamped to form the crib. Photographs of the ballast box assembly, and the Phase 1 base and Phase 2 crib test configurations are provided in Figure 4.4.

The Phase 1 base and Phase 2 crib test preparations were as follows:

(1) The top 150 mm of the base and crib ballast, if applicable, was removed, re-tamped, and levelled to a bulk density of 15.5 kN/m^3 to 16.0 kN/m^3.

(2) The tie was laid and levelled on the freshly-tamped ballast below the vertical ram.

(3) The dead load (loading beam and roller supports) was placed on-top of the tie below the vertical ram.

(4) Two LVDTs were connected, one between the vertical ram and dead load, and one between the tie and ballast box frame.

(5) A horizontal scale was attached from the loading column to the dead load to measure the frictional resistance, if any, in the roller supports.

(6) A normal load was applied to the tie using the vertical ram and the tie was allowed to stabilize under the applied load.

(7) A lateral load was applied to the centre of the steel plate using the horizontal ram. The load was not applied to the hypothetical location of the rails; i.e., the base of the roller supports, to prevent eccentrical loading of the tie.

(8) The tie was pushed laterally across the ballast up to 40 mm at either a 'slow' loading rate of 0.05 mm/sec or a 'fast' loading rate of 0.5 mm/sec. AREMA (2014) suggests displacing the tie at least 50 mm, but the rollers could only displace 40 mm. Larger rollers, capable of displacing at least 50 mm, should be used in future tests. Even though no behaviour change would be expected between 40 mm and 50 mm of displacement (Read et al. 2011, and Le Pen et al. 2014)

(9) Vertical and Horizontal loads and displacements were recorded every two seconds.

Throughout testing the space between the tie and the guide openings was inspected to ensure that no ballast became wedged between the tie and the ballast box sides increasing the tie-lateral resistance being measured.

(A) Un-assembled ballast box

(B) Assembled and lined ballast box

(C) Phase 1 general test configuration

(D) Phase 2 general test configuration

(E) Phase 1 general test configuration

(F) Phase 2 general test configuration

Figure 4.4: Photographs of the ballast box assembly, and Phase 1 base and Phase 2 crib test configurations

4.3.2 Phase 3 Shoulder Tests

The Phase 3 shoulder tests were completed to quantify the shoulder resistance that develops between the end of the tie and the shoulder ballast. For the Phase 3 shoulder tests, the ballast box was moved to the end of the tie, as shown in Figure 4.5. A 0.10 m embedment was provided to support the end of the tie during set-up. Two 0.45 m high support pedestals were assembled to support the tie. Each pedestal consisted of a load cell to measure the normal load transferred to each pedestal and a roller to allow the pedestals to displace across the floor as the tie penetrates into the shoulder ballast. The load cells were used to check for eccentric loading of the tie. The rollers were spaced 0.97 m center-to-center, and were aligned directly below the rollers attached to the dead load. Ballast was placed in the ballast box and hand tamped in three 0.15 m lifts (0.45 m total) with a 10 in steel tamper and rubber mallet to a bulk density of 15.5 kN/m^3 to 16.0 kN/m^3. The ballast was re-surfaced between tests back to a bulk density of 15.5 kN/m^3 to 16.0 kN/m^3 and levelled to provide even support. Once, the tie and dead load were in place, a fourth 0.19 m thick layer of ballast was added and tamped to form the crib and shoulder. Photographs of the Phase 3 test configuration are provided in Figure 4.5

Initially a 0.3 m wide shoulder, measured from the end of the tie to the beginning of the ballast side slope, was considered. AREMA 2014 recommended a shoulder width of not less than 0.3 m. With a 0.3 m wide shoulder the ballast was observed to accumulate in front of the tie, forming a ‘bulge’ that would ‘day-light’ in the side slope of the shoulder, as shown in Figure 4.5E. The bulge, or ‘failure wedge’, represents the volume of ballast being mobilized to resist the lateral displacement of the tie and unless it is fully contained within the slope (i.e., it does not day-light) the maximum shoulder resistance is not being mobilized. Therefore, additional tests were completed with a shoulder width of 0.6 m. No day-lighting of the failure wedge was observed in the 0.6 m wide shoulder, so it was assumed the maximum potential shoulder resistance had been captured and no additional testing was required. Le Pen et al. (2014) concluded that extending the shoulder beyond a limiting shoulder width of approximately 0.75 m, which coincides with the position at which the failure surface day-lights, will not further increase the tie-lateral resistance because the critical failure mechanism is not being affected. This is supported by their previous work (Le Pen 2008, and Le Pen and Powrie 2011) which showed an approximate increase of 130% when the shoulder width was increased from 0.2 m to either 0.3 m or 0.4 m, but only a marginal increase of approximately 15% when the shoulder width was increased from either 0.3 m or 0.4 m to 0.6 m. Samavedam et al. (1995) suggested the limiting shoulder width is generally less than 0.6 m. The side slope was constructed at a slope of 2H:1V slope as suggested in AREMA (2014).

The tests were completed following the same test preparations outlined for the Phase 1 base and Phase 2 crib tests in Section 4.3.1. Except after re-surfacing of the ballast in Step 1 the shoulder ballast needed to be re-graded to the correct width and side slope angle, and in Step 2 the tie was placed on two support pedestals and not the base ballast. Step 5 was also omitted.

(A) Phase 3 general test configuration

(B) A typical 0.6 m shoulder of McAbee Ballast prior to testing

(C) A typical 0.6 m shoulder of McAbee Ballast and failure wedge after testing

(D) A typical 0.3 m shoulder of Gravel Ballast prior to testing

(E) A typical 0.3 m shoulder of Gravel Ballast and failure wedge after testing

Figure 4.5: Photographs of the Phase 3 shoulder test configuration

4.4 Outline of Testing Program

The tie-lateral resistance testing program is outlined in Table 4.1. Proof of concept testing was completed in the McAbee Ballast in June 2015 and in the Gravel Ballast in August 2015 to confirm that the research objectives were achievable in the laboratory and that there was a quantifiable difference in the tie-lateral resistance provided by the two materials. After minor adjustments to the testing apparatus; e.g., replacement of the manual horizontal valve with an automated serval valve, the remainder of the tests were completed between January 2016 and June 2016.

Table 4.1: Outline of the tie-lateral resistance testing program

Ballast Type	Test Configuration	Data Group	Date Completed		Number of tests	Horizontal Valve Used	Loading rate (mm/sec)	Comment
			To	From				
McAbee	Phase 1 Base	1A	2015-06-23	2015-06-25	11	Manual	0.05	Proof of concept
		1B	2016-02-04	2016-02-11		Automated	0.05	
	Phase 2 Crib	2A	2016-01-29	2016-02-02	6	Automated	0.05	
		2B	2016-02-17	2016-02-22		Automated	0.05	
	Phase 3 Shoulder	3A	2016-06-10	2016-06-10	12	Automated	0.05	0.3 m shoulder
		3B	2016-06-09	2016-06-10		Automated	0.05	0.6 m shoulder
Gravel	Phase 1 Base	4A	2015-08-14	2015-08-20	11	Manual	0.05	Proof of concept
		4B	2016-03-11	2016-03-16		Automated	0.05	
		5	2015-08-25	2015-08-25	4	Manual	0.5	Proof of concept
	Phase 2 Crib	6A	2016-03-09	2016-03-11	6	Automated	0.05	
		6B	2016-03-17	2016-03-18		Automated	0.05	
	Phase 3 Shoulder	7A	2016-06-03	2016-06-07	12	Automated	0.05	0.3 m shoulder
		7B	2016-06-03	2016-06-07		Automated	0.05	0.6 m shoulder

The number of tie-lateral resistance tests completed in each material and for each test configuration is summarized in Tables 4.2 and 4.3. In total 72 tests were completed to produce this data set: 29 in the McAbee Ballast, 29 in the Gravel Ballast, and 14 sensitivity tests. Of the 29 tests in the McAbee Ballast and Gravel Ballast, there were 11 Phase 1 base tests, including 2 cyclic tests (see Section 5.4.5); 6 Phase 2 crib tests, including 2 cyclic tests; and 12 Phase 3 shoulder tests, including 6 tests with a 0.3 m wide shoulder and 6 tests with a 0.6 m wide shoulder. These tests were completed at a (slow) loading rate of 0.05 mm/sec. The 14 sensitive tests included 12 tests completed at a (fast) rate of 0.5 mm/sec as part of the loading rate sensitivity analysis (see Section 5.1) and 2 tests completed in the Gravel Ballast as part of the tie-shape sensitivity analysis (see Section 5.4.2). An additional 9 tests were excluded from the data set, 6 tests because of mechanical issues during testing and 3 because they were verification tests; i.e., tests that were conducted to troubleshoot issues with testing apparatus and methodology.

Table 4.2: Number of tie-lateral resistance tests completed in the McAbee Ballast

Data Group		Applied Normal Load (kN)									Additional Sensitivity Tests	Excluded Tests	Total
		Slow Loading Rate – 0.05 mm/sec								Fast Loading Rate – 0.5 mm/sec			
		Non-cyclic						Cyclic					
		5	10	20	40	80	160	80	160	160			
Phase 1 Base	1A	1	2	1	1	1	1	-	-	-	-	2	15
	1B	-	1	-	-	1	1	-	1	1	-	1	
Phase 2 Crib	2A	-	1	-	-	1	1	-	-	-	-	3	10
	2B	-	1	-	-	-	1	1	-	1	-	-	
Phase 3 Shoulder	3A	-	2	-	-	2	2	-	-	1	-	-	14
	3B	-	2	-	-	2	2	-	-	1	-	-	

Table 4.3: Number of tie-lateral resistance tests completed in the Gravel Ballast

Data Group		Applied Normal Load (kN)												Additional Sensitivity Tests	Excluded Tests	Total
		Slow Loading Rate – 0.05 mm/sec								Fast Loading Rate – 0.5 mm/sec						
		Non-cyclic						Cyclic								
		5	10	20	40	80	160	80	160	10	20	80	160			
Phase 1 Base	4A	1	2	1	1	1	1	-	-	-	-	-	-	2	1	15
	4B	-	1	-	-	1	1	-	1	-	-	-	1	-	-	
	5	-	-	-	-	-	-	-	-	1	1	1	1	-	1	5
Phase 2 Crib	6A	-	1	-	-	1	1	-	-	-	-	-	-	-	-	8
	6B	-	1	-	-	-	1	1	-	-	-	-	1	-	1	
Phase 3 Shoulder	7A	-	2	-	-	2	2	-	-	-	-	-	1	-	-	14
	8B	-	2	-	-	2	2	-	-	-	-	-	1	-	-	

CHAPTER 5.0 TIE-LATERAL RESISTANCE TESTS – RESULTS

5.1 Data Processing

Vertical and horizontal loads and displacements were recorded every two seconds during the tie-lateral resistance tests. The normal load was recorded by a load cell attached to the vertical ram and the lateral load by a load cell attached to the horizontal ram. During the Phase 3 shoulder tests, the normal load was also recorded by two loads cells in the support pedestals. The vertical displacement was measured by a LVDT attached to the vertical ram, and the horizontal displacement by a LVDT attached between the tie and ballast box.

For the Phase 1 base and Phase 2 crib tests only a portion of the tie was embedded in the ballast. Thus, to obtain the total lateral resistance per tie the lateral load was multiplied by an embedment ratio, $R_{\text{Embedment}}$ given by equation:

$$\boldsymbol{R}_{\text{Embedment}} = \left(\frac{\boldsymbol{Total\ Tie\ Length}}{\boldsymbol{Embedded\ Tie\ Length}}\right) = \left(\frac{\mathbf{2.59}}{\mathbf{1.52}}\right) = \mathbf{1.70} \qquad \text{Equation 5.1}$$

De Iorio et al. (2016) used a similar ratio when comparing their work to Le Pen and Powrie (2011).

The following outlines how the load and displacement data was processed for each test:

(1) Lateral load and vertical displacement were plotted against horizontal displacement to form a ‘load-horizontal displacement’ and ‘vertical displacement-horizontal displacement’ curve, respectively. Typical curves for a Phase 1 base test completed under a normal load of 160 kN is presented in Figure 5.1. Similar plots are included in Appendix III for each tie-lateral resistance test; however, vertical displacement curves were not plotted for the Phase 3 shoulder tests.

(2) Loads and displacements were recorded for several minutes before and after each test, resulting in pre-test and post-test noise being recorded. This pre-test and post-test noise was removed from each plot.

(3) The curves were shifted, so the first data point, after the pre-test noise was removed, corresponded to zero lateral load and horizontal/vertical displacement.

The lateral load at varying horizontal displacement and the peak-lateral load were determined for each test, as shown in Figure 5.1. Generally, the load-horizontal displacement curve reached a ‘limiting value’ after 20 mm of horizontal displacement, but due to trivial data fluctuations the actual peak-lateral load typically occurred after 20 mm of horizontal displacement (the significance of these fluctuations will be discussed in Section 5.3). It was determined that the lateral load corresponding to the limiting value was a better indication of peak-lateral load then the actual peak-lateral load. The results presented and discussed in this chapter and the succeeding chapters are based on the limiting peak-lateral loads. As discussed in Section 2.2.1, the tie-lateral resistance is being reported as a load and not a stress because of uncertainties in determining the bearing area of the tie in each tie-lateral resistance test.

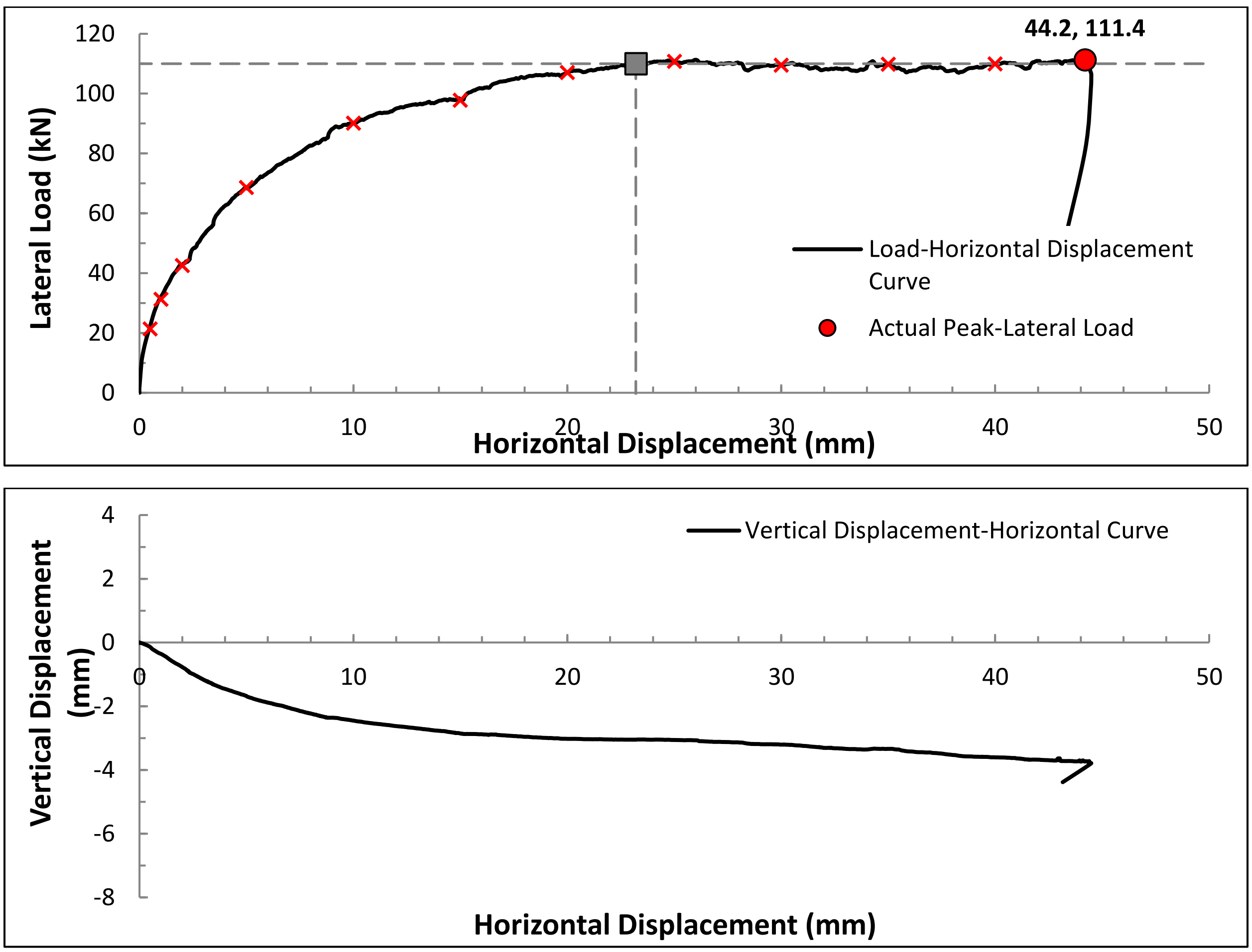

Figure 5.1: Typical Phase 1 base test load-horizontal displacement and vertical displacement-horizontal displacement curve (the test was completed under a normal load of 160 kN in the McAbee Ballast)

5.2 The Tie-lateral Resistance Test Results

Typical load-horizontal displacement and vertical displacement-horizontal displacement curves are presented in Figure 5.2 through 5.4 for the Phase 1 base and Phase 2 crib tests. The tests were completed under normal loads of 10 kN, 80 kN, and 160 kN, respectively, at a loading rate of 0.05 mm/sec. Similar, plots are presented in Figure 5.5 for the Phase 3 shoulder tests. In these plots, the lateral load is initially observed to rapidly increase with horizontal displacement and the rate reducing as the load approaches a limiting value (i.e., the peak-lateral load) at higher horizontal displacements. Overall, the McAbee ballast and Gravel ballast exhibit weak ballast behavior, indicating they were in a freshly-tamped or lightly-consolidated state for each test.

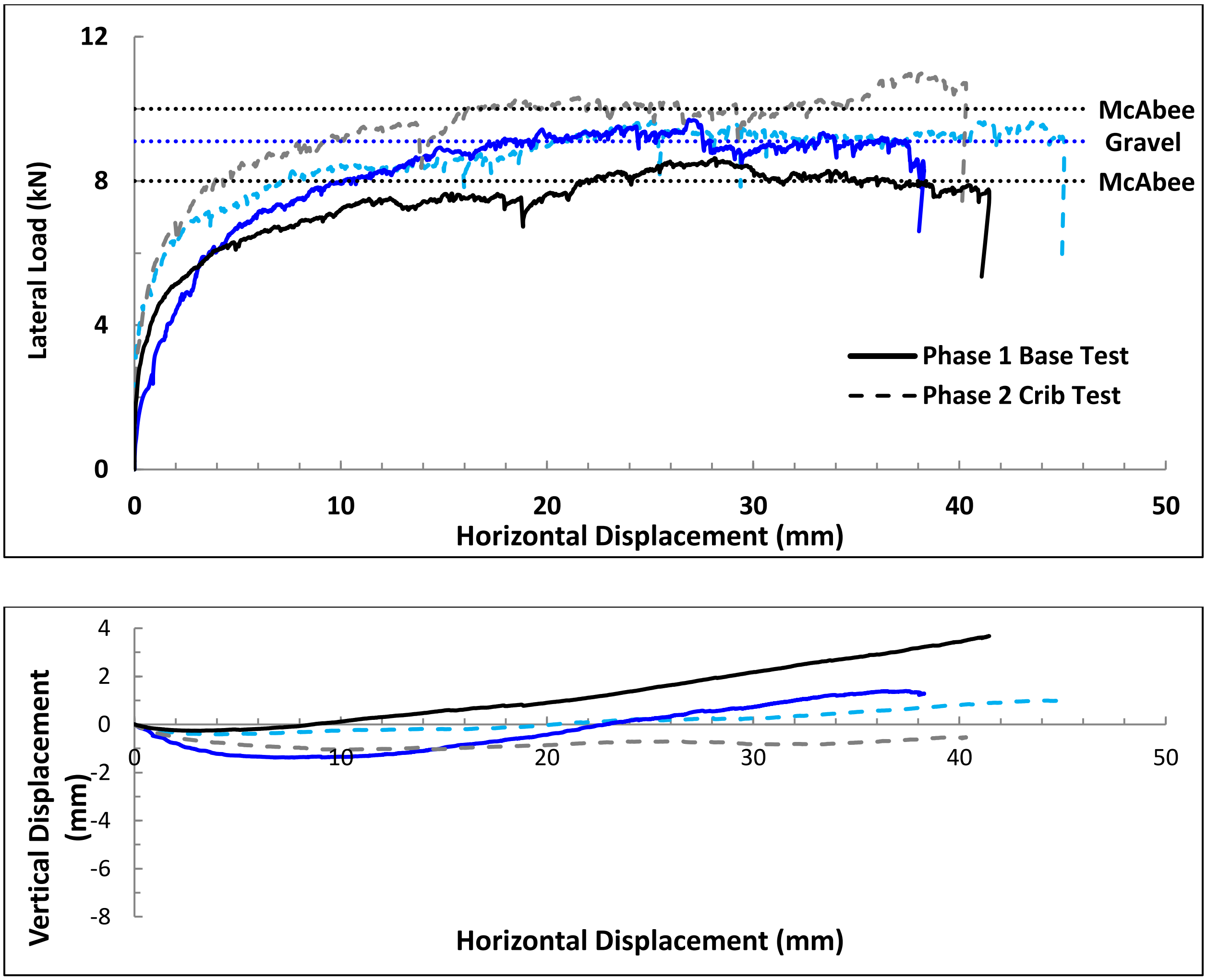

Figure 5.2: Typical load-horizontal displacement and vertical displacement-horizontal displacement curves for the Phase 1 base and Phase 2 crib tests (tests completed under a normal load of 10 kN and a loading rate of 0.05 mm/sec)

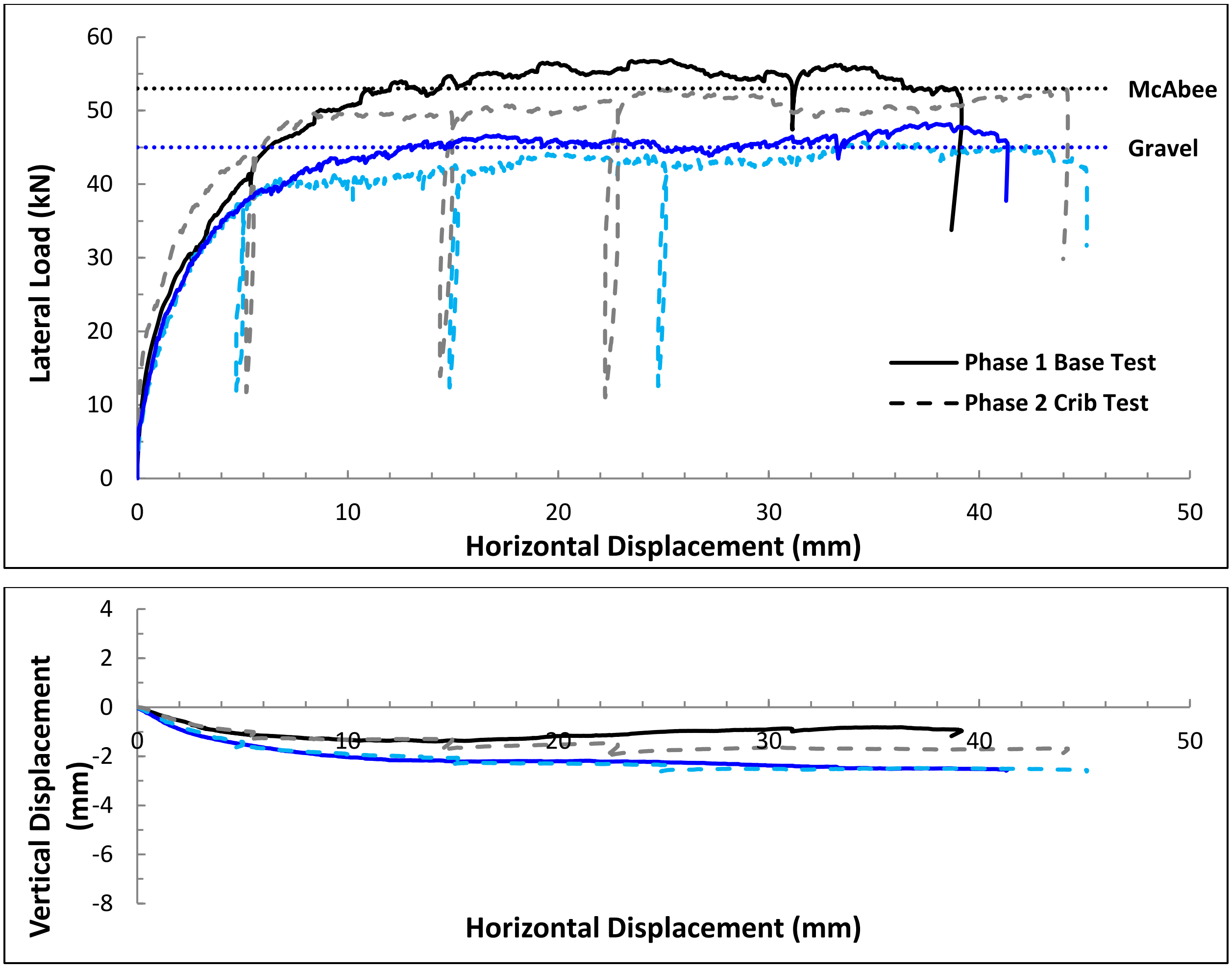

Figure 5.3: Typical load-horizontal displacement and vertical displacement-horizontal displacement curves for the Phase 1 base and Phase 2 crib tests (tests completed under a normal load of 80 kN and a loading rate of 0.05 mm/sec)

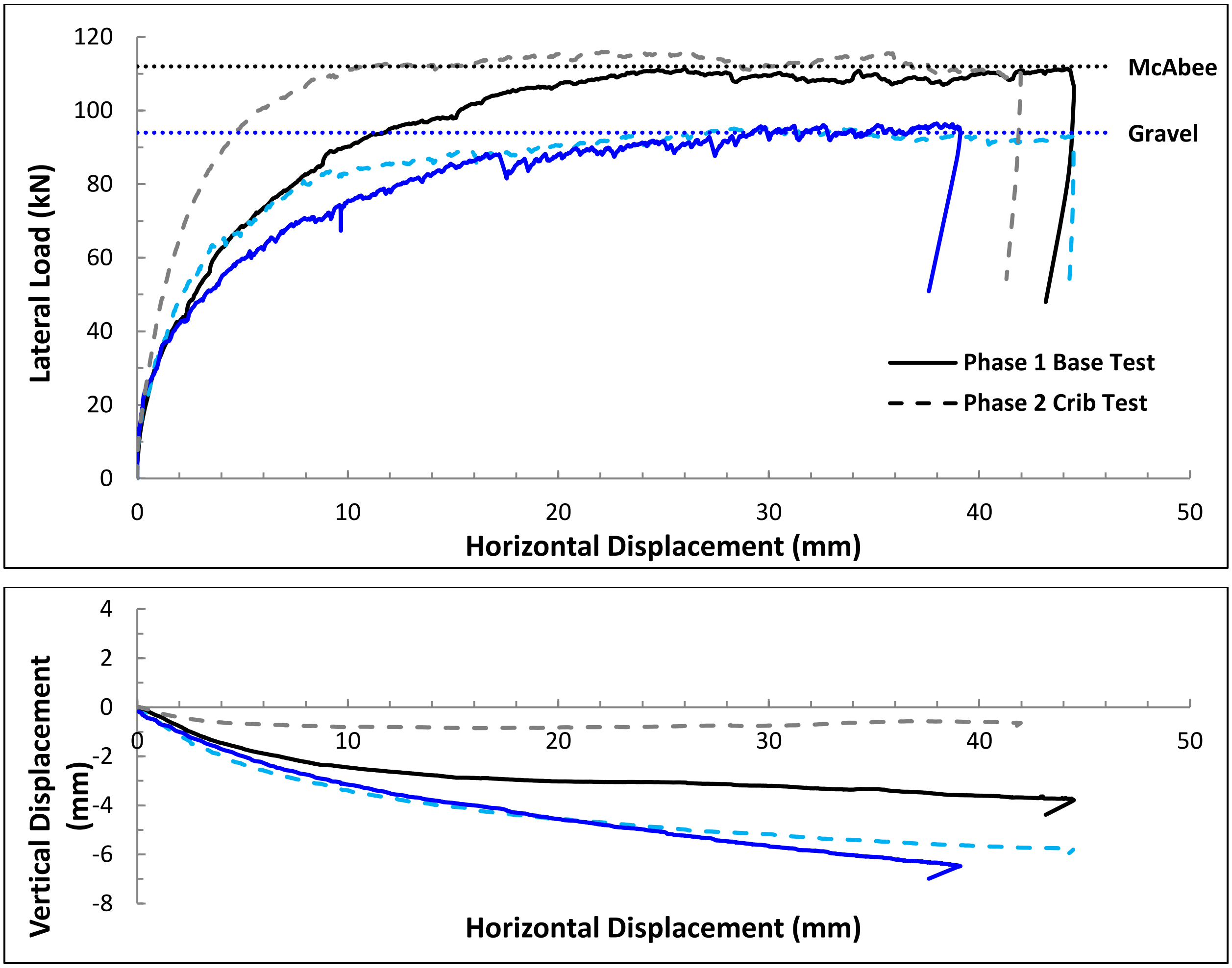

Figure 5.4: Typical load-horizontal displacement and vertical displacement-horizontal displacement curves for the Phase 1 base and Phase 2 crib tests (tests completed under a normal load of 160 kN and a loading rate of 0.05 mm/sec)

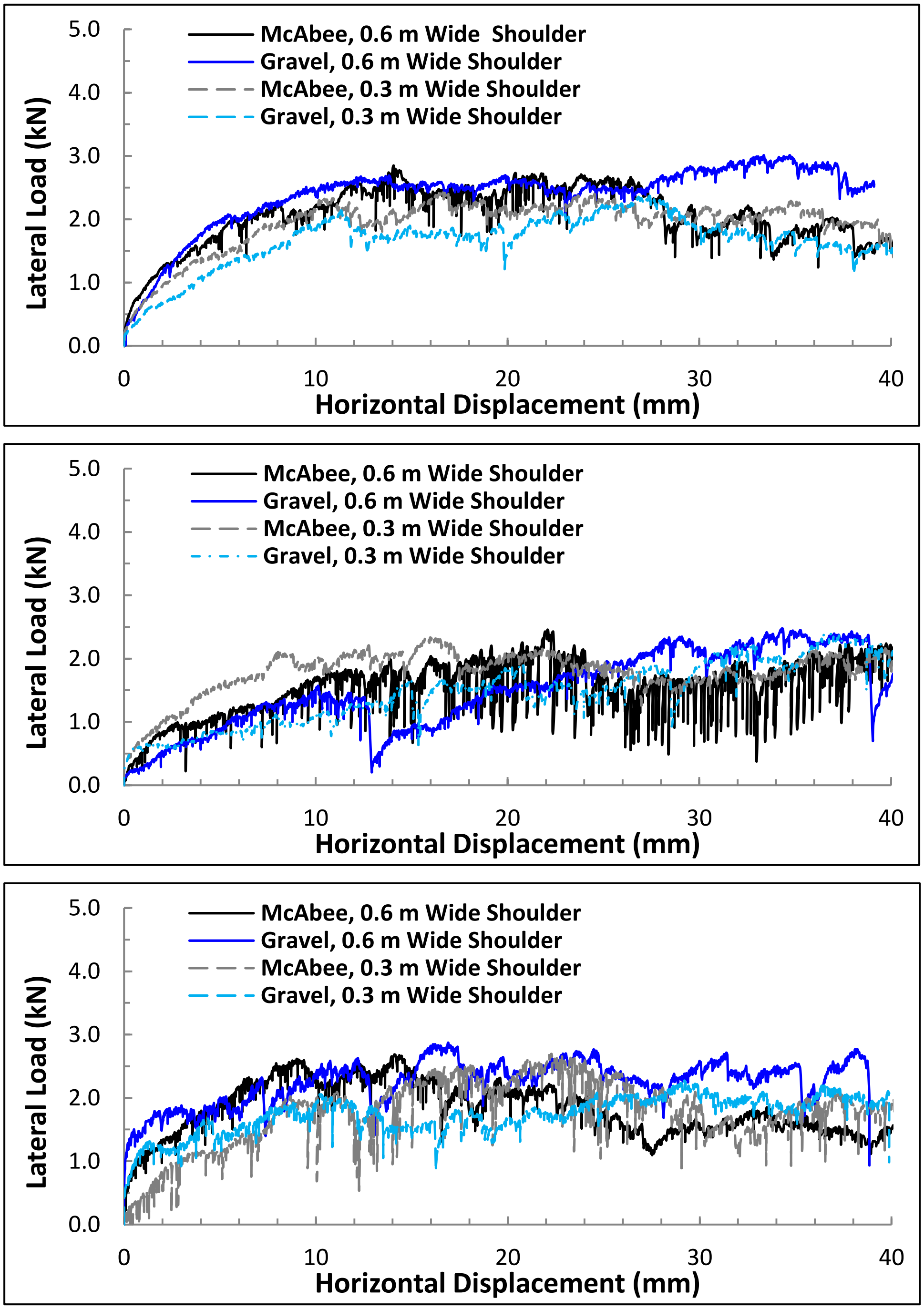

(A)

Completed under a normal load of 10 kN and a loading rate of 0.05 mm/sec

(B)

Completed under a normal load of 80 kN and a loading rate of 0.05 mm/sec

(C)

Completed under a normal load of 160 kN and a loading rate of 0.05 mm/sec

Figure 5.5: Typical load-horizontal displacement curves for the Phase 3 shoulder tests

At horizontal displacements greater than 3 mm, the lateral load is observed to fluctuate, and to randomly drop, followed by a rapid return towards the previous load value. These fluctuations are concurrent with, and thus attributed to, visual and audible observations of ballast breakage and re-arrangement (e.g., fracturing, crushing, rolling, or sliding). Le Pen (2008) and Le Pen and Powrie (2008) made a similar observation. Occasionally, these events were large enough that the load would drop 10 kN to 20 kN while the tie rebounded upwards of 2 mm. These fluctuations are evident in the typical Phase 1 base tests results presented in Figure 5.6.

At horizontal displacements less than 3 mm, the lateral load is observed to rapidly, but consistently increase with displacement and without evidence of ballast breakage or re-arrangement. These results indicate, similarly to Le Pen (2008) and Le Pen and Powrie (2008), that there has been minimal slippage at the tie-ballast interface and most of the movement is still recoverable (i.e., the material is behaving elastically). This hypothesis is also supported by the unload-reload test results (see Section 5.3.5), which show a recoverable (elastic) and non-recoverable (plastic) region in the load-horizontal displacement curves; and in the elastic rebound observed at the end of each Phase 1 base and Phase 2 crib test when the lateral load is removed.

Le Pen (2008) and Le Pen and Powrie (2008) refer to this 'recoverable' zone as the 'pre-failure zone', and suggest that failure begins at the first evidence of ballast breakage and re-arrangement; i.e., a displacement beyond which all further displacement is non-recoverable. The pre-failure zone is shown on Figure 5.6 for typical Phase 1 base tests completed under normal loads of 10 kN, 80 kN, and 160 kN and a loading rate of 0.05 mm/sec. The first evidence of ballast breakage and re-arrangement for these tests are marked in Figure 5.7, and these results normalized to applied normal load are presented in Figure 5.8. From these figures, it can be seen that the pre-failure zone increases with normal load, similarly to the results obtains by Le Pen (2008) and Le Pen and Powrie (2008) (see Figure 2.16C).

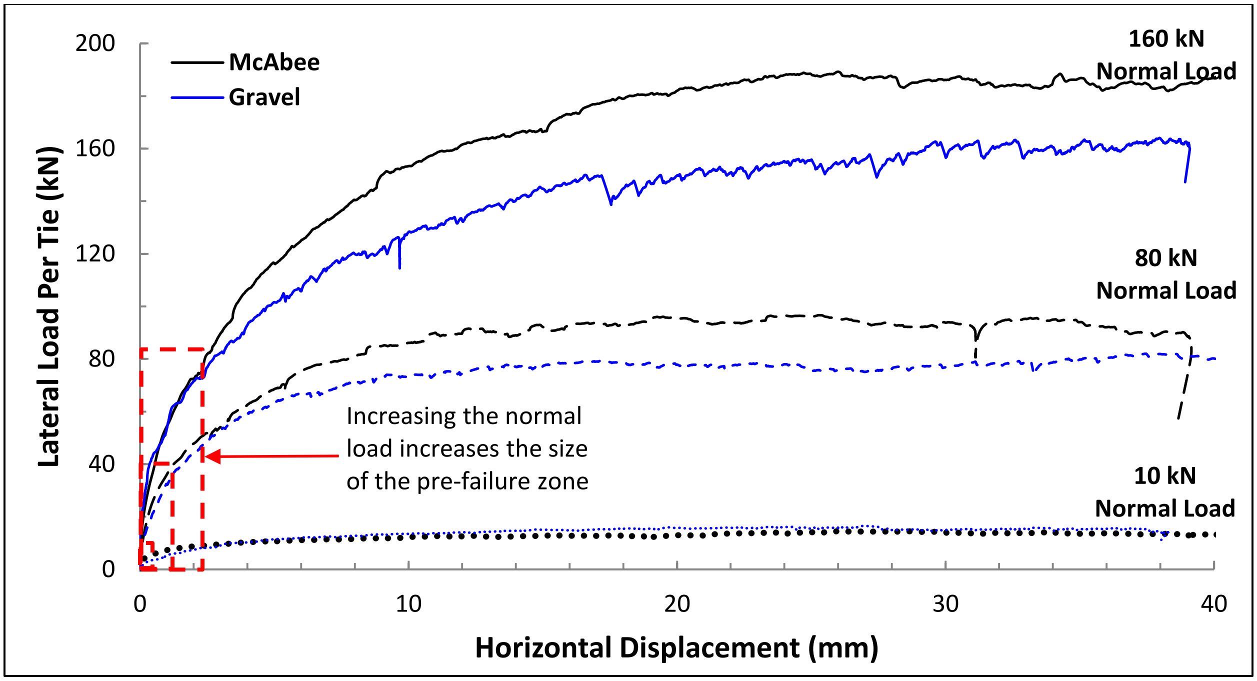

Figure 5.6: Comparison of the pre-failure zone for Phase 1 base tests completed under normal loads of 10 kN, 80 kN, and 160 kN and a loading rate of 0.05 mm/sec

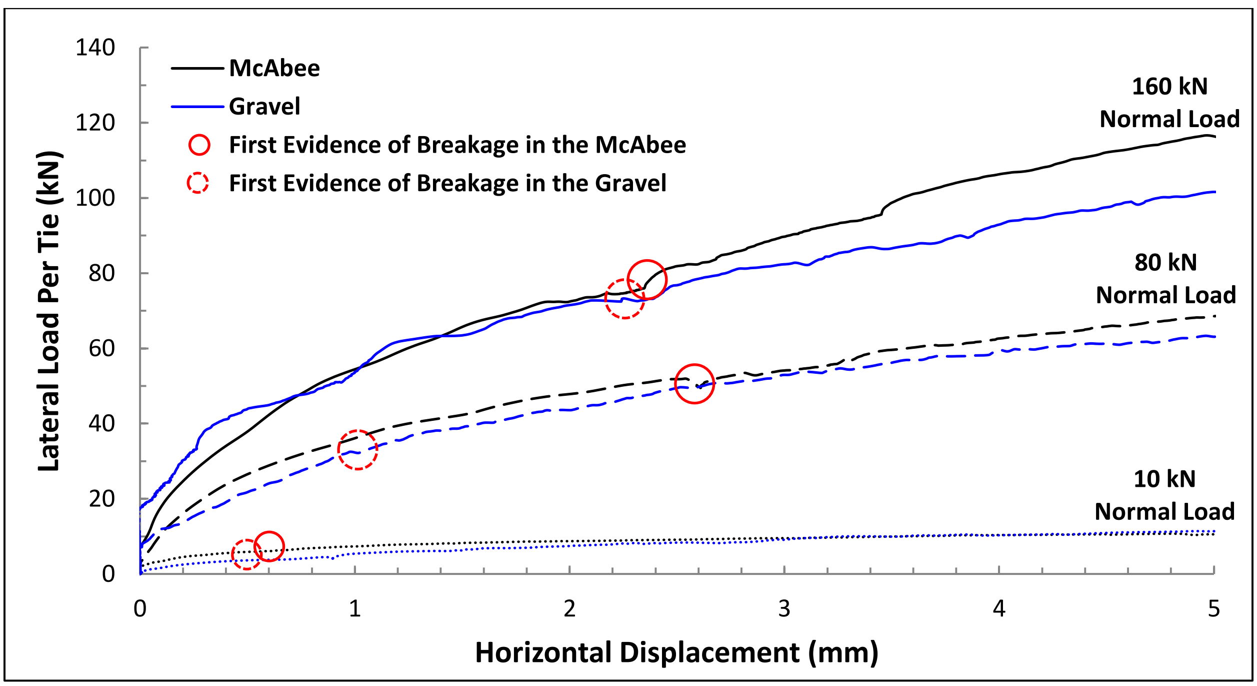

Figure 5.7: Typical Phase 1 base load-horizontal displacement curves showing the first evidence of ballast breakage in the McAbee Ballast and Gravel Ballast (data only plotted up to 5 mm of horizontal displacement)

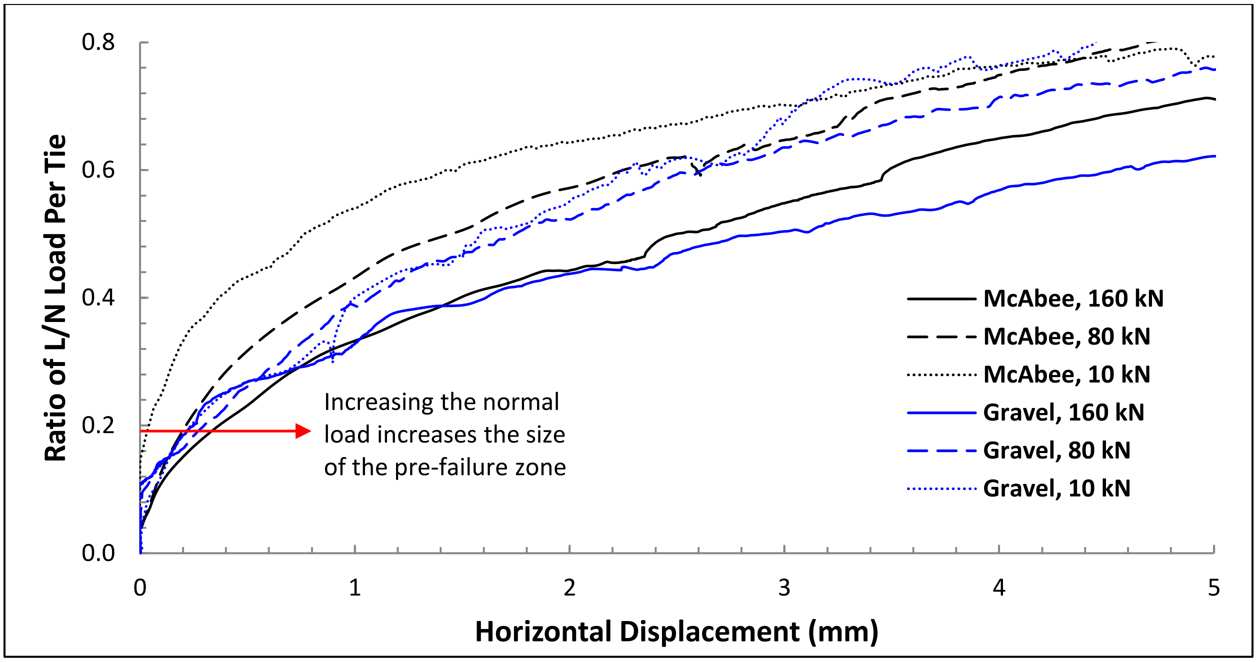

Figure 5.8: Typical Phase 1 base load-horizontal displacement curves normalized to normal load showing the pre-failure zone increasing with displacement (data only plotted up to 5 mm of horizontal displacement)

During the Phase 1 base and Phase 2 crib tests, the ballast was observed to contract under normal loads greater than 80 kN (see Figure 5.3 and Figure 5.4) and to contract then dilate under normal loads less than 40 kN (see Figures 5.2). Dilation was typically observed to occur between 2 mm and 5 mm of horizontal displacement and the initiation of failure at the tie-ballast interface, as shown in Figure 5.2. These results confirm the approximate range of the pre-failure zone shown in Figure 5.2 and discussed in the previous paragraph.

The lateral load per tie versus normal load at varying horizontal displacements is plotted in Figure 5.9 to show how the lateral load develops with horizontal displacement for each material and test configuration. The results were plotted assuming a Mohr-Coulomb failure criterion; i.e., a linear function without cohesion. In these figures, it is shown that the limiting peak-lateral load typically occurs at approximately 20 mm of horizontal. These results are consistent with the findings presented in Sussmann et al. (2003), Le Pen (2008), and Le Pen and Powrie (2008). The relative uneven spacing between the trend-lines for the McAbee Ballast, compared to the even spacing for the Gravel Ballast, indicates that tie-lateral resistance in the McAbee Ballast develops less consistently with horizontal displacement than the Gravel Ballast. This is likely due to the size, shape, and roughness of the McAbee Ballast particles; i.e., the McAbee Ballast is generally finer, rough, and more angular than the Gravel ballast so there are more ballast particles within the failure zone around the tie, and more granular interlock and internal friction preventing slippage from occurring (Indraratna et al. 2011, and Selig and Waters 1994). This hypothesis is supported by visual observations of the McAbee Ballast interlocking quickly during tamping, and being less susceptible to disturbance than the Gravel Ballast during tamping and testing.

For the Phase 1 base test results, the lateral load linearly increases with normal load for the range of applied normal loads, as shown in Figure 5.9. This indicates the base friction component of tie-lateral resistance is dependent on the normal load and that the system is frictional with no significant dilation. For the Phase 3 shoulder test results, the lateral load is constant with lateral loading, as shown in Figure 5.9. This indicates the shoulder resistance component of tie-lateral resistance is independent of the normal load. It is not apparent from the Phase 2 crib test results presented in Figure 5.9, if the crib friction component is dependent on the normal load or not because the contribution from the crib friction is masked by the contribution from the base friction. However, the crib friction is not expected to be dependent on the normal load because the normal load does not provide any confinement to the crib ballast. Le Pen (2008) and Le Pen and Powrie (2011) also reported that the base friction is dependent on the normal load, and the crib friction and shoulder resistance are independent of the normal load.

The relationship between peak-lateral load and normal load, or the ‘failure envelope’, for each material, test configuration, and data group is presented in Figure 5.10. The failure envelopes for the first data group in each material and test configuration are plotted with ‘black circles’ and the second data group with ‘grey squares’. The overall failure envelope for each material and test configuration is plotted as a ‘red dotted line’. Tests completed at a fast rate of 0.5 mm/sec, as part of the loading rate sensitivity analysis (see Section 5.4.1), are plotted with ‘green triangles’. The fast rates test results are plotted for comparison only, and are excluded from the overall failure envelopes for each material and test configuration. Since, the fast and slow rates tests have similar peak-lateral loads it was concluded that loading rate does not impact the tie-lateral resistance for the applied range of normal load.

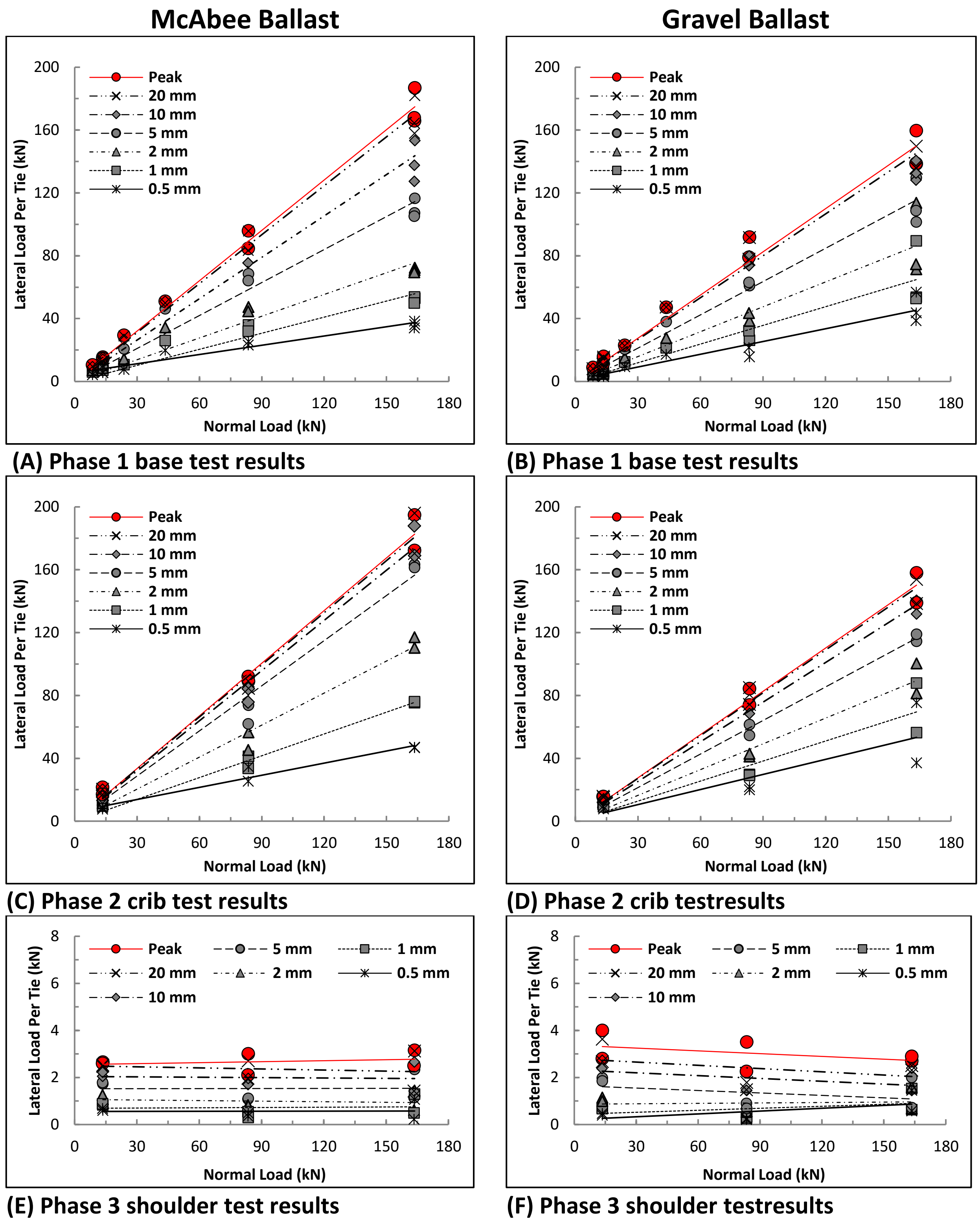

Figure 5.9: Development of peak-lateral load with horizontal displacement for each material and test configuration

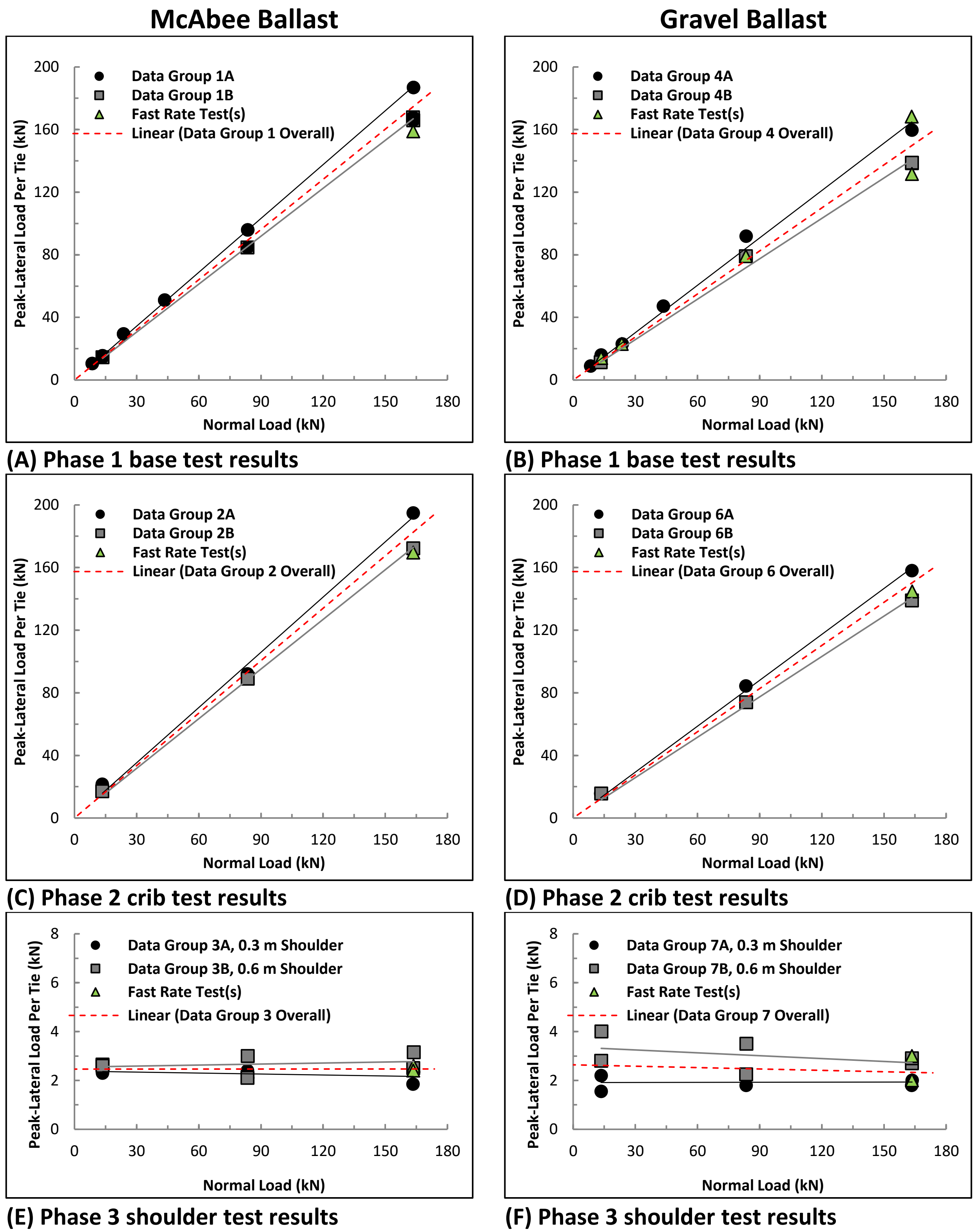

Figure 5.10: Peak-lateral load failure envelopes for each material and test configuration

The overall failure envelopes from the Phase 1 base, Phase 2 crib, and Phase 3 shoulder tests are presented in Figure 5.11 and Figure 5.12. From these figures, it is evident that the contribution from the crib friction and shoulder resistance to overall tie-lateral resistance is small compared to the contribution from the base friction, and that the contribution from a 0.6 m wide shoulder is greater than for a 0.3 m wide shoulder.

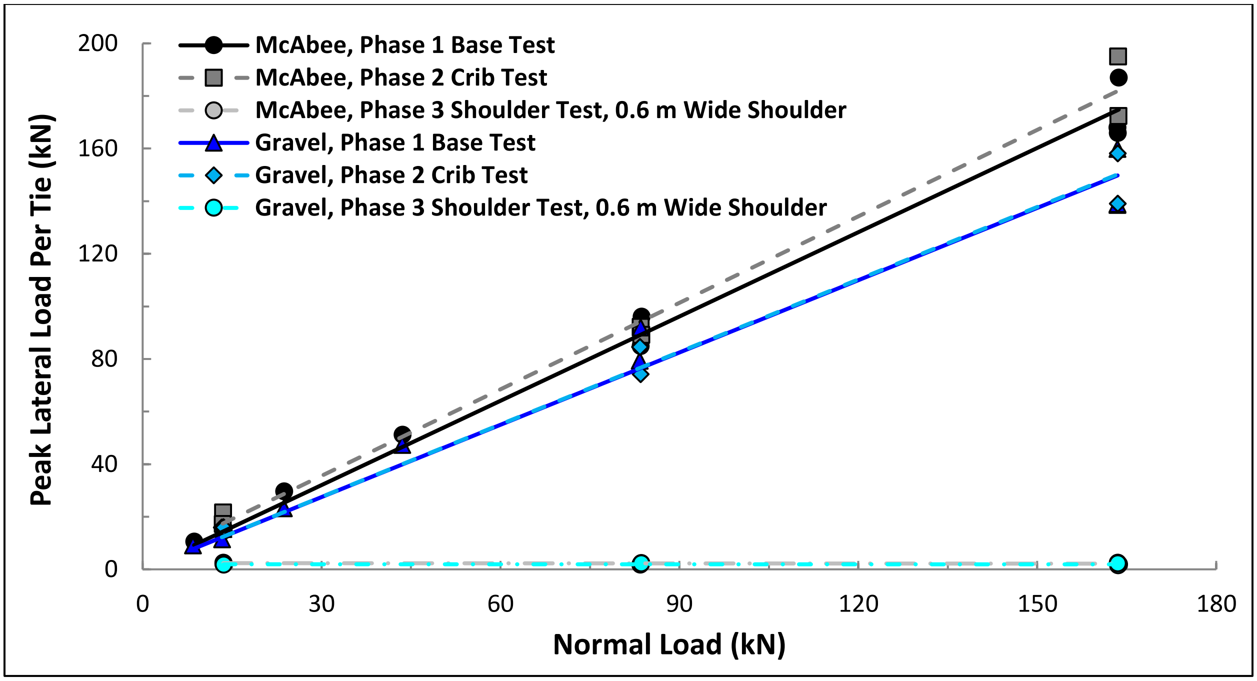

Figure 5.11: Comparison of the peak-lateral load failure envelopes for the Phase 1 base, Phase 2 crib, and Phase 3 shoulder tests

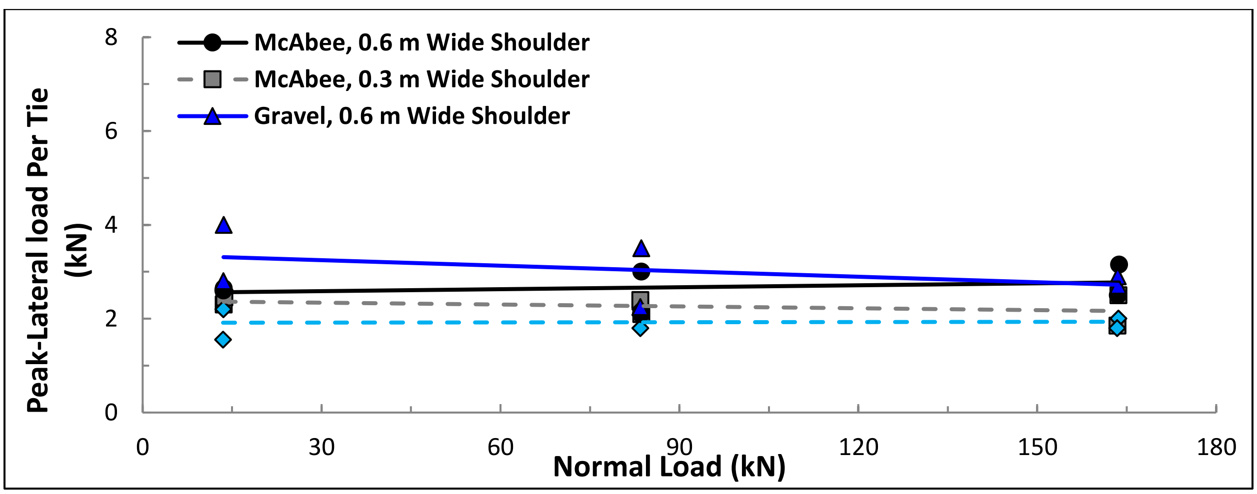

Figure 5.12: Comparison of the peak-lateral load failure envelopes for the Phase 3 shoulder tests

It is also noted in Figures 5.2 through 5.4, that the lateral load increasesmore rapidly with horizontal displacement in the pre-failure zone when the crib ballast is present. So, although the contribution from the crib friction is minimal, compared to the contribution from the base friction, it appears to be making the system stiffer. This is likely because the crib ballast provides additional confinement to the base ballast (Samavedam et al. 1995).

The average results of the Phase 1 base, Phase 2 crib, and Phase 3 shoulder tie-lateral resistance tests are tabulated in Tables 5.1 through 5.6, including the average total normal load (i.e., the average applied normal load plus the setting load of 3.6 kN), the average lateral load per tie at varying horizontal displacements, and the minimum, maximum and average limiting peak lateral load per tie and corresponding horizontal displacement for each material and testing configuration. These values are also tabulated for each individual test in Appendix III. The magnitude and importance of these values will be discussed in Chapter 6.

Overall the tie-lateral resistance test results show a significant amount of scatter. The standard deviation for the Phase 1 base and Phase 2 crib tests ranges between 3% and 14% of the average peak-lateral load, and for the Phase 3 shoulder test between 10% and 19% of the average peak-lateral load. Samavedam et al. (1999) and Sussmann et al. (2003) reported a similar standard deviation ranging from approximately 8% to 15%, and 7% to 10% of the peak-lateral resistance, respectively.

Table 5.1: Summary of Phase 1 base test results in the McAbee Ballast

Loading Rate (mm/sec)	Average Total Normal Load (kN)	Average Lateral Load Per Tie (kN)						Average Limiting Peak Values			
		Horizontal Displacement						Lateral Load Per Tie (kN)			Horizontal Displacement (mm)
		0.5 mm	1 mm	2 mm	5 mm	10 mm	20 mm	Min.	Max.	Ave.	
0.05	8.6	4.4	6.1	7.3	8.8	9.5	9.7	-	-	10.5	34.6
	13.6	7.1	9.0	10.8	12.6	13.9	13.5	14.6	15.6	15.0	17.4
	23.7	7.7	10.8	14.4	20.9	26.8	29.0	-	-	29.6	25.3
	43.6	20.0	26.1	34.5	46.3	51.2	50.1	-	-	51.2	9.9
	83.6	24.5	34.1	46.1	66.4	80.7	89.7	84.8	96.1	90.4	21.4
	163.5	36.3	52.3	71.0	109.8	139.4	168.1	165.9	187.0	173.6	25.4
0.5	163.5	36.5	52.0	74.3	114.6	139.9	158.1	-	-	159.0	19.5
								Average			21.7

Table 5.2: Summary of Phase 2 crib test results in the McAbee Ballast

Loading Rate (mm/sec)	Average Total Normal Load (kN)	Average Lateral Load Per Tie (kN)						Limiting Peak Value			
		Horizontal Displacement						Lateral Load Per Tie (kN)			Horizontal Displacement (mm)
		0.5 mm	1 mm	2 mm	5 mm	10 mm	20 mm	Min.	Max.	Ave.	
0.05	13.4	8.2	10.3	12.7	15.6	17.6	18.8	17.2	21.6	19.4	19.4
	83.5	30.0	37.5	50.9	67.9	80.0	86.9	89.1	92.1	90.6	22.6
	163.6	47.0	75.8	113.8	162.5	178.4	183.3	172.4	195.0	183.7	20.4
0.5	163.5	40.8	54.7	76.6	116.7	149.5	169.0	-	-	169.7	21.5
								Average			20.9

Table 5.3: Summary of Phase 3 shoulder test results in the McAbee Ballast

Loading Rate (mm/sec)	Average Total Normal Load (kN)	Limiting Peak Value							
		0.3 m Wide Shoulder				0.6 m Wide Shoulder			
		Lateral Load Per Tie (kN)			Horizontal Displacement (mm)	Lateral Load Per Tie (kN)			Horizontal Displacement (mm)
		Min.	Max.	Ave.		Min.	Max.	Ave.	
0.05	13.6	-	-	2.38	15.2	-	-	2.63	17.5
	83.5	-	-	2.25	13.4	-	-	2.55	19.4
	163.5	-	-	2.18	8.3	-	-	2.83	17.8
	Average	1.85	2.50	2.27	12.3	2.10	3.15	2.67	18.2
0.5	163.6	-	-	2.60	21.6	-	-	2.40	18.5
		Average			13.6	Average			18.3

Table 5.4: Summary of Phase 1 base test results in the Gravel Ballast

Loading Rate (mm/sec)	Average Total Normal Load (kN)	Average Lateral Load Per Tie (kN)						Limiting Peak Value			
		Horizontal Displacement						Lateral Load Per Tie (kN)			Horizontal Displacement (mm)
		0.5 mm	1 mm	2 mm	5 mm	10 mm	20 mm	Min.	Max.	Ave.	
0.05	8.4	3.4	4.4	5.1	6.7	8.4	8.3	-	-	9.0	5.3
	13.4	4.6	6.3	8.0	10.7	12.4	13.7	11.4	16.0	14.2	8.4
	23.7	9.5	12.5	15.2	20.8	22.7	22.7	-	-	23.1	13.6
	43.5	17.4	21.5	27.8	38.1	46.8	47.5	-	-	47.3	27.8
	83.4	18.7	29.4	41.1	62.1	76.7	84.7	79.2	92.0	85.6	50.4
	163.5	46.5	65.4	86.6	113.4	133.7	140.5	138.6	159.8	145.7	85.7
0.5	13.6	4.5	5.8	8.4	10.4	12.1	13.2	-	-	14.1	8.3
	23.5	9.5	12.5	15.2	20.8	22.7	22.7	-	-	23.1	13.6
	83.4	17.9	24.8	37.6	56.5	71.1	79.0	-	-	79.2	46.6
	163.4	34.6	50.9	68.7	102.9	130.5	152.4	131.8	168.3	150.0	88.3
								Average			17.8

Table 5.5: Summary of Phase 2 crib test results in the Gravel Ballast

Loading Rate (mm/sec)	Average Total Normal Load (kN)	Average Lateral Load Per Tie (kN)						Limiting Peak Value			
		Horizontal Displacement						Lateral Load Per Tie (kN)			Horizontal Displacement (mm)
		0.5 mm	1 mm	2 mm	5 mm	10 mm	20 mm	Min.	Max.	Ave.	
0.05	13.4	8.7	10.1	11.5	13.1	14.0	15.6	15.8	15.8	15.8	18.8
	83.4	21.1	29.5	42.1	58.1	72.8	79.7	74.1	84.5	79.3	26.7
	163.5	56.4	72.2	90.9	116.9	136.2	146.3	139.1	158.1	148.6	19.3
0.5	163.7	32.6	51.3	74.2	113.1	139.6	145.1	-	-	144.8	19.9
								Average			21.3

Table 5.6: Summary of Phase 3 shoulder test results in the Gravel Ballast

Loading Rate (mm/sec)	Average Total Normal Load (kN)	Limiting Peak Value							
		0.3 m Wide Shoulder				0.6 m Wide Shoulder			
		Lateral Load Per Tie (kN)			Horizontal Displacement (mm)	Lateral Load Per Tie (kN)			Horizontal Displacement (mm)
		Min.	Max.	Ave.		Min.	Max.	Ave.	
0.05	13.5	-	-	1.88	17.0	-	-	3.40	25.9
	83.4	-	-	2.00	35.9	-	-	2.88	36.1
	163.5	-	-	1.90	25.7	-	-	2.80	19.1
	Average	1.55	2.20	1.93	26.2	2.25	4.00	3.03	27.0
0.5	163.5	-	-	2.00	14.0	-	-	3.00	28.1
		Average			24.4	Average			27.1

During the Phase 2 crib tests, the tie-lateral resistance provided by both the base friction and crib friction is measured. Thus, the contribution from the base friction must be subtracted from the Phase 2 crib test results to isolate the contribution from the crib friction. Similarly, to Le Pen (2008) and Le Pen and Powrie (2011), this was accomplished by estimating the mean ratio of peak-lateral to normal load for the Phase 1 base tests under a normal load of 10 kN, 80 kN, and a 160 kN and subtracting the results from the mean ratio of peak-lateral to normal load obtained for the Phase 2 crib tests at the same normal load. This calculation is shown in Figure 5.13 and Table 5.7, with the difference being the contribution from the crib friction. The remainder is then multiplied by a normal load of 10 kN, 80 kN, and 160 kN to estimate the crib friction at those normal loads (see Chapter 6).

Table 5.7: Estimation of the crib friction component of tie-lateral resistance from the Phase 1 base and Phase 2 crib test results

Normal Load (kN)	Average Ratio of Peak-lateral to Normal Load Per Tie					
	McAbee Ballast			Gravel Ballast		
	Base Component (Phase 1)	Base + Crib Components (Phase 2)	Calculated Crib Component	Base Component (Phase 1)	Base + Crib Components (Phase 2)	Calculated Crib Component
10	1.17	1.46	0.29	1.07	1.21	0.14
80	1.09	1.16	0.07	0.96	0.97	0.00
160	1.07	1.08	0.01	0.93	0.90	-0.03

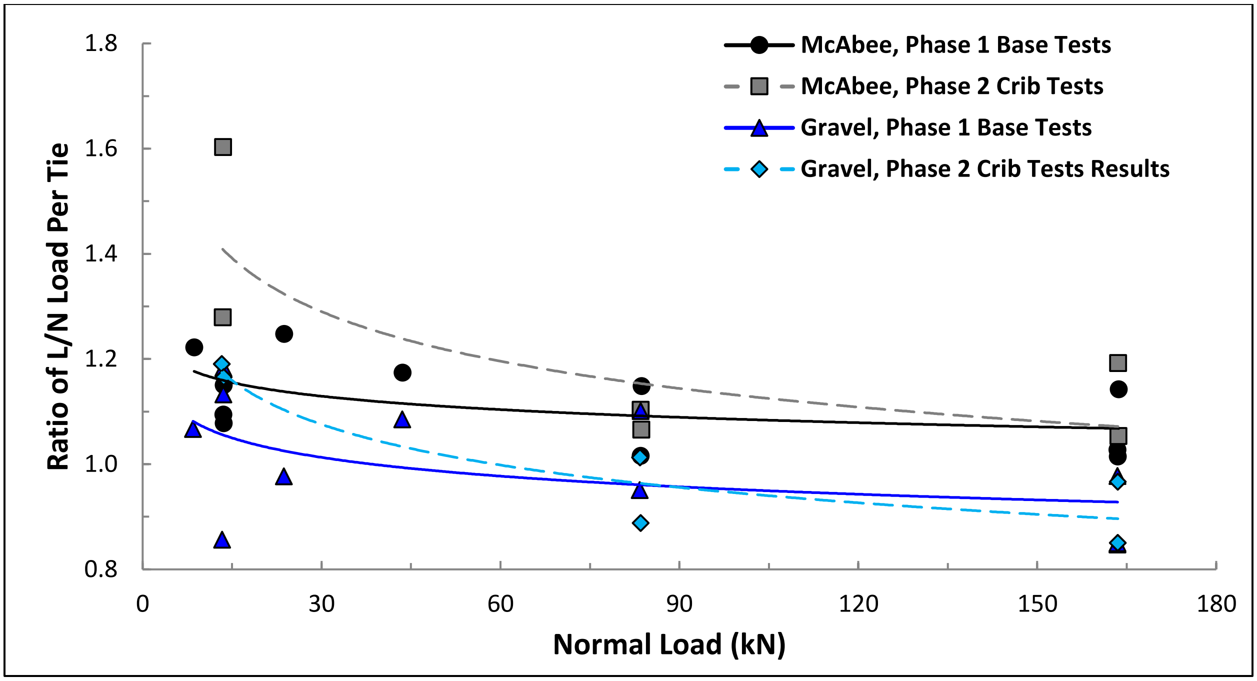

Figure 5.13: Normalized peak lateral load failure envelopes for the Phase 1 base and Phase 2 crib tests

During the Phase 3 tests, the tie is pushed laterally up to 0.05 m into the ballast generating some base friction and crib friction. Assuming the tie is embedded a maximum of 0.15 m into the ballast (the initial embedment of 0.1 m plus the displaced distance of 0.05 m) the tie applies a normal load of approximately 0.6 kN (assumes the tie weighs a 100 kg, which is greater than the weight of the ties used). Since, the sum of normal loads in the support pedestals was equal to the total applied normal load from the vertical ram and dead load, it was assumed no normal load was being transferred from the vertical ram to the base ballast. Using the ratios of peak-lateral to normal load in Figure 5.13 and Table 5.7, and a normal load of 0.6 kN it was estimated that the base friction and crib friction contribute less than 0.008 kN, which is less than 0.3%, of the peak-lateral load measured during the Phase 3 shoulder tests. Therefore, it was assumed the Phase 3 shoulder test results are indicative of the tie-lateral resistance provided by the shoulder ballast only and that the contribution from the base and crib ballast are negligible during the Phase 3 shoulder tests.

In Table 5.7, a negative crib friction is shown for the Gravel Ballast under a normal load of 160 kN, but this is likely a result of the calculation method; i.e., the standard deviation in the Phase 1 base test results ranged from 10 kN to 15 kN under a normal load of 160 kN, so if the crib friction is less than 10 kN, which it is, the base friction component is likely masking the crib friction component in the Phase 2 crib test results. De Iorio et al. (2016) found that the percent contribution of each component of tie-lateral resistance to overall lateral resistance varied depending on the tests used to calculate the contribution, as shown in Table 2.4. Thus, it is suggested that further testing be completed with full ballast, and with full shoulder ballast and no crib ballast to determine the impact of the calculation method.

5.3 Additional Test Results

Additional tie-lateral resistance tests were completed to explore issues of concern that were identified during the tie-lateral resistance tests (e.g., loading rate, tie shape, system degradation, and roller friction) and determine the shear stiffness of the McAbee Ballast and Gravel Ballast. The results of these tests are presented in the following subsections.

5.3.1 Loading Rate

During the proof of concept testing, the horizontal ram was equipment with a manually operated valve, as shown in Figure 4.5A. The manually operated valve could not maintain a constant loading rate. Thus, a sensitivity analysis was completed to assess the impact of varying the loading rate during the tie-lateral resistance tests. It involved repeating the Phase 1 base tests for the Gravel Ballast at a fast rate of 0.5 mm/sec and comparing the results to the results obtained at a slow rate of 0.05 mm/sec. Then replacing the manual valve with an automated servo valve that could maintain a constant loading rate, as shown in Figure 4.5B, and repeating the Phase 1 base tests again at a slow rate of 0.05 mm/sec. In summary, three data groups were collected:

(1) Data Group 4A, which was completed at a slow loading rate of 0.05 mm/sec using the manual horizontal valve in the Gravel Ballast;

(2) Data Group 4B, which was completed at a slow loading rate of 0.05 mm/sec using the automated horizontal servo valve in the Gravel Ballast; and

(3) Data Group 5, which was completed at a fast loading rate of 0.5 mm/sec using the manual horizontal valve in the Gravel Ballast.

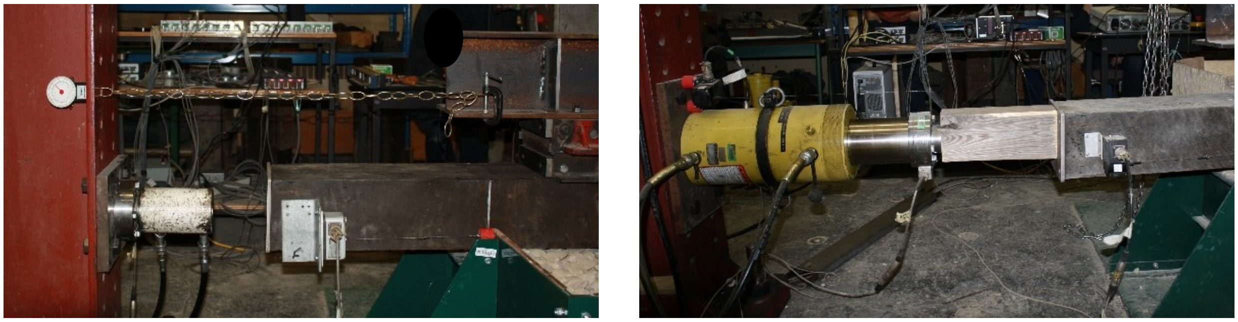

(A) The manually operated horizontal valve. **(B) The automated horizontal servo valve.**

Figure 5.14: Photographs of the horizontal ram valves

The results of the loading rate tests are summarized in Table 5.4**,** and the lateral load per tie at varying horizontal displacements and the peak-lateral load failure envelope for the fast rates tests are shown in Figure 5.15A and 5.15B, respectively. Comparing Figure 5.15 with Figures 5.2 and 5.4, it can be seen that the fast and slow rate tests show a similar peak-lateral load and a similar increase in lateral load with horizontal displacement, with the peak-lateral load still occurring at approximately 20 m of horizontal displacement. Based on these results, it can be concluded that loading rate does not impact the characteristic tie-lateral resistance curve; i.e., the develop of tie-lateral resistance or peak-lateral load, for the range of applied normal loads. These results are consistent with Samavedam et al. (1995) who found that varying the loading rate – Samavedam et al. (1995) considered a slow horizontal loading rate of 0.3 mm to 0.8 mm/sec, a normal rate of 1.7 mm/sec, and a fast rate of 16.9 mm to 25.4 mm/sec – did not influence the STPT characteristic curve. To confirm these results for each material and test configuration a fast rate test was completed for each material and test configuration as shown in Figure 5.10.

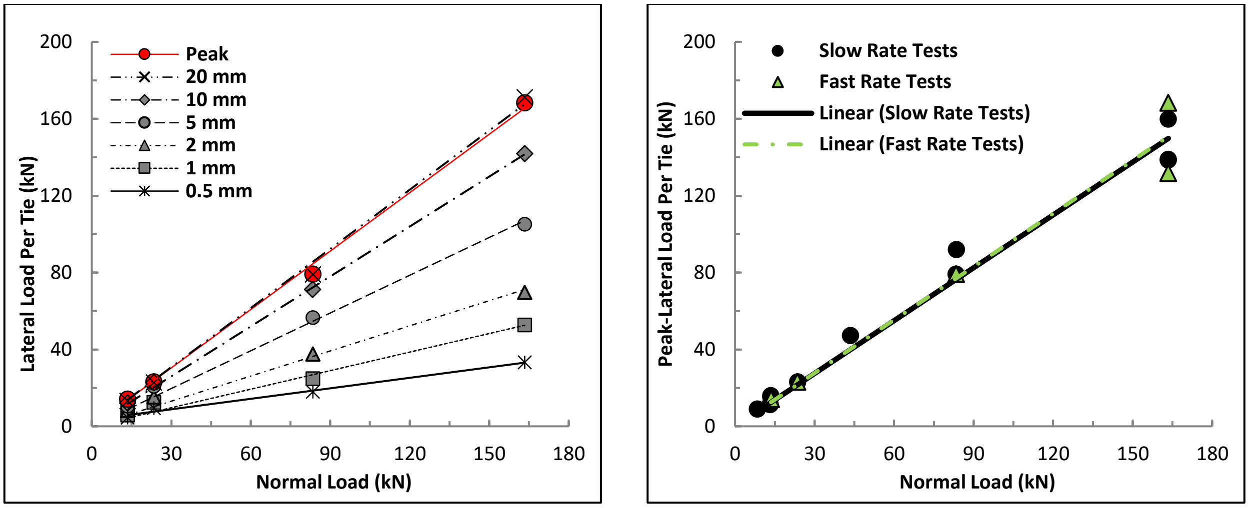

(A) Development of lateral load with horizontal displacement for the fast rate tests

(B) Peak-lateral load failure envelopes

Figure 5.15: Summary of the loading rate test results in the Gravel Ballast

5.3.2 Tie-shape

A sensitivity analysis was completed to determine if the tie-shape affects the tie-lateral resistance of a timber tie. Four Phase 1 base tests were completed under a normal load of 10 kN, two on two timber ties with a misshaped and distorted surface, and two on a timber tie with a relatively constant section width and level surface. A normal load of 10 kN was selected because the tie-lateral resistance under a normal load of 10 kN is small enough (i.e., less than 10 kN) that the effects of tie shape should be evident; whereas, at higher normal loads the effects of the tie-shape may be not be evident because the tie-lateral resistance is governed by the applied normal load.

The results of the tie-shape sensitivity analysis are presented in Figure 5.16. The peak-lateral load, after multiplication by the embedment ratio, was 15.6 kN for the distorted tie surface 1, 13.6 kN for the distorted tie surface 2; and 15.3 kN and 16.0 kN for the levelled tie surface. Overall, the results indicate tie-shape may impact the tie-lateral resistance, but the effect is within the variation observed in tests completed on the same tie surface. However, this may not remain true for ties with more adverse deformities. The remaining tests were conducted on the tie with the relatively constant section width and level surface because it was easier to handle, and would provide a similar pressure distribution in the ballast for each test.

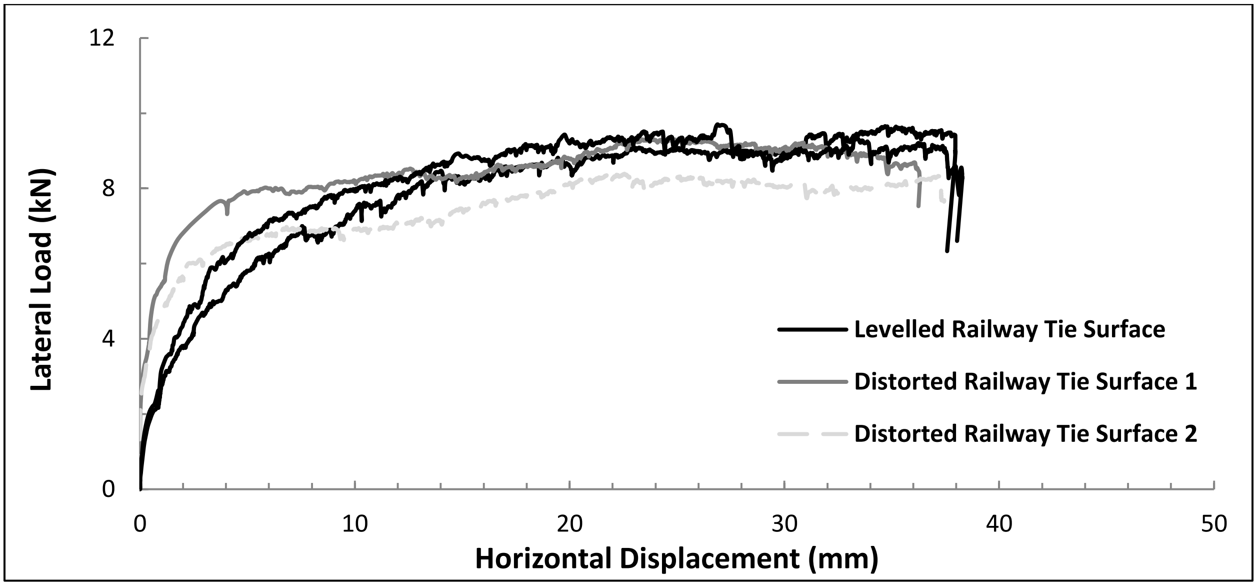

Figure 5.16: Lateral load-horizontal displacement curves for the tie-shape sensitivity analysis

5.3.3 System Degradation

During the proof of concept testing, the tests in each data set were completed in the following sequence of applied normal load: 10 kN, 20 kN, 40 kN, 80 kN, 160 kN, 10 kN, and 5 kN. This testing sequence was selected to determine if the tests were repeatable, and to determine sources of system degradation; e.g., contraction or dilation of the ballast, fragmenting or crushing of the ballast, or damage to the tie or ballast box. The results obtained for the second 10 kN test were similar to the first and the peak-lateral load obtained during the 5 kN test, the last test, aligned with the trend-line for the remaining tests. Based on these results, it was concluded that the tests were repeatable and no significant system degradation was occurring. To confirm this assumption, two data sets were gathered per test configuration and material type.

5.3.4 Roller Friction

Tests were completed to determine the amount of friction generated by the rollers at the base of the dead load (Figure 5.17A), and the rollers at the base of the support pedestals and the concrete floor in the Phase 3 tests (Figure 5.17B).

(A) The roller supports at the base of the dead load

(B) The roller supports at the base of the support pedestals

Figure 5.17: Photographs of the roller supports

To determine the friction generated by the rollers supports at the base of the dead load a horizontal scale was attached from the loading column to the dead load. The maximum frictional load measured in these rollers was 1.25 Kg (0.01 kN) showing the friction generated by these rollers is negligible and does not impact the results of the tie-lateral resistance tests (i.e., it is less than 0.05% of overall tie-lateral resistance). The scale was not observed to consistently increase, but rather to jump concurrently with visual and audible observations of ballast breakage and rearrangement.

To determine the friction generated by the rollers supports at the base of the support pedestals and the concrete floor a Phase 3 test under a normal load of 160 kN was completed with no base, crib or shoulder ballast at the end of the tie. The maximum frictional load measured between the rollers and the concrete floor was 0.02 kN showing the friction generated by these roller support and the concrete floor is negligible and does not impact the results of the tie-lateral resistance tests (i.e., it is less than 0.1% of overall tie-lateral resistance).

5.3.5 Unload-Reload

Unload-reload cycles were purposively triggered during several tests to determine the shear stiffness of the tie-ballast interface. In total, two tests were completed in each material, a Phase 1 base test under a normal load of 160 kN and a Phase crib 2 test under a normal load of 80 kN. These ‘unload-reload tests’ were completed by pausing the tests after 5 mm, 15 mm, and 25 mm of displacement (sometime there was a lag in the horizontal ram, so the displacements are approximate) and then resuming the tests once the lateral load dropped below 20 kN. The results from these tests are presented in Figure 5.18 and Figure 5.19, respectively. For comparison, a particle breakage event, as discussed in Section 5.2, is also labelled on Figure 5.18.

The shear stiffness calculated for each test configuration, applied normal load, material type, and cyclic event is summarize in Table 5.8. The average shear stiffness of the McAbee Ballast and Gravel Ballast was determined to be 0.10 kN/m, and 0.13 kN/m, respectively.

Table 5.8: Shear stiffness of the tie-ballast interface in the McAbee Ballast and Gravel Ballast

Testing Configuration	Applied Normal Load	Material Type	Test Number	Shear Stiffness (kN/m)			
				1	2	3	4
Phase 1	160 kN	McAbee Ballast	1	0.06	0.11	0.10	0.07
		Gravel Ballast	2	0.36 (excluded from average)	0.14	0.13	-
Phase 2	80 kN	McAbee Ballast	3	0.15	0.09	0.11	-
		Gravel Ballast	4	0.12	0.12	0.14	-

From Figure 5.18 and Figure 5.19 it is evident that the tie-lateral response is loading path dependent, and that there is a recoverable (elastic) and non-recoverable (plastic) portion of horizontal displacement during the tests. During in-service conditions, the rail would help return the tie to its original position (Le Pen 2008).

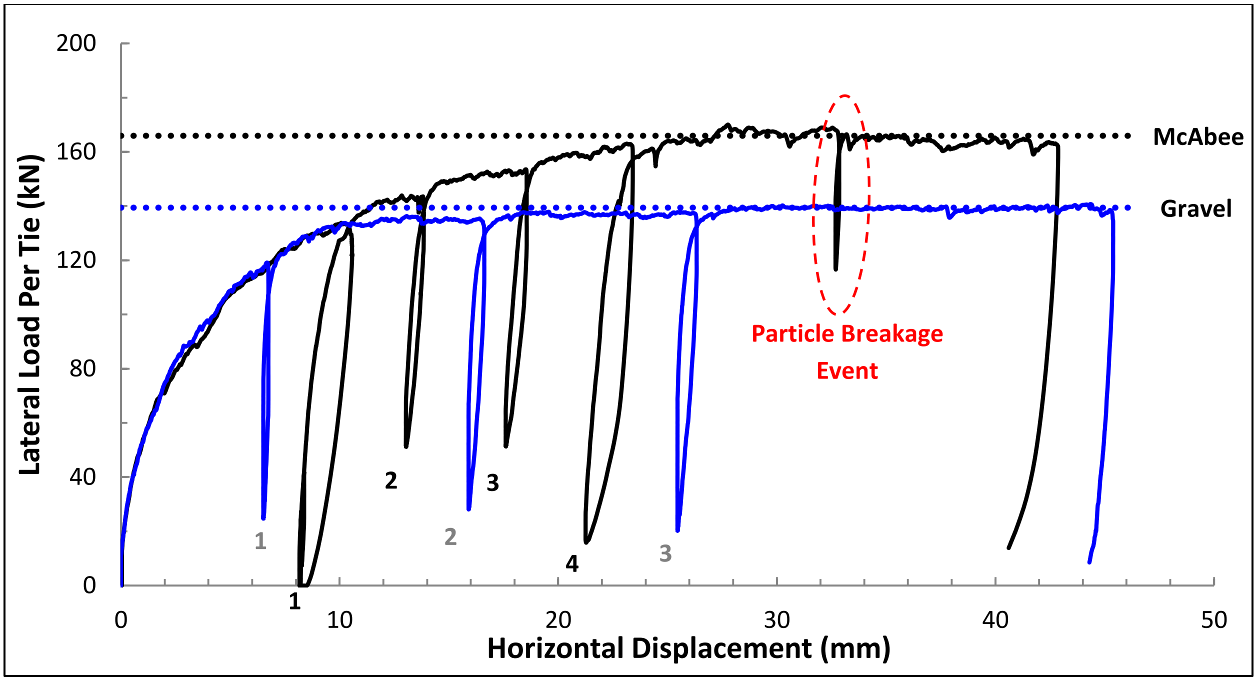

Figure 5.18: Load-horizontal displacement curves for a Phase 1 base unload-reload test completed under a normal load of 160 kN

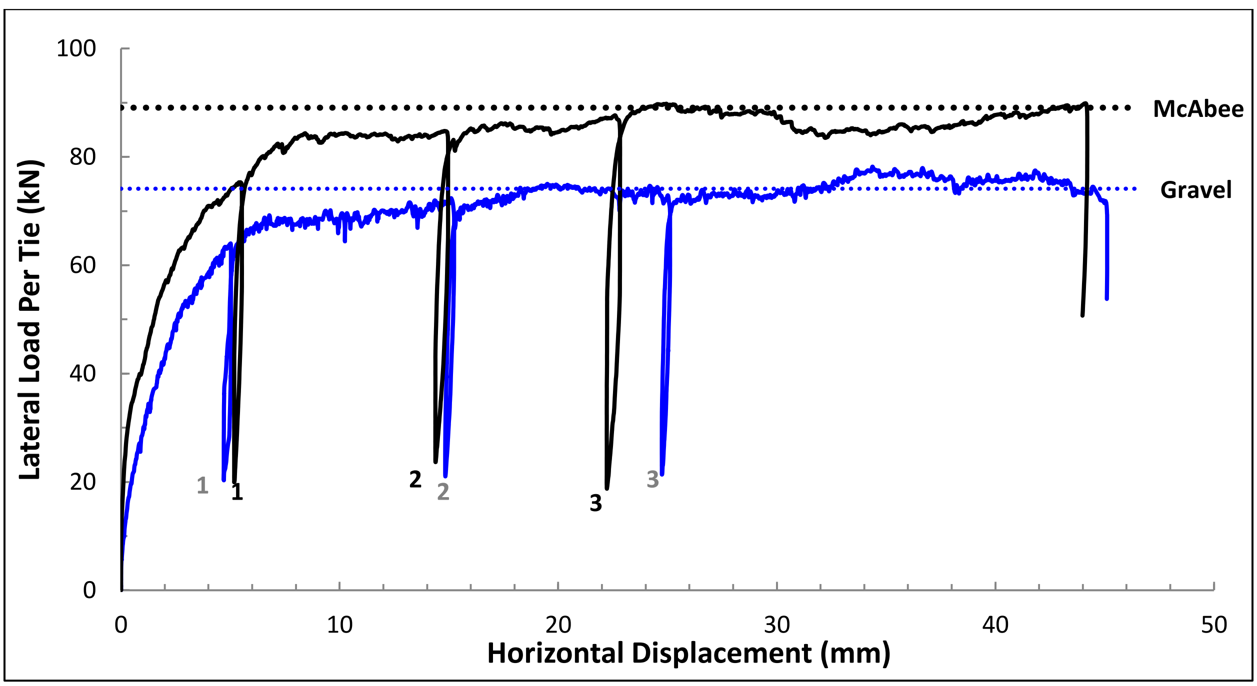

Figure 5.19: Load-horizontal displacement curves for a Phase 2 crib unload-reload test completed under a normal load of 80 kN

5.4 Visual and Audible Observations Made During the Tests

The following visual and audible observations were made during the tie-lateral resistance tests:

- The McAbee Ballast interlocked quickly during tamping and was less susceptible to disturbance than the Gravel Ballast. This was expected based on the material characterization test results, which indicated the Gravel Ballast was less likely to interlock than the McAbee Ballast because it was smoother, less angularity, and contained flakier-aggregates.

- Fluctuations in lateral load coincided with visual and audible observations of ballast breakage and re-arrangement (e.g., fracturing, crushing, rolling, or sliding).

- The ballast surrounding the tie re-arranged (e.g., rolled or slide) during the Phase 1 base and Phase 2 crib tests. The re-arrangement was localized around the tie suggesting stress concentrations within the ballast were negligible at the boundaries, and by extension boundary effects at the rigid interfaces between the ballast and ballast box are minimal.

- The tie moved relative to the ballast by approximately the same distance the tie was pushed, indicating failure occurred at the tie-ballast interface and not within the base ballast or crib ballast.

- The ballast did not penetrate the OSB or plywood liner of the ballast box, suggesting stress concentrations within the ballast were negligible at the boundaries, and by extension boundary effects at the rigid interfaces between the ballast, ballast box, and floor are minimal.

- During the Phase 3 shoulder tests, a 0.6 m wide shoulder of ballast fully contained the failure wedge, indicating a 0.6 m wide shoulder of ballast is sufficient to capture the maximum shoulder resistance.

- The tie underwent a small horizontal rebound, typically on the order of 2 mm to 4 mm, during the Phase 1 base and Phase 2 cribs tests when the lateral load was removed. The rebound indicates there is a recoverable (elastic) and non-recoverable (plastic) portion of horizontal displacement during the Phase 1 base and Phase 2 cribs tests.

5.5 Issues Encountered During the Tie-Lateral Resistance Tests

No significant issues were encounter during the tie-lateral resistance tests, but four modifications were made/are proposed to improve the testing apparatus:

- A manually operated valve in the horizontal ram was replaced with an automated serval valve, so that a constant loading rate could be maintained during the tests.
- A bracing column was installed at the end of the ballast box to resist lateral ballast box movements after the ballast box slide across the concrete floor during a test.
- The end panel of the ballast box was observed to have crept and to have deflected permanently up to one centimeter by the end of the testing program, so additional stiffeners are recommended if additional tests are to be completed.
- The ballast box walls are too short to accommodate the crib ballast, so they need to be extended or replaced with higher panels.
- Pressure sensors or paper are recommended to measure the confining stress in the ballast, and to determine the bearing area of the tie; i.e., how many contact points there are between the tie and the ballast.

CHAPTER 6.0 TIE-LATERAL RESISTANCE TESTS – DISCUSSION

6.1 Comparison of Tie-Lateral Resistance in the McAbee Ballast and Gravel Ballast

The average peak-lateral load per tie provided by the McAbee Ballast and Gravel Ballast is tabulated in Table 6.1. The results are tabulated for normal loads of 10 kN, 80 kN, and 160 kN. The McAbee Ballast and Gravel Ballast provided 17.2 kN and 15.1 kN, respectively, under a normal load of 10 kN; and 174.9 kN and 146.4 kN, respectively, under a normal load of 160 kN. On average, the Gravel Ballast provided 15% less tie-lateral resistance than the McAbee Ballast. These results were expected based on the material characterization tests, which indicated the McAbee Ballast would provide more tie-lateral resistance than the Gravel Ballast because it is rougher, more angular, and contains less flaky-particles.

Table 6.1: Comparison of tie-lateral resistance in the McAbee Ballast and Gravel Ballast

Normal Load (kN)	Average Peak-Lateral Load Per Tie (kN)		Percent Change in Average Peak-Lateral Load from the McAbee Ballast
	McAbee Ballast	Gravel Ballast	
10	17.2	15.1	12%
80	95.5	80.3	16%
160	174.9	146.4	16%
		Average	15%

As discussed in Section 2.1.2, the frictional resistance of the tie-ballast interface can be represented as a friction angle (ϕ) defined as:

$$Friction\ \Phi = \tan^{-1}(lateral\ load/normal\ load) \qquad \text{Equation 6.1}$$

Using the Phase 1 base tests results presented in Figure 5.9, the friction angle between the timber tie and the McAbee Ballast and Gravel Ballast was calculated for varying horizontal displacements and plotted in Figure 6.1. In Figure 6.1, the friction angle is observed to increase with horizontal displacement until it reached a limiting value after approximately 20 mm of horizontal displacemet. The limiting friction angle of the tie-ballast interface was approximately 46.9° and 42.5° in the McAbee Ballast and Gravel Ballast, respectively. On average, the friction angle of the timber tie-ballast interface in the McAbee Ballast was approximately 10% greater than the friction angle of the timber tie-ballast interface in the Gravel Ballast.

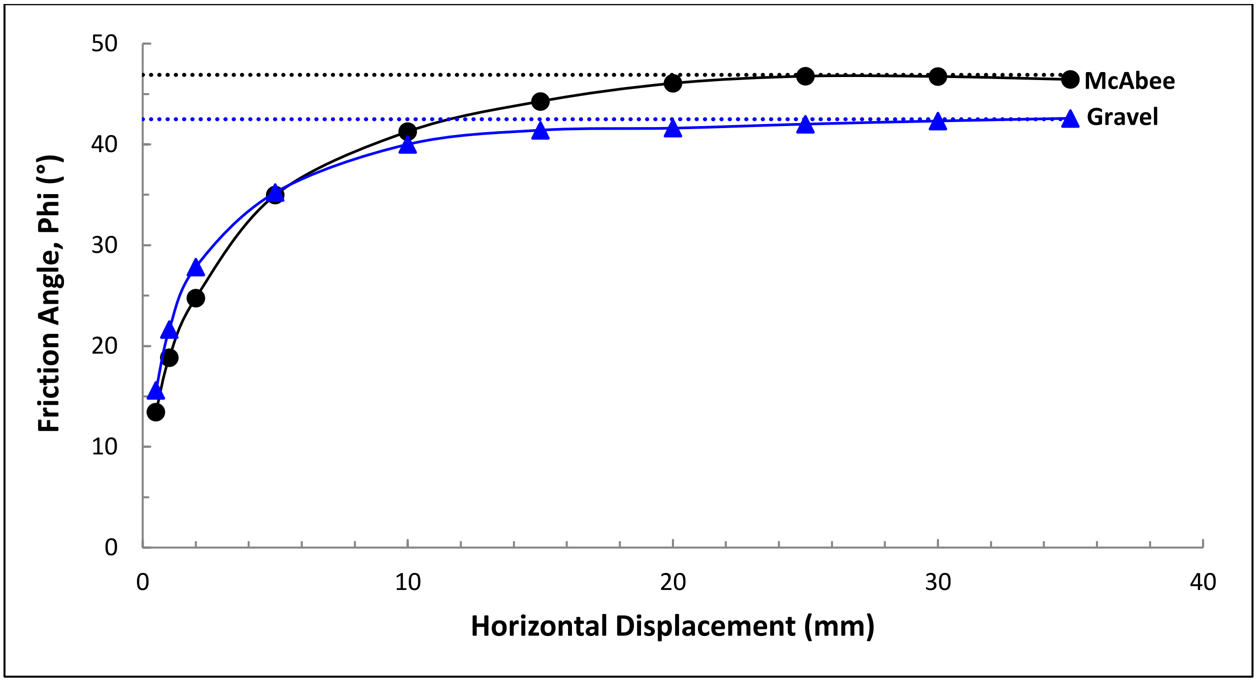

Figure 6.1: Friction angle versus horizontal displacement for the McAbee Ballast and Gravel Ballast

6.2 Contribution of Each Components of Tie-lateral Resistance to Overall Tie-lateral Resistance

The percent contribution of each component of tie-lateral resistance to overall tie-lateral resistance in the McAbee Ballast and Gravel Ballast is tabulated in Table 6.2 and shown in Figure 6.2. The results are tabulated for normal loads of 10 kN, 80 kN, and 160 kN. The percent contribution from the shoulder resistance is based on a 0.6 m wide shoulder. Overall, the base friction, crib friction, and shoulder resistance were determined to contribute 65% to 70%, 10% to 15%, and 15% to 20%, respectively, under a normal load of 10 kN; and to contribute 98%, less than 1%, and less than 2%, respectively, under a normal load of 160 kN.

Table 6.2: Percent contribution of each component of tie-lateral resistance to overall tie-lateral resistance in the McAbee Ballast and Gravel Ballast

Material Type	Normal Load (kN)	Average Peak-Lateral Load Per Tie (kN)				Percentage of Total Peak-Lateral Load		
		Base Friction	Crib Friction	Shoulder Resistance	Overall	Base Friction	Crib Friction	Shoulder Resistance
McAbee Ballast	10	11.7	2.9	2.7	17.2	68%	17%	15%
	80	87.4	5.4	2.7	95.5	92%	6%	3%
	160	170.9	1.3	2.7	174.9	98%	1%	2%
Gravel Ballast	10	10.7	1.4	3.0	15.1	71%	9%	20%
	80	76.9	0.4	3.0	80.3	96%	0%	4%
	160	148.4	-5.0	3.0	146.4	101%	-3%	2%

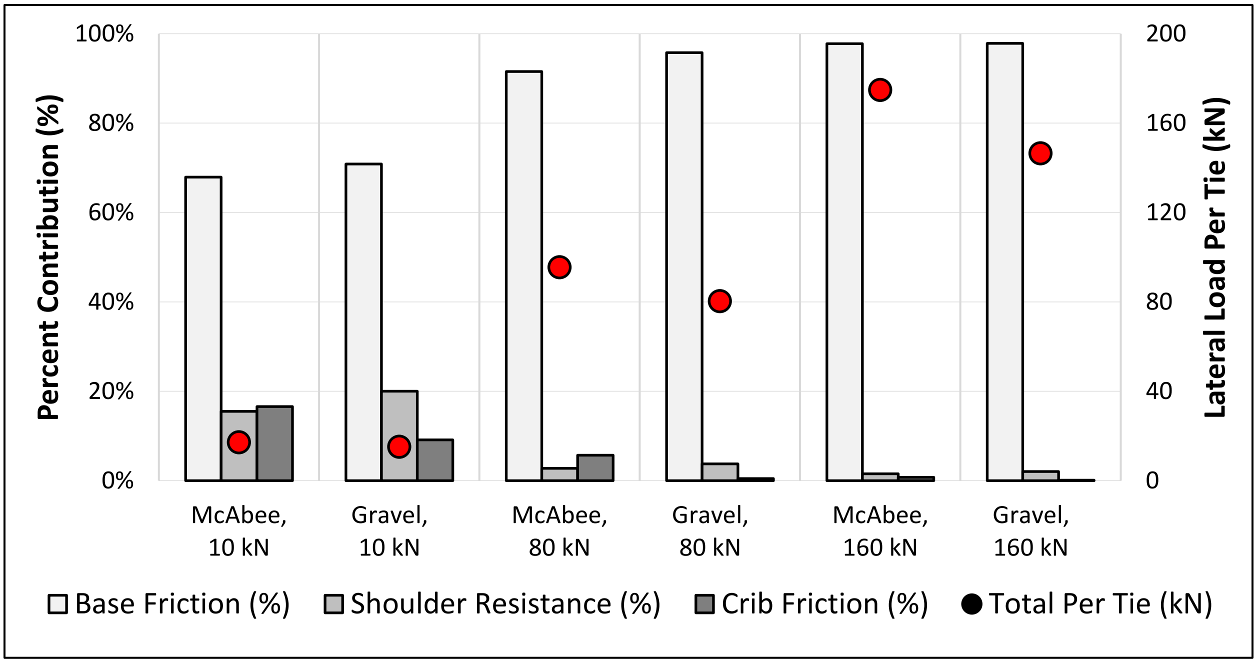

Figure 6.2: Percent contribution of each component of tie-lateral to overall tie-lateral resistance

6.3 Comparison of the Tie-Lateral Resistance Test Results with the Literature

The obtained peak-lateral load per tie and percent contribution of each component of tie-lateral resistance are compared with the literature reviewing findings in Tables 6.3 and 6.4. Since, most of the published literature considers normal loads less than 5 kN, the results were reported for normal loads of 5 kN, 10 kN, and 160 kN. It is clear from Tables 6.3 and 6.4 that there is significant variation in the reported peak-lateral load per tie and percent contribution of each component of tie-lateral resistance. It is difficult to compare our findings with those of other researchers because of variations in test type; tie type; ballast type, geometry and condition; and loading conditions used. Many of which are not reported.

Overall, the obtained peak-lateral load per tie is in general agreement with the values reported in the literature for weak ballast at low normal loads (less than 5 kN), and the percent contribution of each component of tie-lateral resistance is in general agreement with Kish and Samavedam (2013), Lichtberger (2007), and Selig and Waters (1994) who reported the base and crib component contributes the most and least tie-lateral resistance, respectively.

Table 6.3: Comparison of the obtained peak-lateral resistance with the peak-lateral resistance reported in the literature

Reference	Average Peak-Lateral Load		Tie Type	Normal Loading
	'Weak' Track	'Strong' Track		
This research	9 kN to 10 kN	-	Timber	5 kN
	15 kN to 17 kN	-	Timber	10 kN
	146 kN to 175 kN	-	Timber	160 kN
Bakhtiary et al. (2015)	11 kN for timber ties, 13 kN for steel ties and 20 kN for concrete ties		Timber, steel, and concrete	No
Clark et al. (2011) and Read et al. (2011)	8.2 kN to 13.6 kN	40.4 kN	Concrete	-
De Iorio et al. (2014)	Between 4 kN and 10 kN		Concrete	No
De Iorio et al. (2016)	Approximately 5.8 kN		Concrete	Yes, track superstructure, taken to be 3.1 kN
Esmaeili et al. (2015)	Between 6 kN and 17 kN		Concrete	-
Kish (2011)	< 6.2 kN	> 12 kN	-	-
Kish and Samavedam (2013)	8 N/m	53 N/m	Timber	Yes, track superstructure, taken to be 20 lb/in
Le Pen (2008) and Le Pen and Powrie (2008 and 2011)	5.9 kN to 7.3 kN	-	Concrete	Yes, 2 kN seating load plus an applied load up to 75 kN
Samavedam et al. (1999)	8 kN	15 kN	Concrete	-
Sussmann et al. (2003)	6.2 kN to 10.7 kN	13 kN to 22 kN	Concrete	No
van't Zand and Moraal (1997)	5.3 kN to 34.4 kN		Concrete	Yes, -5 kN to 35 kN

Table 6.4: Comparison of the obtained percent contribution with the percent contribution reported in the literature

Reference	The Percent contribution of each component of tie-lateral resistance			Tie Type	Normal Loading
	Base	Crib	Shoulder		
This research	60% to 65%	10% to 20%	20% to 25%	Timber	5 kN
	65% to 70%	10% to 15%	15% to 20%	Timber	10 kN
	> 98%	< 1%	< 2%	Timber	160 kN
De Iorio et al. (2014)	42%	42%	16%	-	-
De Iorio et al. (2016)	25%	50%	25%	Concrete	Yes, track superstructure, taken to be 3.1 kN
Kish (2011)	35% to 40%	30% to 35%	20% to 25%	-	-
Kish and Samavedam (2013)	40% to 55%	20% to 27%	40% to 18%	Timber	Yes, track superstructure, taken to be 20 lb/in
Le Pen (2008) and Le Pen and Powrie (2008 and 2011)	28% to 35%	41% to 50%	15% to 32%	Concrete	Yes, 2 kN seating load plus an applied load up to 75 kN
Lichtberger (2007)	45% to 50%	10% to 15%	35% to 40%	-	-
Samavedam et al. (1995)	25% to 35%	65% to 55%	10% to 20%	Timber	-
Selig and Waters (1994)	50% to 60%	10% to 20%	30% to 40%	-	No
	95% to 100%	0% to 5%	0% to 5%	-	Yes

6.4 Other Considerations

The tie-lateral resistance test results presented herein are based on the peak-lateral resistance obtained for a single timber tie in dry, clean, freshly-tamped McAbee Ballast and Gravel Ballast under normal loads ranging from 5 kN to 160 kN. Thus, these results may have limited applicable when considering other test or in-service conditions; such as, the effects of fouling, moisture, temperature, consolidation, uplift forces, and dynamic or cyclic loading; the tie-lateral resistance offered by different ties or ballast materials; the non-uniform tie-lateral resistance offered by several ties; or the tie-lateral resistance at displacements other than the displacement corresponding to peak-lateral resistance. For example, uplift forces could reduce or eliminate the contribution from the base friction making the contribution from the crib friction and the shoulder resistance more substantial; longitudinal forces could increase the contribution from the crib friction by confining the crib ballast; or failure wedge overlap in the shoulder ballast could reduce the shoulder resistance provided to each tie.

The peak-lateral resistance is the summation of the peak-base friction, peak-crib friction and peak-shoulder resistance in each material, and does not consider whether the base friction, crib friction, and shoulder resistance mobilize simultaneously (i.e., at the same horizontal displacement). The overall tie-lateral resistance, and the percent contribution of each component of tie-lateral versus horizontal displacement is presented in Figures 6.3 and 6.4 for tests completed under a normal load of 80 kN. Similar figures are included in Appendix III for tests completed under normal loads of 10 kN and 160 kN. These figures demonstrate that the base friction, crib friction, and shoulder resistance are not mobilized simultaneously, but generally are mobilized between 10 mm and 20 mm of horizontal displacement. Based on the scatter in the test results, it is reasonable to assume that all three components of tie-lateral resistance could be fully-mobilized at the same time, even if they did not mobilize simultaneously.

It is also noted that the tie-lateral resistance test results presented herein do not account for the influence of tie compressibility, and may not be tabulated at a horizontal displacement that is representative of in-service track conditions (information regarding typical in-situ horizontal displacements was unavailable when this thesis was prepared). It is recommended during a future phase of this research that the influence of tie compressibility be investigated and that the tie-lateral resistance test results be interpreted/tabulated at a horizontal displacement that is representative of in-service track conditions.

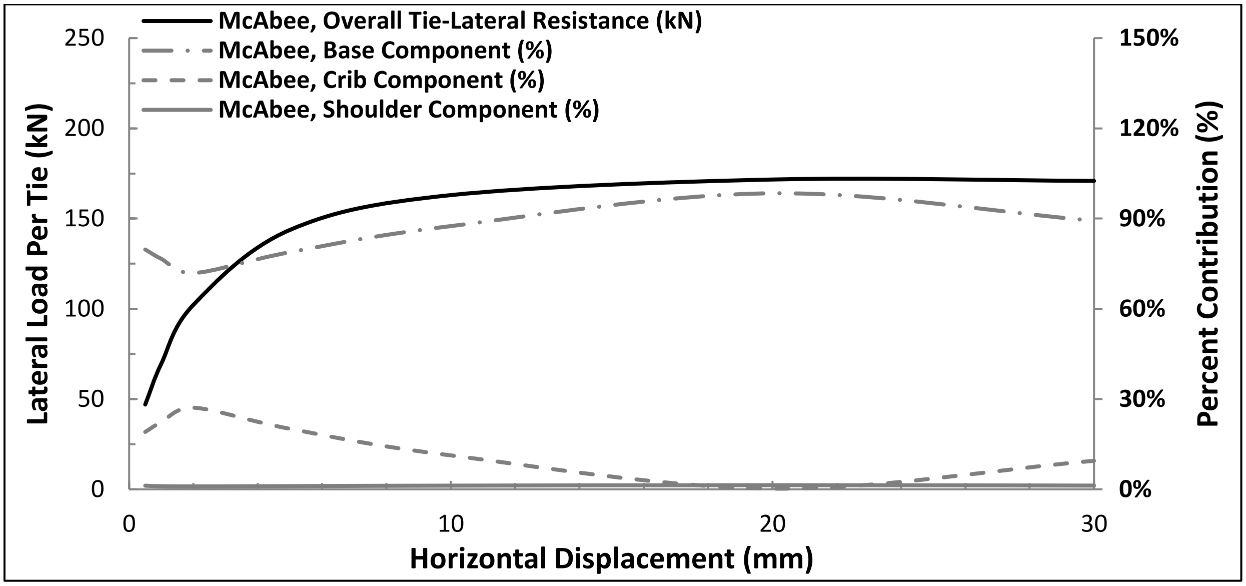

Figure 6.3: Percent contribution of each component of tie-lateral to overall tie-lateral resistance in the McAbee Ballast (tests completed under a normal load of 80 kN)

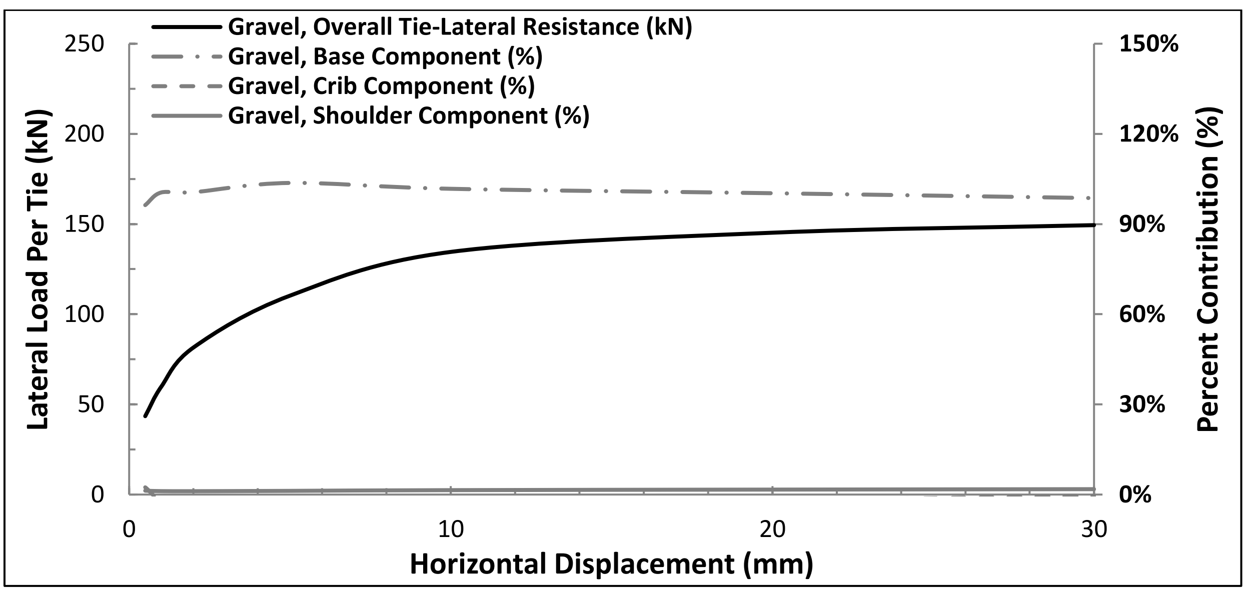

Figure 6.4: Percent contribution of each component of tie-lateral to overall tie-lateral resistance in the Gravel Ballast (tests completed under a normal load of 80 kN)

CHAPTER 7.0 CONCLUSIONS AND FURTHER RESEARCH

For this research, the tie-lateral resistance of the McAbee Ballast and Gravel Ballast and the percent contribution of each component of tie-lateral resistance to overall tie-lateral resistance was determined for the expected range of in-service ballast loads. This was accomplished through material characterization tests and tie-lateral resistance tests. In summary, the key observations, findings, and conclusions of this research are:

- The maximum potential in-service ballast load transferred to a single timber tie is approximately 160 kN based on CN Rail's maximum freight car mass of 130, 000 Kg and the AREMA equation for calculating ballast loads (AREAM 2014).
- The load-horizontal displacement curves reach a limiting peak-lateral resistance after approximately 20 mm of horizontal displacement.
- The lateral load fluctuates concurrently with visual and audible observations of ballast breakage and re-arrangement.
- The pre-failure zone of the base friction increases with normal load.
- The base friction is dependent on the applied normal load; whereas, the crib friction and shoulder resistance are independent of the applied normal load.
- Failure occurs at the tie-ballast interface during the Phase 1 base and Phase 2 crib tests, and not within the base ballast or crib ballast.
- A 0.6 m wide shoulder captures the maximum potential shoulder resistance because the failure wedge is fully-contained within the slope.
- Varying the horizontal loading rate does not impact the tie-lateral resistance test results for the range of applied normal loads.
- The average shear stiffness of the McAbee Ballast and Gravel Ballast is 0.10 kN/m, and 0.13 kN/m, respectively, based on the unload-reload test results.

- The McAbee Ballast and Gravel Ballast provide an average peak-lateral load per tie of 17.2 kN and 15.1 kN, respectively, under a normal load of 10 kN; and 174.9 kN and 146.4 kN, respectively, under a normal load of 160 kN.

- The contact between the timber tie and McAbee Ballast and Gravel Ballast (i.e., the tie-ballast interface) has a friction angle of 46.9° and 42.5°, respectively.

- On average, the Gravel Ballast provides 15% less tie-lateral resistance than the McAbee Ballast. The McAbee Ballast was expected to provide more tie-lateral resistance than the Gravel Ballast because it is rougher, more angular, and contains less flaky-particles.

- Overall, the base friction, crib friction, and shoulder resistance contribute 65% to 70%, 10% to 15%, and 15% to 20%, respectively, under a normal load of 10 kN; and 98%, less than 1%, and less than 2%, respectively, under a normal load of 160 kN.

7.1 Further Research

Suggestions for continuing this research:

- Complete additional tie-lateral resistance tests to determine the tie-lateral resistance provided by other tie types and ballast materials.

- Complete additional tie-lateral resistance tests to investigate the influence of fouling, moisture, temperature, consolidation, uplift forces, dynamic and cyclic loading, and tie-compressibility on tie-lateral resistance.

- Complete additional tests with full base, crib, and shoulder ballast and re-calculate the percent contribution for each component of tie-lateral resistance. As shown in Table 2.4, De Iorio et al. (2016) found that the percent contribution varied depending on the test configurations used.

- Complete panel pull tests to determine the non-uniform lateral resistance offered by multiple ties, and to study the interaction between the different components of tie-lateral resistance.

- Complete tie-lateral resistance tests on in-service track and correlate the results to the laboratory results. De Iorio et al. (2016) expresses a concern that the results obtained from laboratory STPTs often overestimates the ballast strength.

- Determine the in-situ horizontal displacements that would typically occur in in-service track. Then determine the peak-lateral resistance and the percent contribution of each component of tie-lateral resistance to overall tie-lateral resistance at that displacement.

REFERENCES

Abadi, T., Le Pen, L., Zervos, A., and Powrie, W. 2015. Measuring the Area and Number of Ballast Particle Contacts at Sleeper/Ballast and Ballast/Subgrade Interfaces. International Journal of Railway Technology, **4**(2):45-72.

Al-Rousan, T. 2004. Characterization of Aggregate Shape Properties Using a Computer Automated System. Ph.D. Thesis, Department of Civil Engineering, Texas A&M University, College Station, Texas, USA.

Al-Rousan, T. Masad, E., Tutumluer, E., and Pan, T. 2007. Evaluation of Image Analysis Techniques for Quantifying Aggregate Shape Characteristics. Journal of Construction and Building Materials, **21**(5): 978–990.

American Railway Engineering and Maintenance-of-Way Association (AREMA). 2014. Manual for Railway Engineering. AREMA, Lanham, Maryland, USA.

American Society for Testing and Materials (ASTM). 2010. ASTM D6928-10, Standard Test Method for Resistance of Coarse Aggregate to Degradation by Abrasion in the Micro-Deval Apparatus. ASTM International, West Conshohocken, Pennsylvania, USA. Available from https://www.astm.org/Standards/D6928.htm.

American Society for Testing and Materials (ASTM). 2011a. ASTM C702/C702M-11 Standard Practice for Reducing Samples of Aggregate to Testing Size. ASTM International, West Conshohocken, Pennsylvania, USA. Available from https://www.astm.org/Standards/C702.htm.

American Society for Testing and Materials (ASTM). 2011b. ASTM D2487-11 Standard Practice for Classification of Soils for Engineering Purpose (Unified Soil Classification System). ASTM International, West Conshohocken, Pennsylvania, USA. Available from https://www.astm.org/Standards/D2487.htm.

American Society for Testing and Materials (ASTM). 2014a. ASTM D75/D75M-14 Standard Practice for Sampling Aggregates. ASTM International, West Conshohocken, Pennsylvania, USA. Available from https://www.astm.org/Standards/D75.htm.

American Society for Testing and Materials (ASTM). 2014b. ASTM C136/C136M-14 Standard Test Method for Sieve Analysis of Fine and Coarse Aggregates. ASTM International, West Conshohocken, Pennsylvania, USA. Available from https://www.astm.org/Standards/C136.htm.

American Society for Testing and Materials (ASTM). 2014c. ASTM C131/C131M-14 Standard Test Method for Resistance to Degradation of Small-Size Coarse Aggregate by Abrasion and Impact in the Los Angeles Machine. ASTM International, West Conshohocken, Pennsylvania, USA. Available from https://www.astm.org/Standards/C131.htm.

American Society for Testing and Materials (ASTM). 2016. ASTM C535-16 Standard Test Method for Resistance to Degradation of Large-Size Coarse Aggregate by Abrasion and Impact in the Los Angeles Machine. ASTM International, West Conshohocken, Pennsylvania, USA. Available from https://www.astm.org/Standards/C535.htm.

Bakhtiary, A. Zakeri, J.A., Fang, H.J., and Kasraiee, A. 2015. An Experimental and Numerical Study of the Effect of Different Types of Sleepers on Track Lateral Resistance. International Journal of Transportation Engineering, **3**(1):7-15.

Balideh, S. 2015. Influence of Particle Shape and Texture on Broken Sandstone Strength Behavior. Ph.D. Thesis, Department of Civil and Environmental Engineering, University of Alberta, Edmonton, Alberta, Canada.

British Standard Institute (BSI). 1989. BS 812: Section 105.1:1989, British Standard Testing aggregates, Part 105. Methods for determination of particle shape, Section 105.1 Flakiness index. British Standard Institute, London, UK.

Canadian National Rail Company (CN Rail). 1990. An Investigation into Ballast Failures in Concrete Tie Track on the Ashcroft Subdivision, B.C. South District.

Canadian National Rail Company (CN Rail). 2003. Appendix 'D' CN Crushed Rock Ballast Material Specification.

Clark, D.W., Read, D.M., Gehringer, E. and Thompson, R. 2011. Track Panel Shift Tests on the Union Pacific Railroad. *In* Proceedings of the IHHA Specialist Technical Sessions 2011: Railroading in Extreme Condition, Calgary, Alberta. International Heavy Haul Association (IHHA).

Clifton Associates Ltd. 1991. Final Report Geologic Evaluation McAbee Quarry. Report prepared for CN Rail by Clifton Associates, Regina, Saskatchewan, Canada.

De Iorio, A., Grasso, M., Penta, F., Pucillo, G.P. and Rosiello, V. 2014. Transverse Strength of Railway Track: Part 1. Planning and Experimental Setup. Frattura ed Intergrità Strutturale **30**: 478-485.

De Iorio, A., Grasso, M., Penta, F., Pucillo, G.P. and Rosiello, V. 2014. Transverse Strength of Railway Track: Part 2. Test System for Ballast Resistance in Line Measurement. Frattura ed Intergrità Strutturale **30**: 593-601.

De Iorio, A., Grasso, M., Penta, F., Pucillo, G.P. and Rosiello, V. 2014. Transverse Strength of Railway Track: Part 3. Multiple Scenarios Test Field. Frattura ed Intergrità Strutturale **30**: 578-592.

De Iorio, A., Grasso, M., Penta, F., Pucillo, G.P., Rosiello, V., Testa, M. 2016. On the Ballast-Sleeper Interaction in the Longitudinal and Lateral Directions. Institution of Mechanical Engineers Part F: Journal of Rail and Rapid Transit **0**(0):1-12.

Esmaeili, M., Nouri, R., and Yousefian, K. 2017. Experimental Comparison of the Lateral Resistance of Tracks with Steel Slag Ballast and Limestone Ballast Material. Institution of Mechanical Engineers Part F: Journal of Rail and Rapid Transit **231**(2):175-184.

Hay, W, W. 1982. Railway Road Engineering. John Wiley & Sons Inc., New York, USA.

Hayano, K., Koike, Y., Nakamura, T., and Momoya, Y. 2014. Effects of Sleeper Shape on Lateral Resistance of Railway Ballasted Tracks. American Society of Civil Engineers (ASCE).

Indraratna, B., Salim, W. and Rujikiatkamjorn, C. 2011. Advanced Rail Geotechnology: Ballasted Track. CRC Press, London, New York, USA.

Jeong, D.Y. 2013. Analyses for Lateral Deflection of Railroad Track Under Quasi-Static Loading. *In* Proceedings of the ASME 2013 Rail Transportation Division Fall Technical Conference, Altoona, Pennsylvania, USA, 15-17 October 2013. American Society of Mechanical Engineers (ASME).

Kish, A. 2011. On the Fundamentals of Track Lateral Resistance. AREMA.

Kish, A., and Samavedam, G. 2013. Track Buckling Prevention: Theory, Safety, Concepts, and Application. U.S. Department of Transportation, Federal Railroad Administration Report DOT/FRA/ORD-13/16), Washington, District of Columbia, USA.

Le Pen, L. 2008. Track Behaviour: The Importance of the Sleeper to Ballast Interface. Ph.D. Thesis, School of Civil Engineering and the Environment, University of Southhampton, Southhampton, England.

Le Pen, L., and Powrie, W. 2008. Testing the ultimate resistance at the sleeper/ballast interface. *In* Proceedings of the Third International Conference on Advances in Transportation Geotechnics, Nottingham, UK, 25-27 August 2008. Taylor & Francis Group, London, UK, pp. 607-613.

Le Pen, L., and Powrie, W. 2011. Contribution of base, crib, and shoulder ballast to the lateral sliding resistance of railway track: a geotechnical perspective. Institution of Mechanical Engineers Journal of Rail and Rapid Transit, **225**(2):113-128.

Le Pen, L., Bhandari, A.R., and Powrie, W. 2014. Sleeper End Resistance of Ballasted Railway Tracks. Journal of Geotechnical and Geoenvironmental Engineering, **140**(5):04014004-1-14.

Litchtberger, B. 2007. The Lateral Resistance of the Track. European Railway Review 3 and 4.

Little, D., Button, J., Jayawickrama, P., Solaimanian, M., and Hudson, B. 2003. Quantify Shape, Angularity and Surface Texture of Aggregates Using Image Analysis and Study Their Effect on Performance. Texas Transportation Institute, The Texas A&M University System, College Station, Texas, USA.

Masad, E. 2001. Review of Imaging Techniques For Characterizing The Shape of Aggregates Used in Asphalt Mixes. *In* Proceedings of the International Center for Aggregates Research 9th Annual Symposium: Aggregates - Concrete, Bases and Fines Austin, Texas, USA, 22-25 April 2001. University of Texas, International Center for Aggregates Research, Austin, Texas, USA.

Masad, E., Al-Rousan, T., Button, J., Little, D., and Tutumluer, E. 2007. Test Methods for Characterizing Aggregate Shape, Texture, and Angularity. National Cooperative Highway Research Program (NCHRP), Washington, District of Columbia, USA, NCHRP Report 555.

McHenry, M. 2013. Pressure Measurement at the Ballast-Tie Interface of Railroad Track Using Matrix Based Tactile Surface Sensors. Ph.D. Thesis, Department of Civil Engineering, University of Kentucky, Lexington, Kentucky, USA.

Mulhall, C., Balideh, S., Macciotta, R., Hendry, M., Martin, D., and Edwards, T. 2016. Large-Scale Testing of Tie Lateral Resistance in Two Ballast Materials. *In* Proceedings of the Third International Conference on Railway Technology: Research, Development and Maintenance Cagliari, Sardinia, Italy, 5-8 April 2016. Civil-Comp Press, Stirlingshire, UK, Paper 4.

Mulhall, C., Balideh, S., Macciotta, R., Hendry, M., Martin, D., and Edwards, T. 2016. "Large-scale Laboratory Testing of the Lateral Resistance of a Timber Tie". *In* Proceedings of the Symposium of Railroad Ballast Testing and Properties, Sheraton New Orleans, New Orleans, Louisiana, USA, 24 January 2018. American Society for Testing and Materials (ASTM) International, West Conshohocken, Pennsylvania, USA, Manuscript STP-2017-0030.R1 (in press).

Prud'homme, A. 1967. Resistance of the track to lateral loads exerted by rolling stock. Trvue Generale des Chemins de Fer.

Read, D., Thompson, R., Clark, D., and Gehringer, E. 2011. Results of Union Pacific Concrete Tie Track Panel Shift Tests. Technology Digest, **11**(4).

Samavedam, G., and Kish, A. 1991. Continuous Welded Rail Track Buckling Safety Assurance Through Field Measurements of Track Resistance and Rail Force. *In* Proceedings of Lateral Track Stability, St. Louis, Missouri, USA, 15-17 May 1990. Transportation Research Record No. 1289, pp. 39-52.

Samavedam, G., Kish, A., Purple, A., and Schoengart, J. 1993. Parametric Analysis and Safety Concepts of CWR Track Buckling. U.S. Department of Transportation, Federal Railroad Administration Report DOT/FRA/ORD-93/26, Washington, District of Columbia, USA.

Samavedam, G. Kanann, A., Peitrack, J., Kish, A., and Sluz, A. 1995. Wood Tie Track Resistance Characterization and Correlations Study. U.S. Department of Transportation, Federal Railroad Administration Report DOT/FRA/ORD-94/07, Washington, District of Columbia, USA.

Samavedam, G., Sluz, A., and Kish, A. 1999. The Effect of Realignment on Track Lateral Stability. *In* Proceedings of the AREMA 1999 Track and Structure Annual Conference, Chicago, Illinois, USA, 12-15 September 1999. American Railway Engineering and Maintenance-of-Way Association (AREMA), Paper 19.

Selig, E. T., and Waters, J. M. 1994. Track Geotechnology and Substructure Management. Thomas Telford, London, UK.

Smith, T. 2014. Manual on Test Sieving Methods: Guidelines for Establishing Sieve Analysis Procedures, MNL32-5TH-EB. ASTM International, West Conshohocken, Pennsylvania, USA. Available from https://www.astm.org/DIGITAL_LIBRARY/MNL/SOURCE_PAGES/MNL32-5TH.htm.

Sussmann, T., Kish, A., and Trosino, M. 2003. Influence of Track Maintenance on the Lateral Resistance of Concrete-Tie Track. Journal of the Transportation Research Board, Transportation Research Record **1825**(3):56-63.

van't Zand, J., and Moraal, J. 1997. Ballast Resistance Under Three-Dimensional Loading. Delft University of Technology, Delft, Netherlands.

Appendix I CN Rail’s (2003) Ballast Specifications

APPENDIX 'D'

CN CRUSHED ROCK BALLAST MATERIAL SPECIFICATION

12-20C
(July 2003)

Superseding
Specification
12-20B

CRUSHED ROCK BALLAST

1 SCOPE: This specification covers two classes of crushed rock ballast and one class of trowelling stone.

Class 1 - Crushed rock ballast for use primarily on main line track.

Class 2 - Crushed rock ballast for use only on other than main line track.

Trowelling stone shall be supplied in one class only.

GENERAL REQUIREMENTS

2 Material

2.1 The ballast and trowelling stone shall be composed of hard, strong and durable particles, clean and free from clay and shale and from an excess of dust or elongated pieces.

2.2 Before crushed rock ballast is accepted from any new pit, or from a new seam, bed or formation in any existing pit that in the judgement of the Inspector is substantially different from material previously inspected and approved, the material shall be inspected by a qualified petrologist and approved by the Senior Geotechnical Engineer of the Railway.

2.3 The word "Inspector" occurring in this specification shall mean the duly authorized representative of the Railways' Chief Engineer.

DETAILED REQUIREMENTS

3 Methods of Test

All tests shall be carried out according to the latest revision of the standard test methods referred to in this specification.

4 Fractured Faces

The crushed rock ballast or trowelling stone shall have at least 75% of the particles by mass with two or more fractured faces and at least 98% of the particles by mass with one fractured face. The above percentages will be required within each sieve size coarser than 3/4-inch (19 mm).

5 Flat Pieces

The crushed rock ballast or trowelling stone shall contain less than 30% by mass of flat pieces. In cases of dispute the test method "Determination of Flakiness Index" contained in British Standard 812 shall be used.

6 Absorption

The absorption of the ballast or trowelling stone shall be less than 0.5%. ASTM C 127

Note: Vertical bar on left margin indicates location of latest revision.

7 Soundness and Resistance to Abrasion

Property	Requirement		Tested in Accordance with ASTM Method	Testing Remarks
Soundness	Class 1 Ballast & Trowelling Stone	Class 2 Ballast	C 88	Coarse aggregate only, magnesium sulphate solution.
	Less than 7.0% at 5 cycles.	Less than 10.0% at 5 cycles.		
Abrasion Loss	Less than 20%.	Less than 30%.	C 535	ASTM Grading "2".

8 Grading

The ballast and trowelling stone shall conform to the grading requirements shown below.

% Passing by Mass

Sieve Size		Class 1 & 2 Ballast	Trowelling Stone
2-1/2"	(63 mm)	100	-
2"	(50 mm)	70-90	-
1-1/2"	(37.5 mm)	40-70	-
1"	(25 mm)	0-25	100
3/4"	(19 mm)	0-3	90-100
1/2"	(12.5 mm)	-	15-55
No. 4	(4.75 mm)	-	0-5
No. 200)	(0.75 mm	0-1	0-1

ASTM C 136
ASTM C 117 (for material passing the No. 200 sieve).

9 Ballast Resistivity

9.1 When tested as described in Appendix A, ballast resistivity shall not be less than 3000 ohm-meters.

10 Frequency of Testing

10.1 At the start of production the Producer shall carry out all tests described in Sections 4 to 9 inclusive to establish compliance with this specification.

10.2 During production the Producer shall carry out the grading test twice per day, the abrasion loss test once on each 10,000 metric tonnes of production, and all other tests once on each 30,000 metric tonnes of production thereafter. The ballast or trowelling stone shall be tested more frequently if there is any indication of a change in quality.

11.1 Ballast and trowelling stone shall be handled, stockpiled and/or loaded into cars in such a manner as to minimize the abrasion of particles and the segregation of sizes.

11.2 Under no circumstances shall rubber tired or crawler type vehicles be allowed to operate or traverse repeatedly over the stockpile of crushed material.

11.3 The handling and loading procedures shall have the prior approval of the Senior Geotechnical Engineer of the Railway.

12 Weighing

12.1 All ballast and trowelling stone delivered to the Railway shall be weighed by the Producer at his expense and proof of such weight shall be supplied to the Inspector.

12.2 All measurement shall be by actual weight in net tonnes (1000 kg).

12.3 The weighing device or method used must be approved by the Railway in writing. The Producer shall arrange for and obtain certification by the Weights and Measures Division of the Federal Department of Consumer and Corporate Affairs of any weighing device before it goes into service and thereafter as required by the Inspector. In no case shall calibration be done less than once after each 100,000 tonnes of production.

12.4 The accuracy of any weighing device may be checked by the Inspector at any time and should any discrepancies be found in the reading adjustments to the production quantities will be made by the Inspector.

QUALITY ASSURANCE

13 Application

Material ordered to this specification is subject to inspection by the Railway with respect to all the requirements of this specification.

14 Plant Access

The Inspector shall have, during working hours, free entry to all parts of the producer's plant and laboratory facilities used in the production or testing of material ordered to this specification.

15 Quality Assurance Provisions

It is the producer's responsibility to satisfy the Inspector that the ballast and trowelling stone conforms to this specification. This may be accomplished either by performing the tests (preferably on-site) prescribed in this specification or by demonstrating to the Inspector that the production, handling and stockpiling are so controlled that conformity to this specification is assured.

The Railway reserves the right to perform any of the tests set forth in the specification where such tests are deemed necessary to assure conformity to the prescribed requirements.

16 Test Samples

The incidence of sampling and the location at which samples are selected for testing by the Railway shall be at the discretion of the Inspector. The samples shall be taken in such a manner as to ensure that they truly represent the material being produced. The sample size for complete testing shall be not less than 50 kg.

17 Defective Material

Material which has been or is being produced which does not comply with this specification shall be rejected by the Inspector. The Producer shall stop further production until the fault has been corrected and shall dispose of all rejected material without cost to the Railway.

APPENDIX A

Ballast Resistivity Testing

1. Load ballast into the covered plexiglass resistivity box (see Diagram A below – minimum dimensions h=0.15m and L=0.2m). Ensure that the box is filled level. If necessary, shake the box to settle material.

2. Measure and record the resistance of the material as produced / received.

3. Record ambient temperature.

4. Using an atomizer, add de-ionized water 50 ml at a time waiting 3 minutes between applications until bottom of sample is wet. Water may not be allowed to accumulate at the base of the box. Record volume of water added and cover sample.

5. The resistivity of the material will decreases as water disperses through the sample. Record resistivity every hour for the first 6 hours and then take a minimum of three additional measurements over the next 36 hours.

6. Minimum resistivity will be calculated by multiplying the lowest recorded resistivity by the ballast box factor (h^2/L where h and L are the ballast box dimensions shown in Diagram A)

7. Replace sample and repeat test a minimum of 4 times. Ballast resistivity shall be the average of the minimum resistivity of all valid tests.

Appendix II Material Characterization Test Results

II.1 Sieve Analysis Results

II.2 Photogrammetry Analysis Results

II.3 Los Angeles Abrasion and Micro-Deval Test Results

Supporting tables and figures for Chapter 3 are included in this appendix, including the complete data set for the sieve analysis, photogrammetry analysis, Los Angeles Abrasion, and Micro-Deval tests.

II.1 Sieve Analysis Results

The results of the sieve analyses on the McAbee Ballast and Gravel ballast samples are tabulated in Tables II.1 and II.2, respectively.

Table II.1: Sieve analysis results for the McAbee Ballast samples

Sieve Size	Mass Retained on Sieve (Kg)													
	Bulk Sample													Representative Sample
	Individual Portions												Combined	
	1	2	3	4	5	6	7	8	9	10	11	12		
Sample Mass (Kg)	19.72	23.24	21.66	19.84	19.32	20.6	21.72	20.14	21.32	22.48	19.62	22.32	251.98	14.54
63.0 (2½ in)	0.38	0.00	0.00	0.00	0.00	0.00	0.00	0.00	0.00	0.00	0.00	0.00	0.38	0.00
50.0 (2 in)	2.54	2.82	1.68	1.44	0.68	1.08	1.56	1.12	1.12	0.64	0.96	1.32	16.96	1.26
37.5 (1½ in)	7.14	7.74	6.18	6.02	6.24	5.38	7.82	5.74	6.04	3.28	4.16	8.20	73.94	3.92
25.0 (1 in)	7.58	8.52	7.20	8.38	8.32	8.44	9.20	6.68	8.30	7.74	8.32	8.30	96.98	5.84
19.0 (¾ in)	1.16	1.98	2.30	2.24	2.10	2.52	1.94	2.10	2.56	3.26	2.90	1.90	26.96	1.74
12.5 (½ in)	0.54	1.18	2.42	1.22	1.40	1.84	0.84	2.14	2.14	3.42	2.40	1.44	20.98	1.36
9.5 (No. 4)	0.06	0.24	0.56	0.20	0.18	0.38	0.08	0.64	0.38	0.90	0.30	0.20	4.12	0.20
4.75 (No. 200)	0.02	0.22	0.42	0.08	0.08	0.28	0.04	0.54	0.30	1.00	0.16	0.10	3.24	0.18
												Total	243.56	14.50

Table II.2: Sieve analysis results for the Gravel Ballast samples

Sieve Size (mm)	Mass Retained on Sieve (Kg)													
	Bulk Sample													Representative Sample
	Individual Portions												Combined	
	1	2	3	4	5	6	7	8	9	10	11	12		
Sample Mass (Kg)	16.72	15.88	20.06	19.56	17.12	19.36	17.84	17.32	15.86	17.98	14.32	18.54	210.56	12.66
63.0 (2½ in)	0.00	0.00	0.00	0.00	0.00	0.00	0.00	0.00	0.00	0.00	0.00	0.00	0.00	0.00
50.0 (2 in)	0.00	0.30	0.20	0.00	0.00	0.00	0.46	0.24	0.40	0.00	0.00	0.22	1.82	0.27
37.5 (1½ in)	1.18	1.00	1.32	1.96	1.10	1.34	1.74	0.94	1.00	1.74	1.44	1.86	16.62	1.28
25.0 (1 in)	8.80	8.31	8.46	10.06	8.96	8.32	8.02	7.16	6.78	8.16	7.94	9.06	100.03	5.92
19.0 (¾ in)	4.62	4.16	5.90	4.96	4.96	6.12	4.76	5.60	4.84	5.38	4.18	5.06	60.54	3.64
12.5 (½ in)	1.83	1.83	3.70	2.25	1.79	2.82	2.50	2.92	2.38	2.30	0.58	2.04	26.95	1.32
9.5 (No. 4)	0.13	0.13	0.20	0.17	0.15	0.36	0.18	0.22	0.20	0.20	0.12	0.14	2.21	0.14
4.75 (No. 200)	0.04	0.02	0.07	0.00	0.02	0.14	0.04	0.10	0.02	0.06	0.04	0.04	0.59	0.04
												Total	208.76	12.61

The particle size distribution plots for the McAbee Ballast and Gravel Ballast samples are shown in Figures II.1 and II.2, respectively.

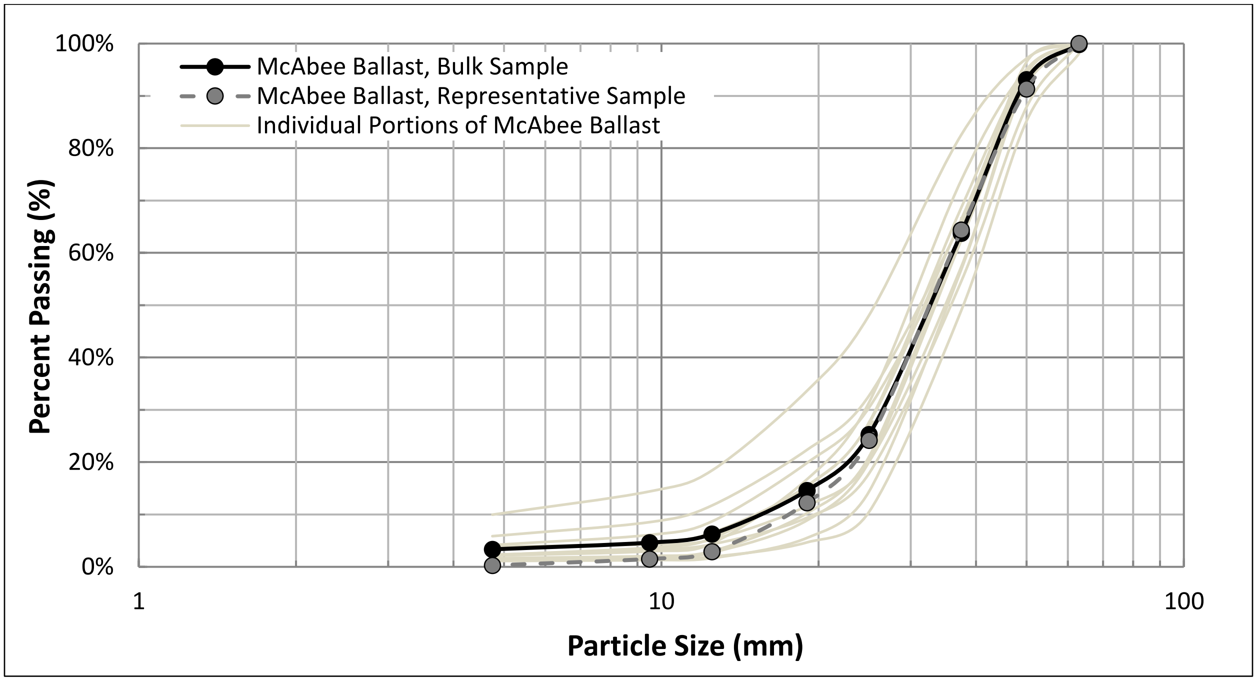

Figure II.1: Particle size distribution plots for the McAbee Ballast samples

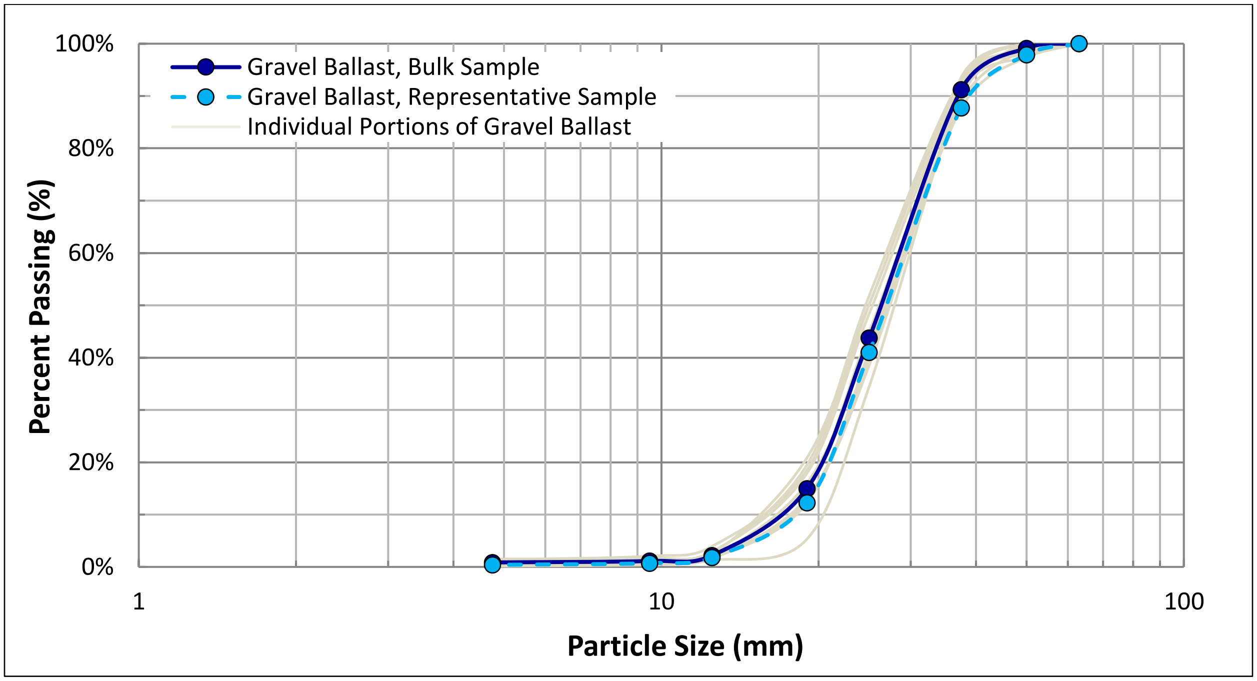

Figure II.2: Particle size distribution plots for the Gravel Ballast samples

II.2 Photogrammetry Analysis Results

II.2.1 Photographs of the McAbee Ballast

The three perpendicular photographs taken of each McAbee Ballast particle, in each size fraction, are presented in Figures II.3 through II.9.

 **(A) Photograph in x-direction**	 **(A) Photograph in x-direction**
 **(B) Photograph in y-direction**	 **(B) Photograph in y-direction**
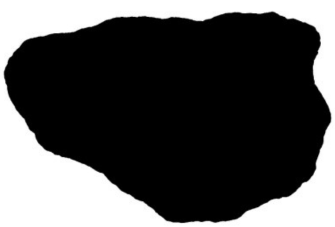 **(C) Photograph in z-direction**	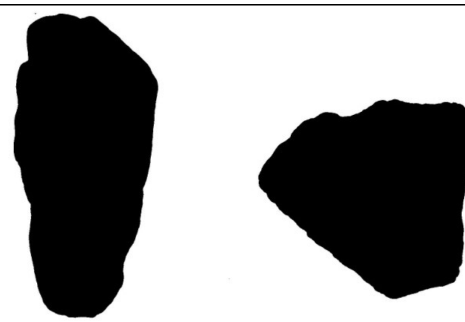 **(C) Photograph in z-direction**
Figure II.3: McAbee Ballast size fraction 1 (63.0 mm to 50.0 mm)	**Figure II.4: McAbee Ballast size fraction 2 (50.0 mm to 37.5 mm)**

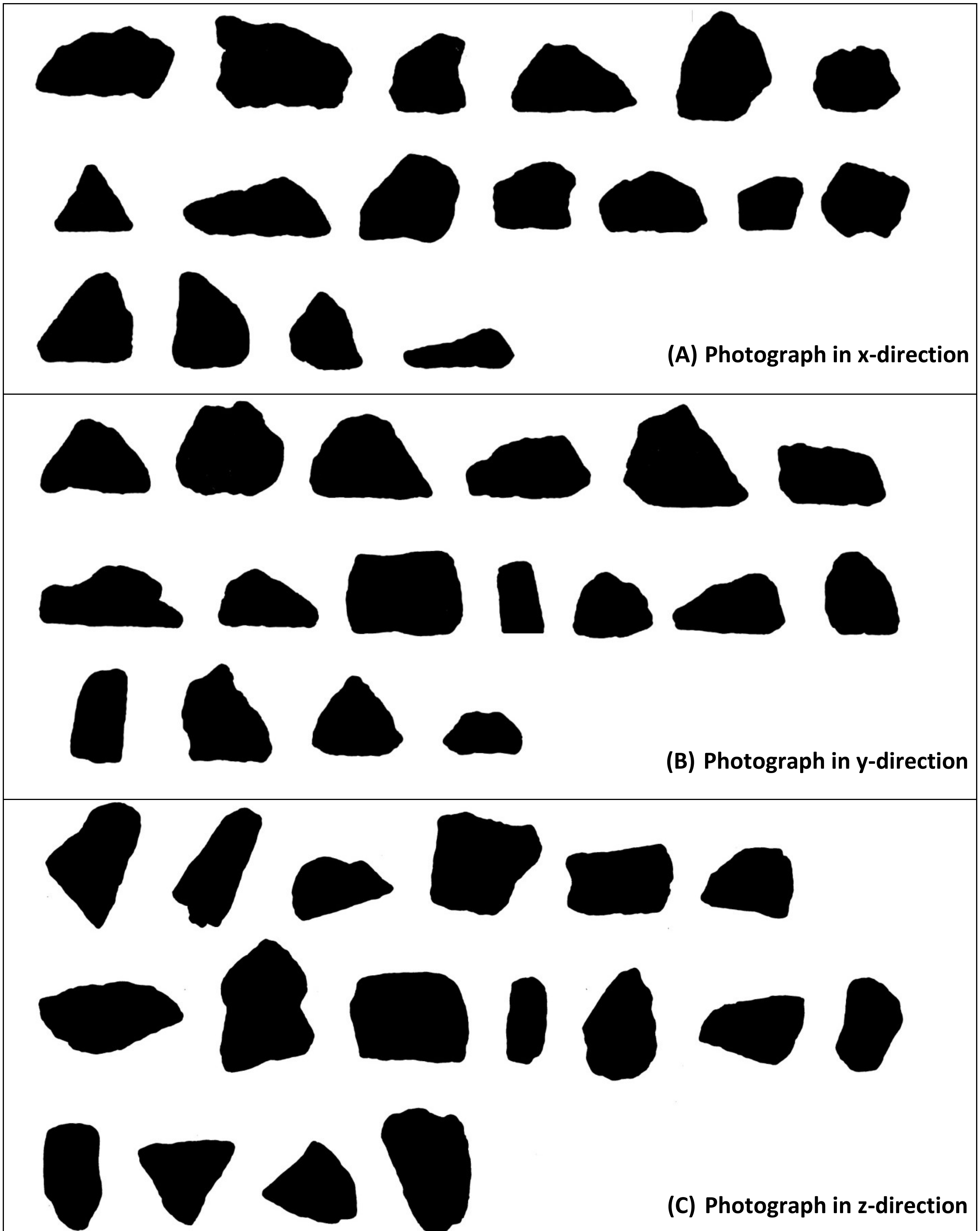

Figure II.5: McAbee Ballast size fraction 3 (37.5 mm to 25.0 mm)

(A) Photograph in x-direction

(B) Photograph in y-direction

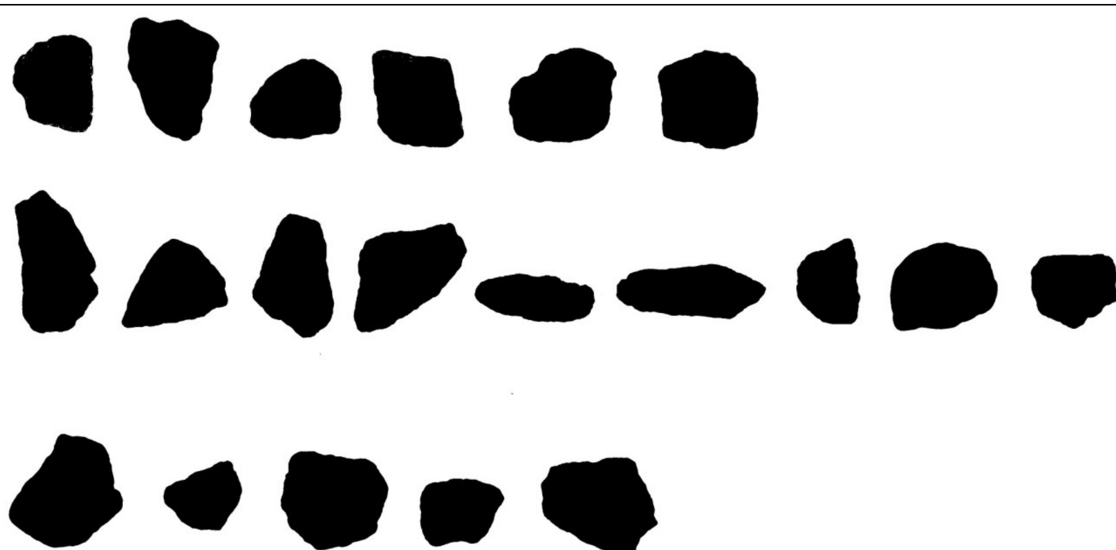

(C) Photograph in z-direction

Figure II.6: McAbee Ballast size fraction 4 (25.0 mm to 19.0 mm)

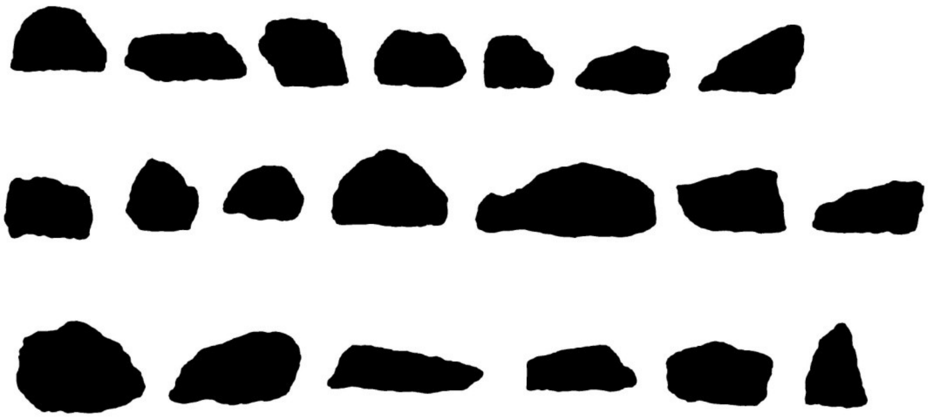

(A) Photograph in x-direction

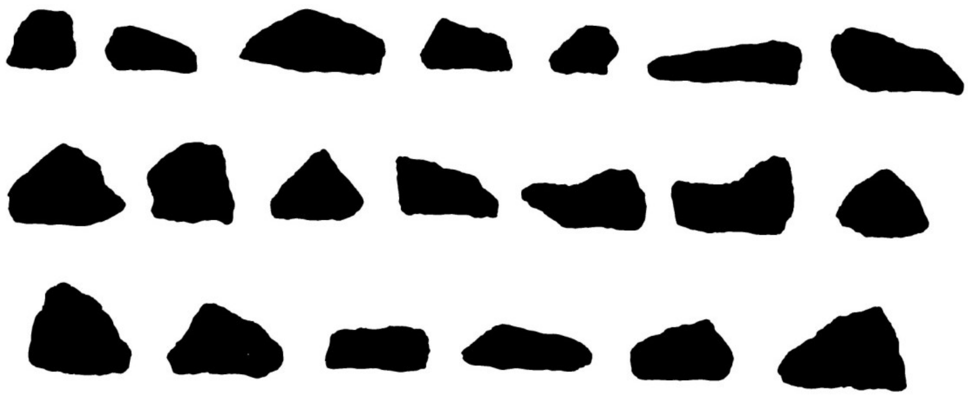

(B) Photograph in y-direction

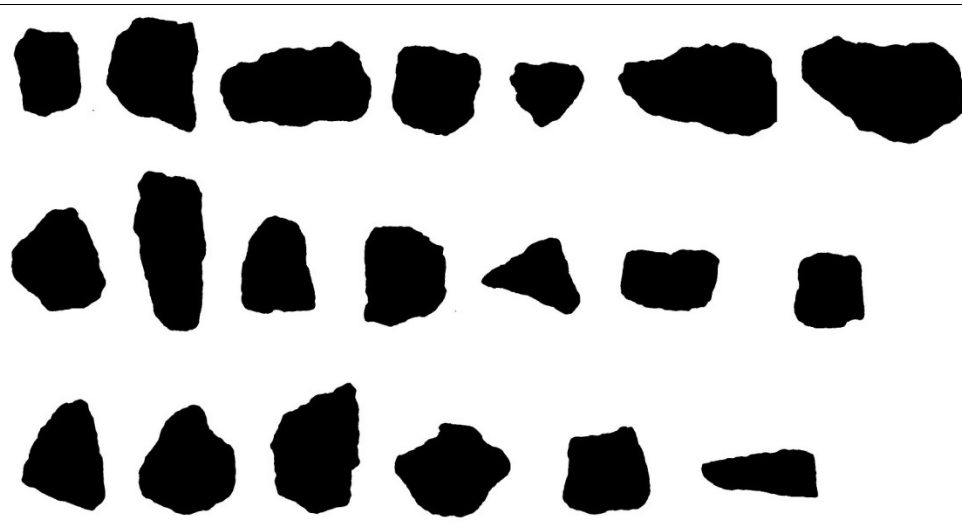

(C) Photograph in z-direction

Figure II.7: McAbee Ballast size fraction 5 (19.0 mm to 12.5 mm)

(A) Photograph in x-direction

(B) Photograph in y-direction

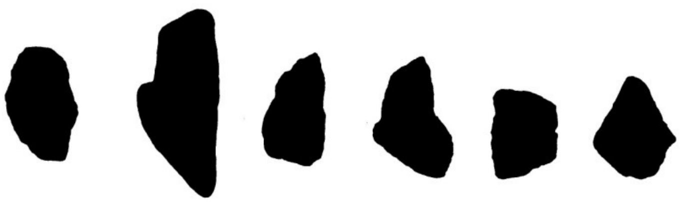

(C) Photograph in z-direction

Figure II.8: McAbee Ballast size fraction 6 (12.5 mm to 9.5 mm)

(A) Photograph in x-direction

(B) Photograph in y-direction

(C) Photograph in z-direction

Figure II.9: McAbee Ballast size fraction 7 (9.5 mm to 4.75 mm)

II.2.2 Photographs of the Gravel Ballast

The three perpendicular photographs taken of each Gravel Ballast particles, in each size fraction, are presented in Figures II.10 through II.16.

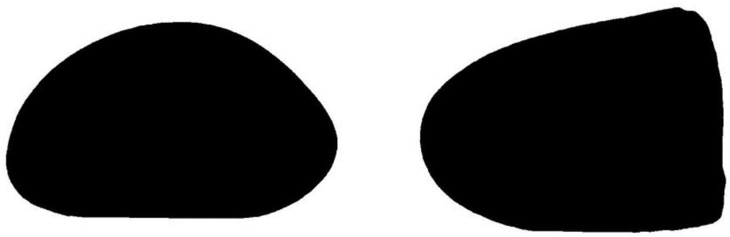

(A) Photograph in x-direction

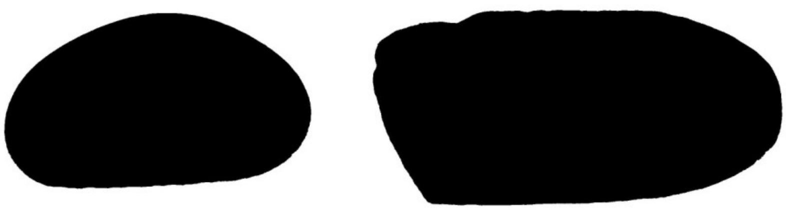

(B) Photograph in y-direction

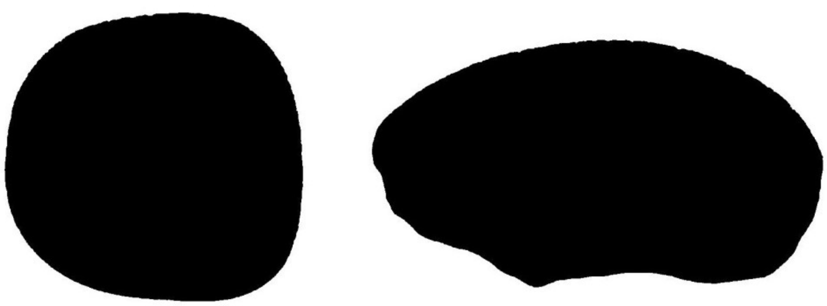

(C) Photograph in z-direction

Figure II.10: Gravel Ballast size fraction 1 (63.0 mm to 50.0 mm)

(A) Photograph in x-direction

(B) Photograph in y-direction

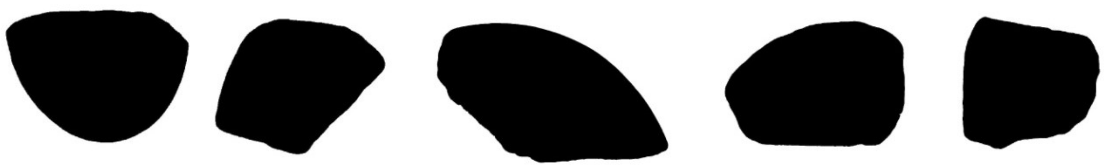

(C) Photograph in z-direction

Figure II.11: Gravel Ballast size fraction 2 (50.0 mm to 37.5 mm)

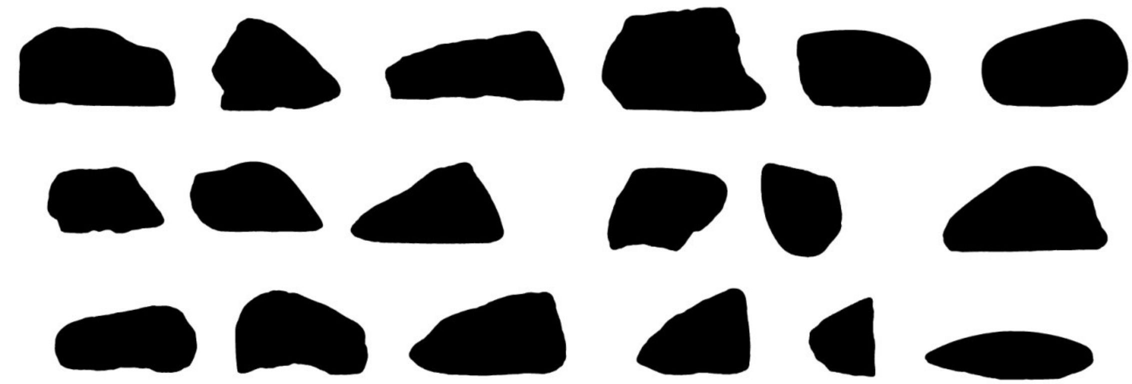

(A) Photograph in x-direction

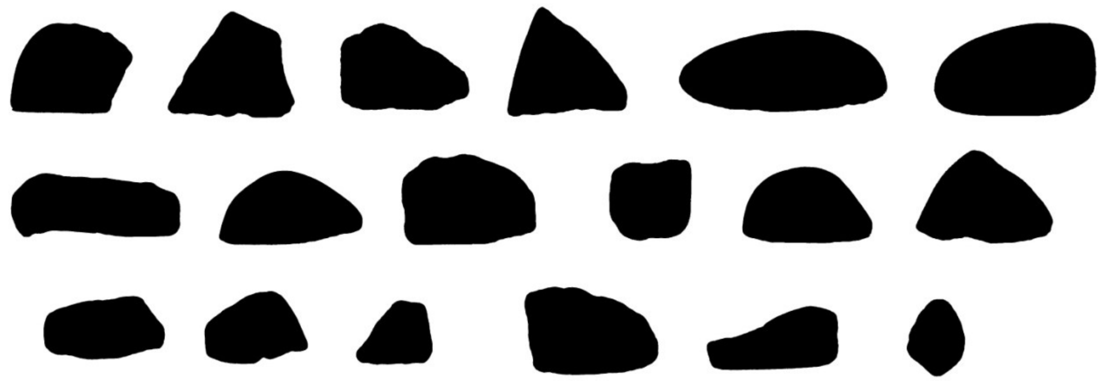

(B) Photograph in y-direction

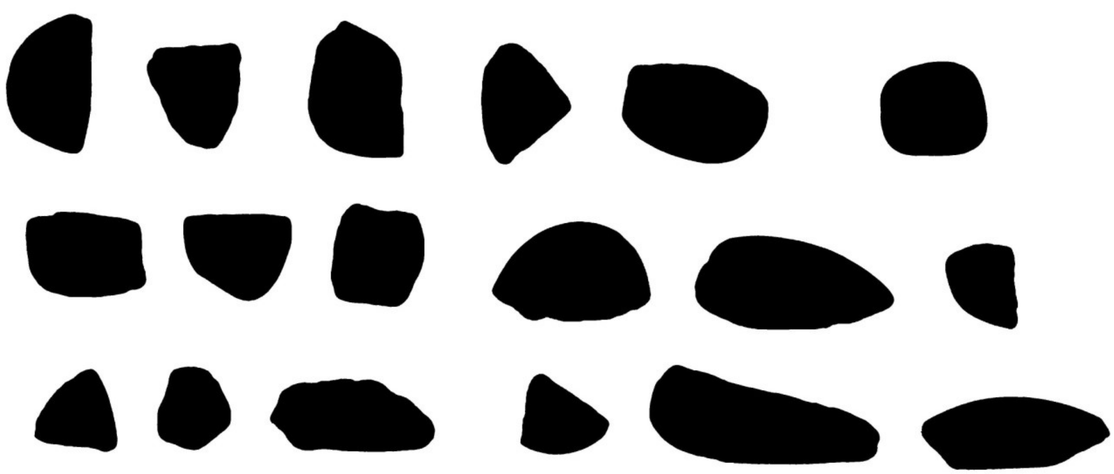

(C) Photograph in z-direction

Figure II.12: Gravel Ballast size fraction 3 (37.5 mm to 25.0 mm)

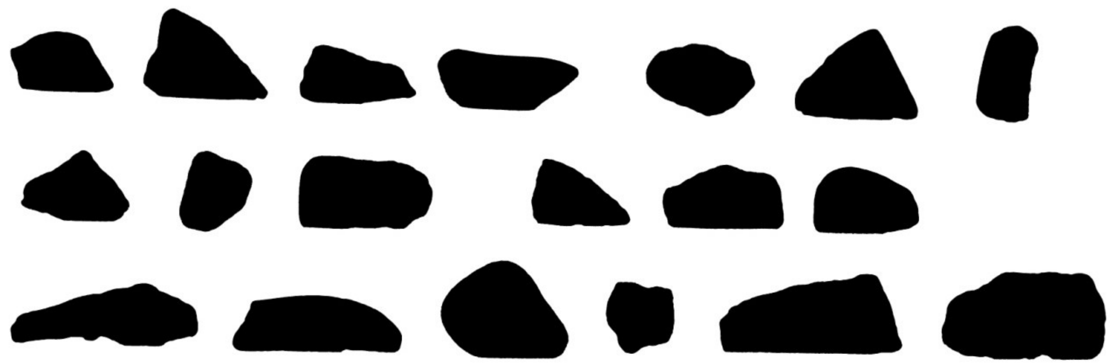

(A) Photograph in x-direction

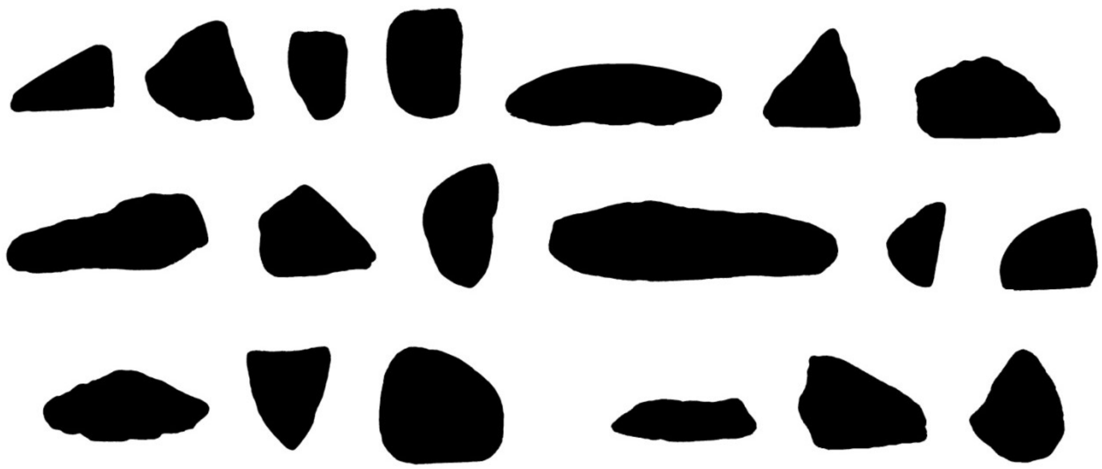

(B) Photograph in y-direction

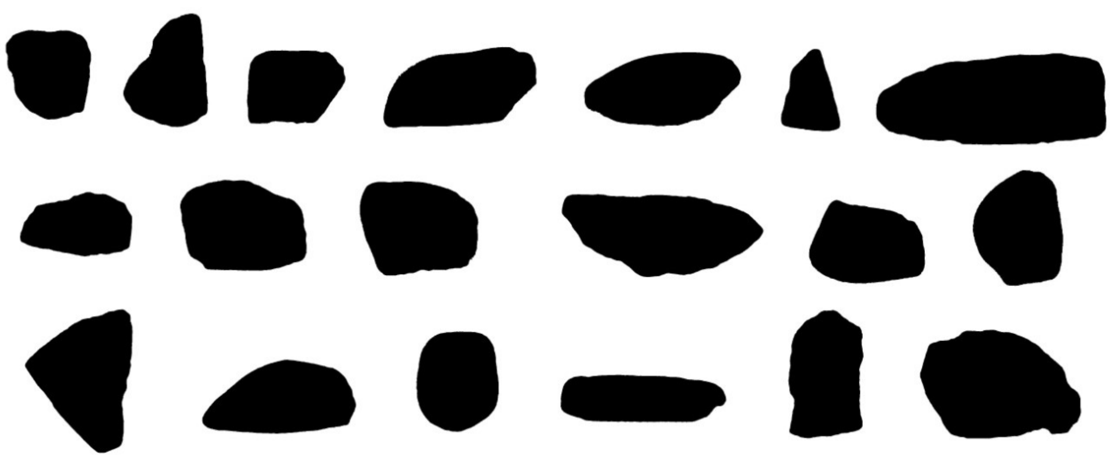

(C) Photograph in z-direction

Figure II.13: Gravel Ballast size fraction 4 (25.0 mm to 19.0 mm)

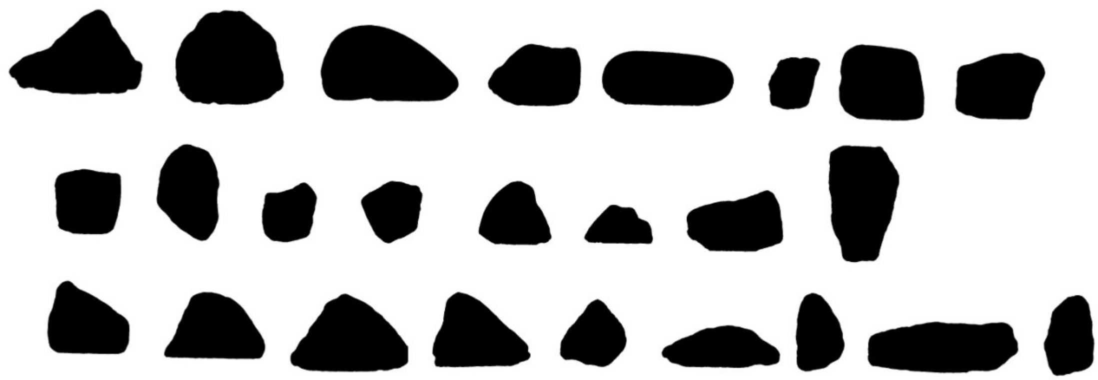

(A) Photograph in x-direction

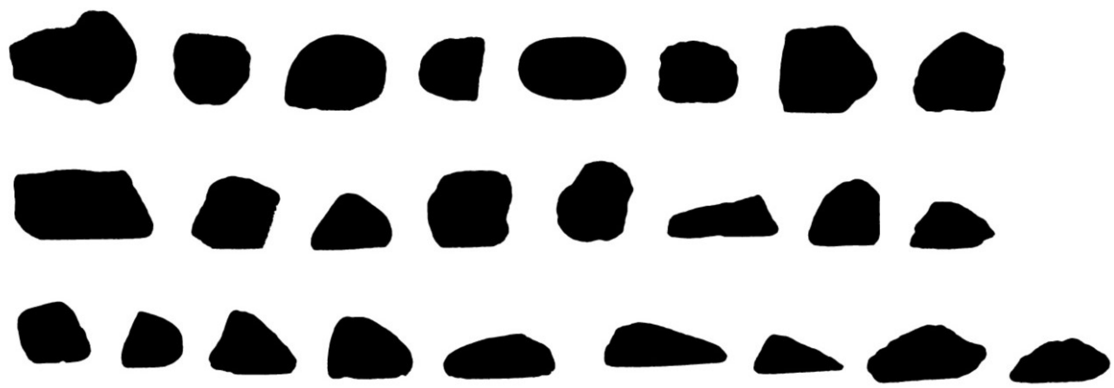

(B) Photograph in y-direction

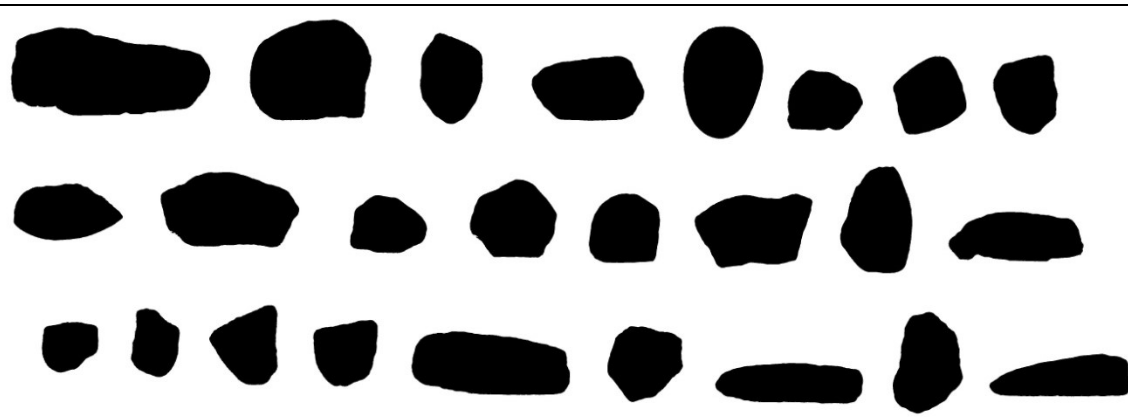

(C) Photograph in z-direction

Figure II.14: Gravel Ballast size fraction 5 (19.0 mm to 12.5 mm)

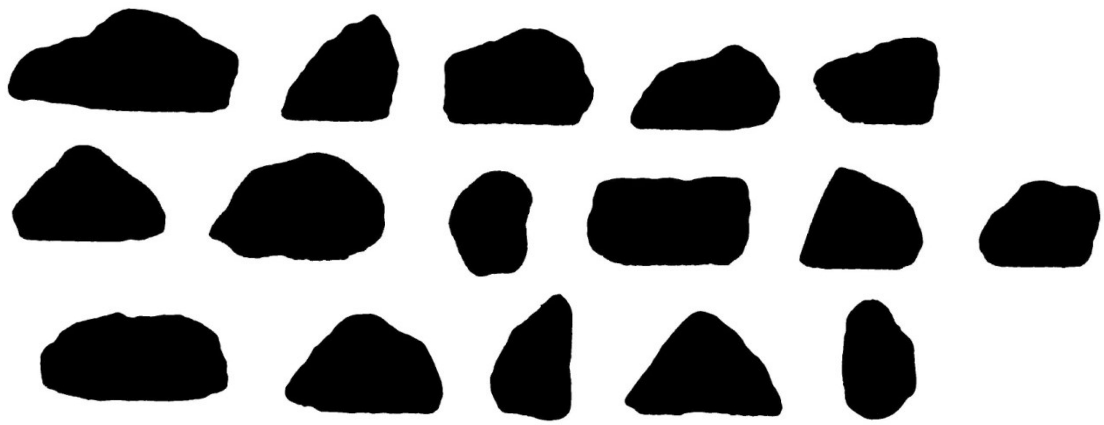

(A) Photograph in x-direction

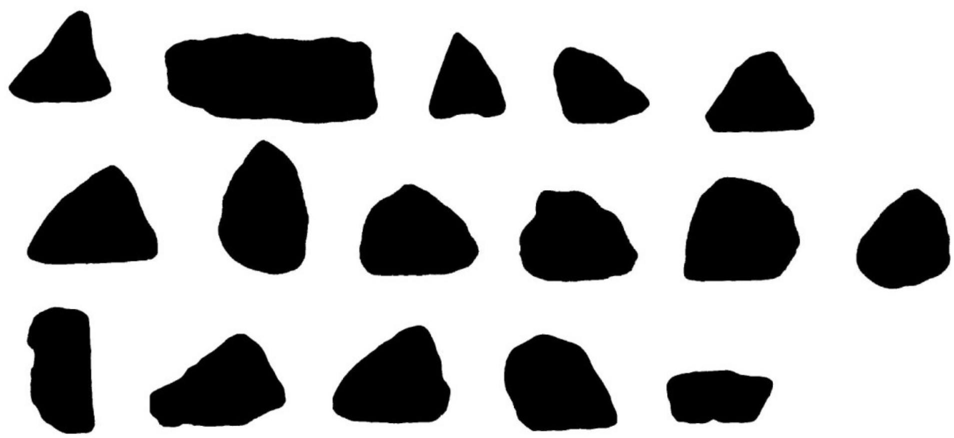

(B) Photograph in y-direction

(C) Photograph in z-direction

Figure II.15: Gravel Ballast size fraction 6 (12.5 mm to 9.5 mm)

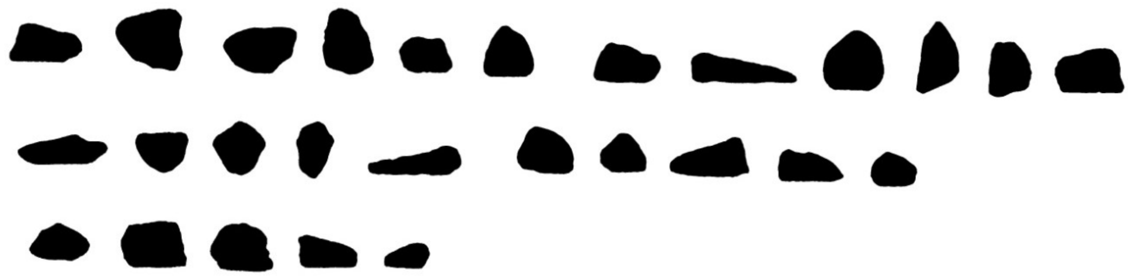

(A) Photograph in x-direction

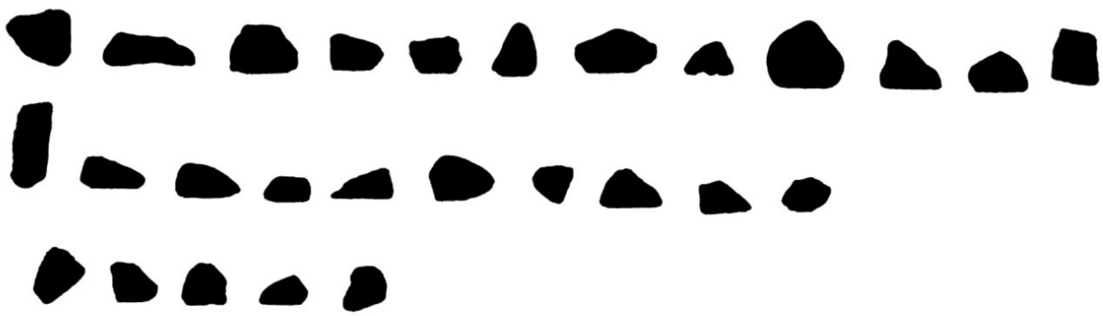

(B) Photograph in y-direction

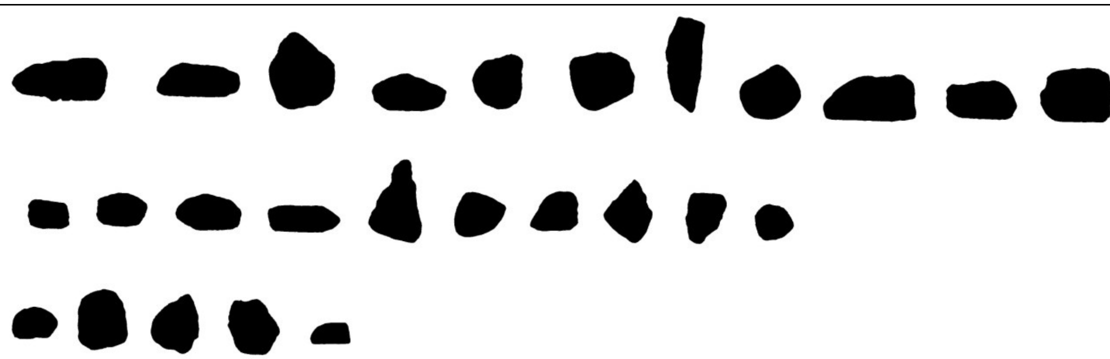

(C) Photograph in z-direction

Figure II.16: Gravel Ballast size fraction 7 (9.5 mm to 4.75 mm)

II.2.3 2D Form and Angularity Indices

The 2D form and angularity indices are plotted for each material and size fraction in Figures II.17 through II.19 and Figures II.20 through II.22 respectively.

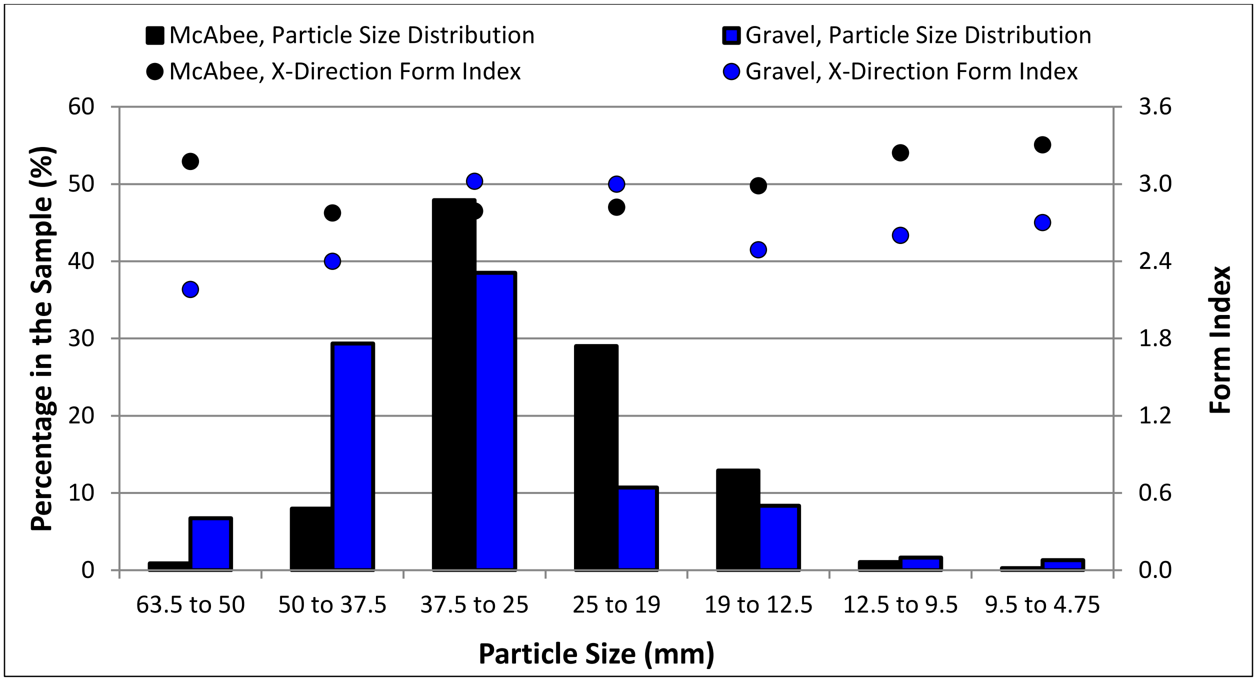

Figure II.17: 2D form index in the x-direction for the McAbee Ballast and Gravel Ballast samples

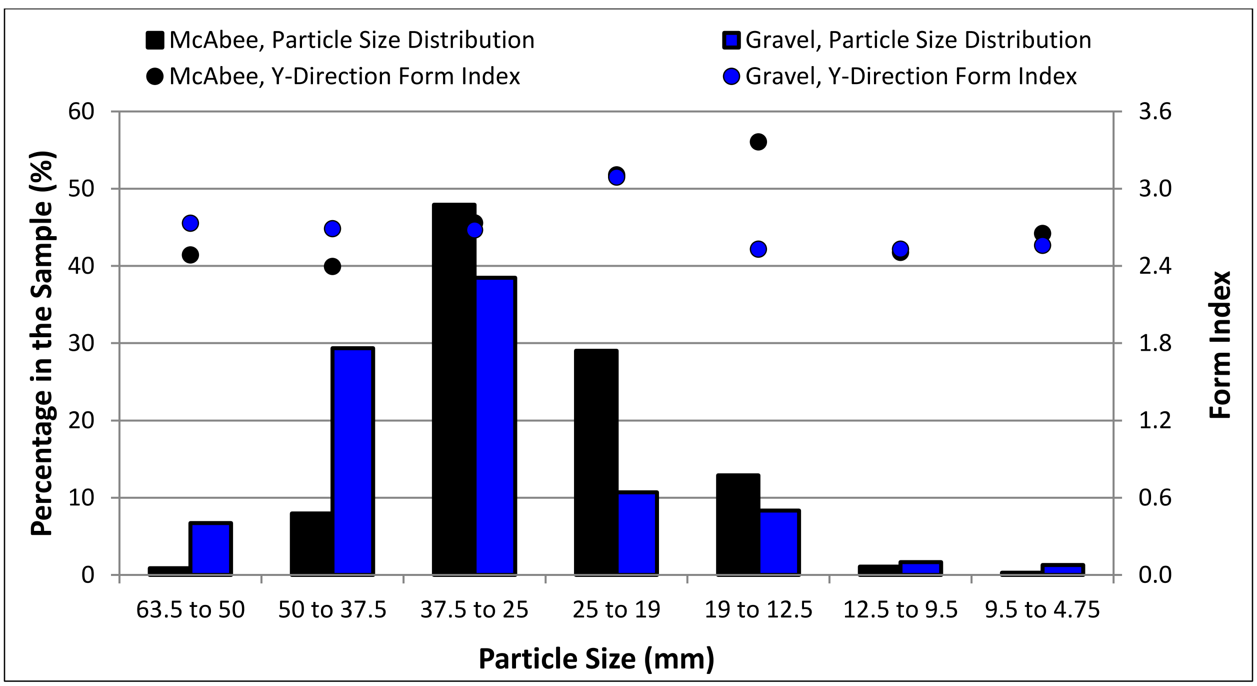

Figure II.18: 2D form index in the y-direction for the McAbee Ballast and Gravel Ballast samples

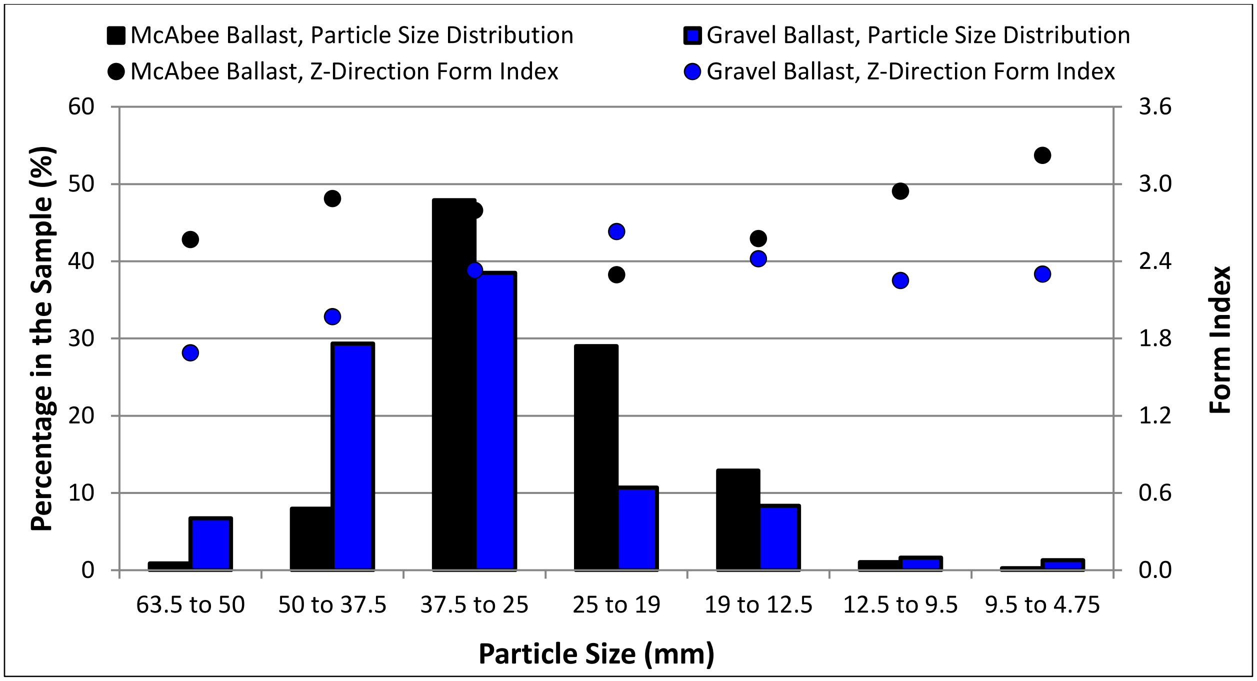

Figure II.20: 2D form index in the z-direction for the McAbee Ballast and Gravel Ballast samples

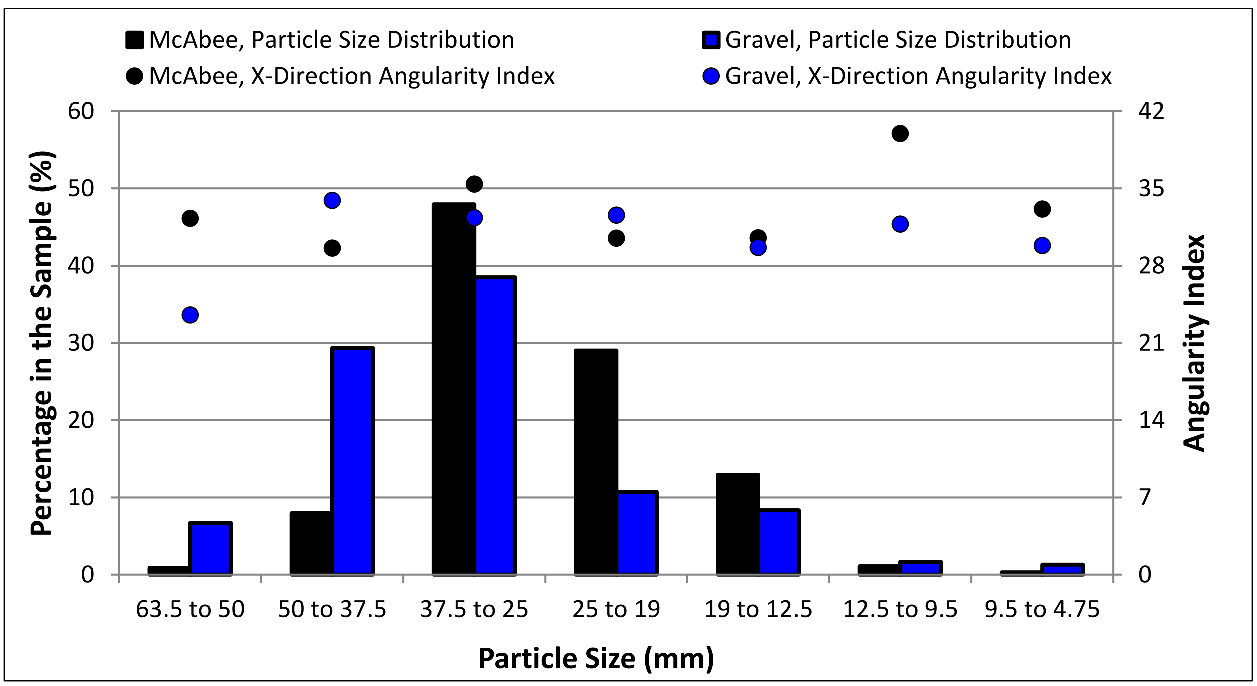

Figure II.20: 2D angularity index in the x-direction for the McAbee Ballast and Gravel Ballast samples

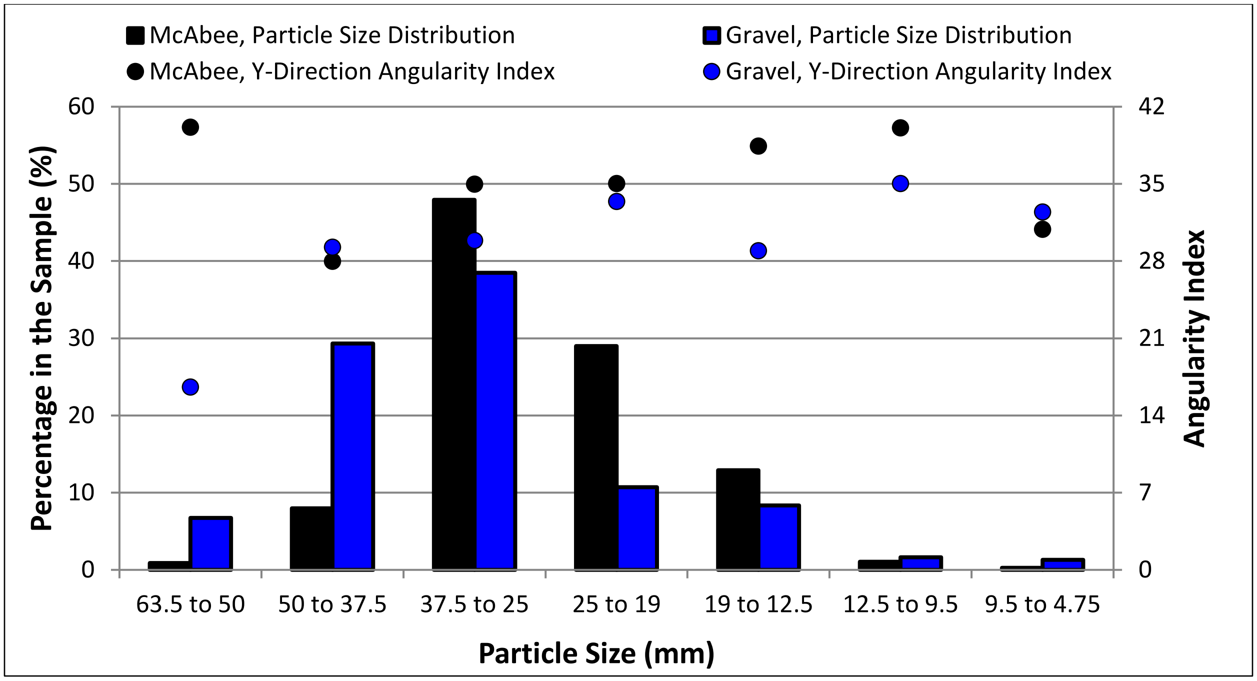

Figure II.21: 2D angularity index in the y-direction for the McAbee Ballast and Gravel Ballast samples

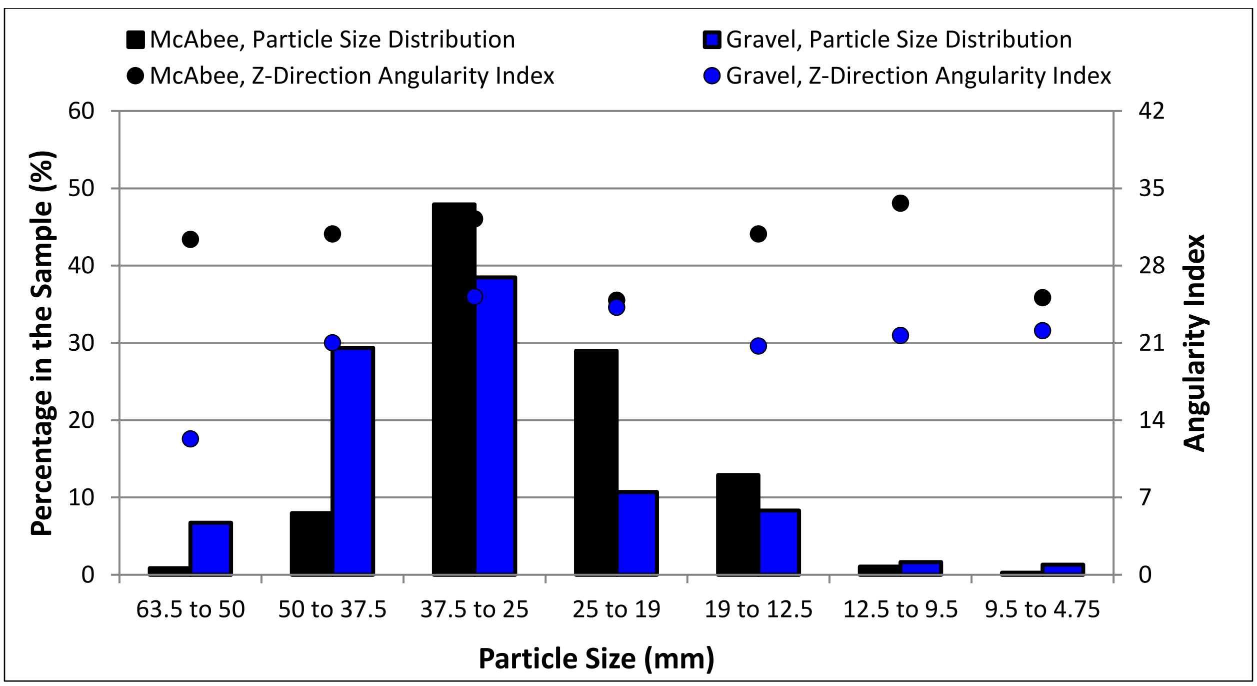

Figure II.22: 2D angularity index in the z-direction for the McAbee Ballast and Gravel Ballast samples

II.3 Los Angeles Abrasion and Micro-Deval Test Results

The Los Angeles Abrasion and Micro-Deval test results are tabulated in Tables II.3 and II.4, respectively.

Table II.3: Los Angeles Abrasion test results for the McAbee Ballast and Gravel Ballast samples

Material Type	Grading	Sample Number	Sample Mass (Kg)					Percent Loss (%)
			Initial				Final	
			Size Fraction (mm)			Total		
			50.0 – 37.5	37.5 – 25.0	25.0 – 19.0			
McAbee Ballast	2	1	4999.3	5003.5		10002.8	8733.8	12.7
	3	1	-	5000.5	5001.6	10002.1	8349.7	16.5
		2	-	4998.5	5000.7	9999.1	8376.1	16.2
		3	-	5002.8	4999.0	10001.8	8328.7	16.7
		4	-	5004.6	4996.8	10001.4	8303.9	17.0
		Average	-	-	-	-	-	16.6
Gravel Ballast	2	1	5000.25	4994.8	-	9995.0	8280.9	17.1
		2	5006.84	5004.6	-	10011.5	8170.5	18.4
		3	5003.06	4999.4	-	10002.4	8241.8	17.6
		4	4982.41	5020.2	-	10002.6	8383.5	16.2
		Average	-	-	-	-	-	17.3

Table II.4: Micro-Deval test results for the McAbee Ballast and Gravel Ballast samples

Material Type	Sample Number	Sample Mass (Kg)					Percent Loss (%)
		Initial				Final	
		Size Fraction (mm)			Total		
		19.0 - 16.0	16.0 - 12.5	12.5 - 9.5			
McAbee Ballast	1	374.83	375.22	750.30	1500.35	1440.93	4.0
	2	375.92	375.11	750.11	1501.14	1444.45	3.8
	3	375.70	374.97	750.20	1500.87	1443.37	3.8
	Average	-	-	-	-	-	3.9
Gravel Ballast	1	373.99	373.94	750.30	1498.72	1439.46	4.0
	2	375.67	375.34	750.11	1500.39	1424.63	5.0
	3	374.71	375.46	750.20	1500.31	1435.52	4.3
	Average	-	-	-	-	-	4.4

Appendix III Tie-Lateral Resistance Test Results

III.1 Supporting Tables for Chapter 5

III.2 Supporting Figures for Chapter 6

III.3 Load-Horizontal Displacement and Vertical Displacement-Horizontal Displacement Curves

Supporting tables and figures for Chapters 5 and 6 are included in this appendix, including load-displacement and vertical displacement-horizontal-displacement curves for each tie-lateral resistance test.

III.1 Supporting Tables for Chapter 5

The results of the Phase 1 base, Phase 2 crib, and Phase 3 shoulder tests are tabulated for the McAbee Ballast in Tables III.1 through III.3, and for the Gravel Ballast in Table III.4 through III.6. Tests excluded from the data set are typed in '~~grey~~' text.

Table III.1: Summary of the Phase 1 base test results in the McAbee Ballast

Test ID	Date of Test	Horizontal Loading Rate (mm/sec)	Average Applied Normal Load (kN)	Average Total Normal Load (kN)	Lateral Load Per Tie (kN)						Actual Peak Value		Limiting Peak Value		Comments
					Horizontal Displacement (mm)						Lateral Load Per Tie (kN)	Horizontal Displacement (mm)	Lateral Load Per Tie (kN)	Horizontal Displacement (mm)	
					0.5	1	2	5	10	20					
~~M_1A_10 (EXCLUDED)~~	~~23-Jun-15~~	~~0.05~~	~~10.3~~	~~14.0~~	~~4.5~~	~~5.7~~	~~7.1~~	~~8.7~~	~~9.2~~	~~9.8~~	~~10.1~~	~~20.7~~	~~0.0~~	~~0.0~~	~~Mechanical issues~~
M_1A_10	23-Jun-15	0.05	10.0	13.6	5.8	6.7	7.6	8.3	9.1	8.1	9.3	14.0	15.6	11.4	
M_1A_20	23-Jun-15	0.05	20.1	23.7	4.5	6.4	8.5	12.3	15.8	17.0	17.9	26.6	29.6	25.3	
~~M_1A_40 (EXCLUDED)~~	~~24-Jun-15~~	~~0.05~~	~~37.8~~	~~41.4~~	~~0.0~~	~~4.1~~	~~11.4~~	~~19.5~~	~~26.6~~	~~0.0~~	~~32.0~~	~~12.4~~	~~0.0~~	~~0.0~~	~~Mechanical issues~~
M_1A_40	24-Jun-15	0.05	40.0	43.6	11.7	15.3	20.3	27.2	30.1	29.5	31.0	14.7	51.2	9.9	
M_1A_80	24-Jun-15	0.05	80.0	83.7	15.0	21.2	27.9	40.3	50.7	56.4	56.9	25.3	96.1	19.5	
M_1A_160	24-Jun-15	0.05	160.0	163.7	21.3	31.3	42.6	68.6	90.2	107.0	111.4	44.2	187.0	23.2	
M_1A_10 (2)	25-Jun-15	0.05	9.9	13.5	3.3	4.9	6.4	7.8	8.3	8.0	8.8	13.4	14.8	12.8	
M_1A_5	25-Jun-15	0.05	5.0	8.6	2.6	3.6	4.3	5.2	5.6	5.7	6.3	35.1	10.5	34.6	
M_1B_160 (CYCLIC)	4-Feb-16	0.05	159.9	163.5	22.6	31.7	41.8	63.2	74.9	92.9	100.0	27.8	165.9	27.2	Unload-reload test
M_1B_160 (FAST)	10-Feb-16	0.50	159.9	163.5	21.5	30.6	43.7	67.4	82.3	93.0	97.3	48.9	159.0	19.5	Fast rate test
M_1B_160	10-Feb-16	0.05	159.8	163.4	20.1	29.4	40.9	62.0	80.9	96.7	99.9	28.6	168.0	25.7	
M_1B_80	10-Feb-16	0.05	79.9	83.5	13.7	18.9	26.3	37.8	44.3	49.1	52.6	29.3	84.8	23.2	
~~M_1B_10 (EXCLUDED)~~	~~10-Feb-16~~	~~0.05~~	~~9.9~~	~~13.6~~	~~2.7~~	~~3.7~~	~~4.7~~	~~6.1~~	~~5.7~~	~~5.9~~	~~7.6~~	~~32.3~~	~~0.0~~	~~0.0~~	~~Mechanical issues~~
M_1B_10	11-Feb-16	0.05	9.9	13.6	3.5	4.3	5.1	6.2	7.2	7.6	8.6	28.1	14.6	28.0	

Table III.2: Summary of the Phase 2 crib test results in the McAbee Ballast

Test ID	Date of Test	Horizontal Loading Rate (mm/sec)	Average Applied Normal Load (kN)	Average Total Normal Load (kN)	Lateral Load Per Tie (kN)						Actual Peak Value		Limiting Peak Value		Comments
					Horizontal Displacement (mm)						Lateral Load Per Tie (kN)	Horizontal Displacement (mm)	Lateral Load Per Tie (kN)	Horizontal Displacement (mm)	
					0.5	1	2	5	10	20					
M_2A_10	29-Jan-16	0.05	9.9	13.5	8.8	10.9	13.7	16.7	19.7	20.4	12.8	24.4	21.6	22.1	
~~M_2A_10 (2)~~	~~29-Jan-16~~	~~0.05~~	~~8.6~~	~~12.2~~	~~7.0~~	~~9.6~~	~~13.1~~	~~16.7~~	~~17.3~~	~~17.9~~	~~11.1~~	~~42.0~~	~~0.0~~	~~0.0~~	~~Verification test~~
~~M_2A_160 (EXCLUDED)~~	~~1-Feb-16~~	~~0.05~~	~~159.8~~	~~163.4~~	~~31.5~~	~~48.5~~	~~69.7~~	~~109.2~~	~~146.5~~	~~176.4~~	~~104.2~~	~~20.5~~	~~0.0~~	~~0.0~~	~~Mechanical issues~~
M_2A_160	1-Feb-16	0.05	159.9	163.5	46.8	75.5	110.4	163.5	187.9	196.1	116.1	26.0	195.0	18.7	
M_2A_80	2-Feb-16	0.05	79.9	83.5	25.5	33.7	45.3	62.0	75.8	89.2	54.8	21.6	92.1	21.4	
~~M_2A_80 (2)~~	~~2-Feb-16~~	~~0.05~~	~~79.9~~	~~83.5~~	~~33.1~~	~~46.6~~	~~65.0~~	~~88.5~~	~~91.3~~	~~89.8~~	~~55.5~~	~~16.7~~	~~0.0~~	~~0.0~~	~~Verification test~~
M_2B_160 (FAST)	17-Feb-16	0.50	159.9	163.5	40.8	54.7	76.6	116.7	149.5	169.0	101.4	42.1	169.7	21.5	
M_2B_160	17-Feb-16	0.05	160.0	163.6	47.2	76.1	117.2	161.6	168.9	170.4	102.8	25.0	172.4	22.0	
M_2B_10	22-Feb-16	0.05	9.8	13.4	7.7	9.7	11.6	14.4	15.4	17.1	11.0	38.2	17.2	16.6	
M_2B_80 (CYCLIC)	22-Feb-16	0.05	80.0	83.6	34.6	41.3	56.6	73.9	84.2	84.6	52.9	44.1	89.1	23.8	Unload-reload test

Table III.3: Summary of the Phase 3 shoulder test results in the McAbee Ballast

Test ID	Date of Test	Horizontal Loading Rate (mm/sec)	Average Applied Normal Load (kN)	Average Total Normal Load (kN)	Lateral Load Per Tie (kN)						Actual Peak Value		Limiting Peak Value		Comments
					Horizontal Displacement (mm)						Lateral Load Per Tie (kN)	Horizontal Displacement (mm)	Lateral Load Per Tie (kN)	Horizontal Displacement (mm)	
					0.5	1	2	5	10	20					
M_3A_10	10-Jun-16	0.05	10.0	13.6	0.5	0.7	0.9	1.4	2.2	2.1	2.4	16.9	2.3	10.2	
M_3A_80	10-Jun-16	0.05	80.0	83.6	0.6	0.7	1.0	1.6	2.0	2.1	2.5	48.1	2.1	8.0	
M_3A_160	10-Jun-16	0.05	160.0	163.6	0.9	1.1	1.3	1.9	2.3	2.0	2.7	14.1	2.5	7.9	
M_3A_160 (FAST)	10-Jun-16	0.50	160.0	163.6	0.9	1.1	1.3	1.6	2.3	2.2	5.4	42.5	2.6	21.6	Fast rate test
M_3A_10 (2)	10-Jun-16	0.05	10.1	13.7	0.6	0.8	1.0	1.6	2.1	2.4	2.6	25.8	2.5	20.2	
M_3A_80 (2)	10-Jun-16	0.05	79.8	83.5	0.6	0.8	0.9	1.4	1.9	2.4	2.5	23.7	2.4	18.7	
M_3A_160 (2)	10-Jun-16	0.05	159.8	163.5	0.6	0.7	0.8	1.2	1.6	1.9	2.1	20.5	1.9	8.7	
M_3B_10	9-Jun-16	0.05	9.9	13.6	0.6	0.8	1.1	1.7	2.0	2.5	3.0	27.5	2.7	21.6	
M_3B_80	9-Jun-16	0.05	79.9	83.5	0.3	0.5	0.8	1.1	1.7	2.0	2.5	22.1	2.1	21.4	
M_3B_160	9-Jun-16	0.05	159.9	163.5	0.2	0.5	0.6	1.1	1.4	1.4	2.7	22.3	2.5	18.0	
M_3B_160 (FAST)	9-Jun-16	0.50	159.9	163.6	0.8	0.7	0.6	1.7	1.8	2.0	8.0	50.5	2.4	18.5	Fast rate test
M_3B_10 (2)	9-Jun-16	0.05	9.9	13.5	0.7	0.9	1.2	1.8	2.2	2.5	2.9	14.1	2.6	13.4	
M_3B_80 (2)	9-Jun-16	0.05	80.0	83.6	0.5	0.3	0.8	1.1	2.0	2.7	3.3	42.2	3.0	17.4	
M_3B_160 (2)	10-Jun-16	0.05	160.1	163.7	1.1	1.3	1.4	2.3	2.7	3.1	3.3	17.6	3.2	17.5	

Table III.4: Summary of the Phase 1 base test results in the Gravel Ballast

Test ID	Date of Test	Horizontal Loading Rate (mm/sec)	Average Applied Normal Load (kN)	Total Normal Load (kN)	Lateral Load Per Tie (kN)						Actual Peak Value		Limiting Peak Value		Comments
					Horizontal Displacement (mm)						Lateral Load Per Tie (kN)	Horizontal Displacement (mm)	Lateral Load Per Tie (kN)	Horizontal Displacement (mm)	
					0.5	1	2	5	10	20					
G_4A_10	14-Aug-15	0.05	9.7	13.4	6.7	8.0	9.6	11.2	11.8	13.8	8.4	22.6	13.6	20.0	Sensitivity test
G_4A_10 (2)	14-Aug-15	0.05	9.9	13.5	7.6	9.2	11.2	13.4	14.0	14.9	9.3	24.8	15.6	22.3	Sensitivity test
G_4A_10 (3)	17-Aug-15	0.05	9.9	13.5	3.2	4.7	6.4	9.9	12.6	14.6	9.7	34.7	15.3	22.7	
G_4A_20	17-Aug-15	0.05	20.1	23.7	9.5	12.5	15.2	20.8	22.7	22.7	14.0	18.9	23.1	9.6	
~~G_4A_40 (EXCLUDED)~~	~~18-Aug-15~~	~~0.05~~	~~39.8~~	~~43.4~~	~~15.9~~	~~21.6~~	~~27.7~~	~~36.8~~	~~42.4~~	~~46.8~~	~~30.8~~	~~35.1~~	~~0.0~~	~~0.0~~	~~Mechanical issues~~
G_4A_40	18-Aug-15	0.05	39.9	43.5	17.4	21.5	27.8	38.1	46.8	47.5	28.8	35.6	47.3	10.5	
G_4A_80	19-Aug-15	0.05	79.9	83.5	15.7	26.3	38.7	61.1	79.9	91.7	54.6	23.3	92.0	19.5	
G_4A_160	19-Aug-15	0.05	159.8	163.5	43.8	53.7	71.5	101.6	128.2	149.7	96.5	38.0	159.8	29.2	
G_4A_10 (4)	20-Aug-15	0.05	9.9	13.5	3.6	5.4	7.4	11.4	13.5	15.6	9.7	26.9	16.0	19.7	
G_4A_5	20-Aug-15	0.05	4.8	8.4	3.4	4.4	5.1	6.7	8.4	8.3	5.4	40.3	9.0	24.9	
G_5_20 (FAST)	25-Aug-15	0.50	19.8	23.5	9.5	12.5	15.2	20.8	22.7	22.7	14.0	18.9	23.1	9.6	
G_5_160 (FAST)	25-Aug-15	0.50	159.8	163.4	33.3	52.8	69.6	105.2	141.8	171.2	100.9	22.9	168.3	17.8	
~~G_5_160 (FAST) (2)~~	~~25-Aug-15~~	~~0.50~~	~~159.9~~	~~163.5~~	~~27.7~~	~~43.6~~	~~64.4~~	~~103.2~~	~~128.6~~	~~158.6~~	~~101.6~~	~~39.3~~	~~0.0~~	~~0.0~~	Fast rate test
G_5_10 (FAST)	25-Aug-15	0.50	9.9	13.6	4.5	5.8	8.4	10.4	12.1	13.2	8.7	27.3	14.1	22.0	
G_5_80 (FAST)	25-Aug-15	0.50	79.8	83.4	17.9	24.8	37.6	56.5	71.1	79.0	48.7	31.1	79.2	20.0	
G_4B_160	11-Mar-16	0.05	159.8	163.5	56.9	89.6	113.7	129.7	140.5	135.7	83.4	31.7	138.6	9.3	
G_4B_160 (FAST)	11-Mar-16	0.50	159.8	163.4	36.0	48.9	67.8	100.6	119.3	133.5	80.8	44.1	131.8	16.2	Fast rate test
G_4B_80	15-Mar-16	0.05	79.7	83.3	21.6	32.5	43.6	63.1	73.6	77.8	48.2	37.5	79.2	17.1	
G_4B_10	15-Mar-16	0.05	9.7	13.3	7.2	8.9	10.1	10.8	11.1	11.0	7.3	40.1	11.4	8.2	
G_4B_160 (CYCLIC)	16-Mar-16	0.05	159.8	163.4	38.7	53.0	74.6	108.8	132.5	136.2	82.8	44.4	138.9	28.0	Unload-reload test

Table III.5: Summary of the Phase 2 crib test results in the Gravel Ballast

Test ID	Date of Test	Horizontal Loading Rate (mm/sec)	Average Applied Normal Load (kN)	Total Normal Load (kN)	Lateral Load Per Tie (kN)						Actual Peak Value		Limiting Peak Value		Comments
					Horizontal Displacement (mm)						Lateral Load Per Tie (kN)	Horizontal Displacement (mm)	Lateral Load Per Tie (kN)	Horizontal Displacement (mm)	
					0.5	1	2	5	10	20					
G_6A_10	9-Mar-16	0.05	9.7	13.3	9.5	11.0	12.2	13.8	13.7	15.9	9.5	17.8	15.8	16.3	
G_6A_80	10-Mar-16	0.05	79.8	83.4	22.0	29.8	41.2	61.5	77.2	85.0	51.0	23.6	84.5	19.7	
G_6A_160	11-Mar-16	0.05	159.9	163.5	37.3	56.4	81.4	114.6	140.6	154.0	95.6	30.0	158.1	23.3	
G_6B_160 (FAST)	17-Mar-16	0.50	160.1	163.7	32.6	51.3	74.2	113.1	139.6	145.1	87.0	27.0	144.8	19.9	Fast rate test
~~G_6B_80 (EXCLUDED)~~	~~17-Mar-16~~	~~0.05~~	~~79.8~~	~~83.4~~	~~18.3~~	~~27.0~~	~~40.1~~	~~60.7~~	~~69.9~~	~~9.2~~	~~41.6~~	~~12.7~~	~~0.0~~	~~0.0~~	~~Mechanical issues~~
G_6B_80 (CYCLIC)	18-Mar-16	0.05	79.9	83.5	20.1	29.1	42.9	54.6	68.4	74.3	46.0	34.4	74.1	33.6	Unload-reload test
G_6B_10	18-Mar-16	0.05	10.0	13.6	8.0	9.2	10.8	12.4	14.4	15.2	9.7	29.0	15.8	21.3	
G_6B_160	18-Mar-16	0.05	159.9	163.5	75.4	88.1	100.4	119.1	131.7	138.6	83.7	26.4	139.1	15.3	

Table III.6: Summary of the Phase 3 shoulder test results in the Gravel Ballast

Test ID	Date of Test	Horizontal Loading Rate (mm/sec)	Average Applied Normal Load (kN)	Total Normal Load (kN)	Lateral Load Per Tie (kN)						Actual Peak Value		Limiting Peak Value		Comments
					Horizontal Displacement (mm)						Lateral Load Per Tie (kN)	Horizontal Displacement (mm)	Lateral Load Per Tie (kN)	Horizontal Displacement (mm)	
					0.5	1	2	5	10	20					
G_7A_10	3-Jun-16	0.05	9.9	13.5	0.5	0.6	0.8	1.2	1.5	1.5	1.7	38.3	1.6	9.2	
G_7A_160	3-Jun-16	0.05	159.9	163.6	0.9	1.2	1.2	1.4	1.9	1.7	2.3	29.2	2.0	10.1	
G_7A_160 (FAST)	3-Jun-16	0.50	159.9	163.5	0.5	0.6	0.7	1.4	1.1	1.7	2.3	45.8	2.0	14.0	Fast rate test
G_7A_80	7-Jun-16	0.05	79.9	83.5	0.2	0.3	0.6	0.7	1.3	1.4	2.3	49.9	1.8	39.5	
G_7A_10 (2)	7-Jun-16	0.05	9.9	13.5	0.3	0.5	0.7	1.3	1.8	1.5	2.4	27.4	2.2	24.7	
G_7A_160 (2)	7-Jun-16	0.05	159.8	163.4	0.6	0.5	0.5	0.8	1.1	1.2	2.0	42.6	1.8	41.2	
G_7A_80 (2)	7-Jun-16	0.05	79.8	83.4	0.6	0.6	0.6	0.8	1.1	1.8	2.4	36.9	2.2	32.3	
G_7B_160	3-Jun-16	0.05	159.9	163.5	1.5	1.5	1.6	2.0	2.4	2.3	2.9	16.9	2.7	15.6	
G_7B_10	3-Jun-16	0.05	9.9	13.5	0.5	0.7	1.1	2.0	2.4	2.7	3.0	33.4	2.8	29.4	
G_7B_160 (FAST)	3-Jun-16	0.50	159.9	163.5	0.5	0.6	0.7	0.7	1.3	2.4	3.3	55.6	3.0	28.1	Fast rate test
G_7B_80	7-Jun-16	0.05	79.8	83.4	0.2	0.3	0.5	0.9	1.5	1.5	2.5	34.3	2.3	27.9	
G_7B_80(2)	7-Jun-16	0.05	80.0	83.6	0.3	0.3	0.6	0.7	1.4	1.8	4.0	48.4	3.5	44.2	
G_7B_10(2)	7-Jun-16	0.05	10.0	13.6	0.4	0.7	1.0	1.9	2.7	3.6	4.3	29.8	4.0	22.3	
G_7B_160(2)	7-Jun-16	0.05	159.9	163.5	0.6	0.6	0.7	0.7	1.4	2.5	3.3	43.7	2.9	22.5	

III.2 Supporting Figures for Chapter 6

The percent contribution of the base friction, crib friction, and shoulder resistance to overall tie-lateral resistance is presented in Figure III.1 and Figure III.2 for the tie-lateral resistance tests completed under a normal load of 10 kN and 160 kN at a loading rate of 0.05 mm/sec.

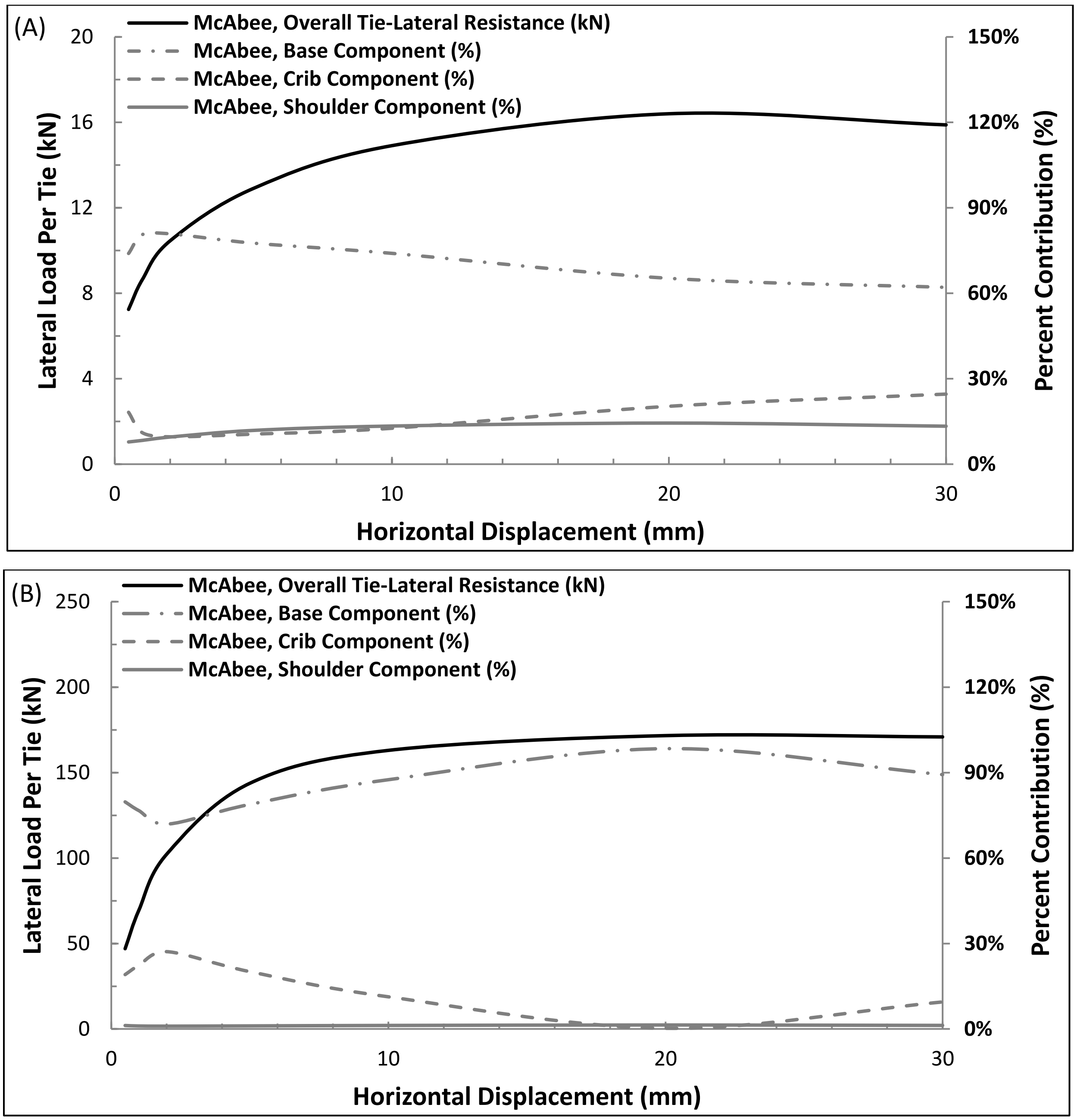

Figure III.1: Percent contribution of each component of tie-lateral to overall tie-lateral resistance for tests completed in the McAbee Ballast under a normal load of (A) 10 kN and (B) 160 kN at a loading rate of 0.05 mm/sec

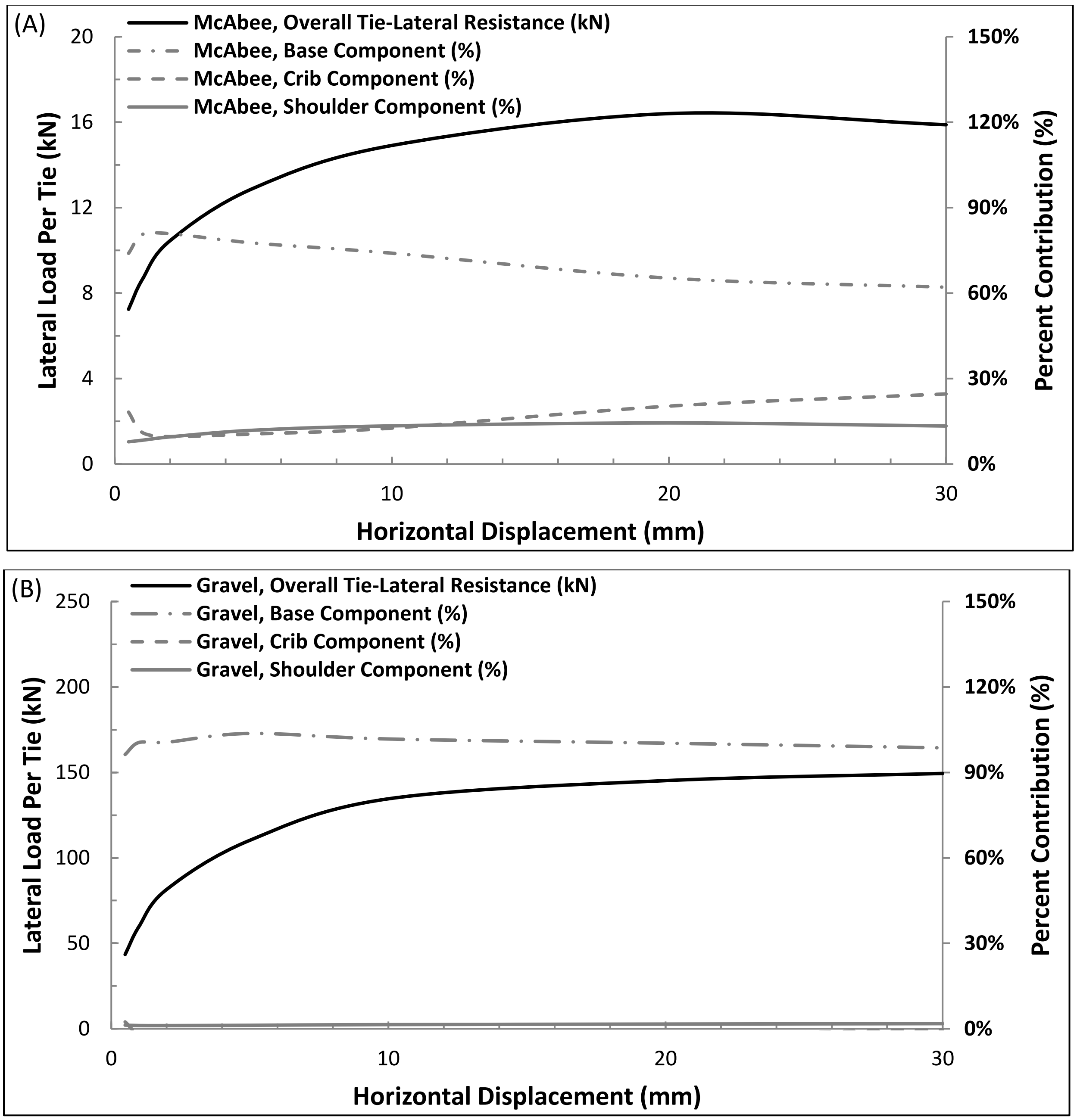

Figure III.2: Percent contribution of each component of tie-lateral to overall tie-lateral resistance for tests completed in the Gravel Ballast under a normal load of (a) 10 kN and (b) 160 kN at a loading rate of 0.05 mm/sec

III.3 Load-Horizontal Displacement, and Vertical Displacement-Horizontal Displacement Curves

Load-horizontal displacement and vertical displacement-horizontal displacement curves (if applicable) are presented in the following subsections for each material and test configuration.

III.3.1 Phase 1 base tests results in the McAbee Ballast

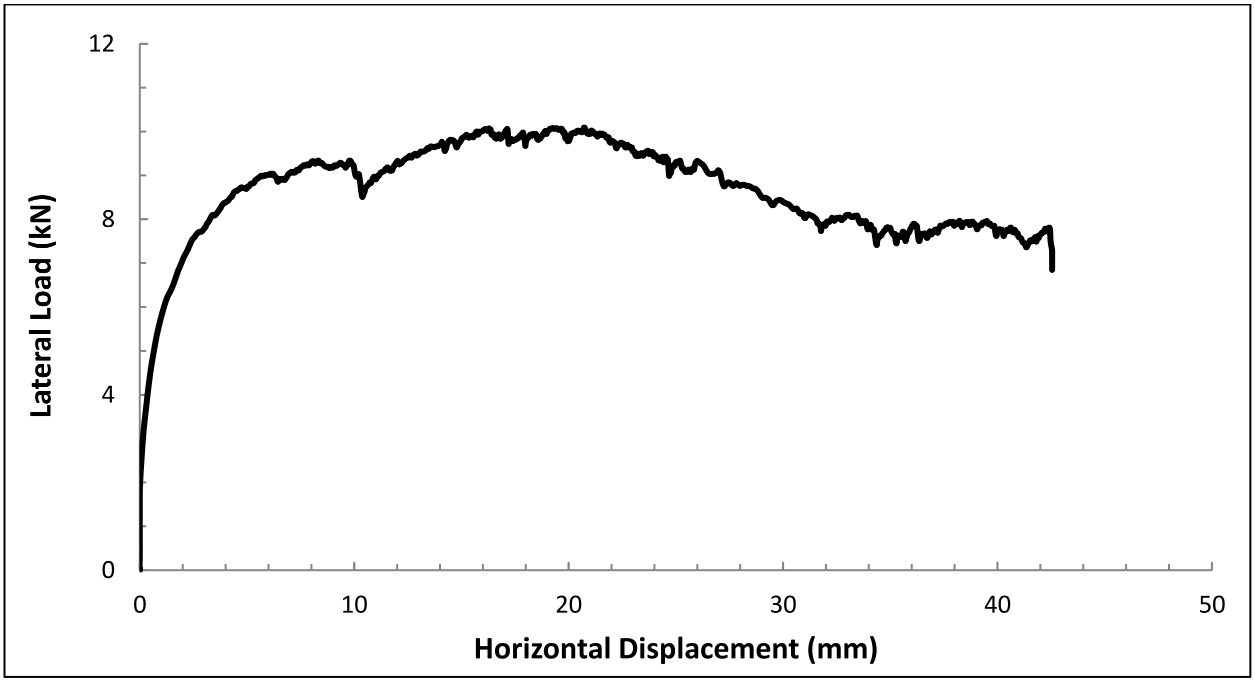

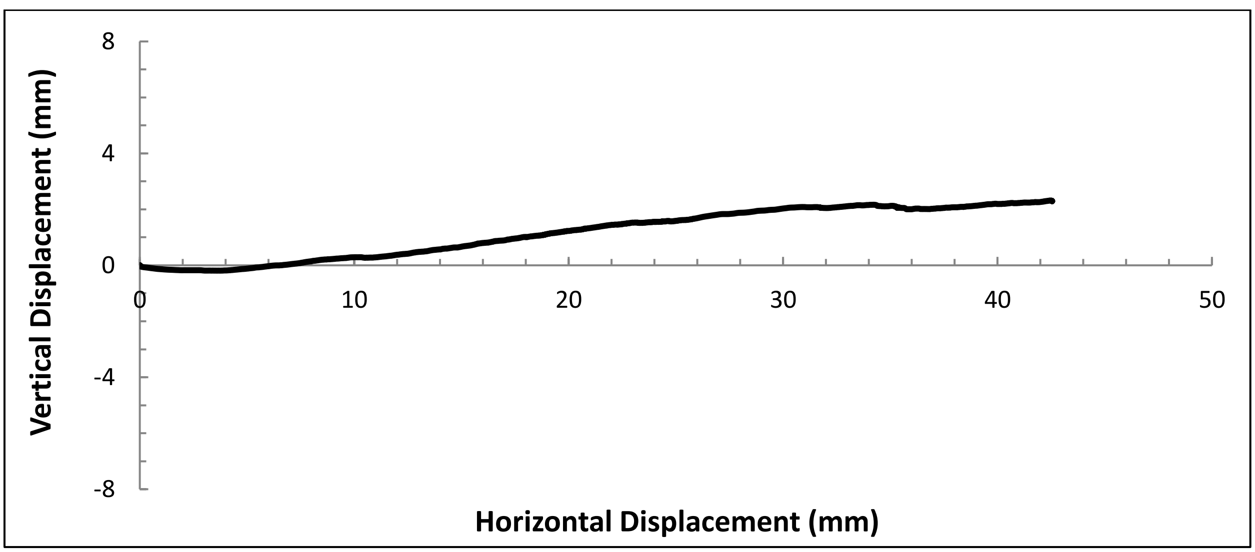

Test ID: M_1A_10 (EXCLUDED)

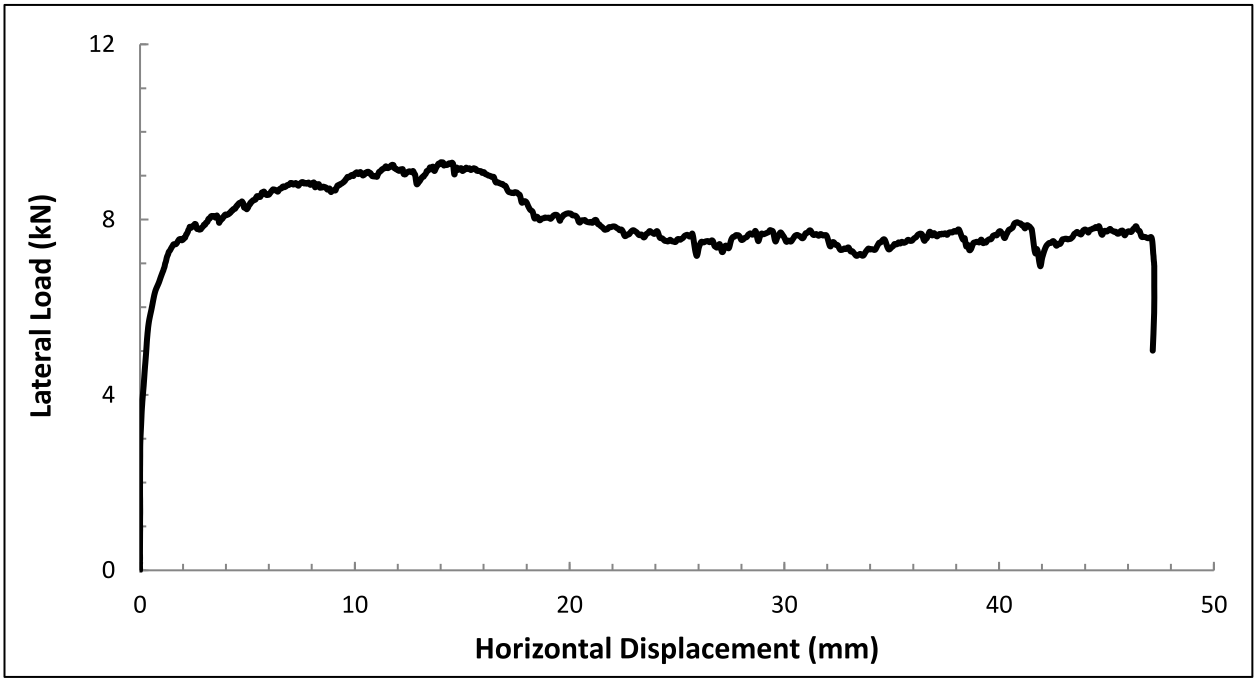

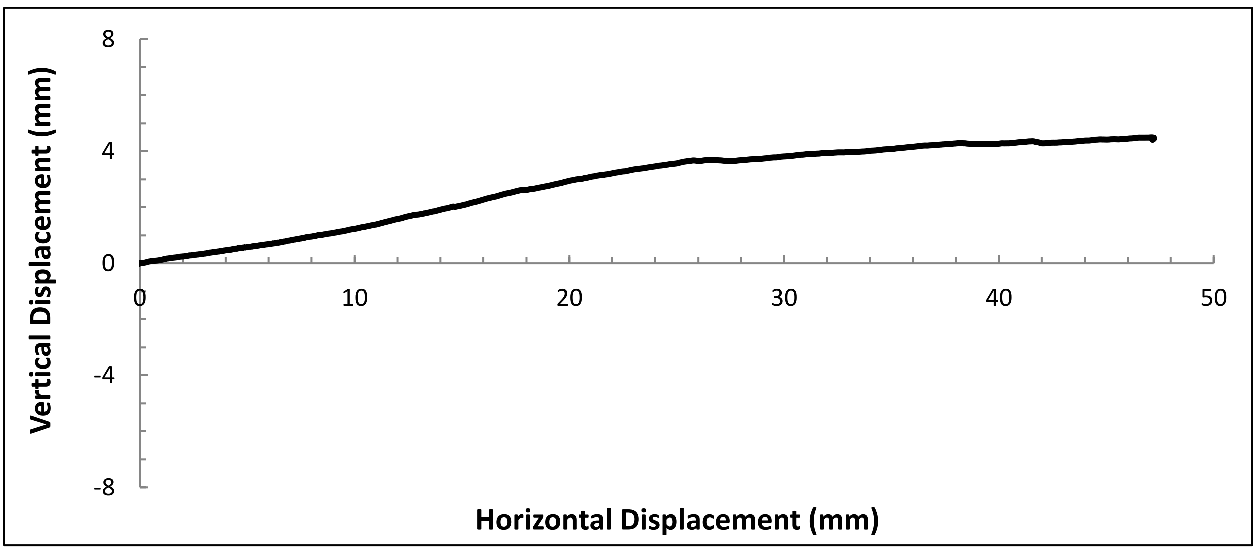

Test ID: M_1A_10

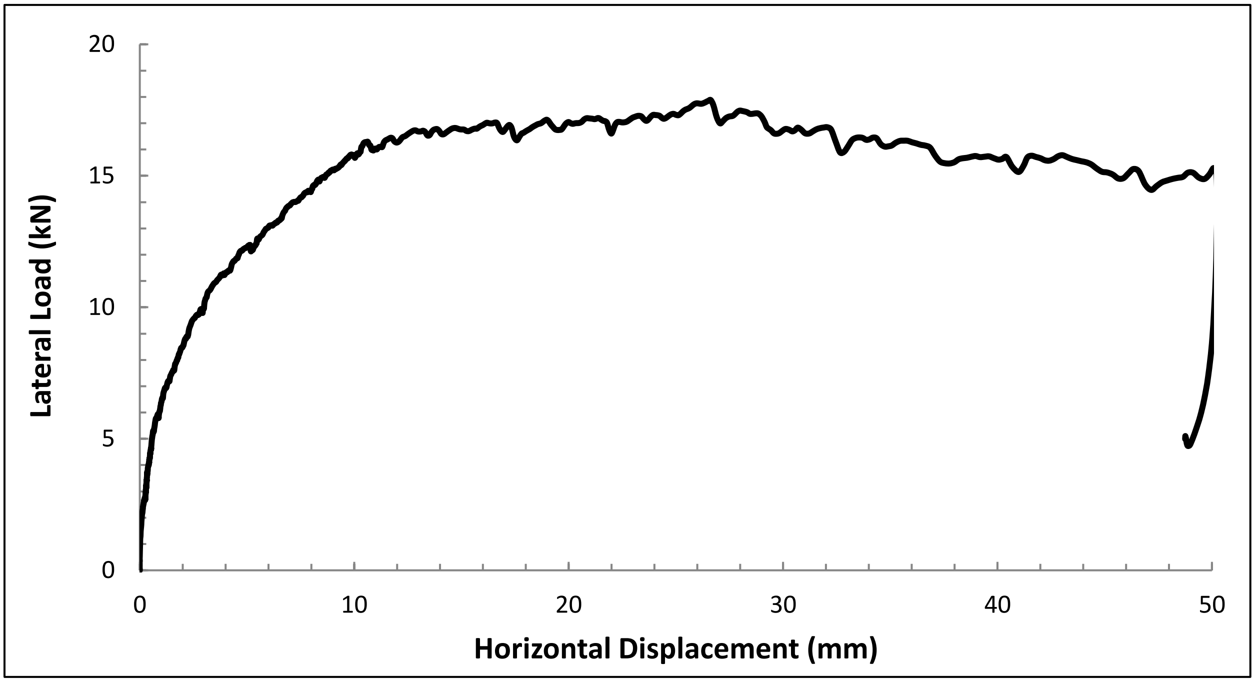

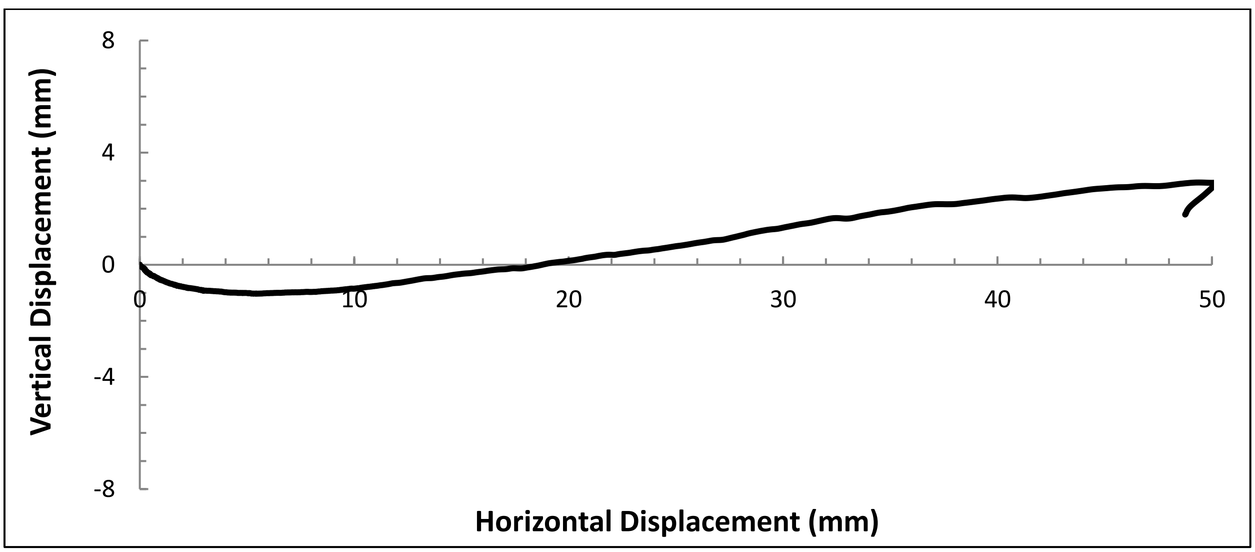

Test ID: M_1A_20

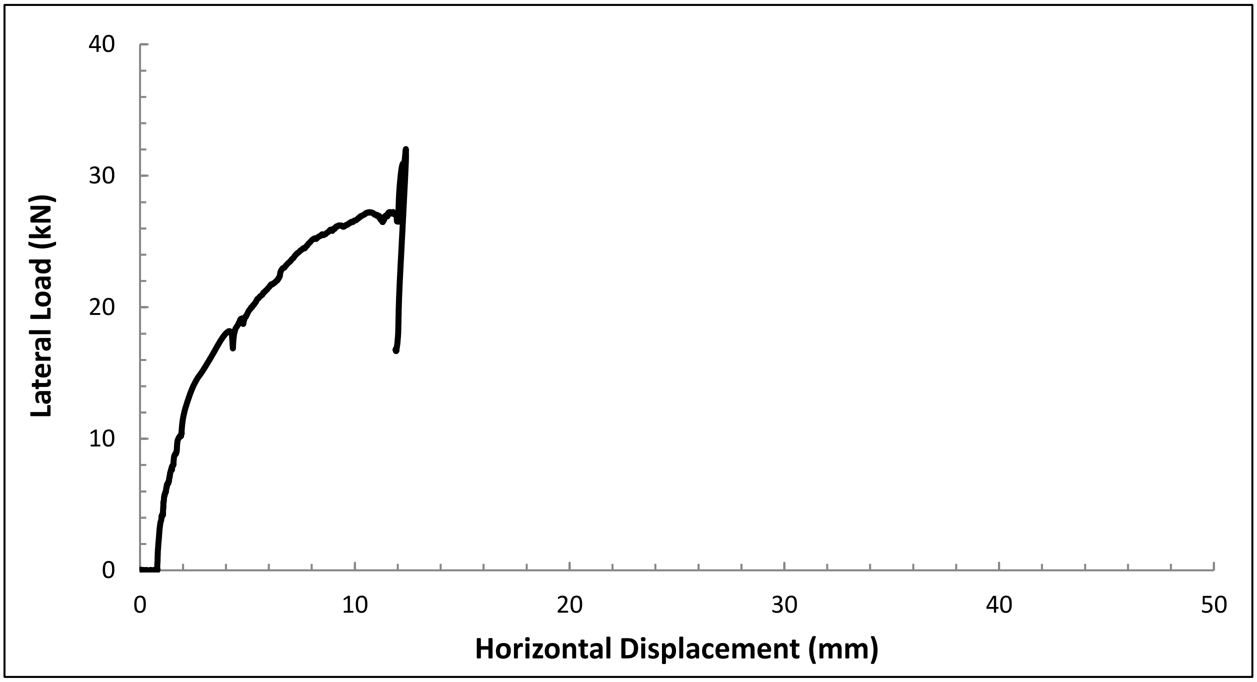

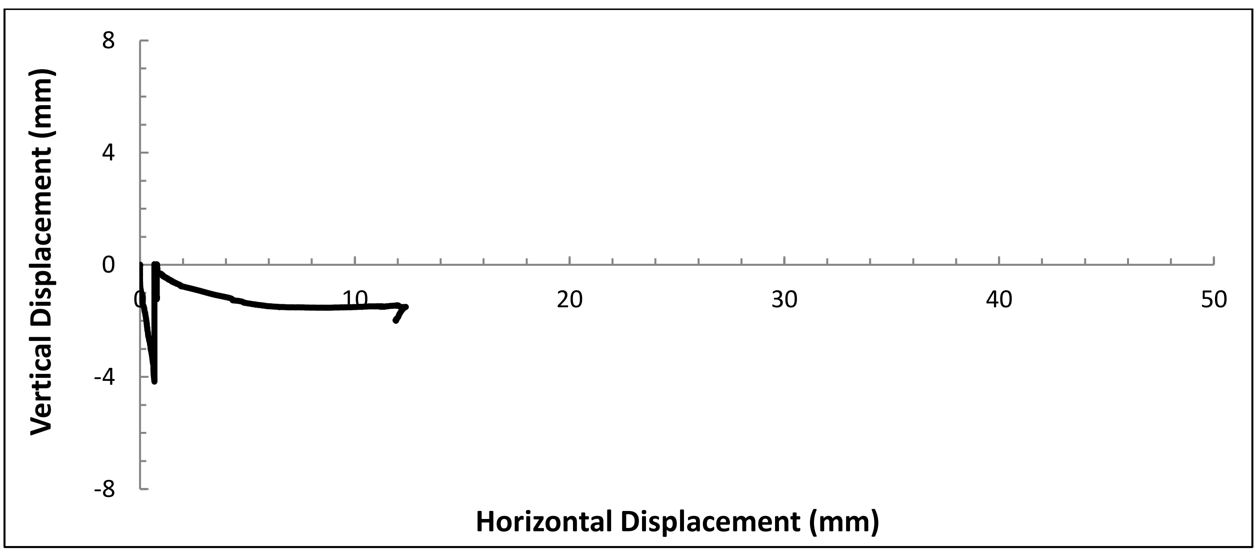

Test ID: M_1A_40 (EXLCLUDED)

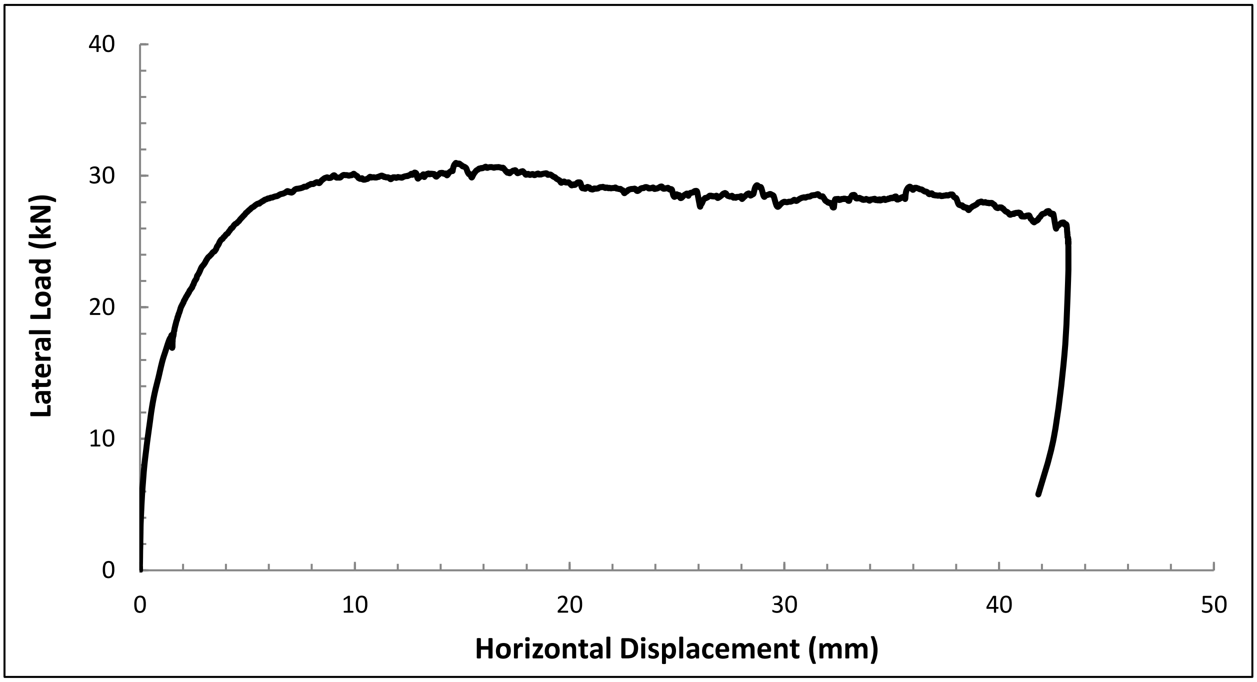

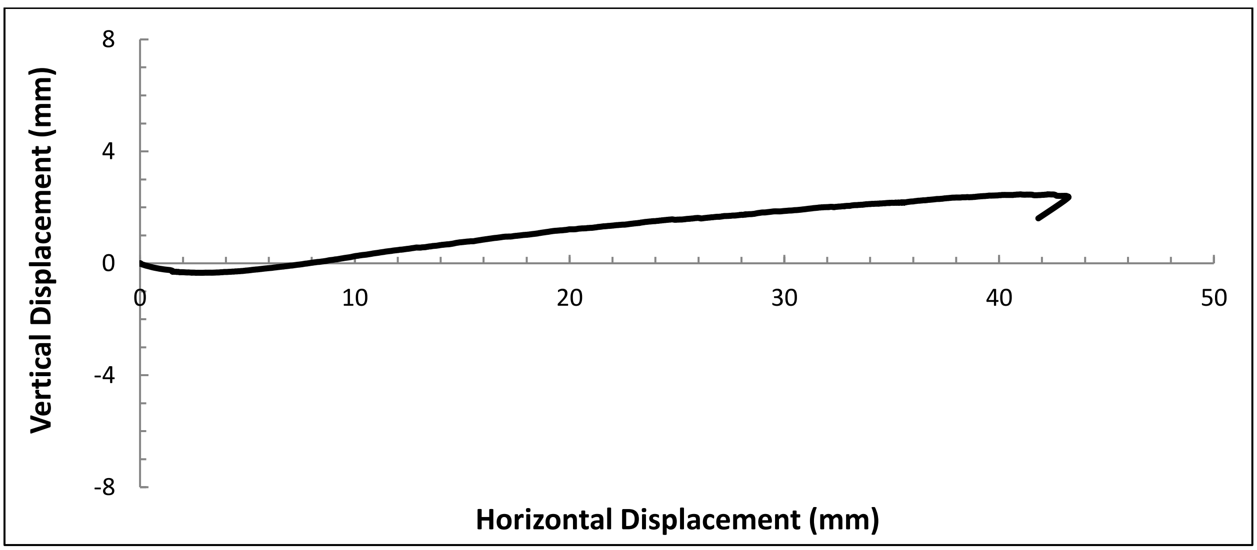

Test ID: M_1A_40

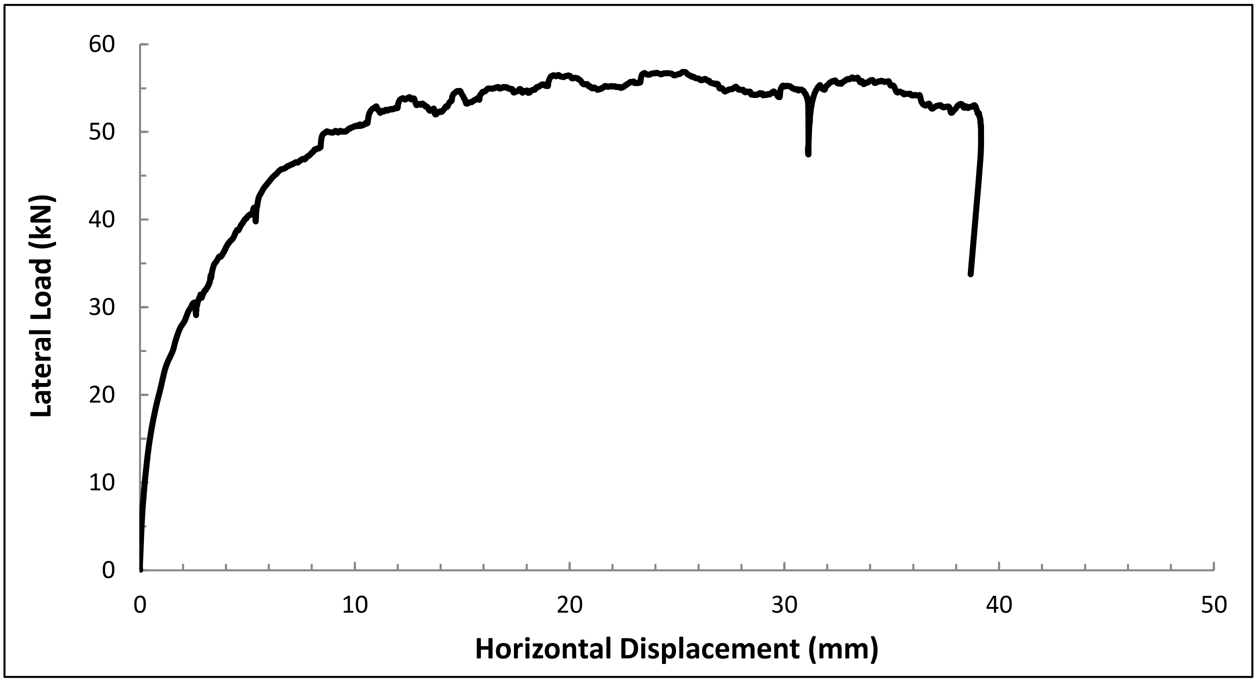

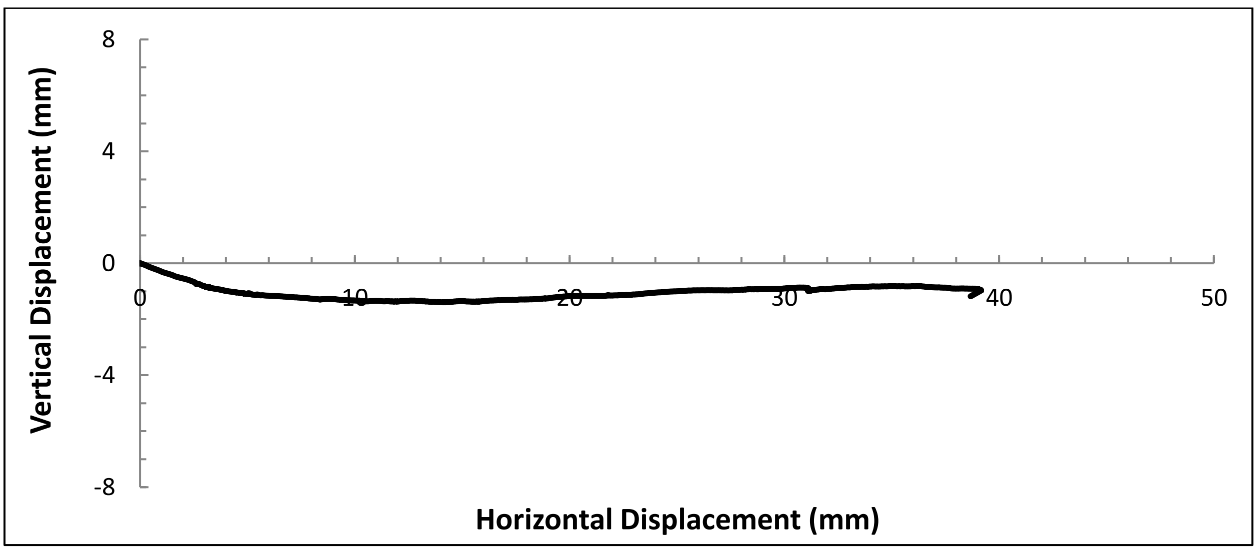

Test ID: M_1A_80

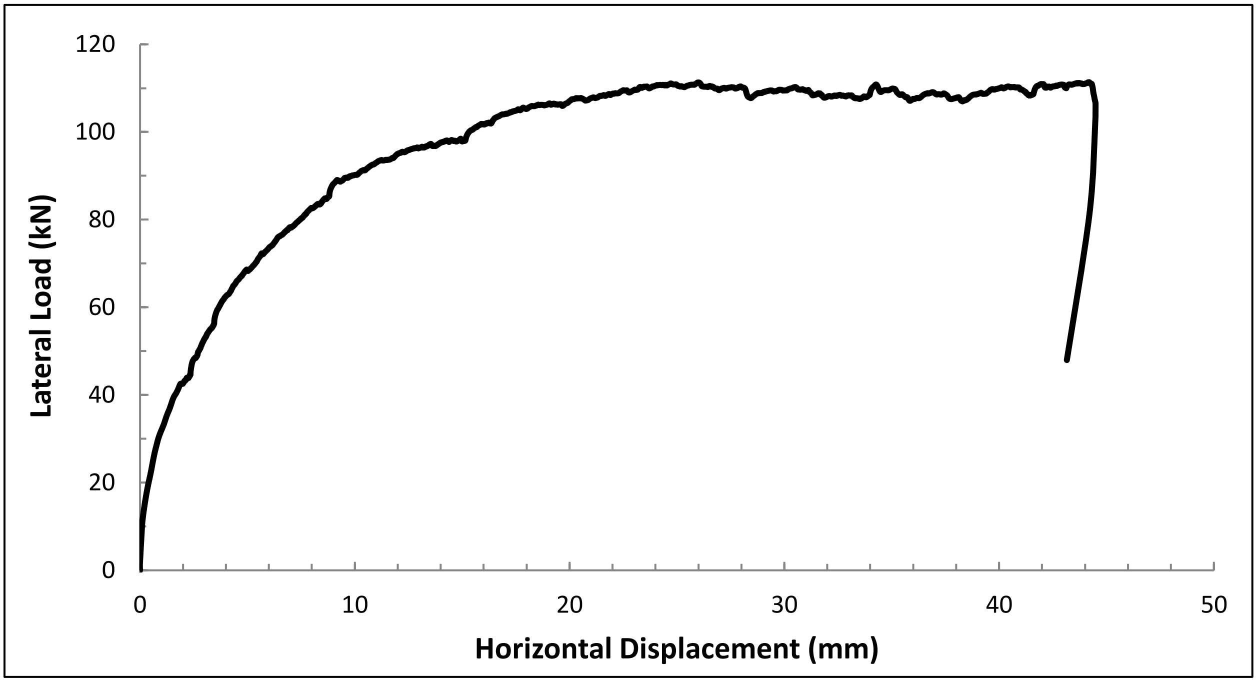

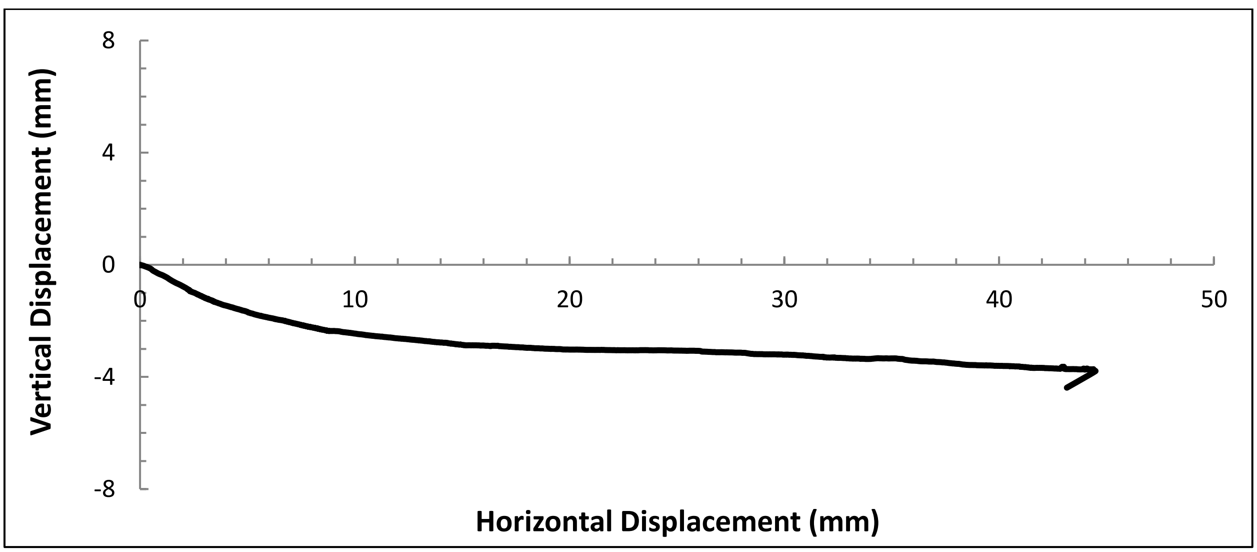

Test ID: M_1A_160

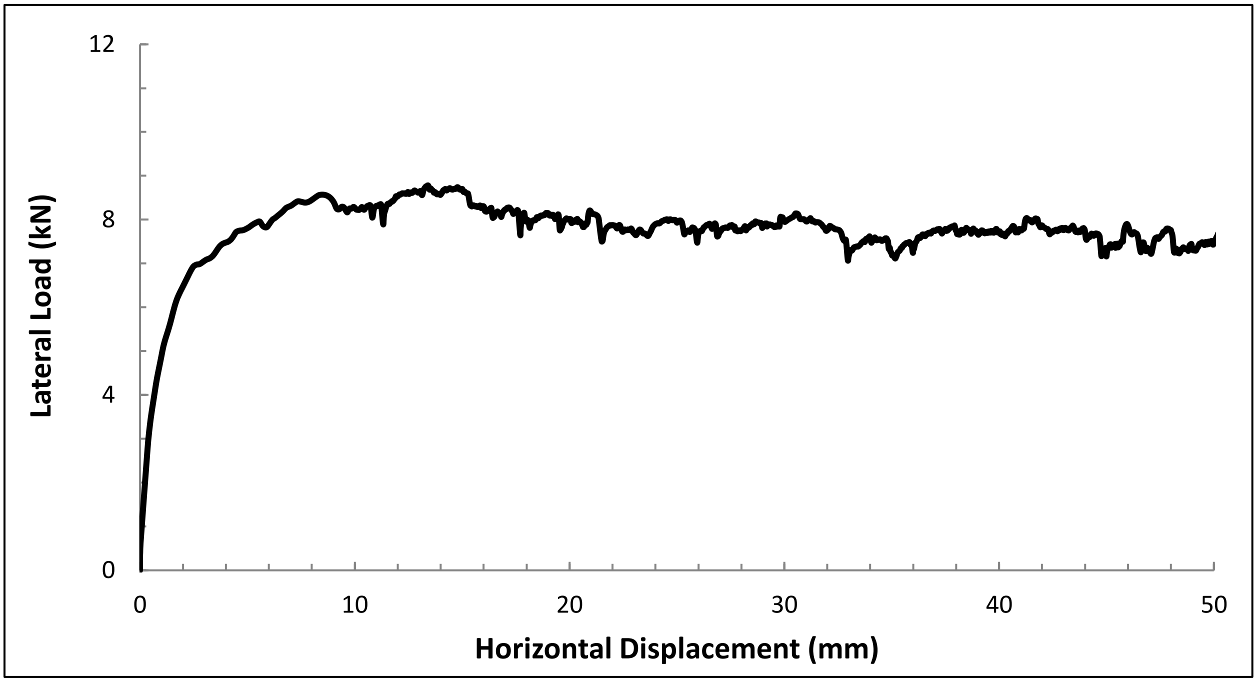

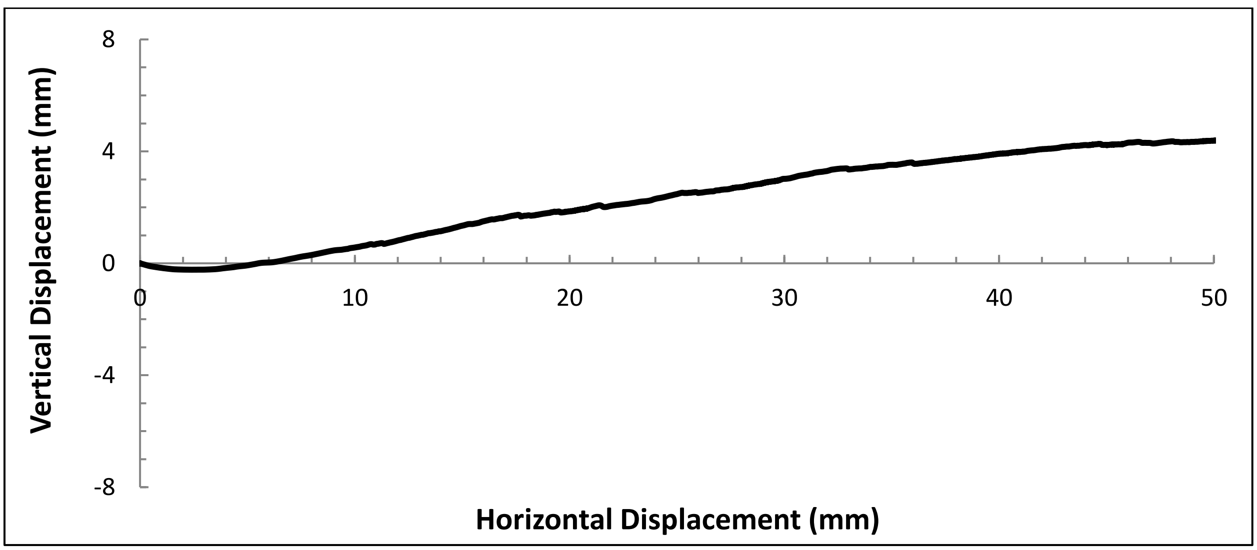

Test ID: M_1A_10 (2)

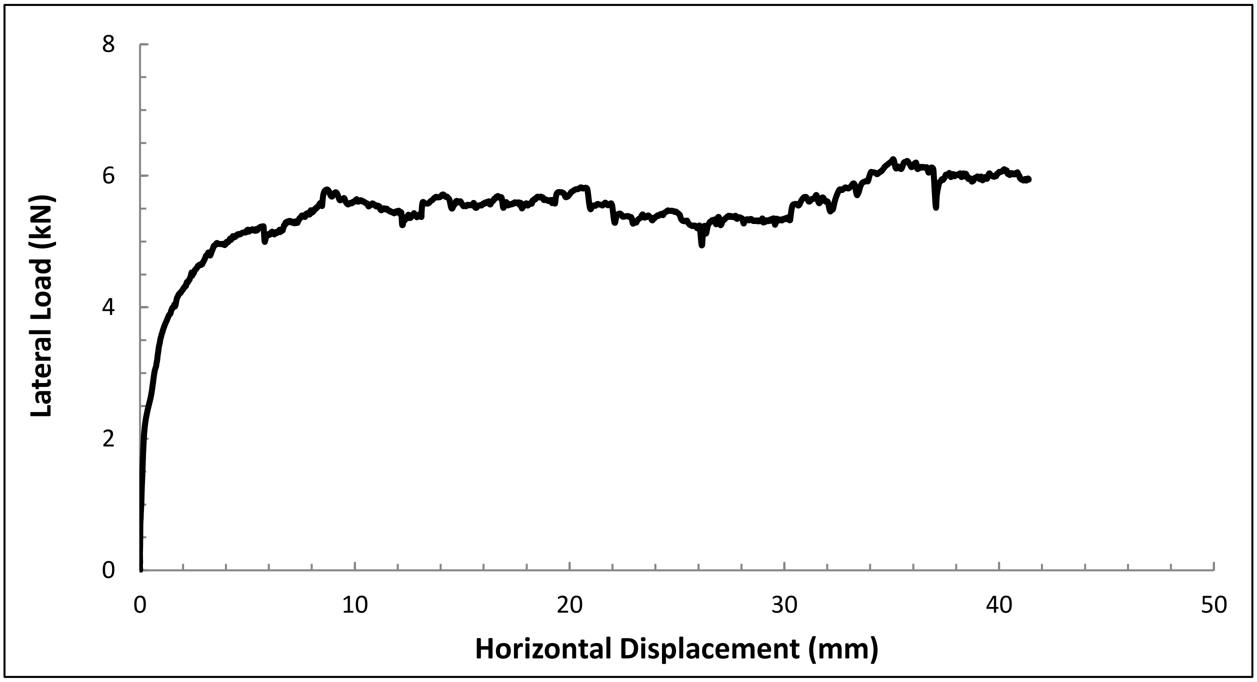

Lateral Load (kN)
8
6
4
2
0
0
10
20
30
40
50
Horizontal Displacement (mm)

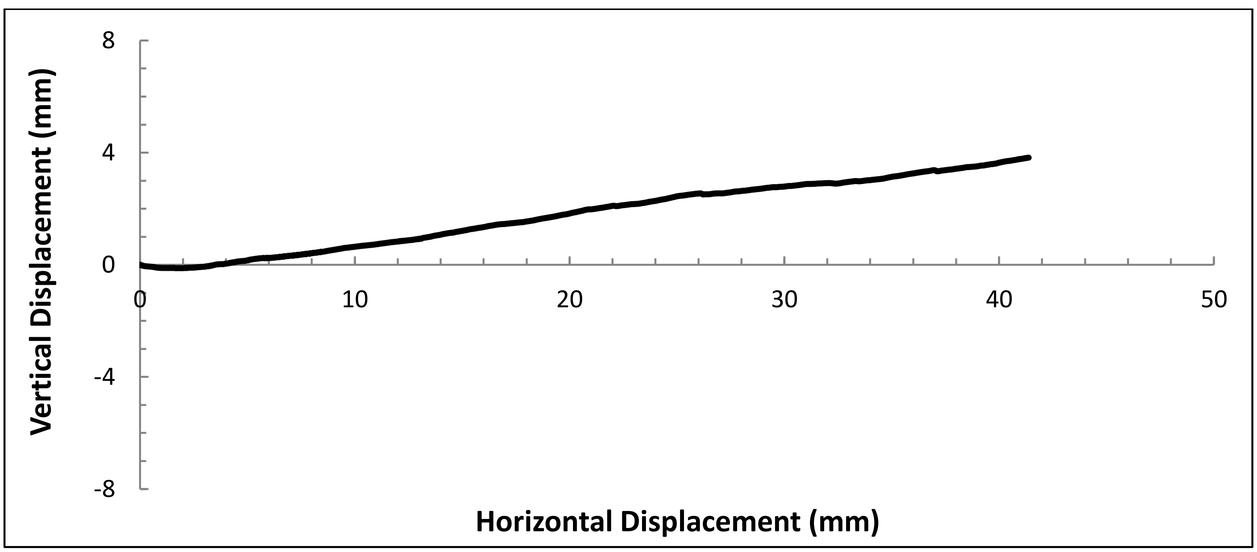

Vertical Displacement (mm)
8
4
0
-4
-8
0
10
20
30
40
50
Horizontal Displacement (mm)

Test ID: M_1A_5

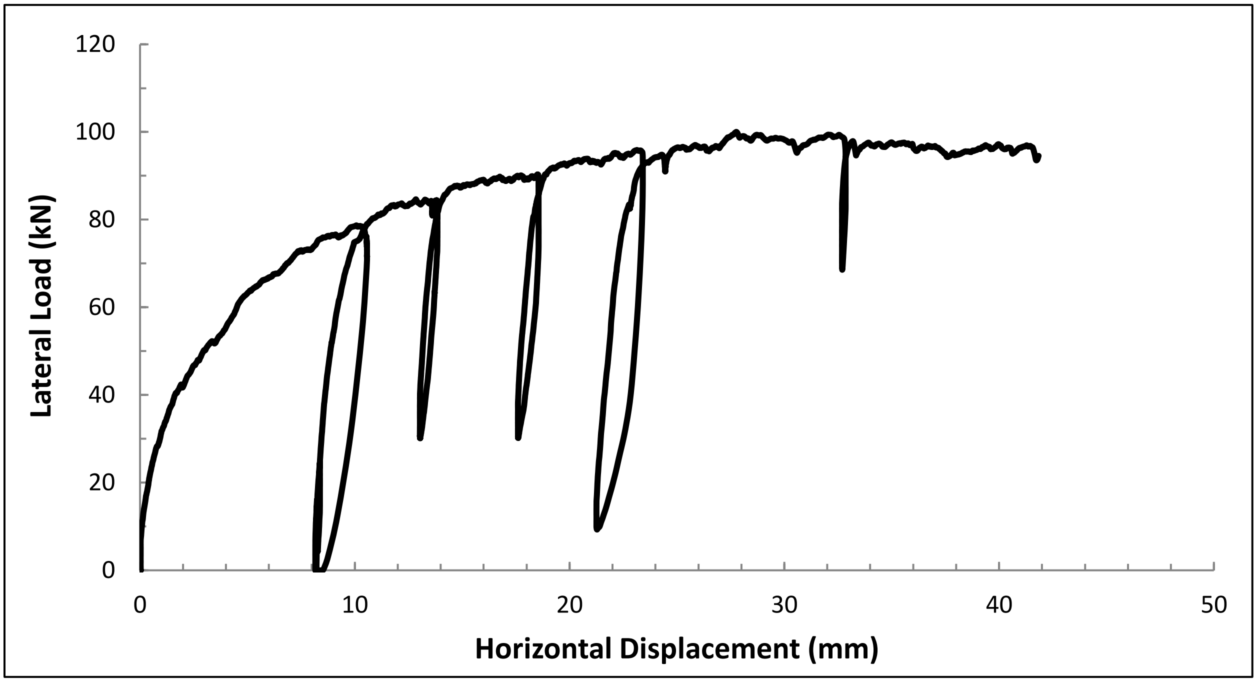

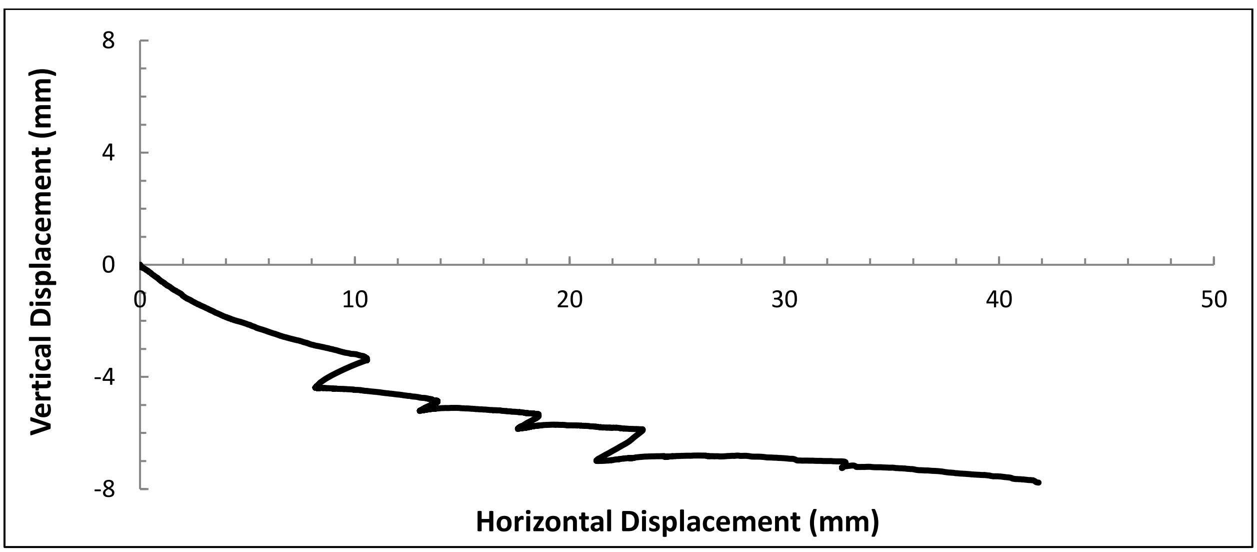

Test ID: M_1B_160 (CYCLIC)

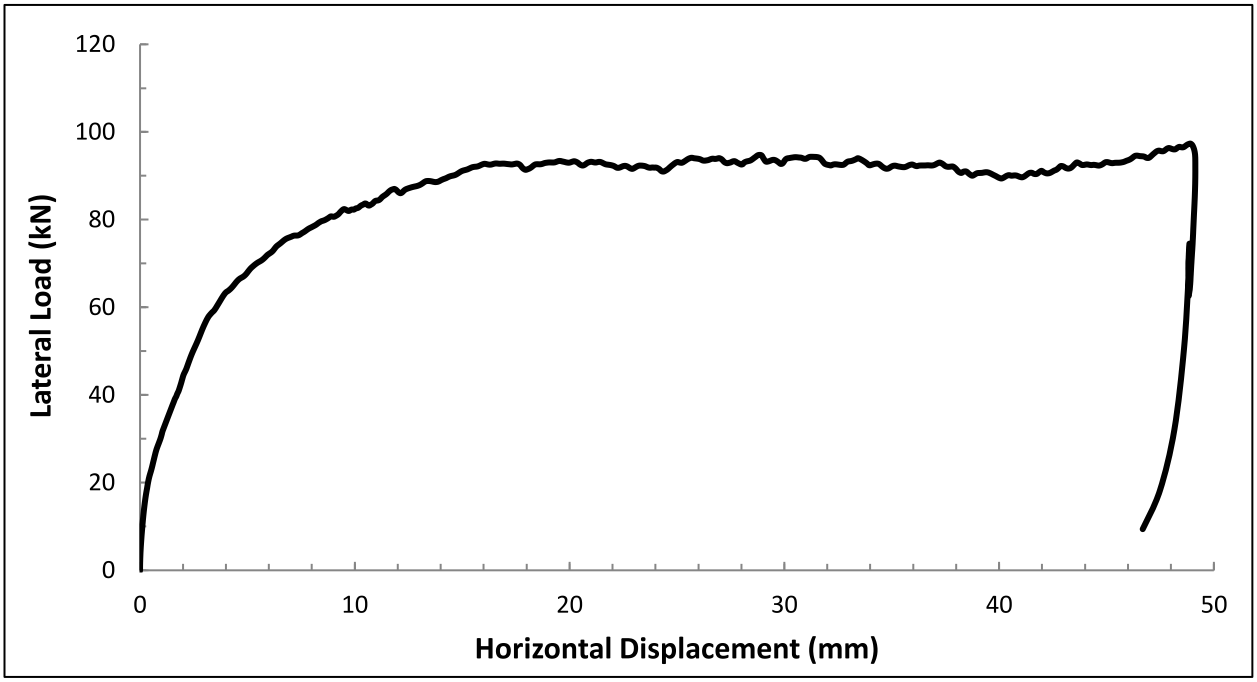

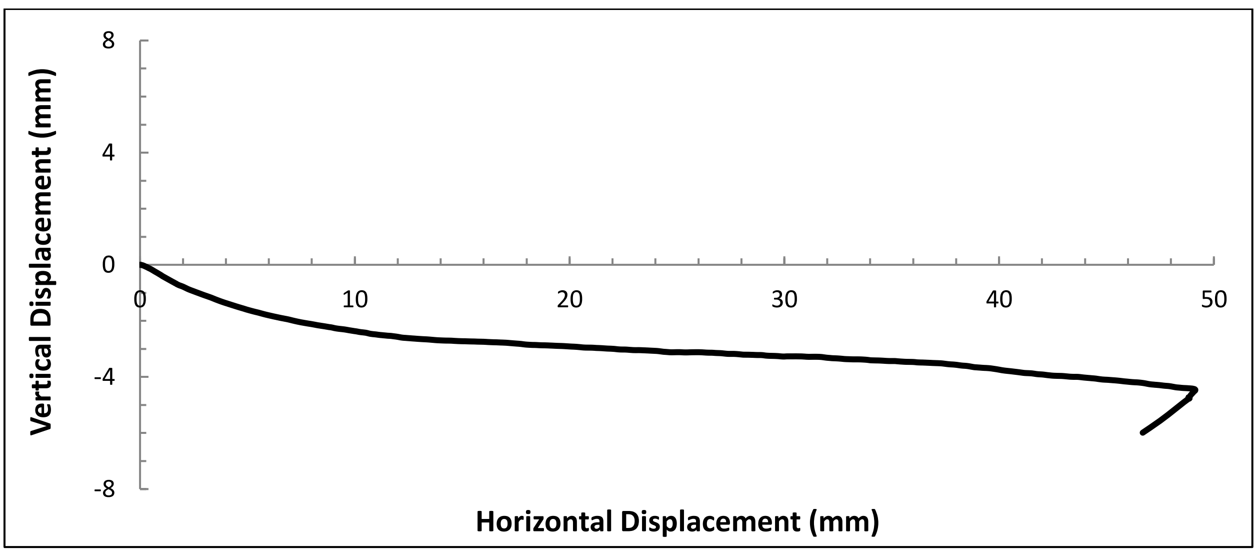

Test ID: M_1B_160 (FAST)

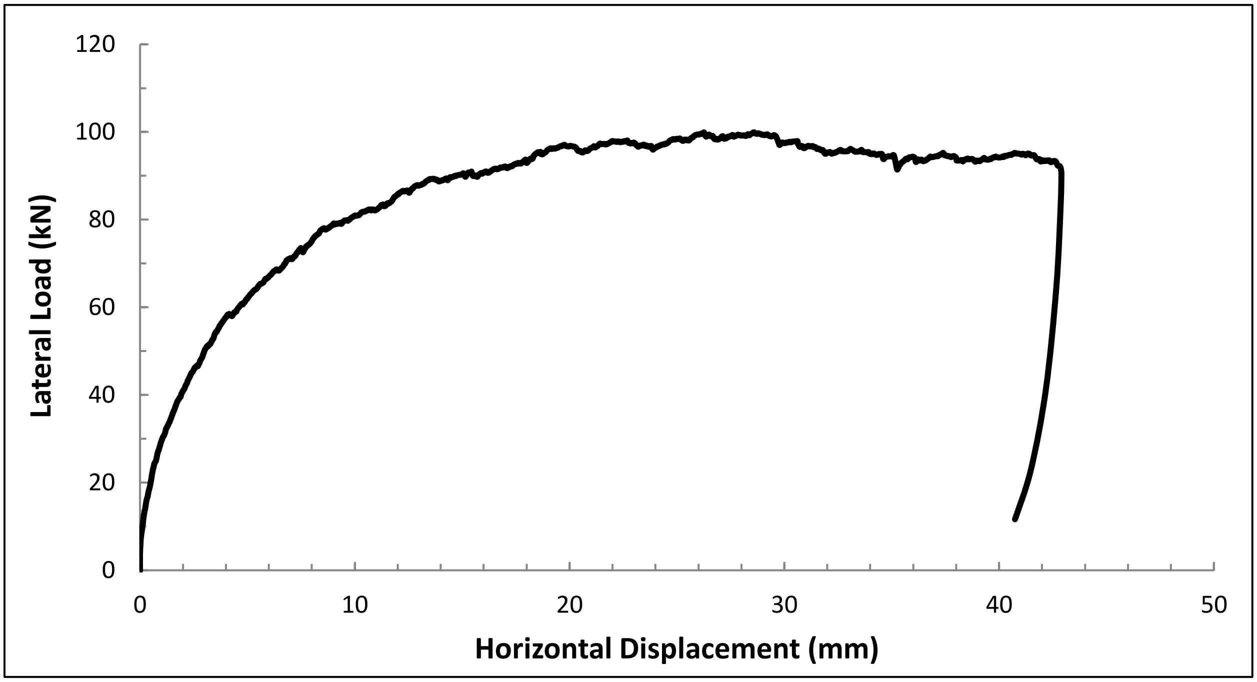

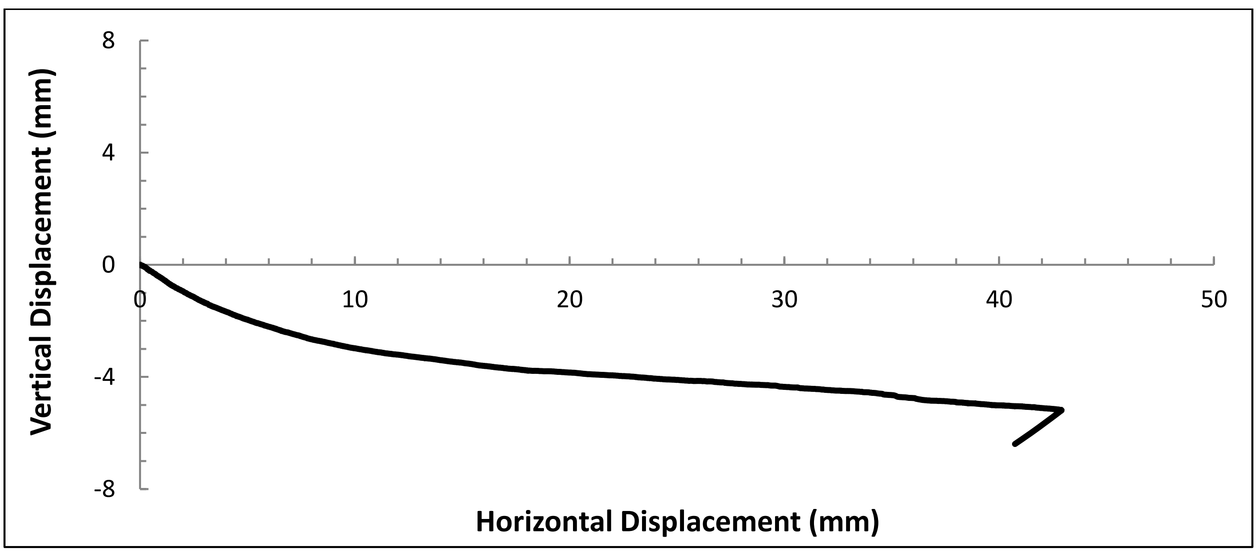

Test ID: M_1B_160

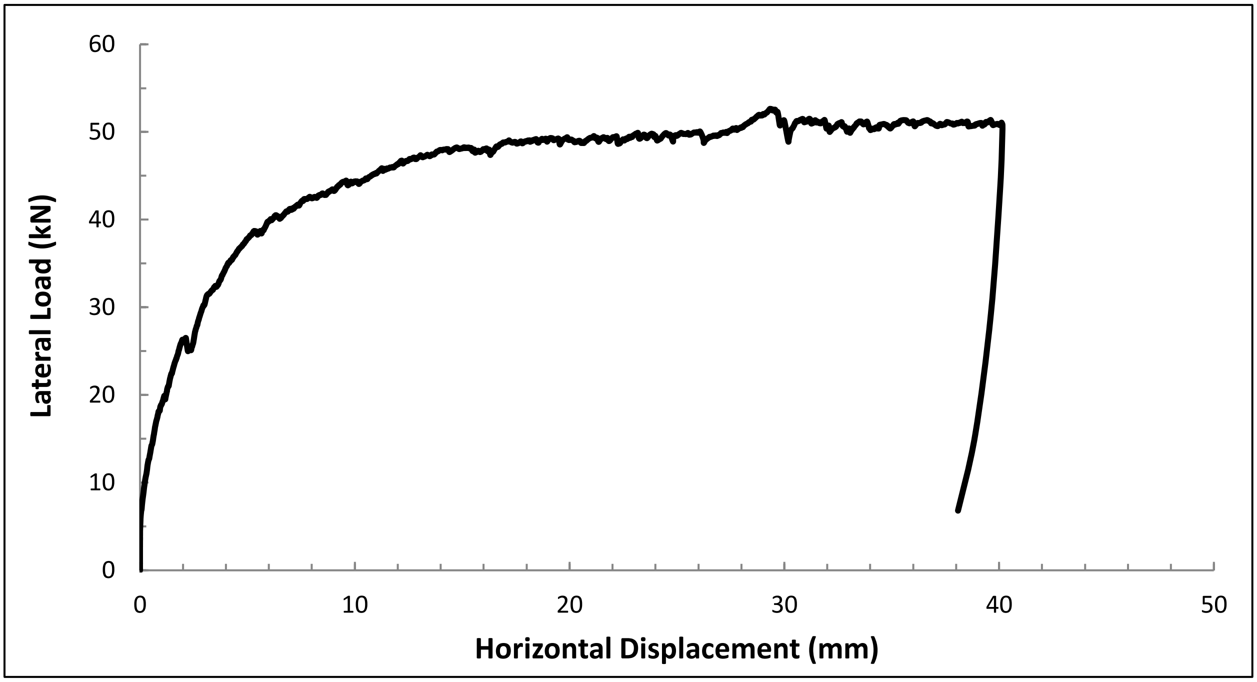

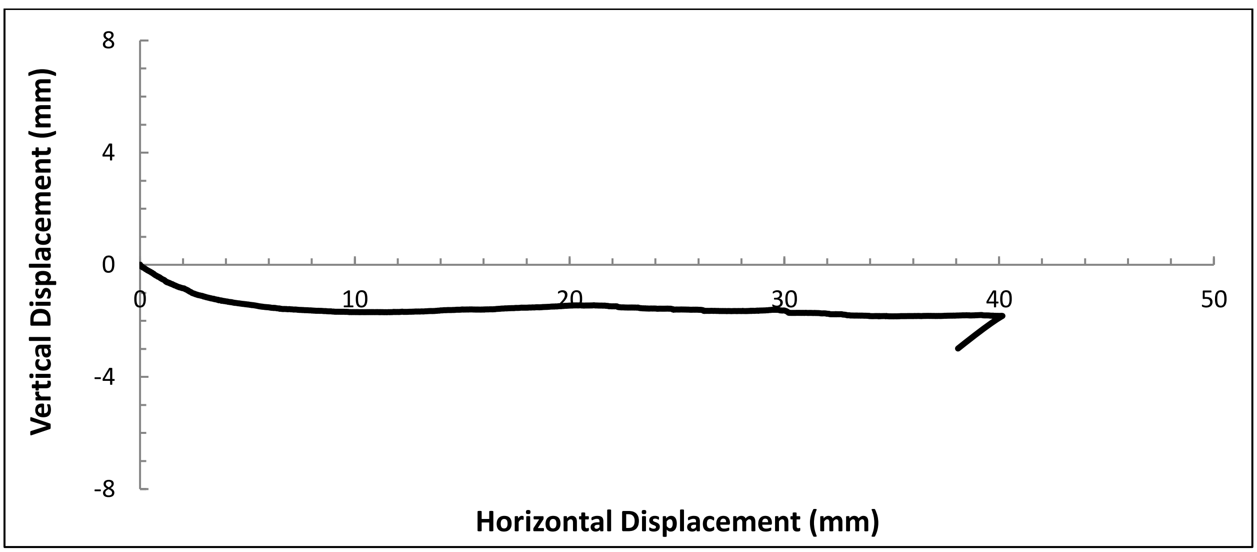

Test ID: M_1B_80

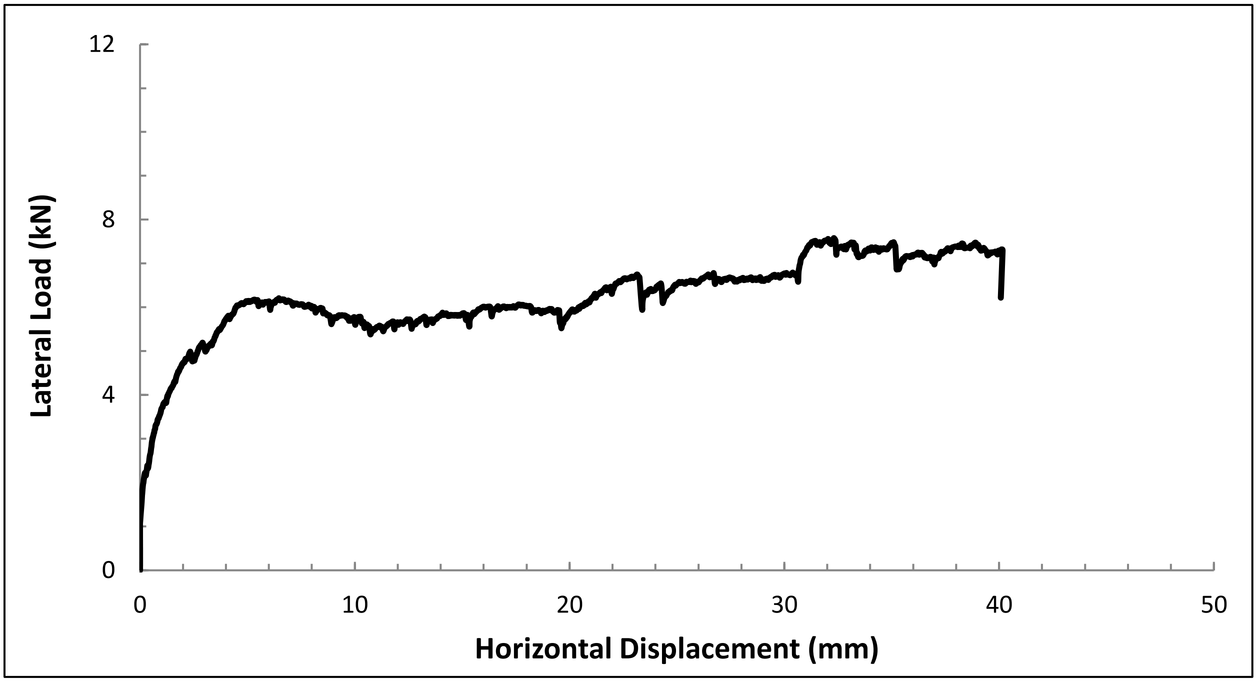

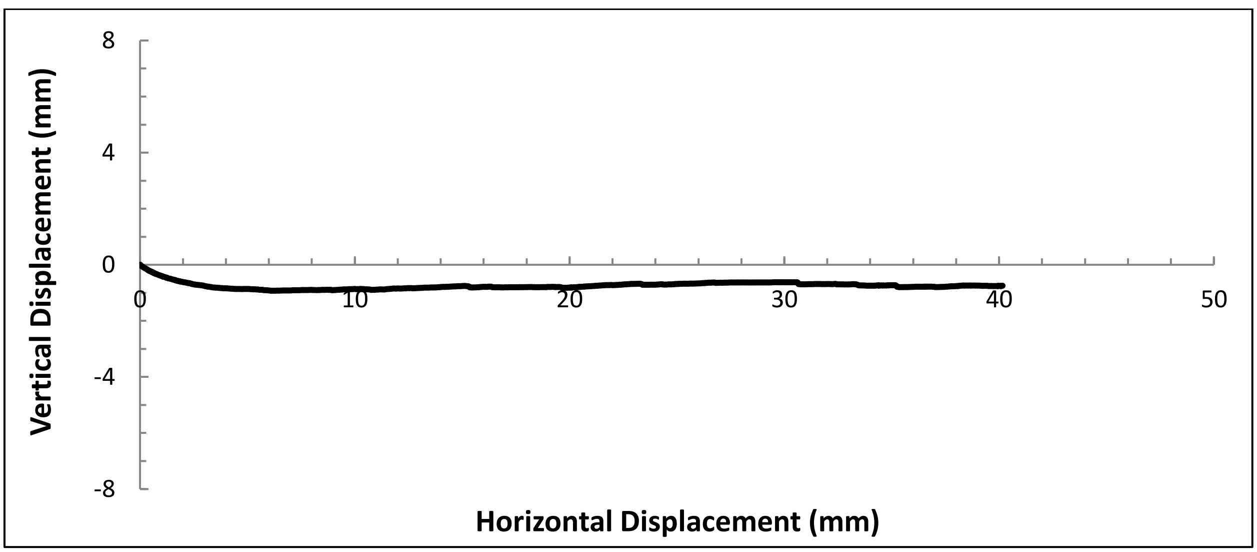

Test ID: M_1B_10 (EXCLUDED)

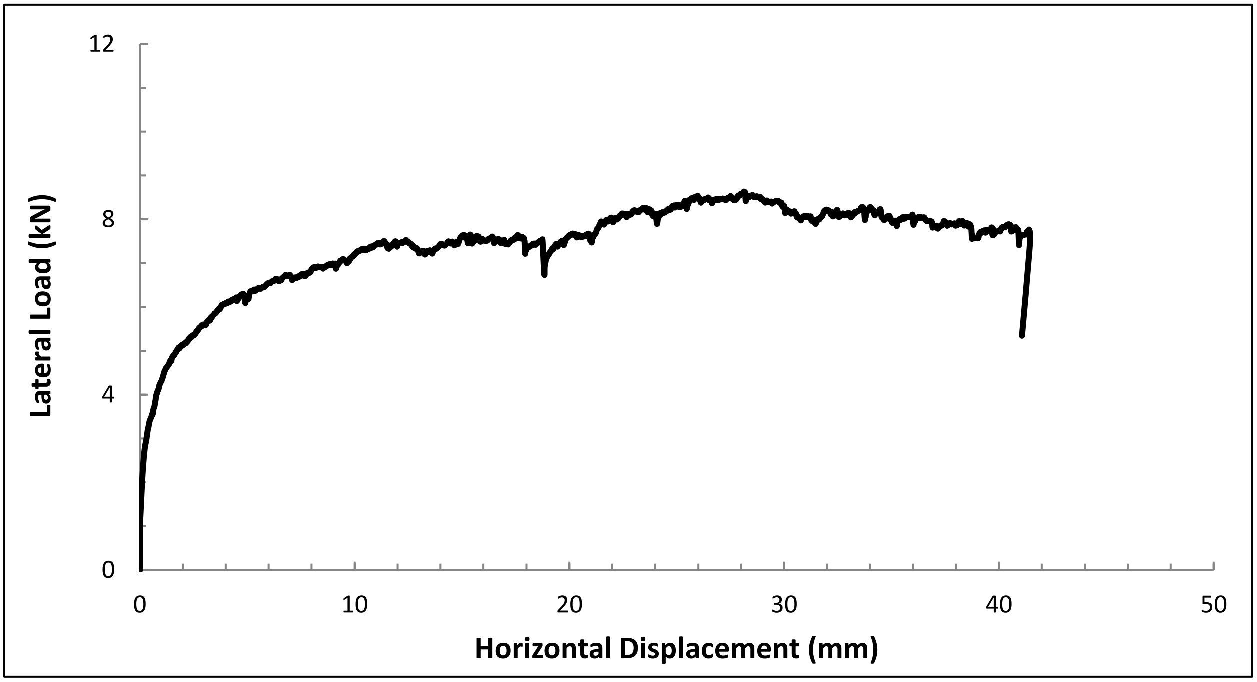

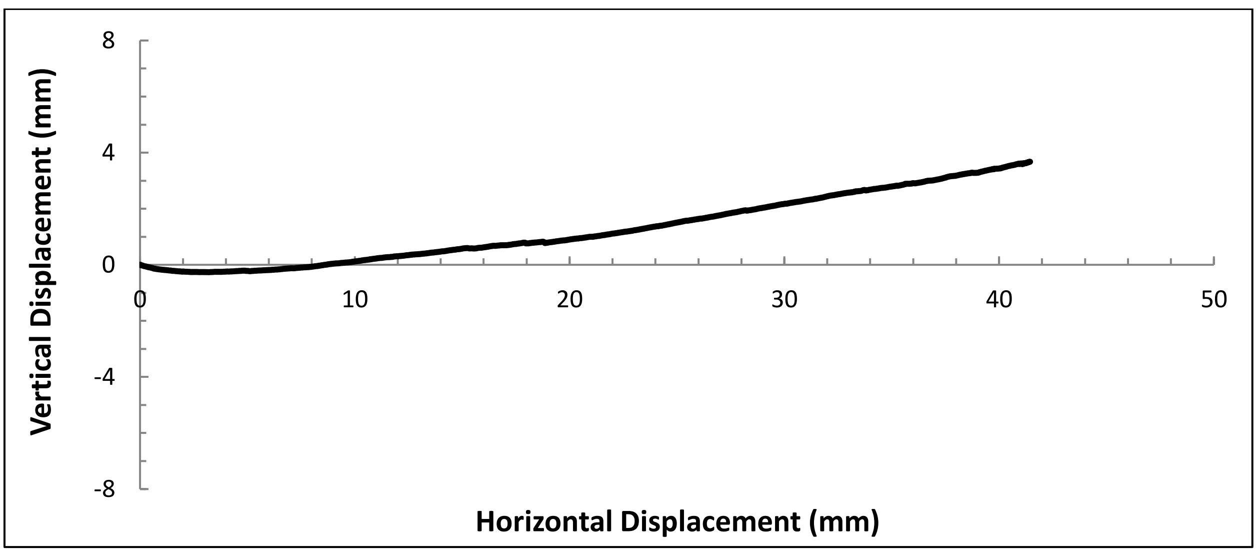

Test ID: M_1B_10

III.3.2 Phase 2 crib test results in the McAbee Ballast

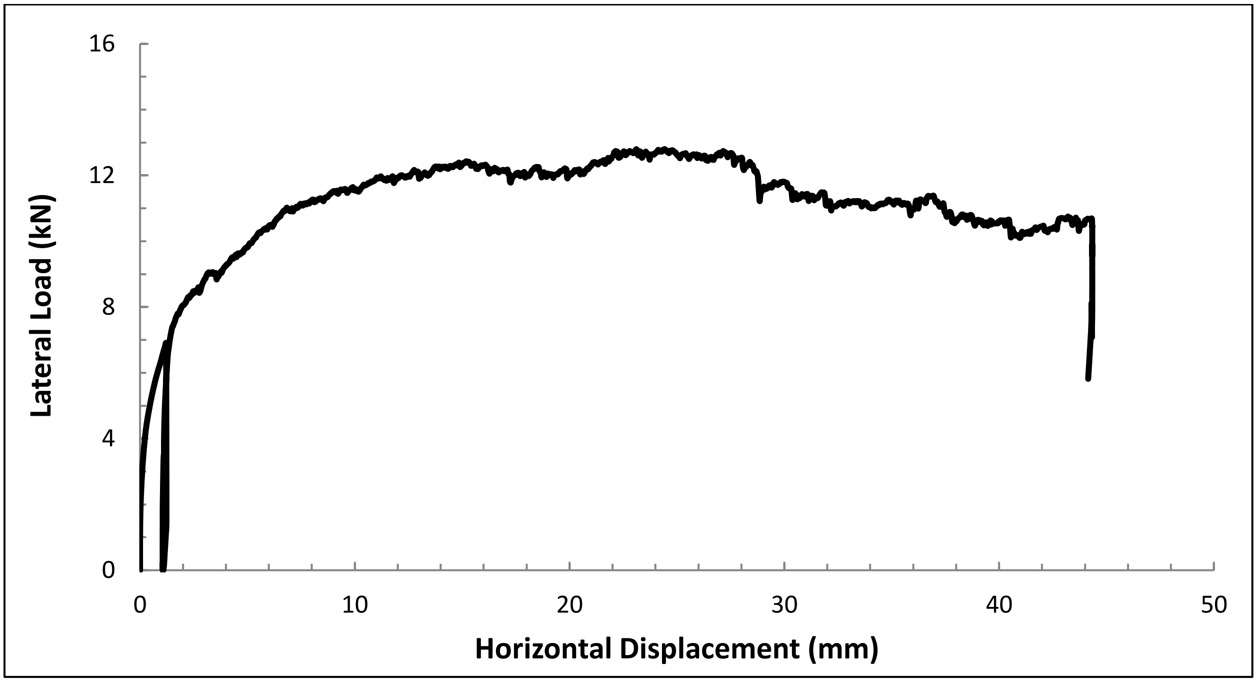

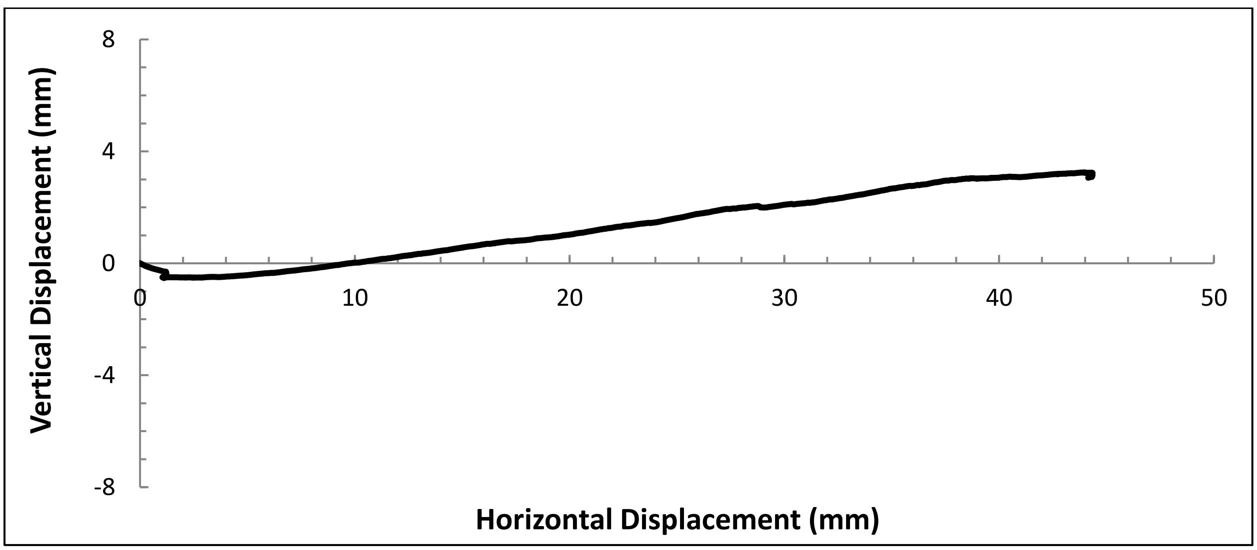

Test ID: M_2A_10

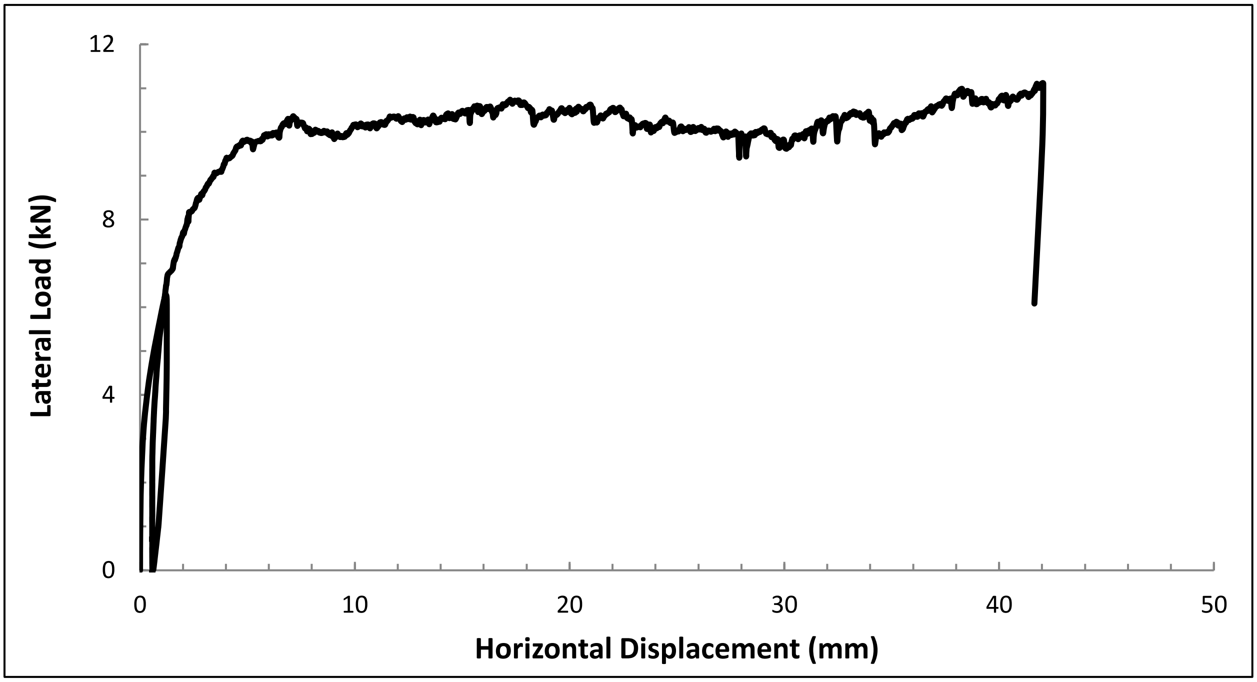

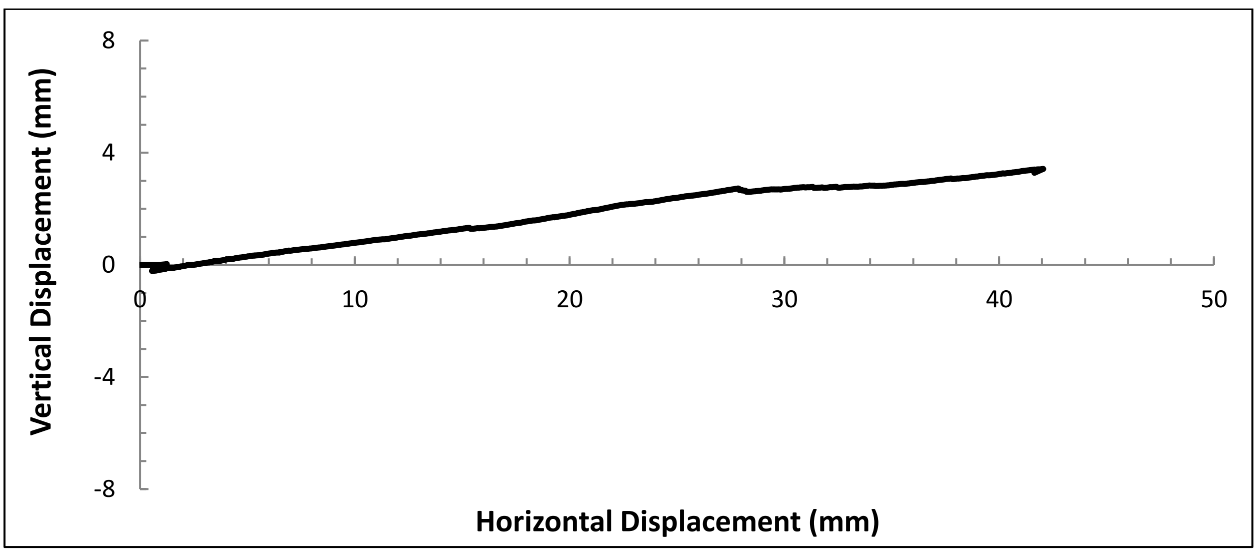

Test ID: M_2A_10 (2)

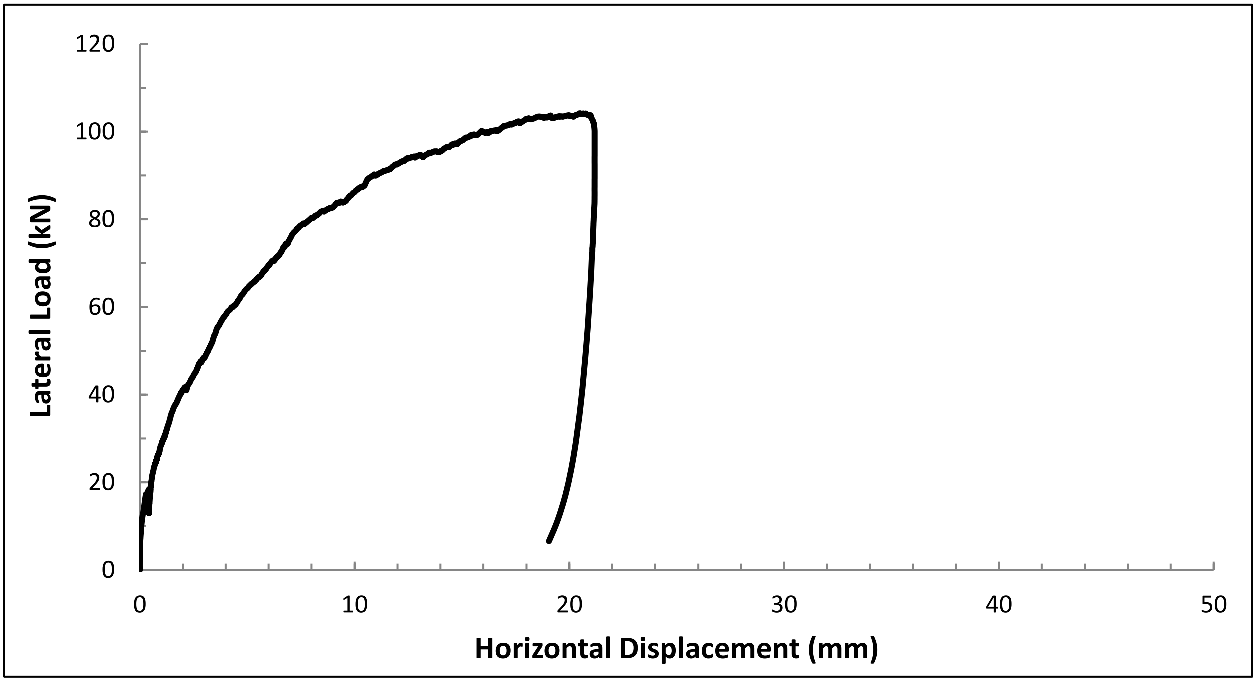

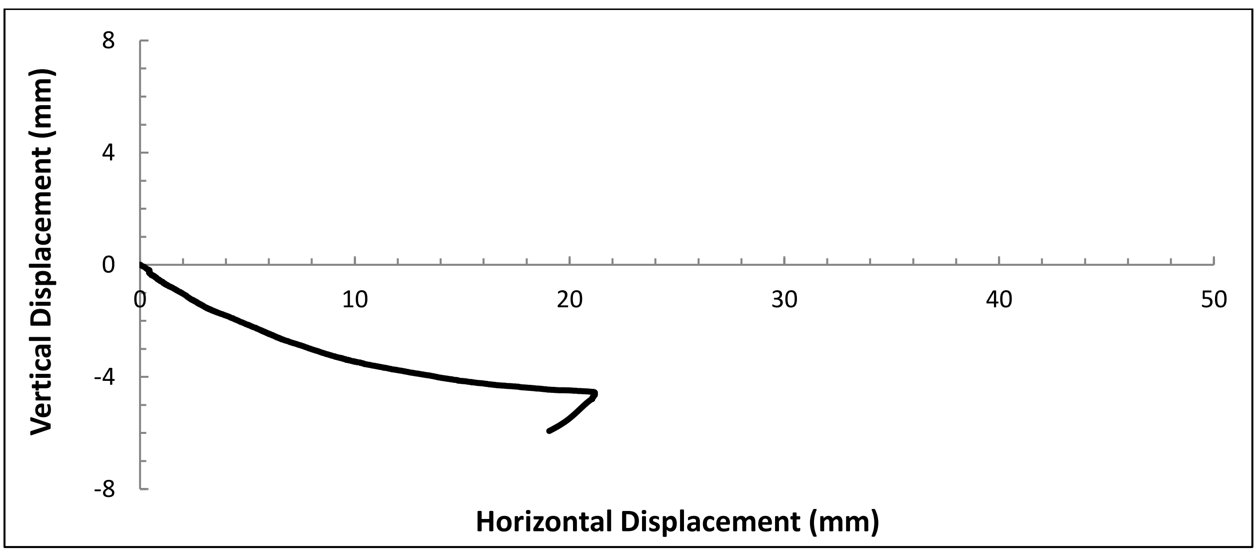

Test ID: M_2A_160 (EXCLUDED)

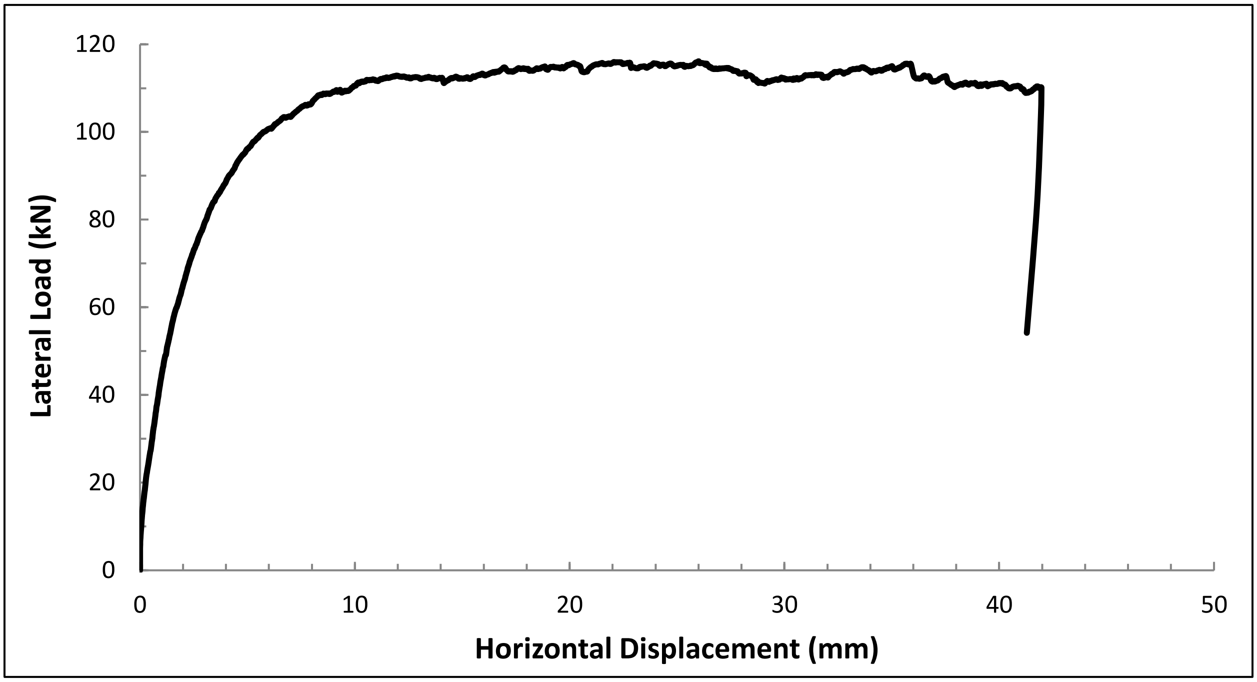

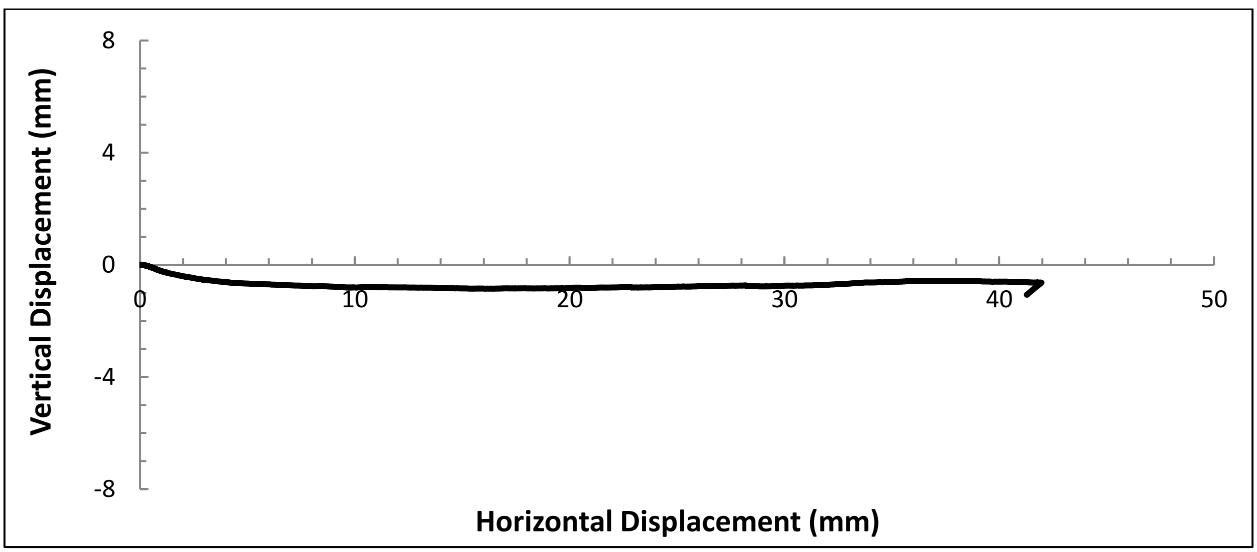

Test ID: M_2A_160

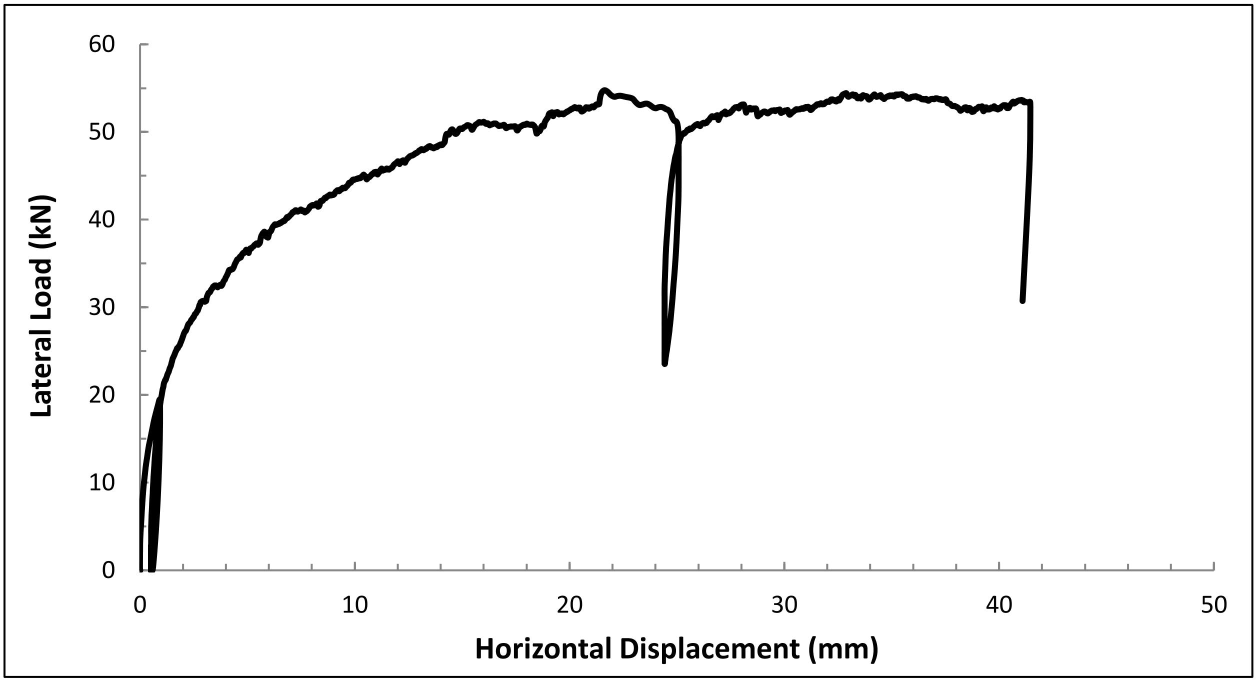

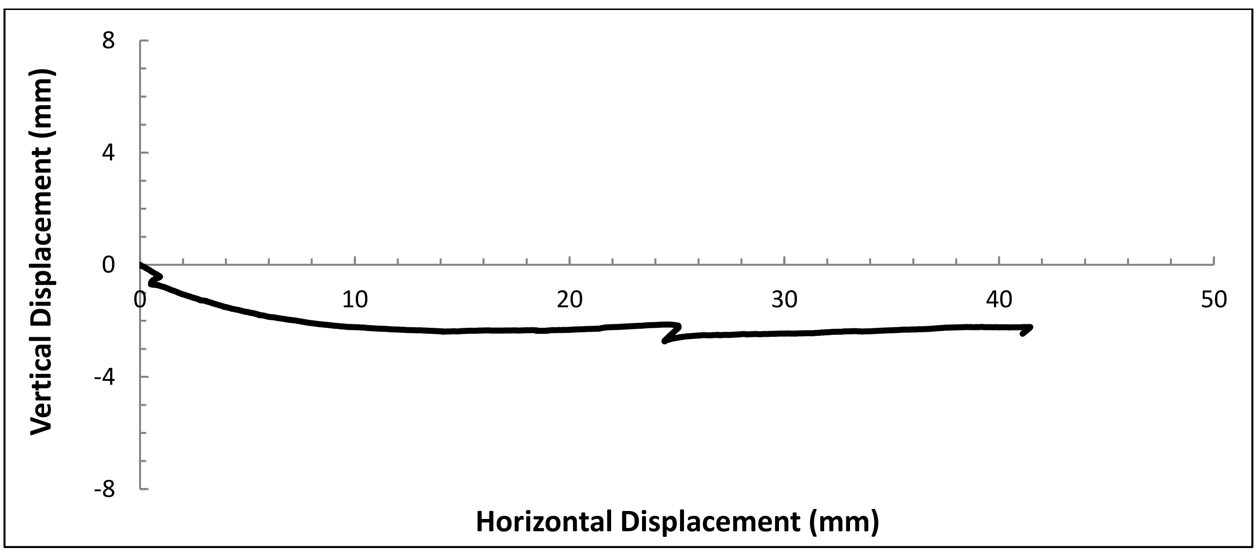

Test ID: M_2A_80

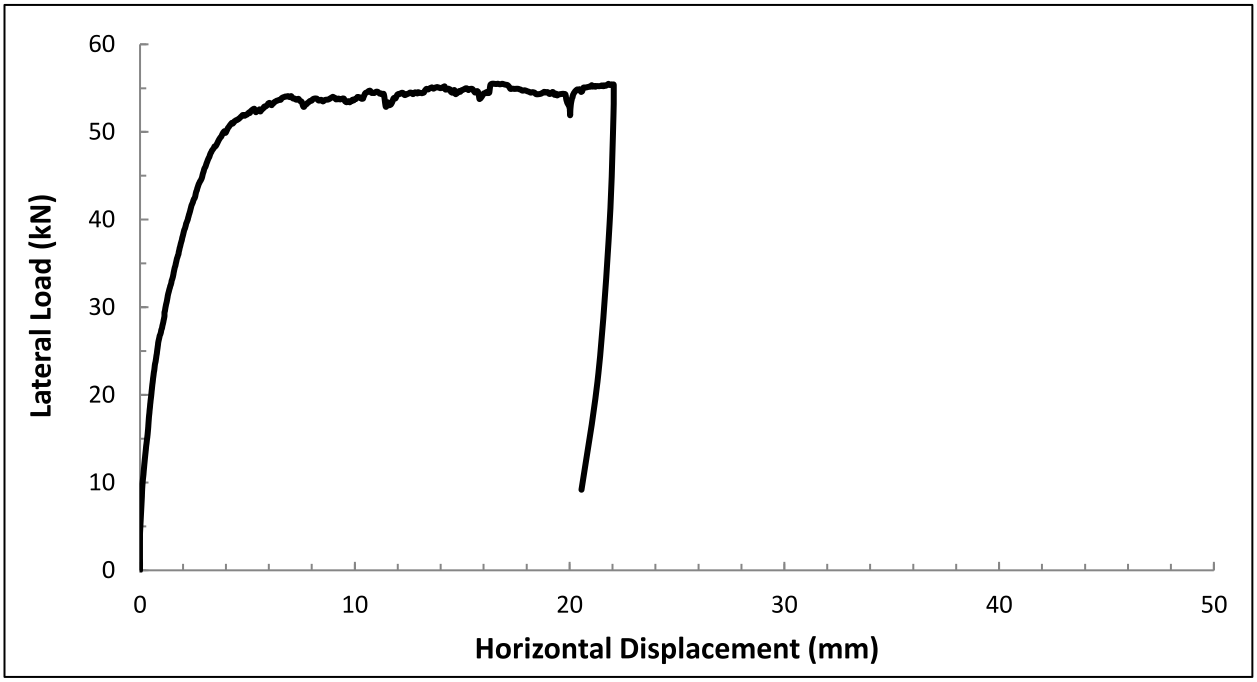

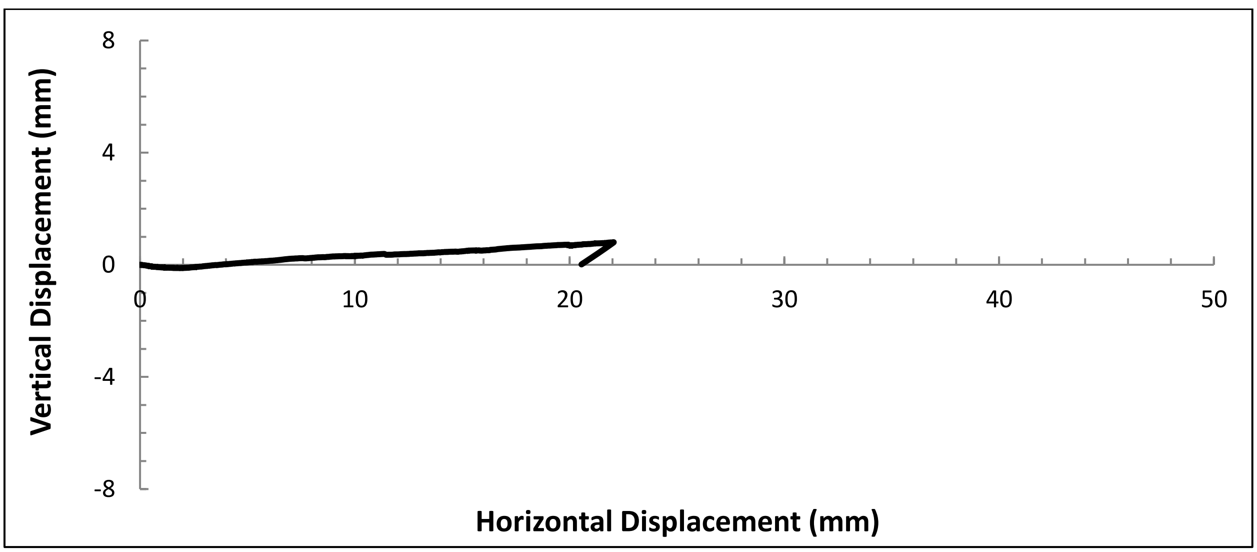

Test ID: M_2A_80 (2)

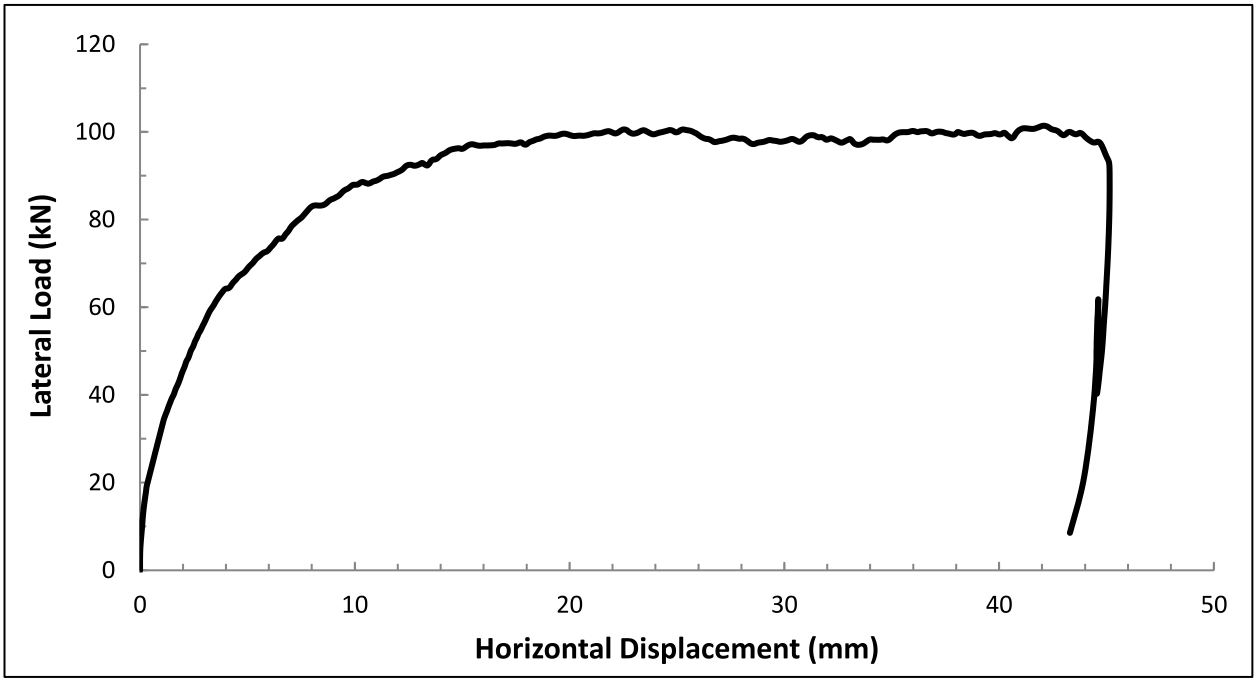

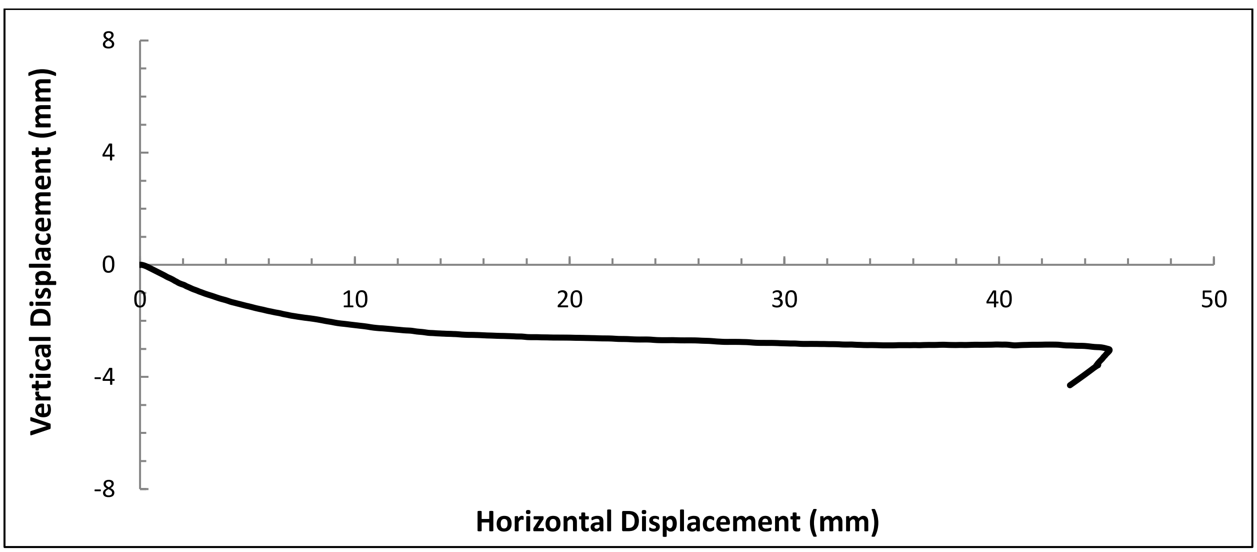

Test ID: M_2B_160 (F)

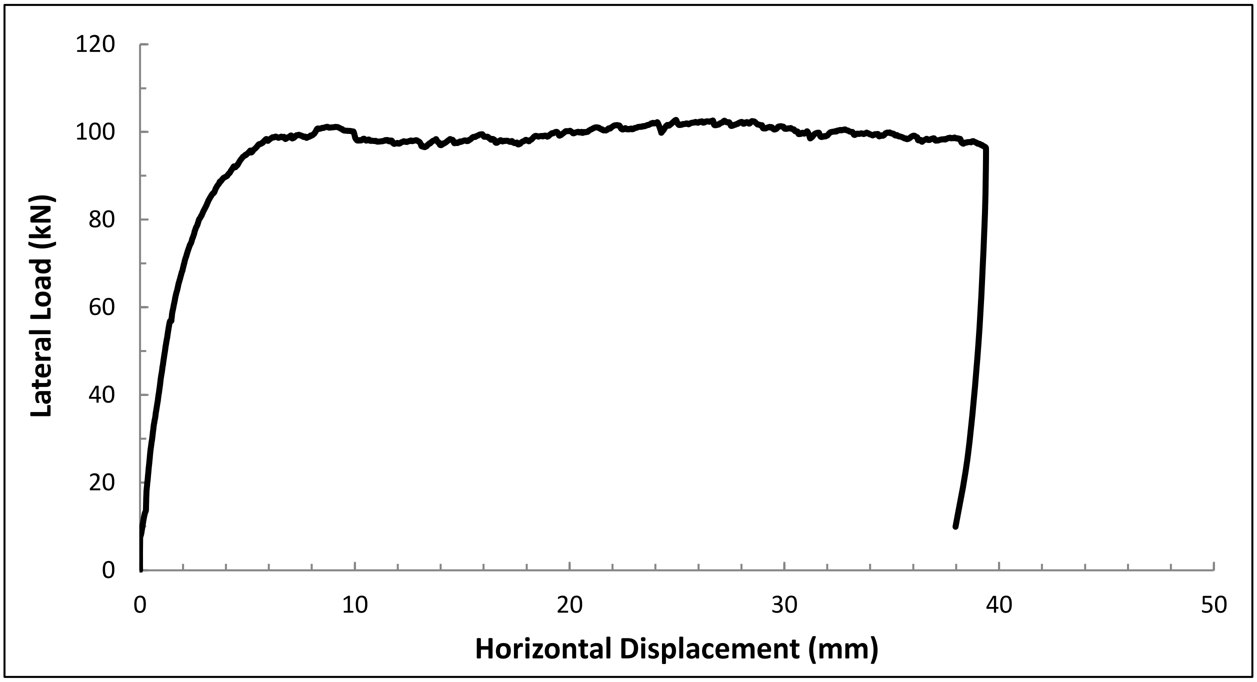

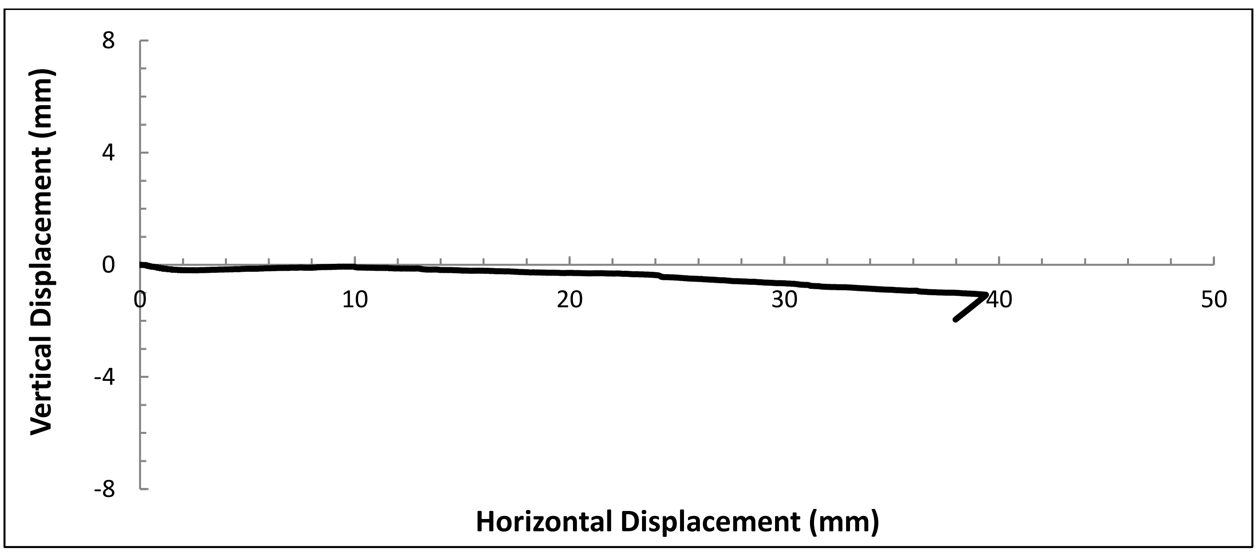

Test ID: M_2B_160

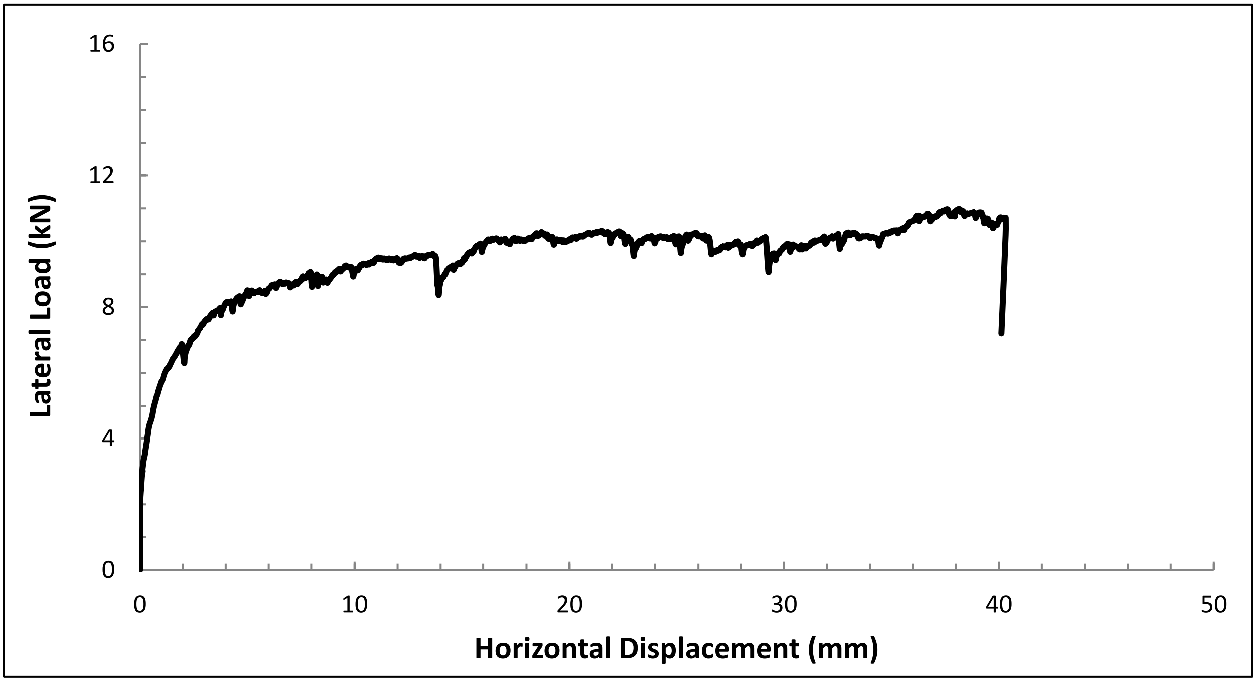

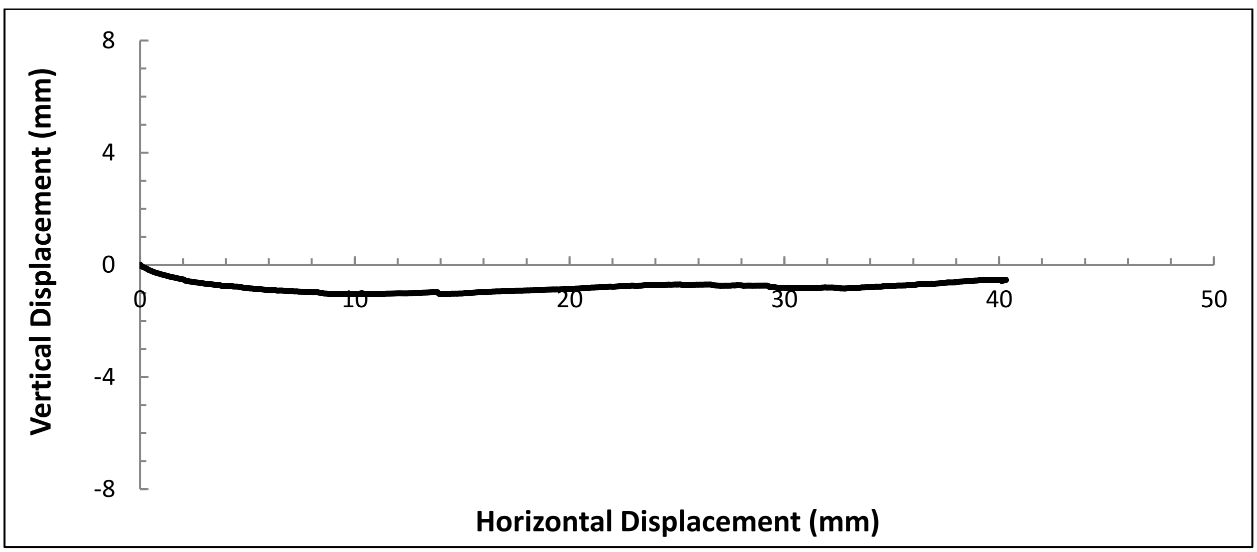

Test ID: M_2B_10

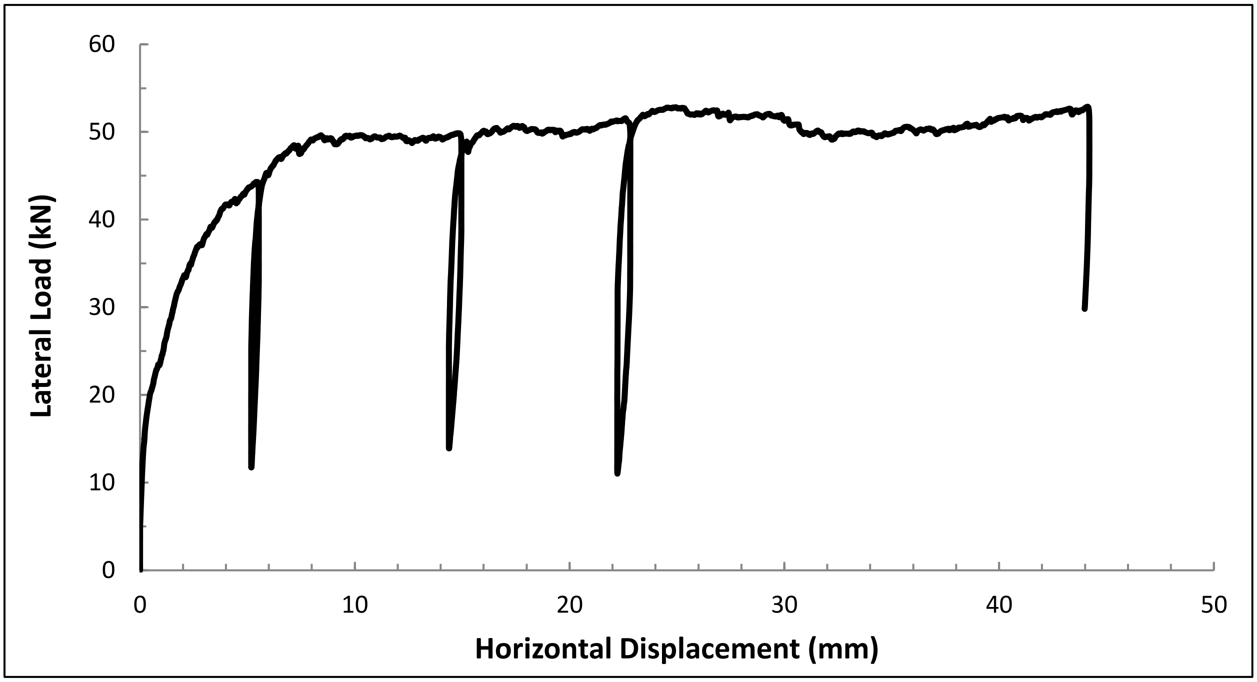

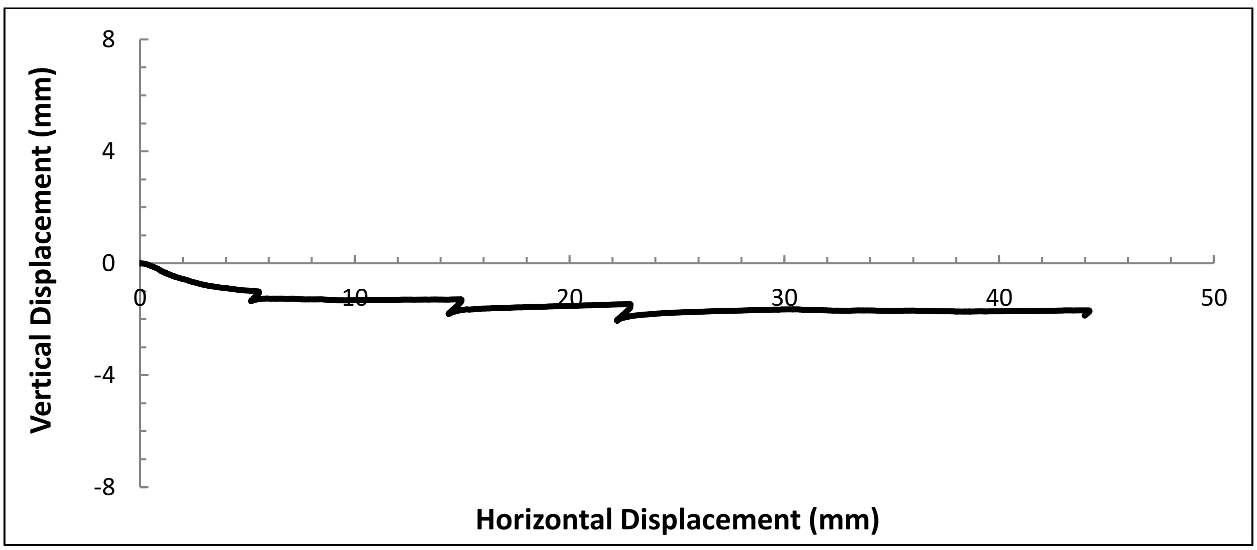

Test ID: M_2B_80 (CYCLIC)

III.3.3 Phase 3 shoulder test results in the McAbee Ballast

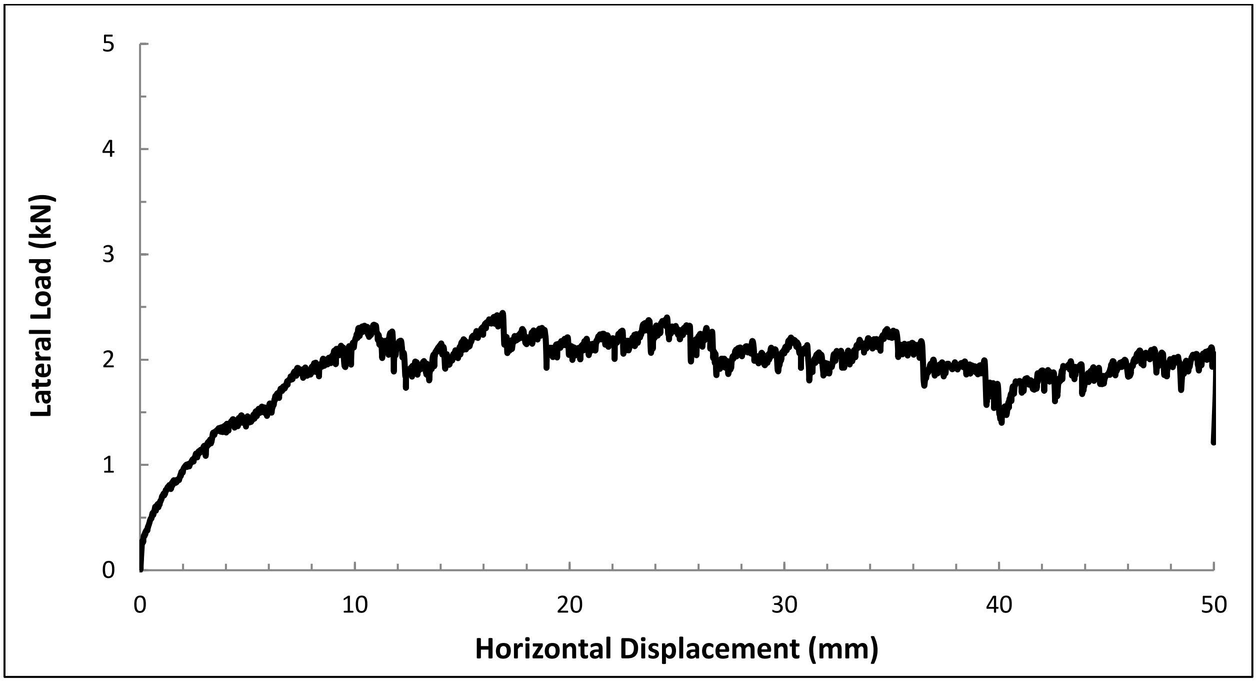

Test ID: M_3A_10

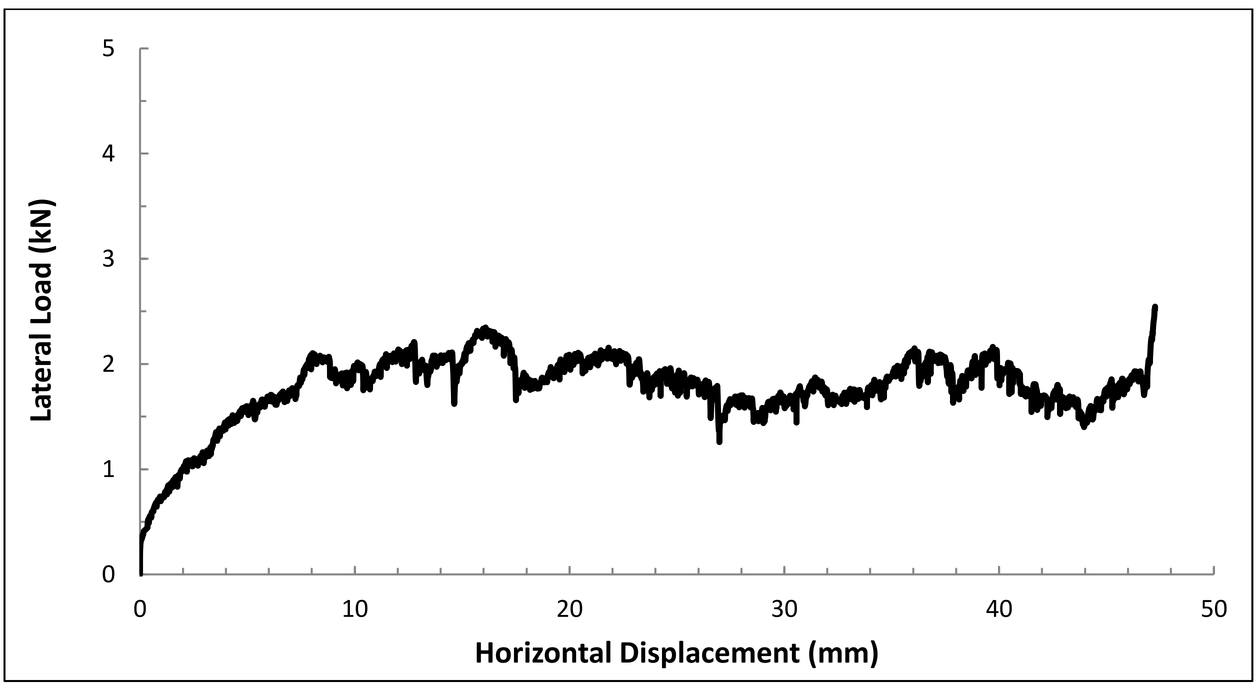

Test ID: M_3A_80

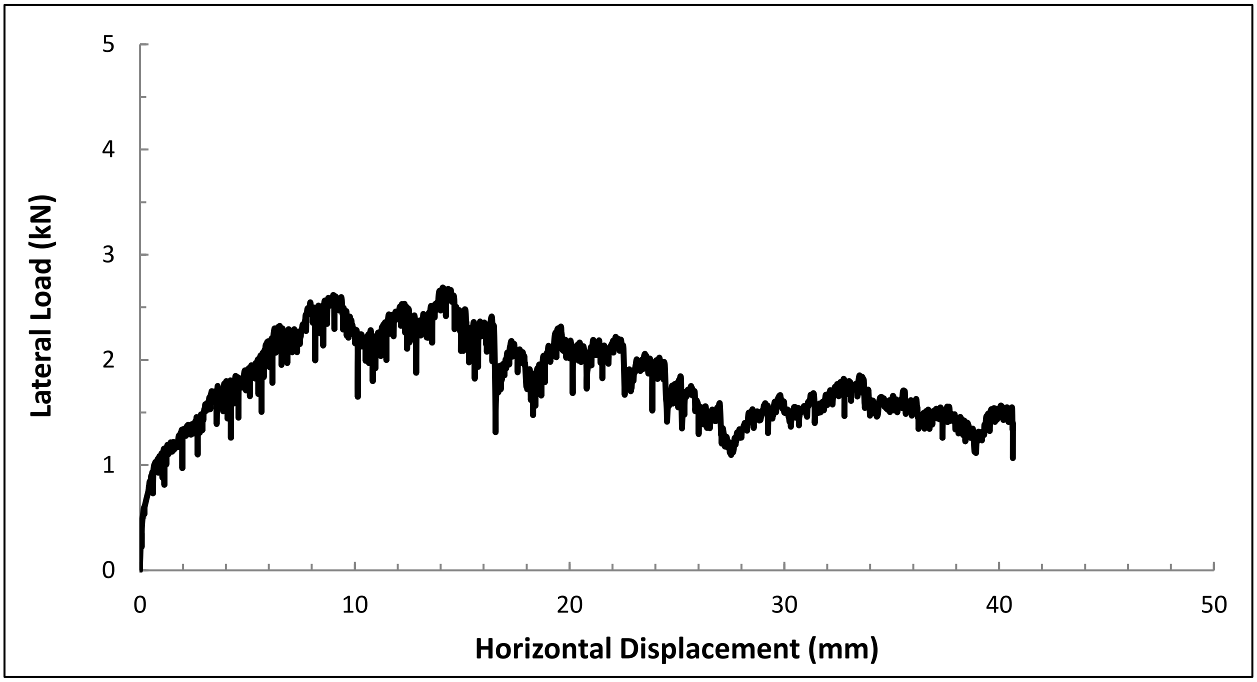

Test ID: M_3A_160

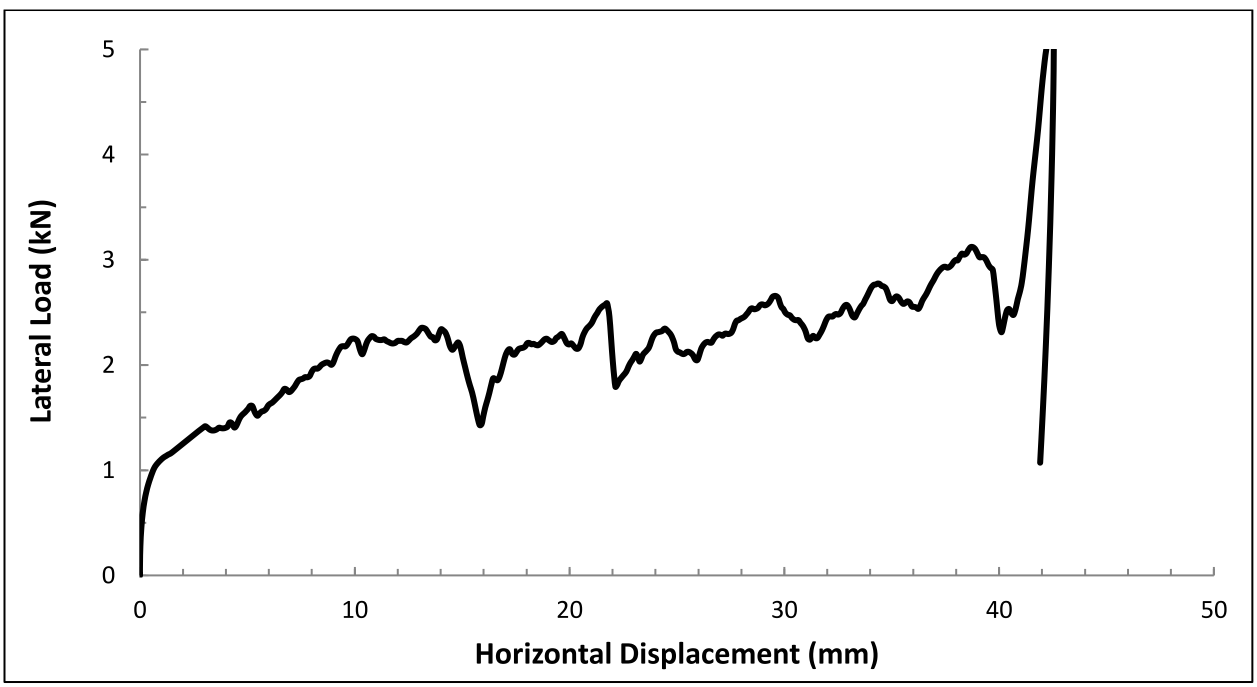

Test ID: M_3A_160 (F)

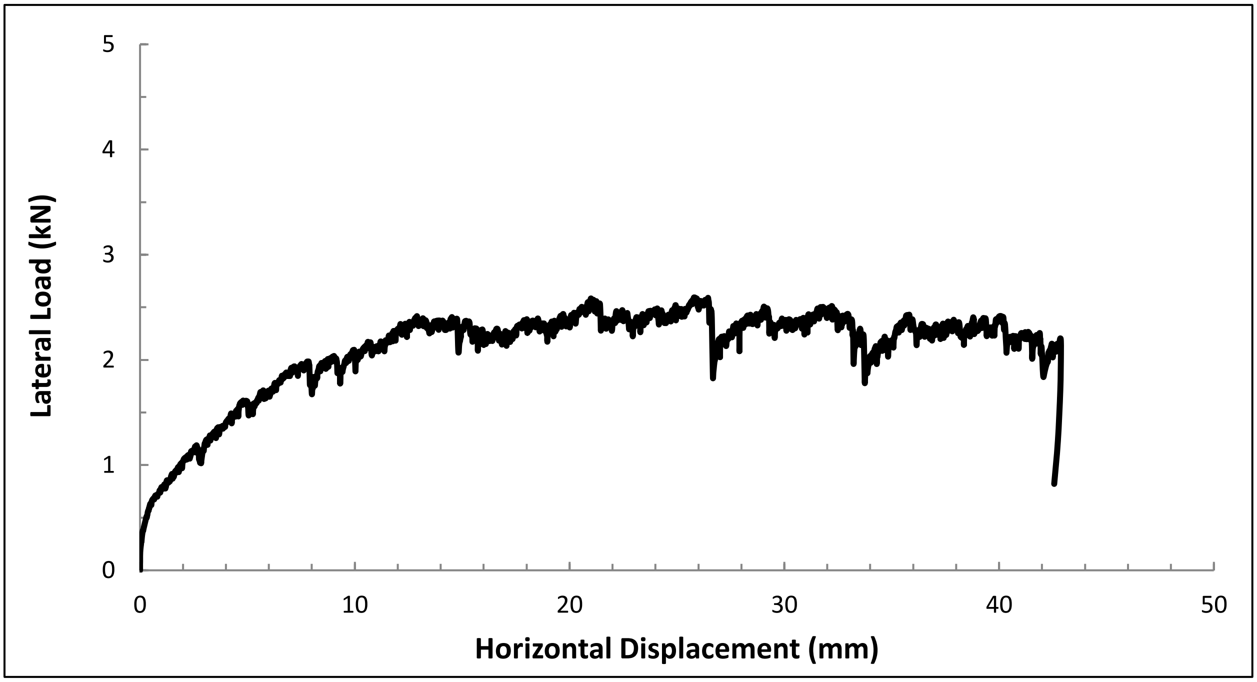

Test ID: M_3A_10 (2)

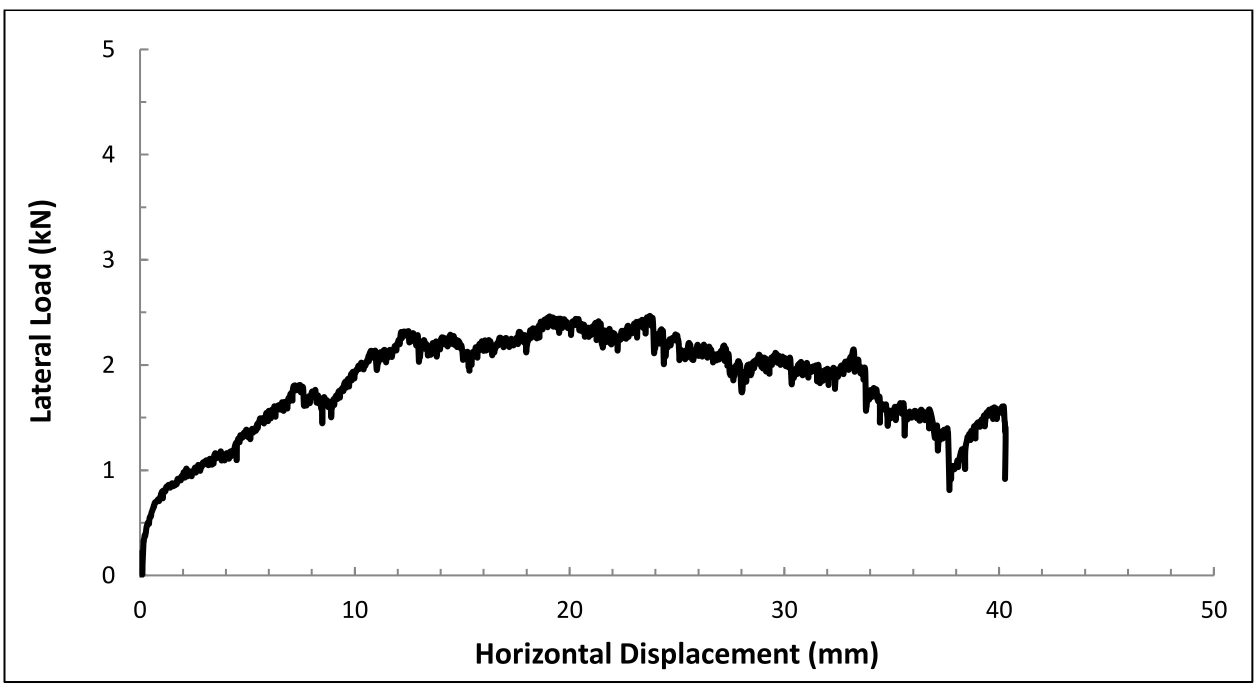

Test ID: M_3A_80 (2)

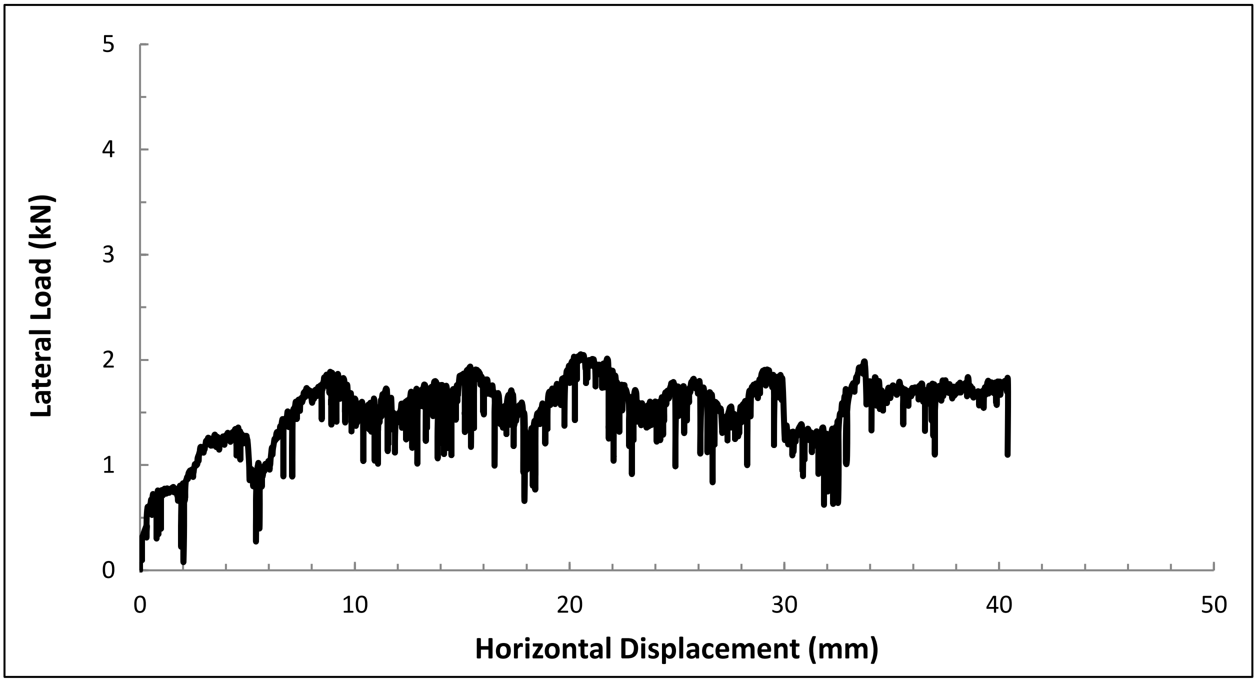

Test ID: M_3A_160 (2)

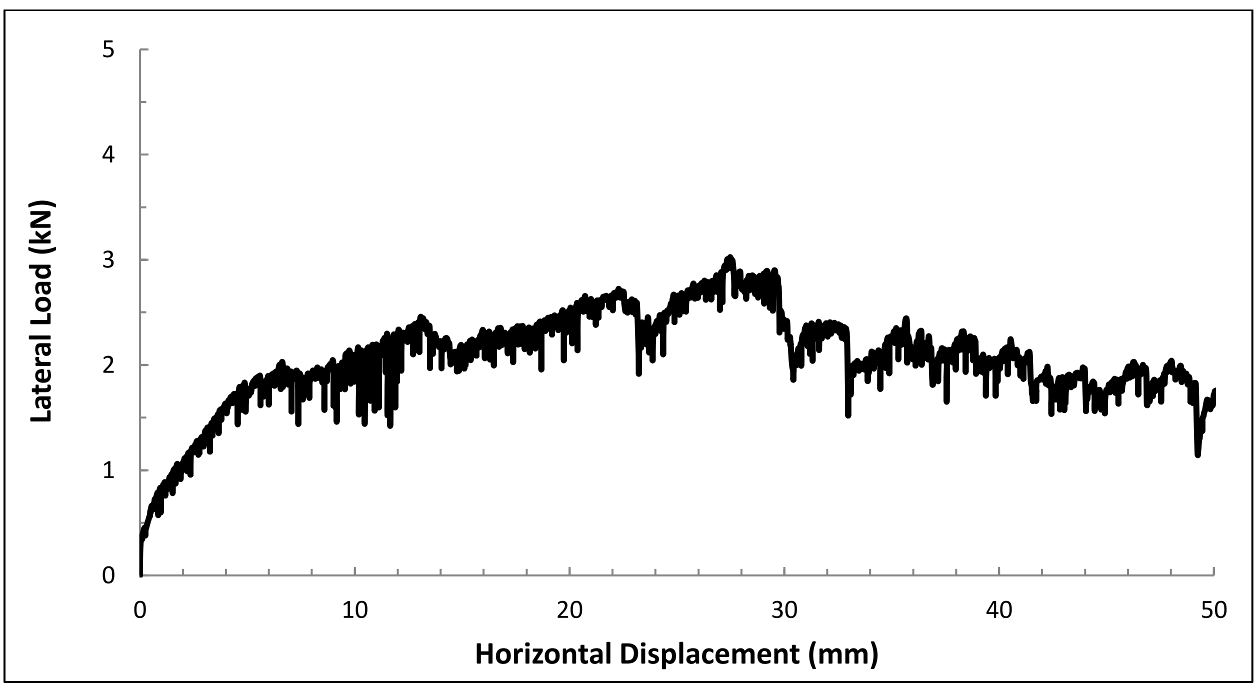

Test ID: M_3B_10

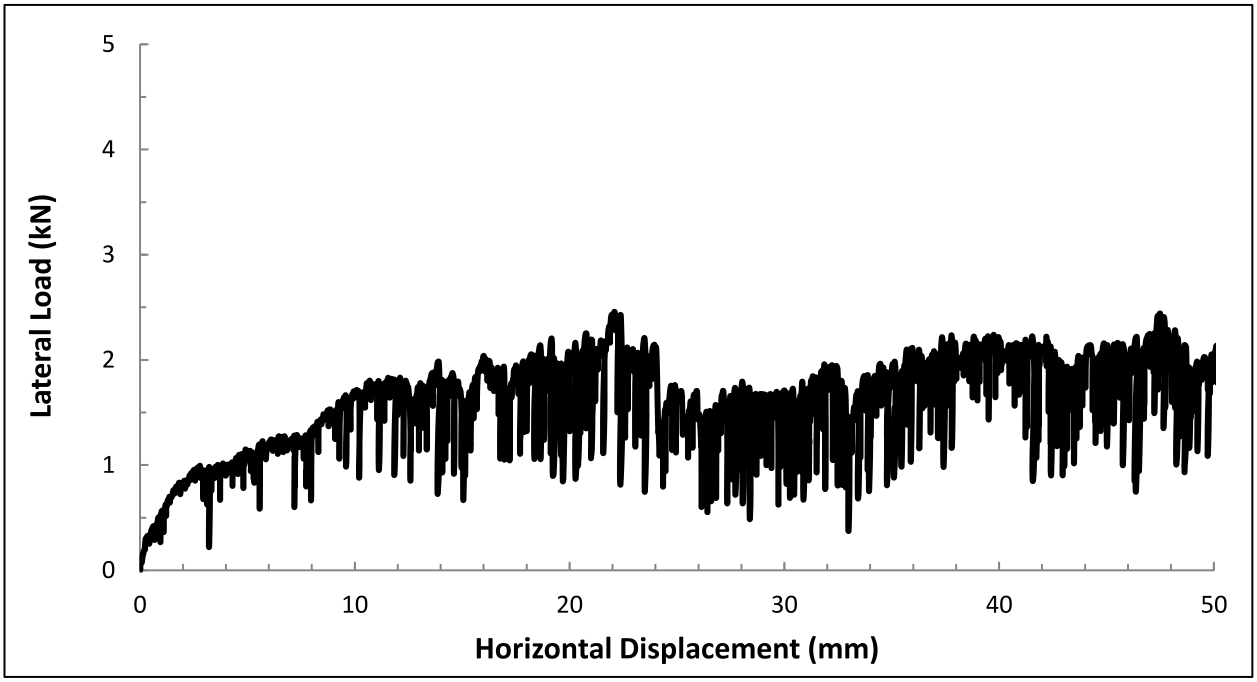

Test ID: M_3B_80

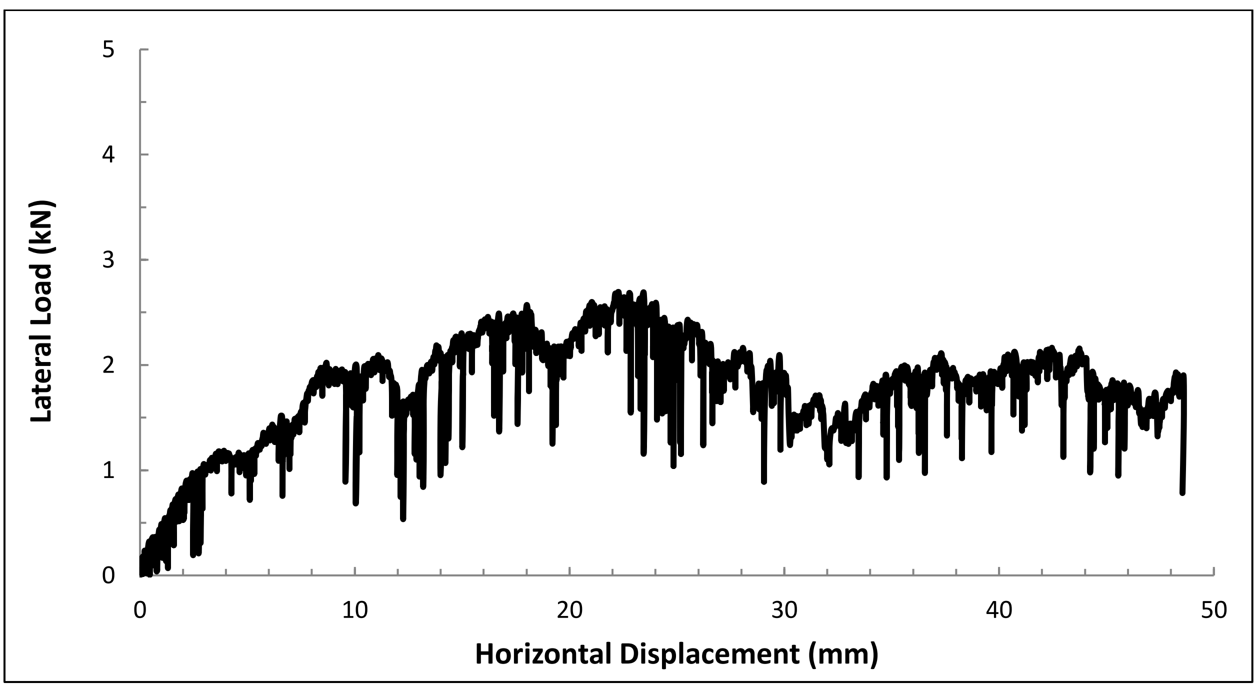

Test ID: M_3B_160

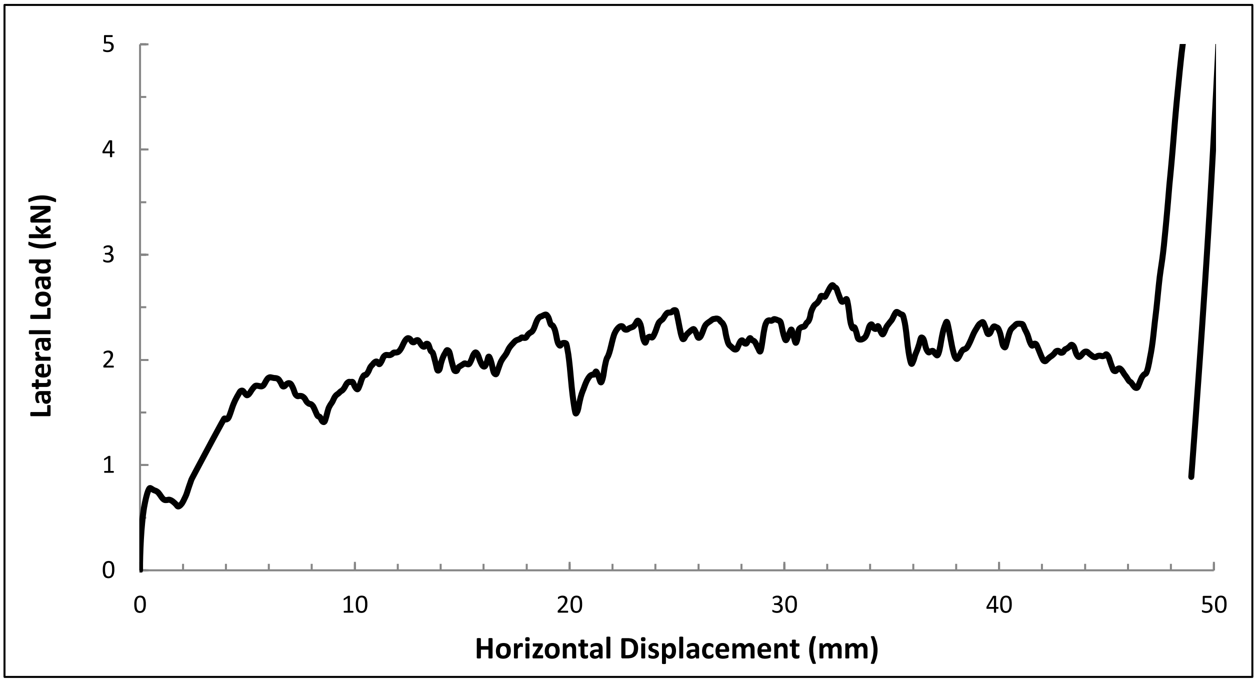

Test ID: M_3B_160 (F)

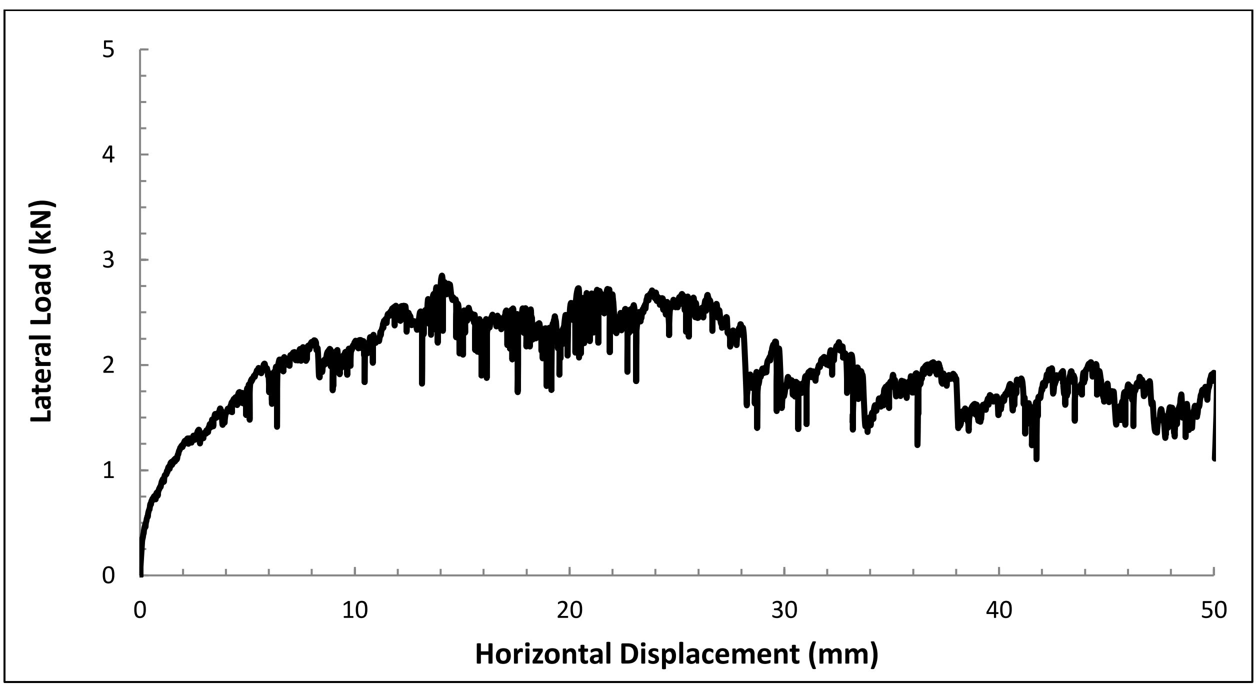

Test ID: M_3B_10 (2)

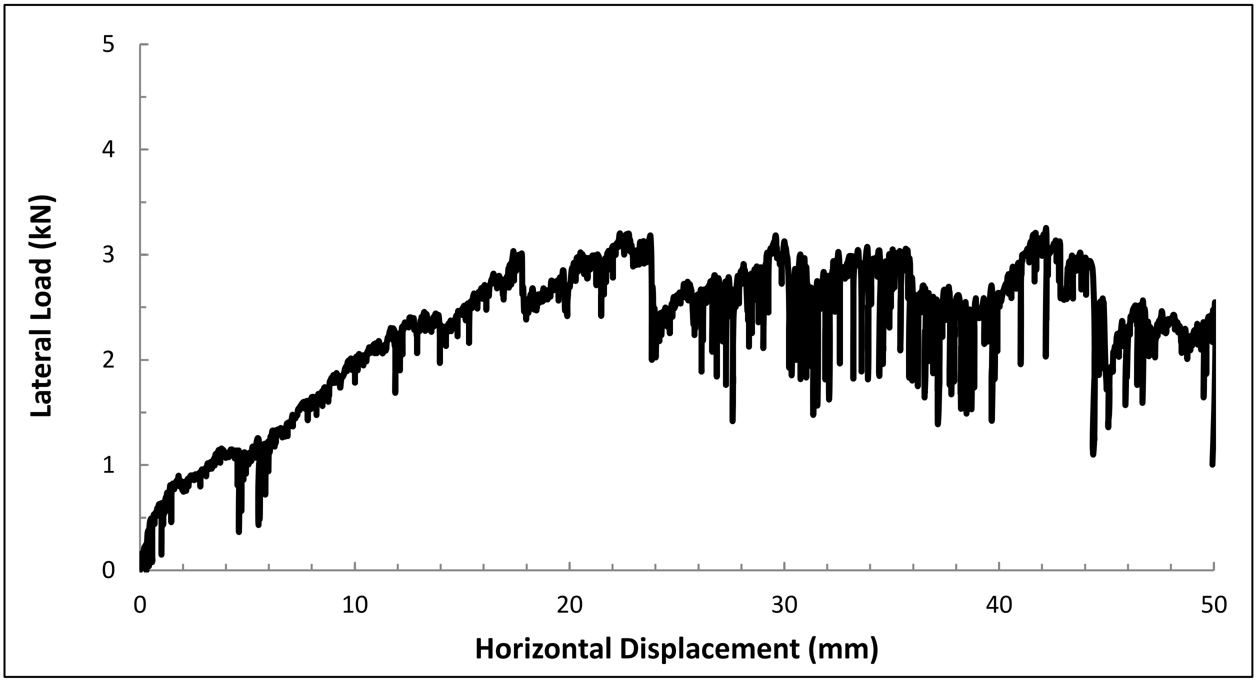

Test ID: M_3B_80 (2)

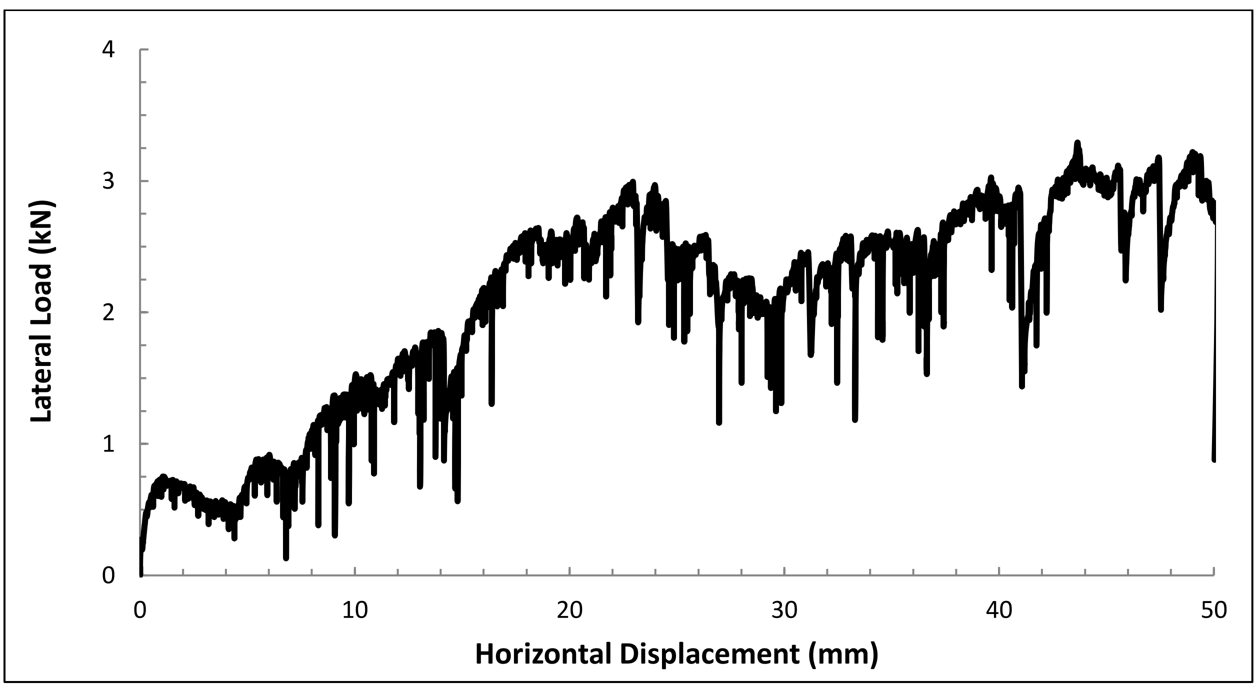

Test ID: M_3B_160 (2)

III.3.4 Phase 1 base tests results in the Gravel Ballast

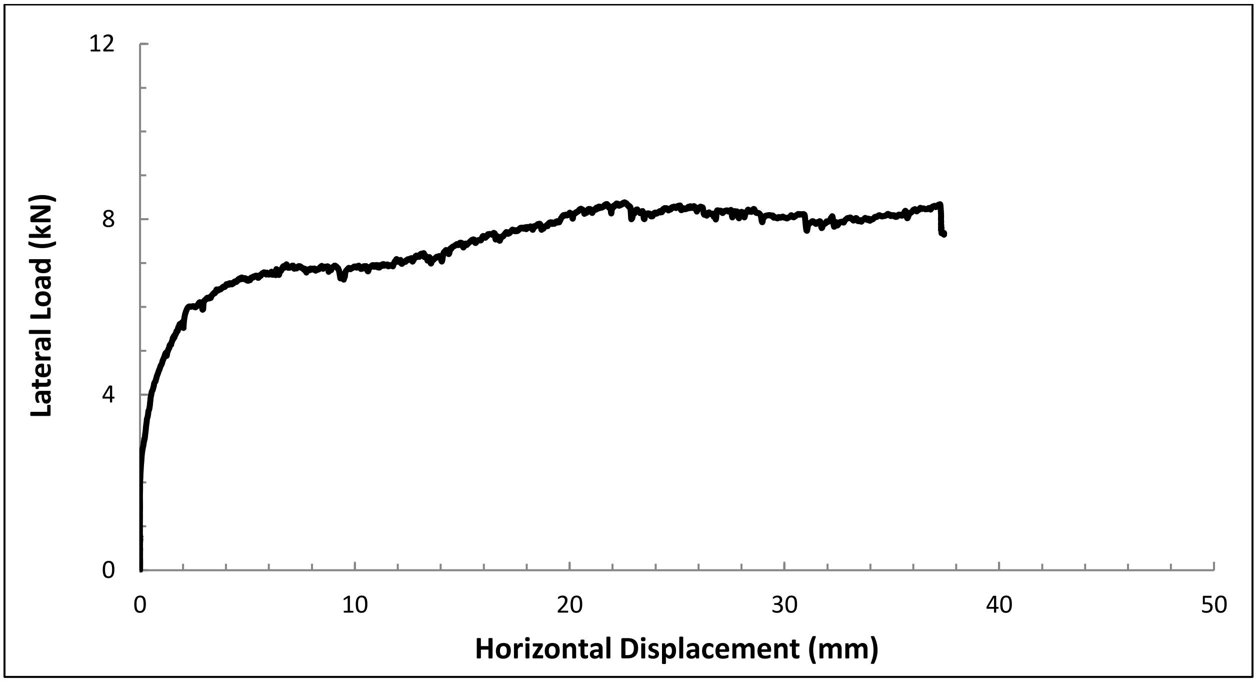

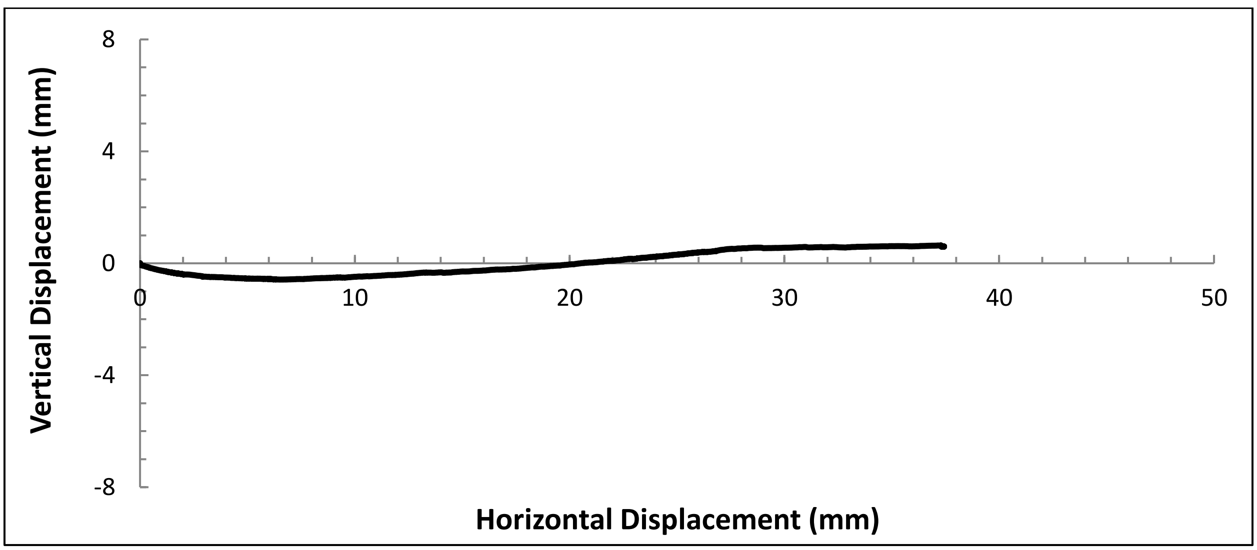

Test ID: G_4A_10

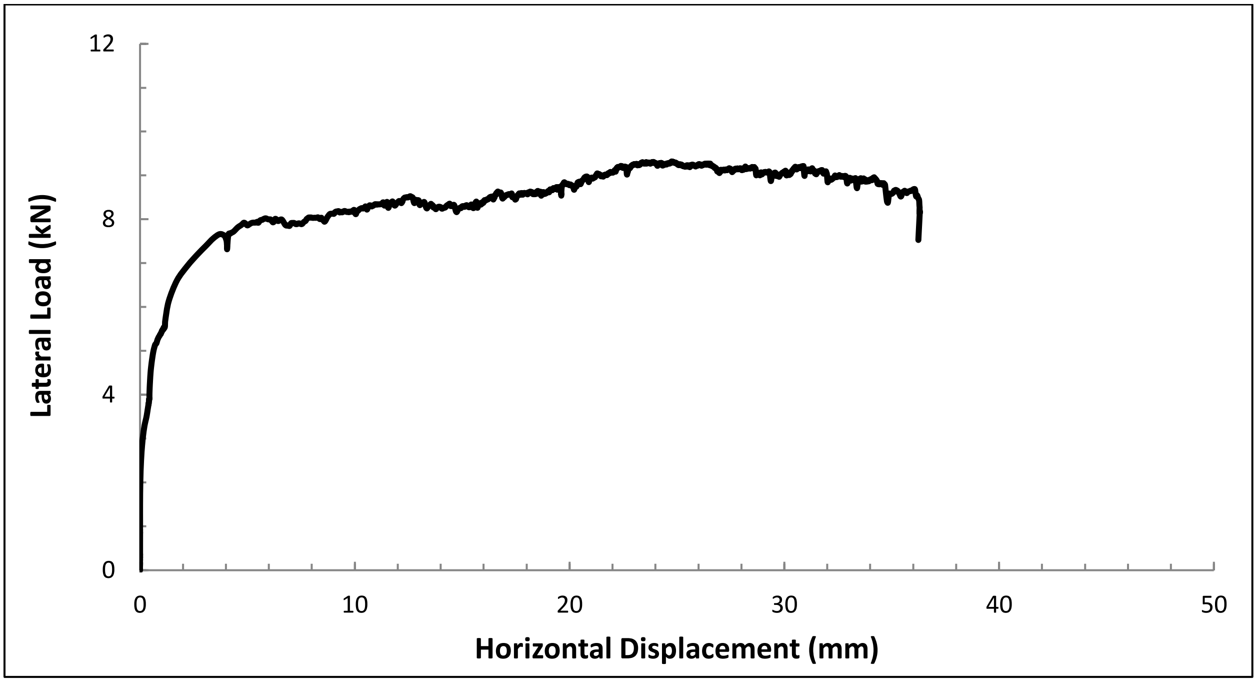

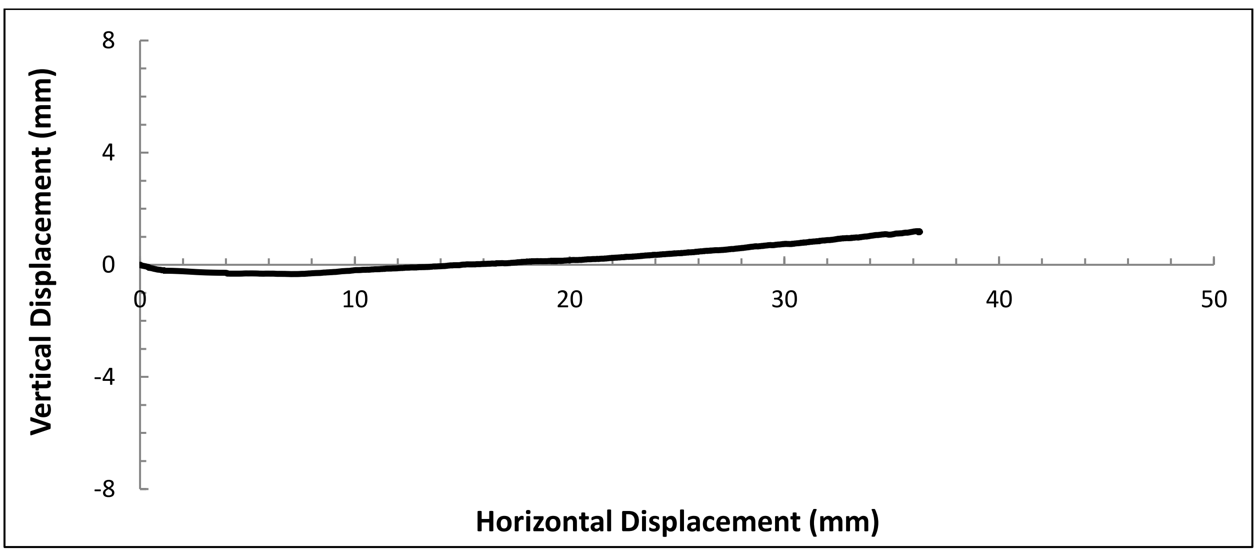

Test ID: G_4A_10 (2)

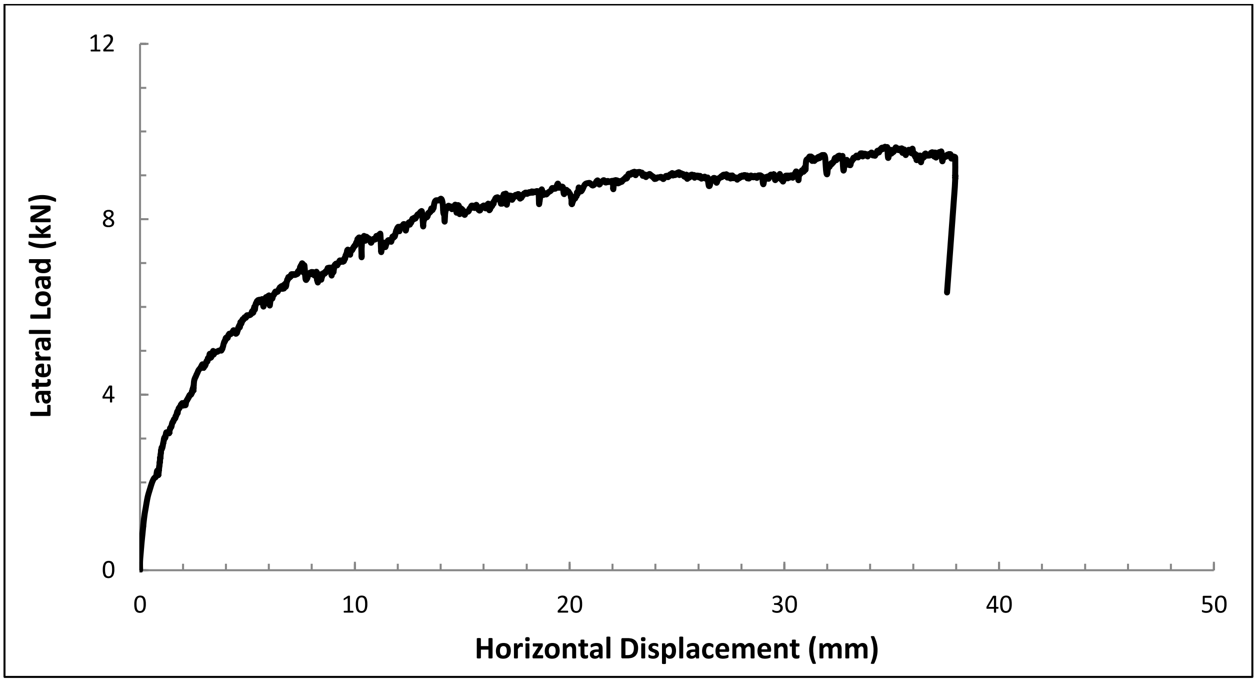

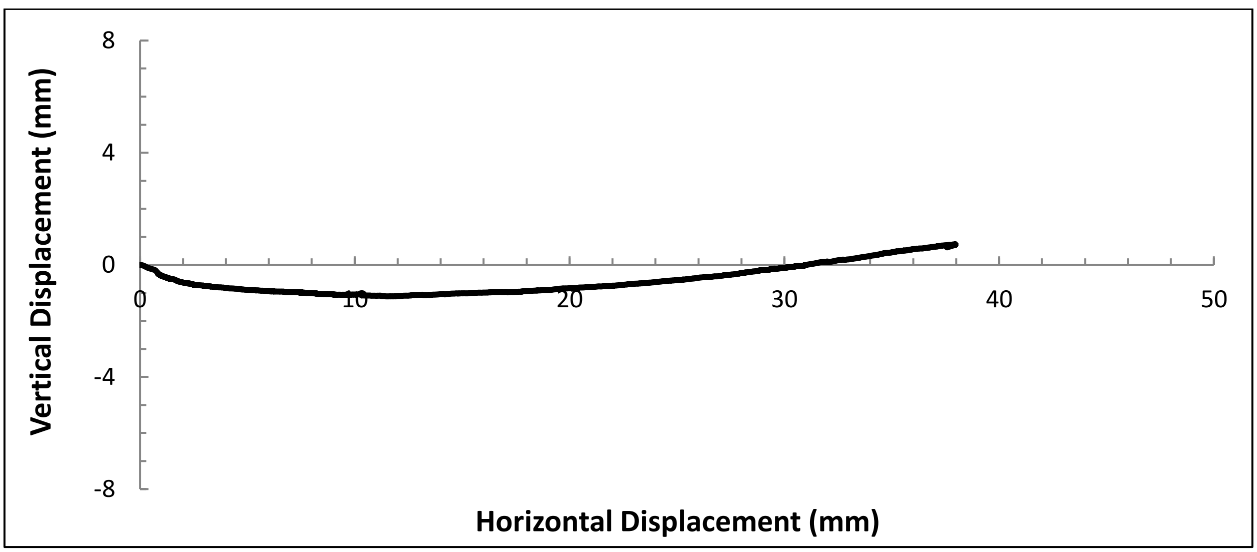

Test ID: G_4A_10 (3)

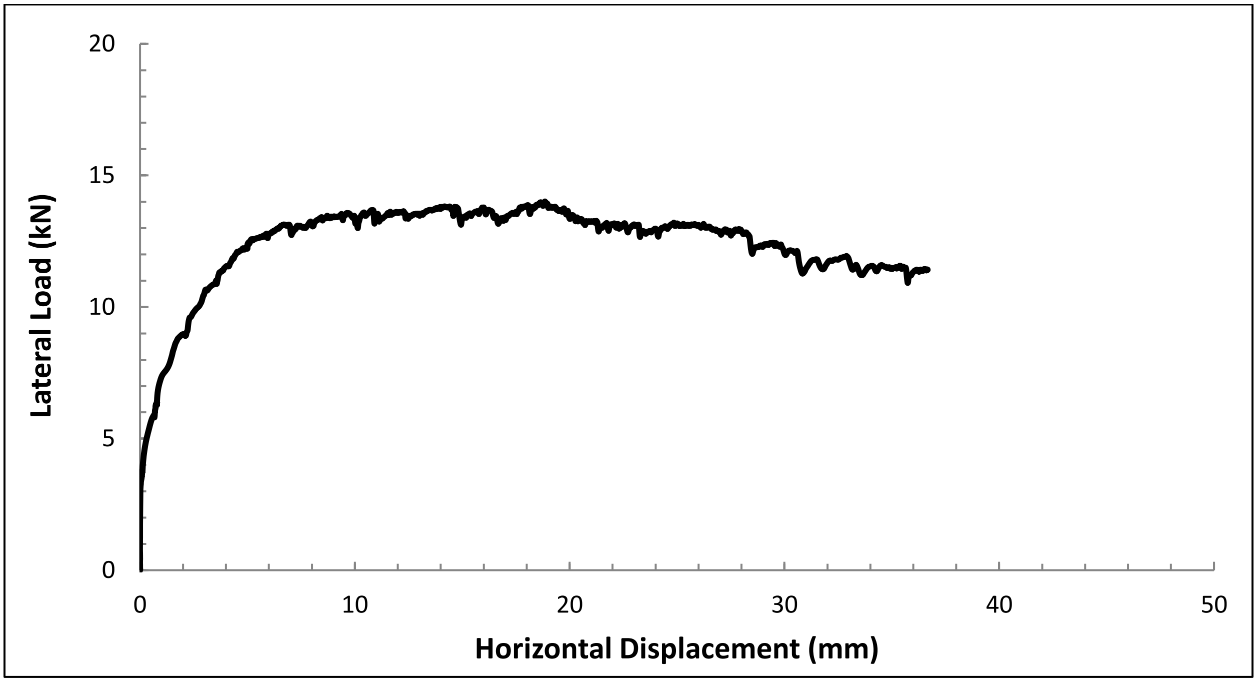

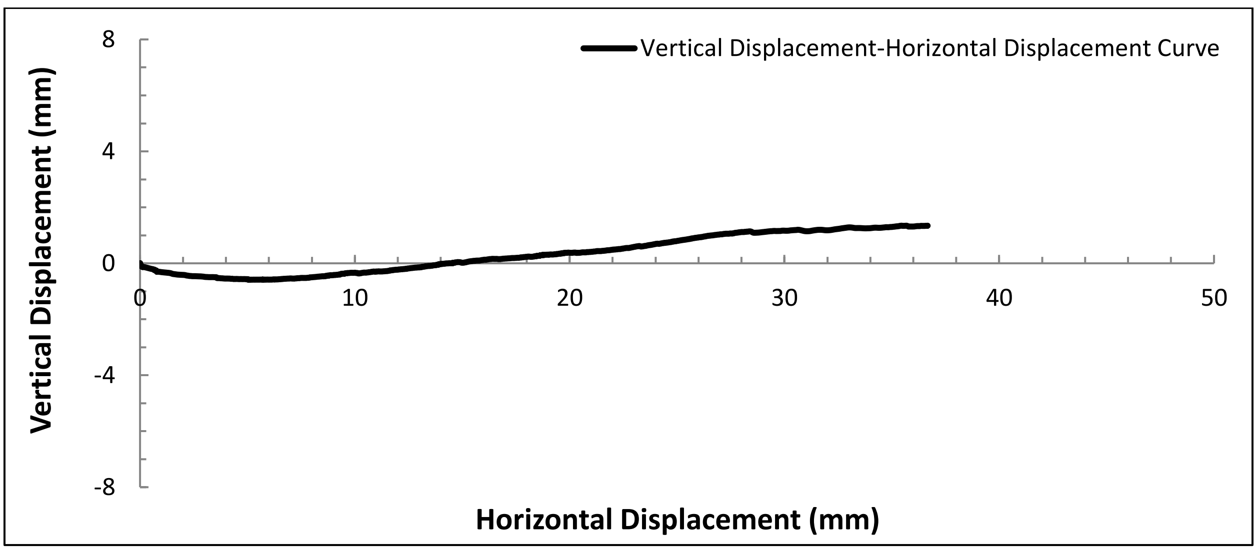

Test ID: G_4A_20

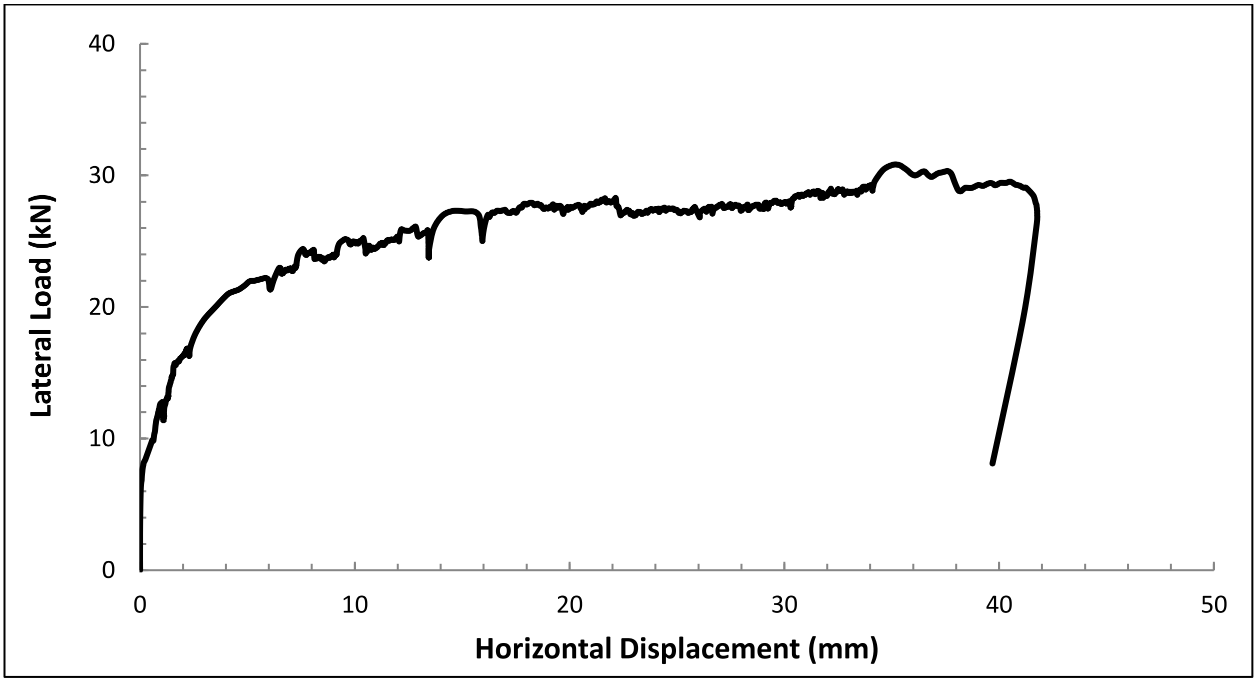

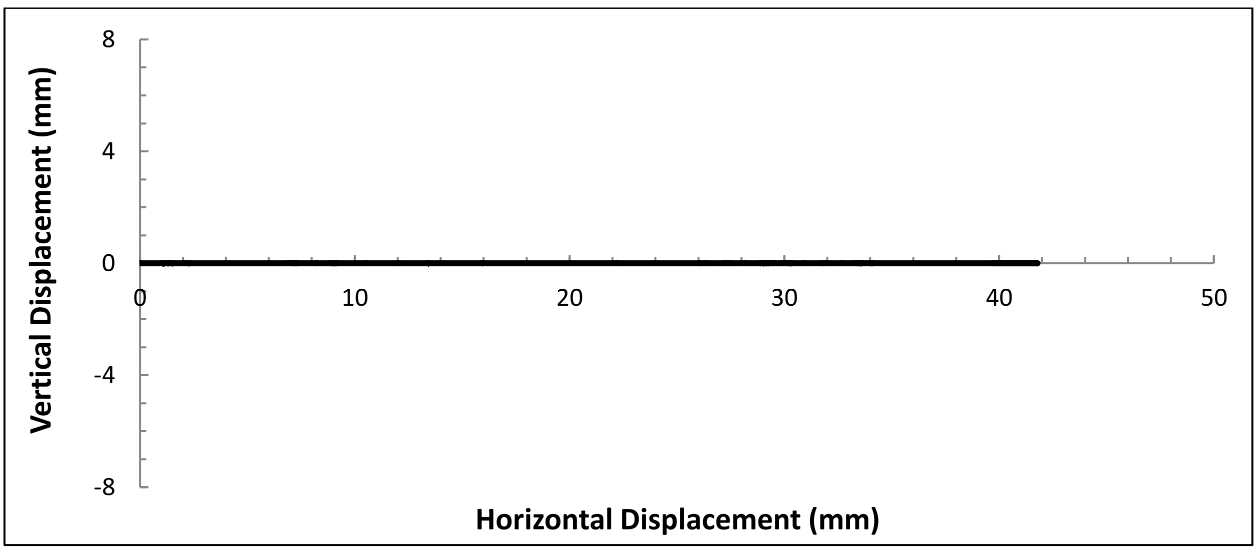

Test ID: G_4A_40 (EXCLUDED)

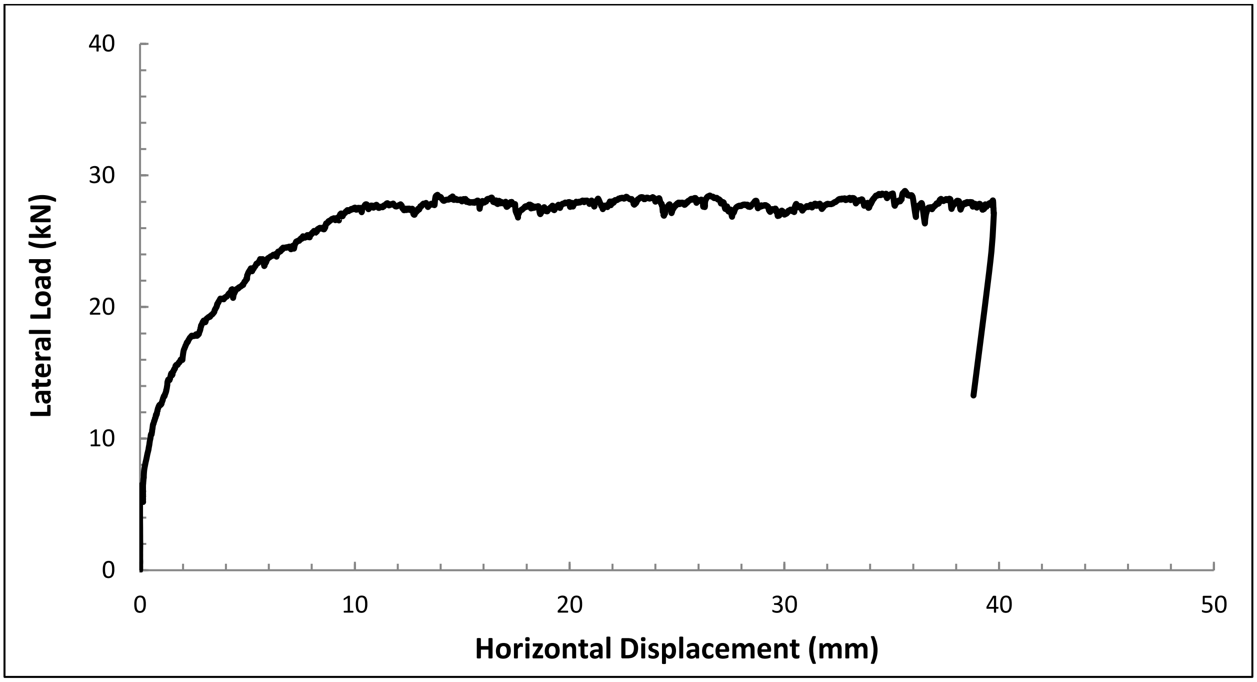

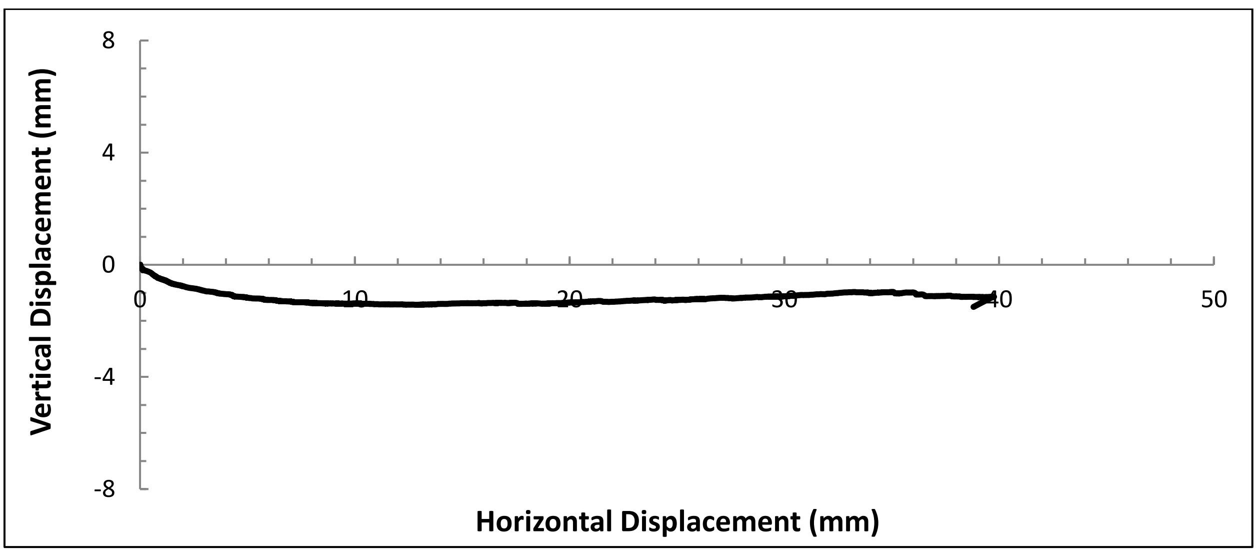

Test ID: G_4A_40

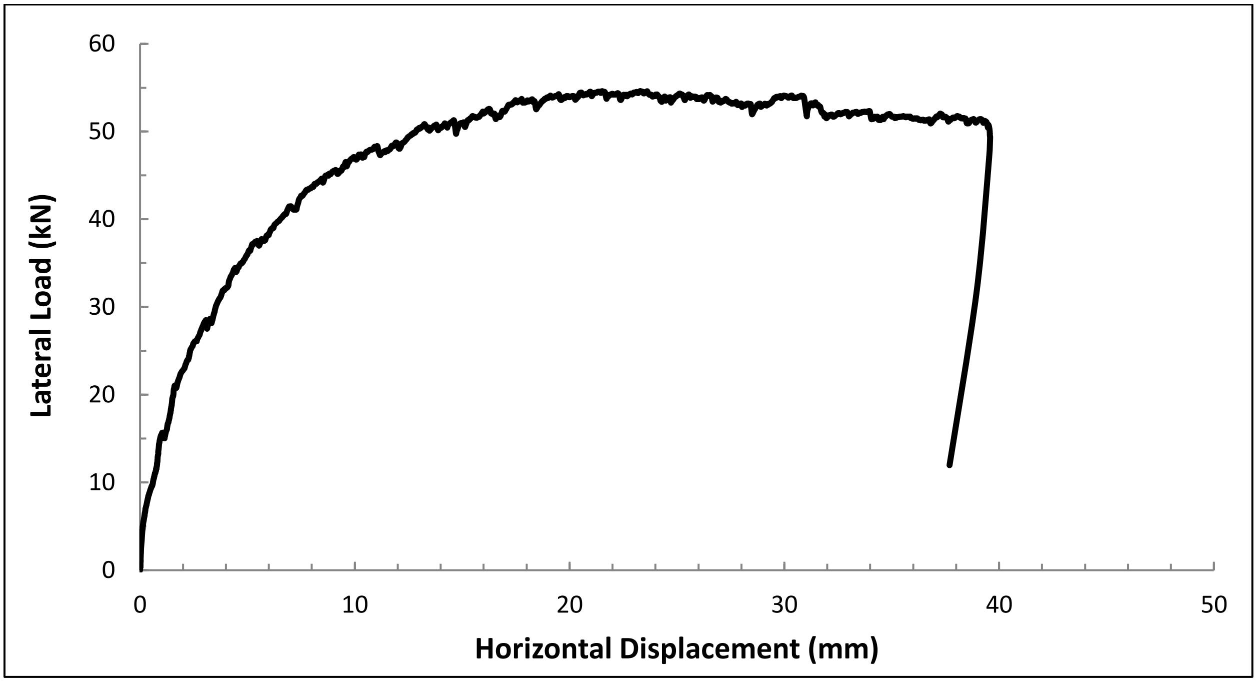

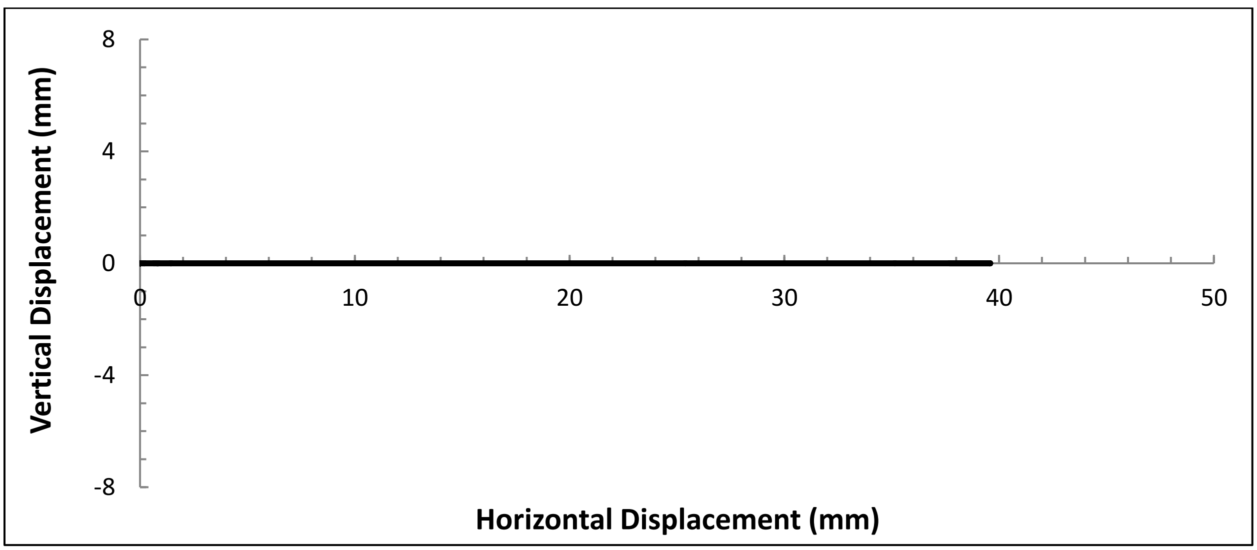

Test ID: G_4A_80

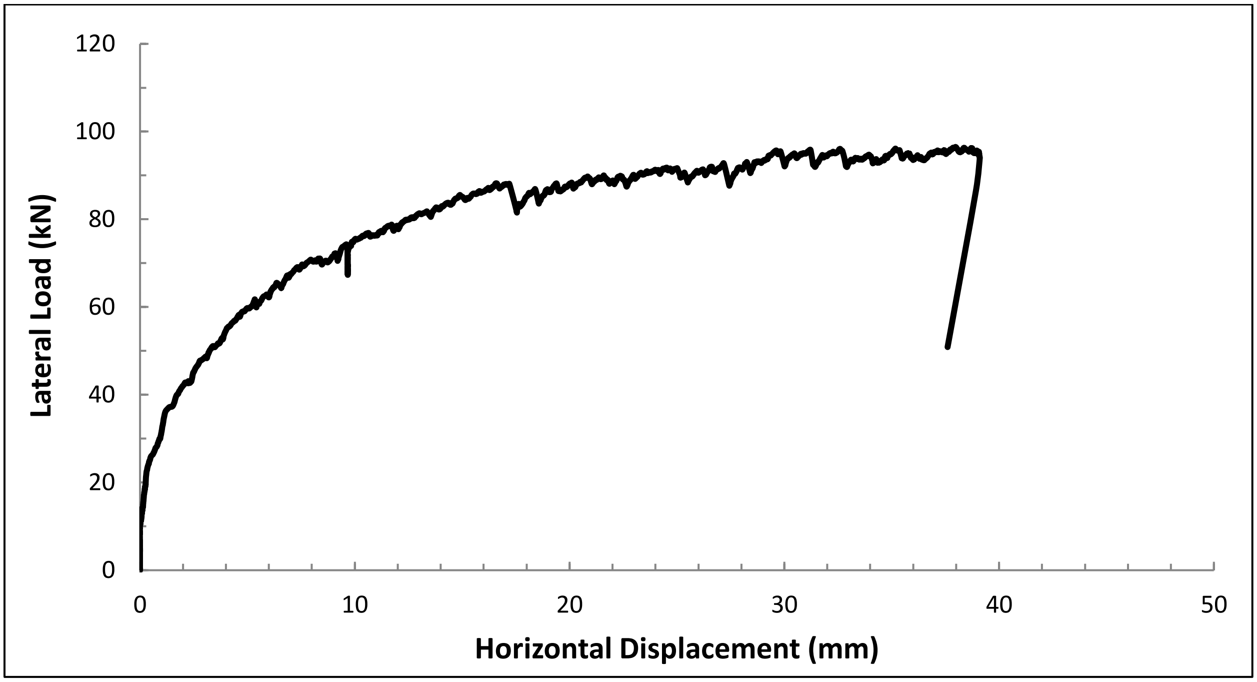

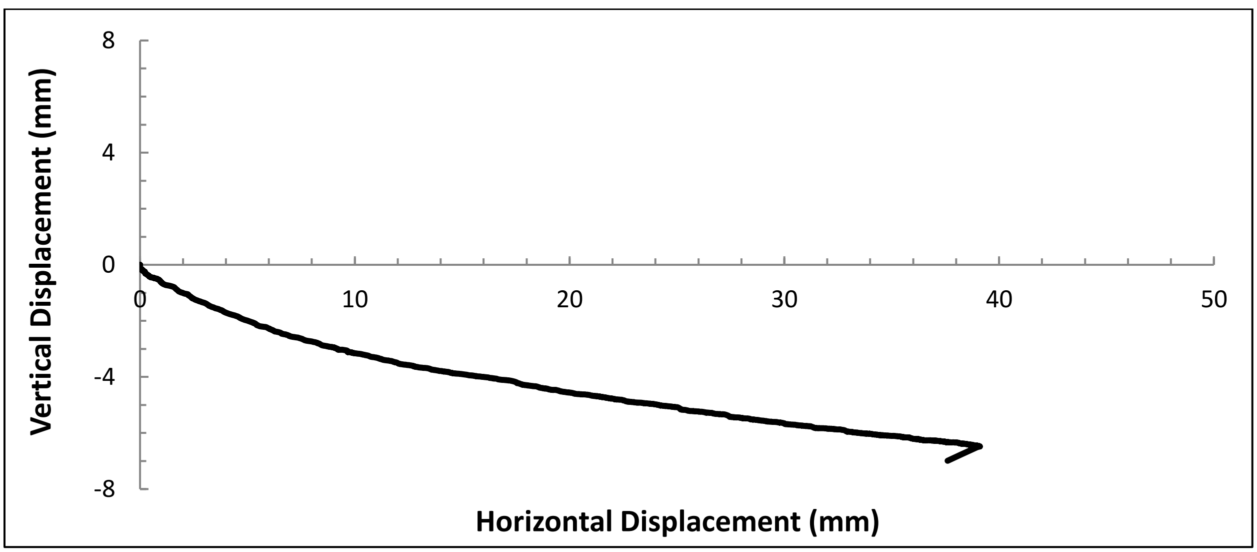

Test ID: G_4A_160

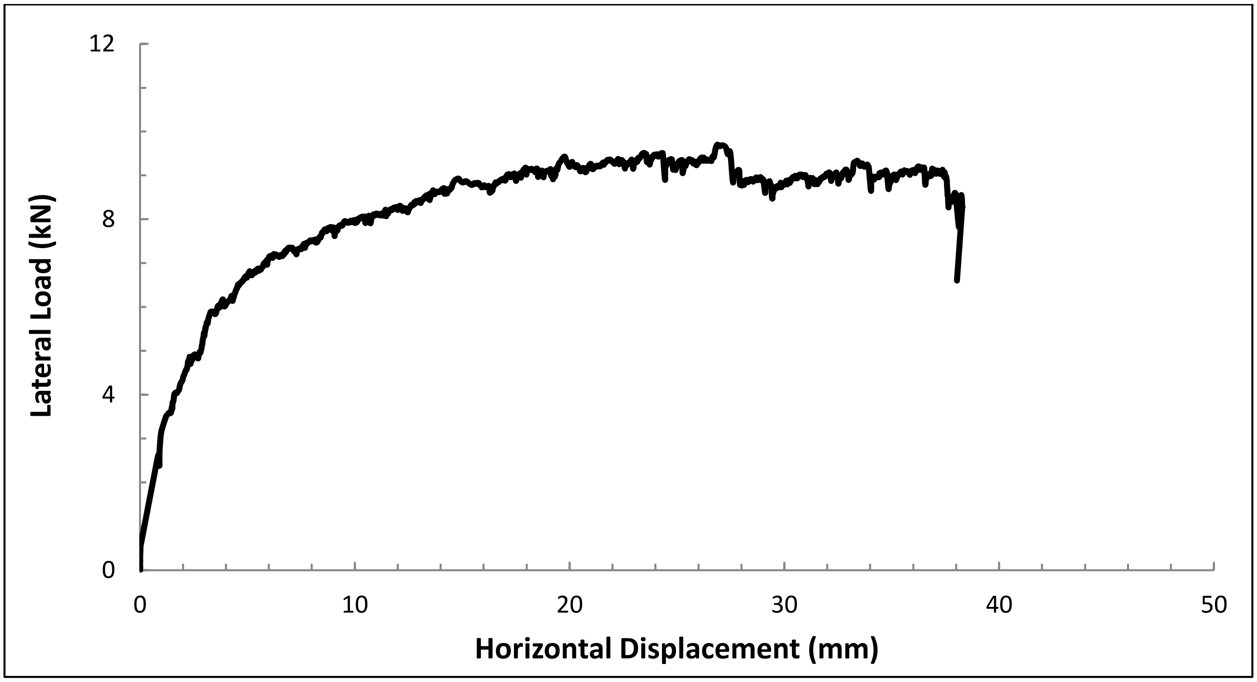

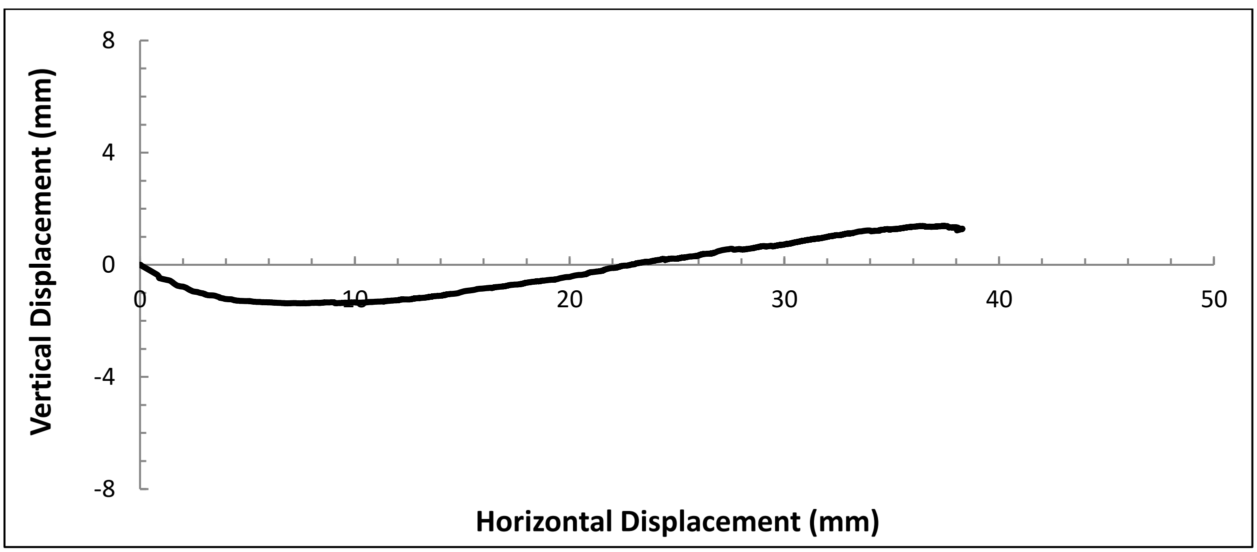

Test ID: G_4A_10 (4)

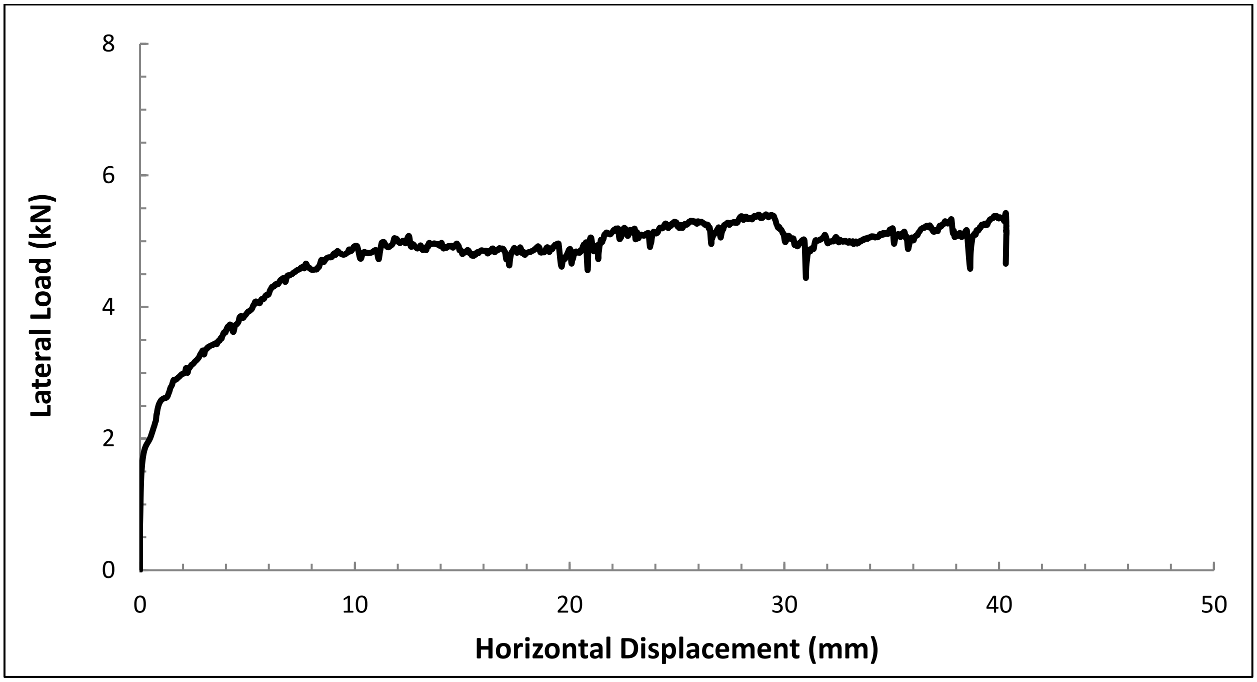

8
6
4
2
0
0
10
20
30
40
50
Lateral Load (kN)
Horizontal Displacement (mm)

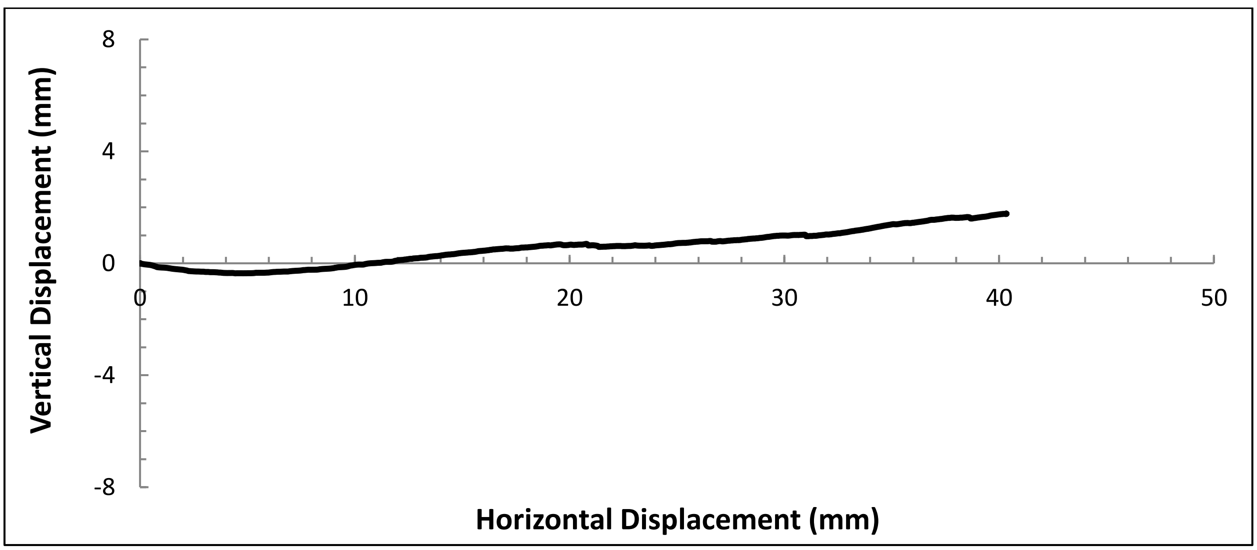

8
4
0
-4
-8
0
10
20
30
40
50
Vertical Displacement (mm)
Horizontal Displacement (mm)

Test ID: G_4A_5

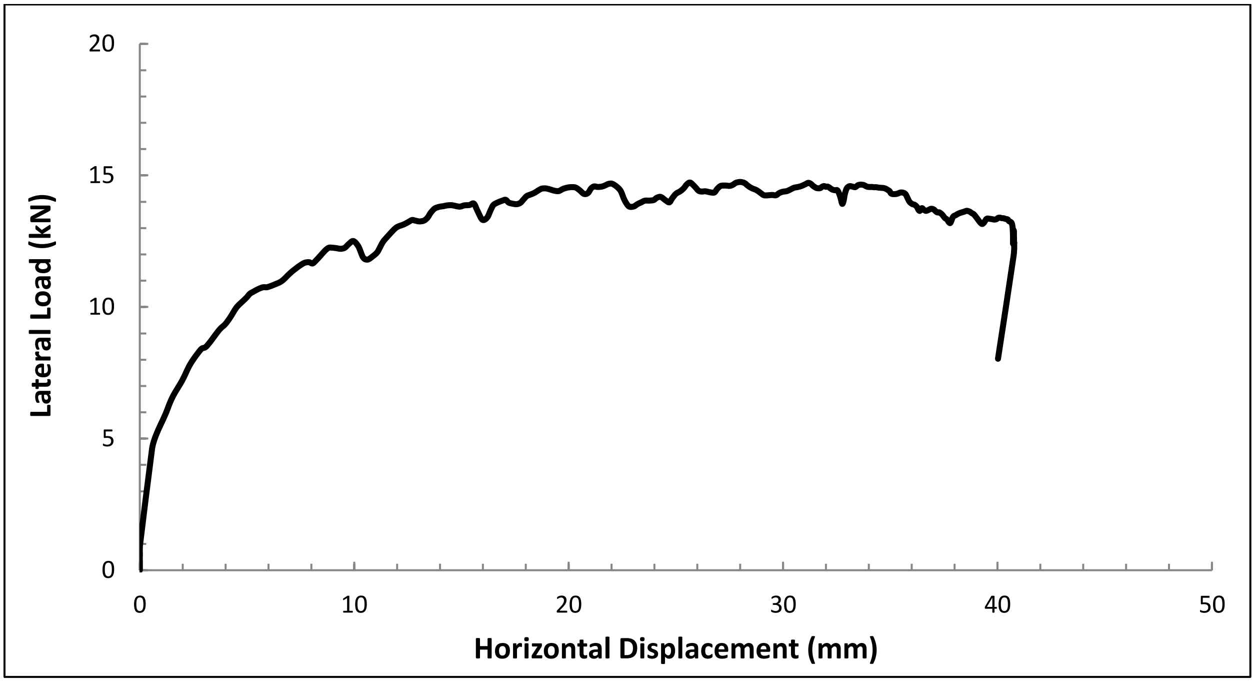

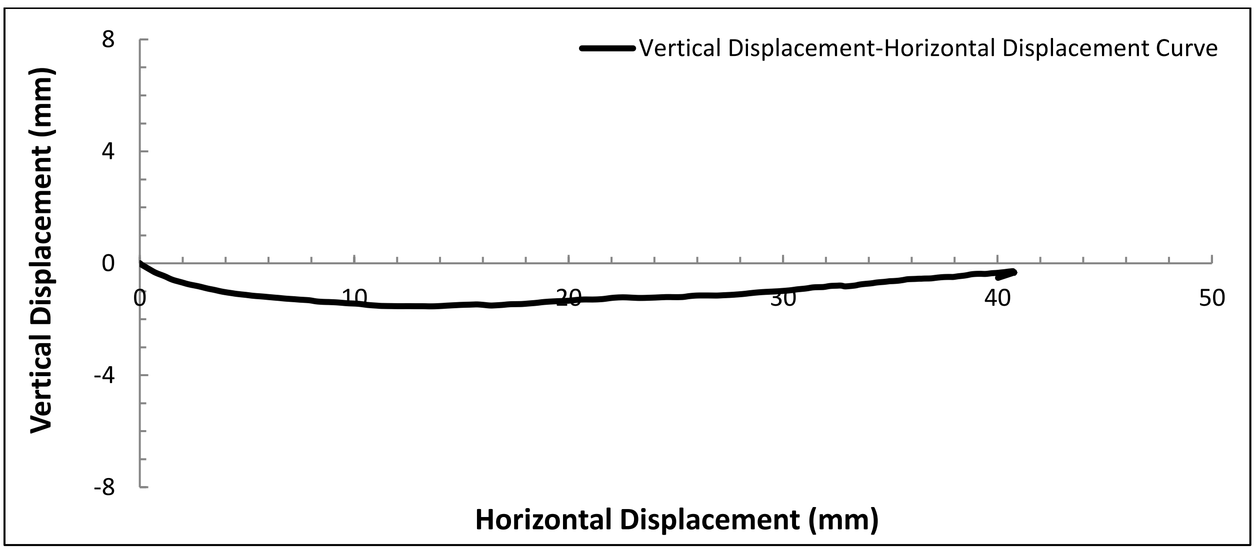

Test ID: G_5_20 (FAST)

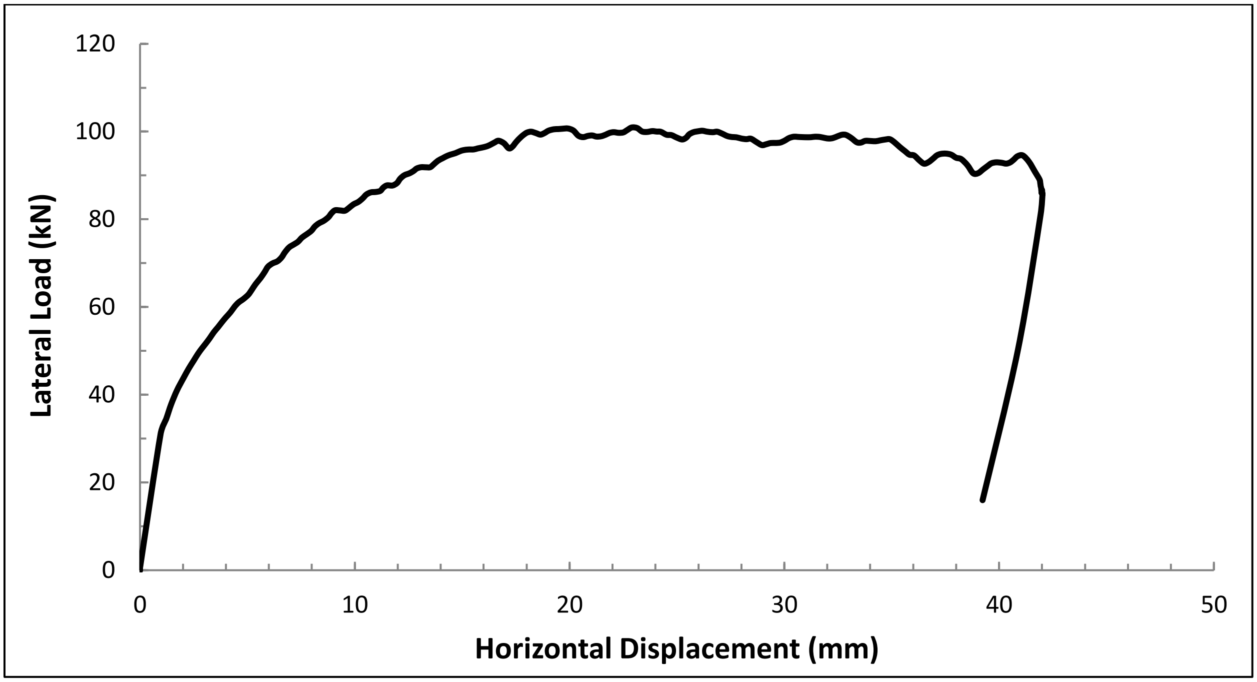

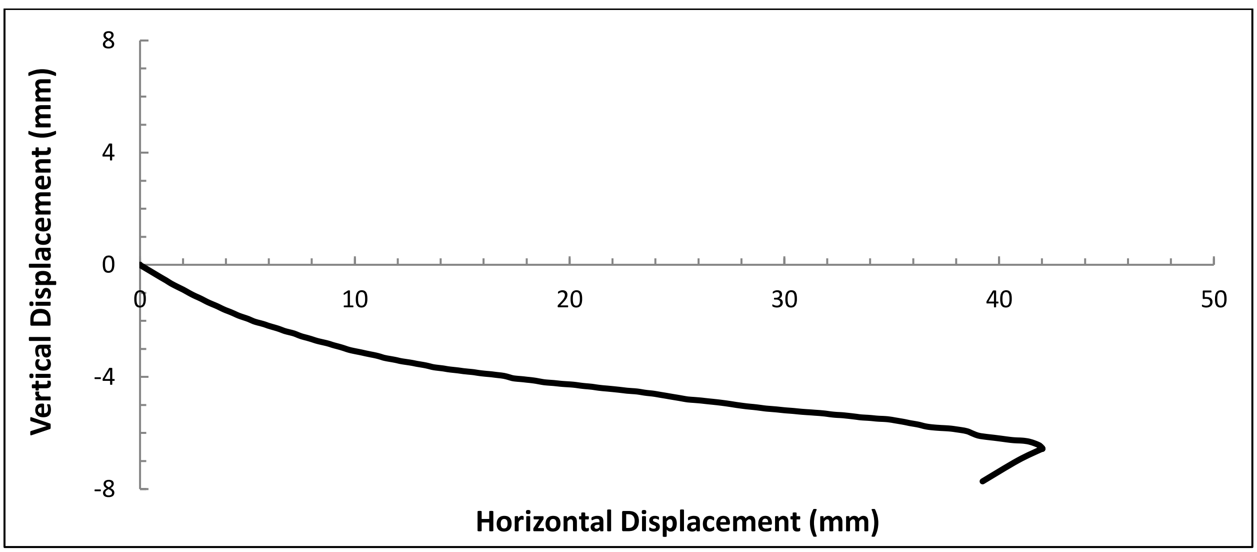

Test ID: G_5_160 (FAST)

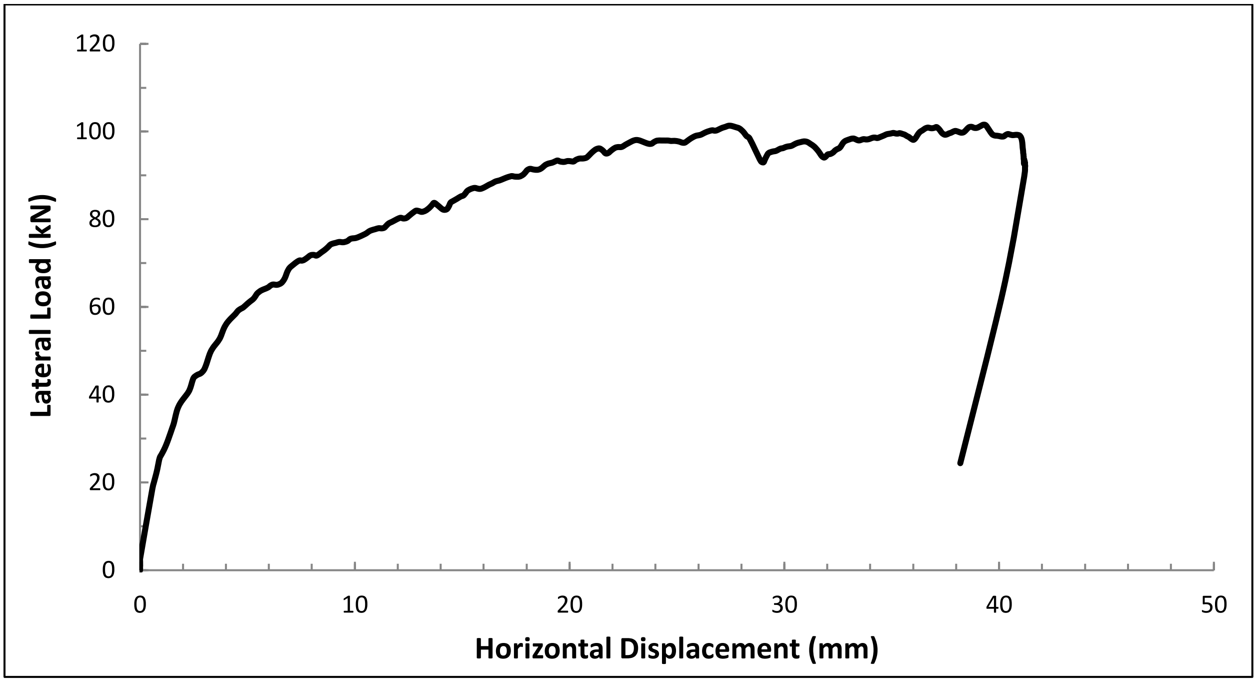

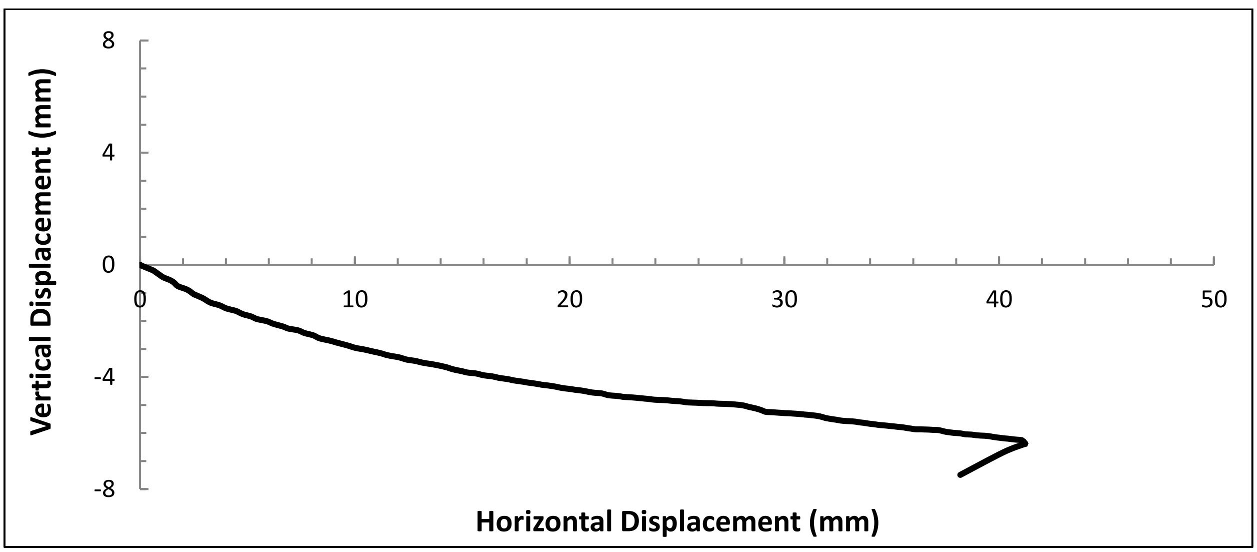

Test ID: G_5_160 (FAST) (2)

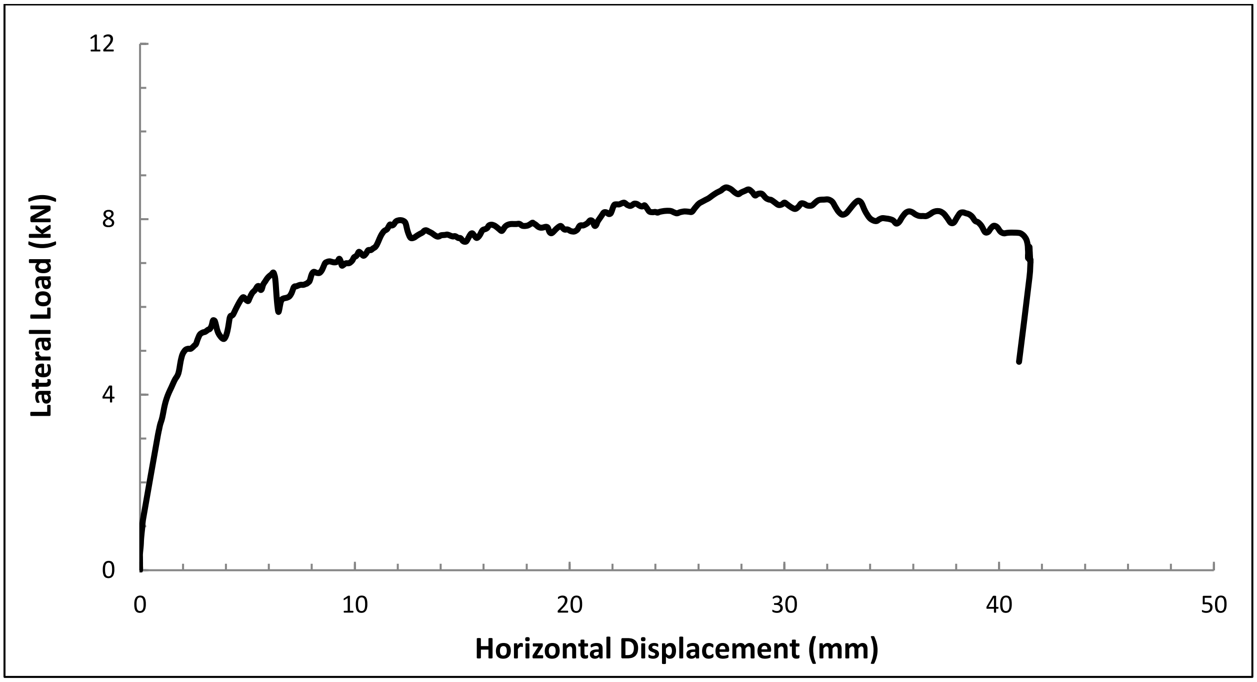

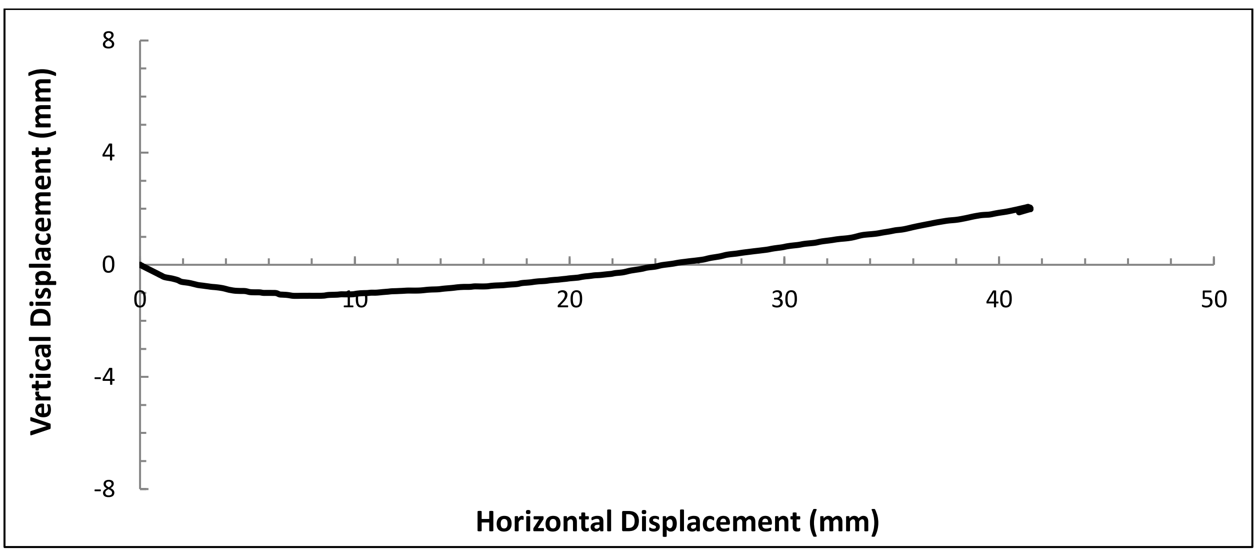

Test ID: G_5_10 (FAST)

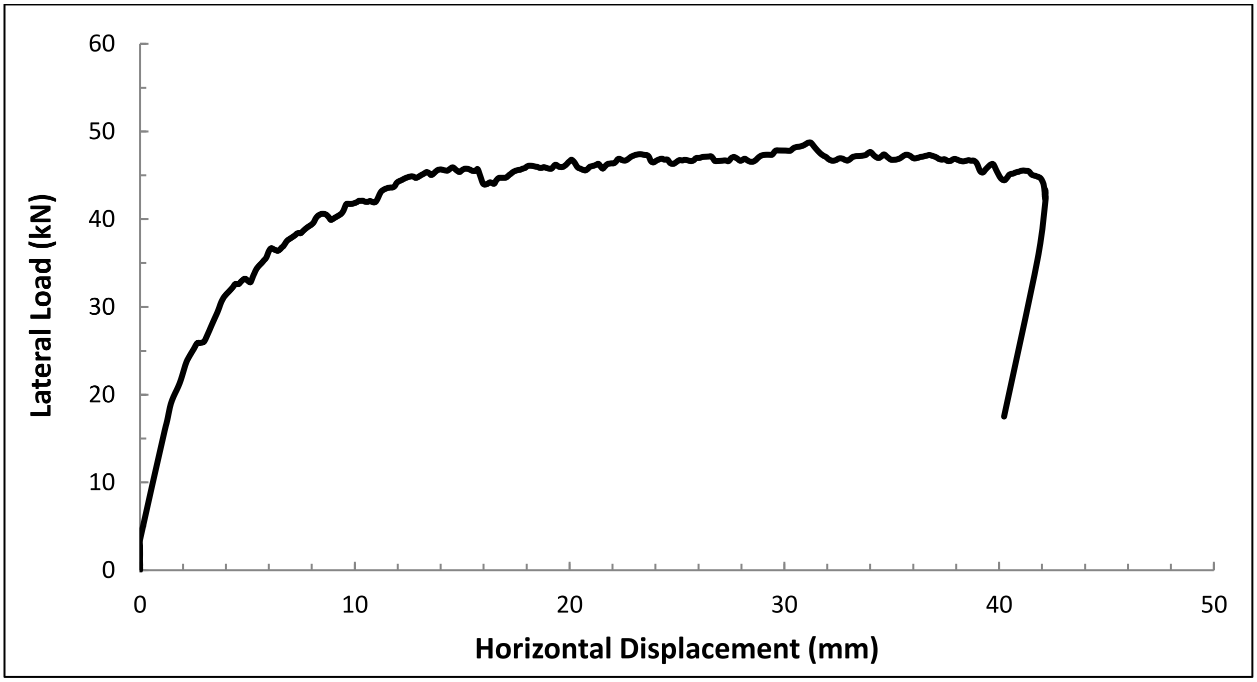

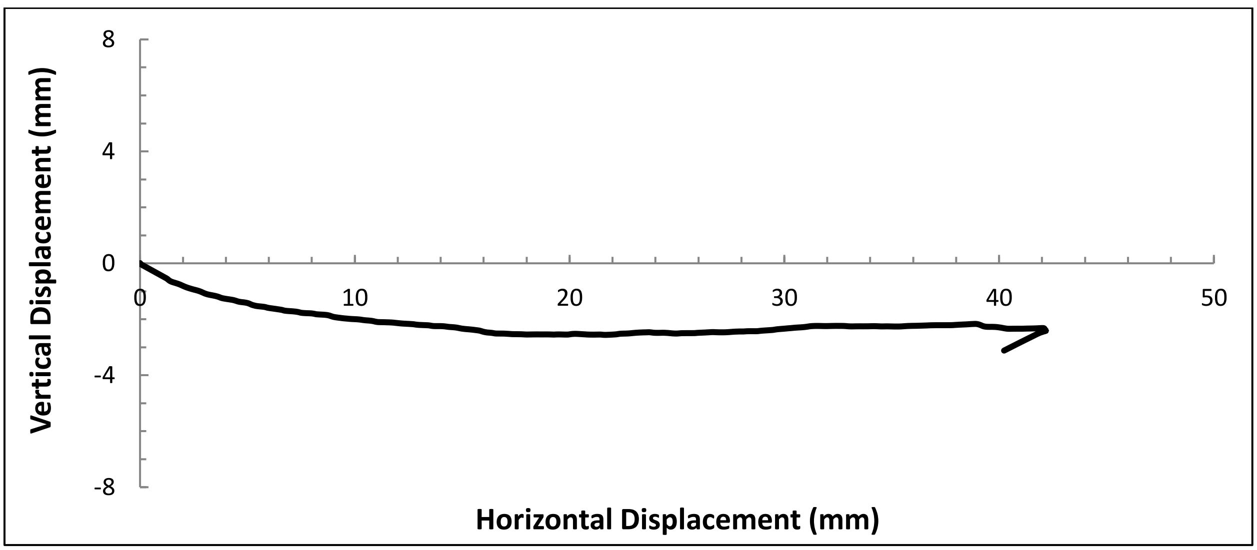

Test ID: G_5_80 (FAST)

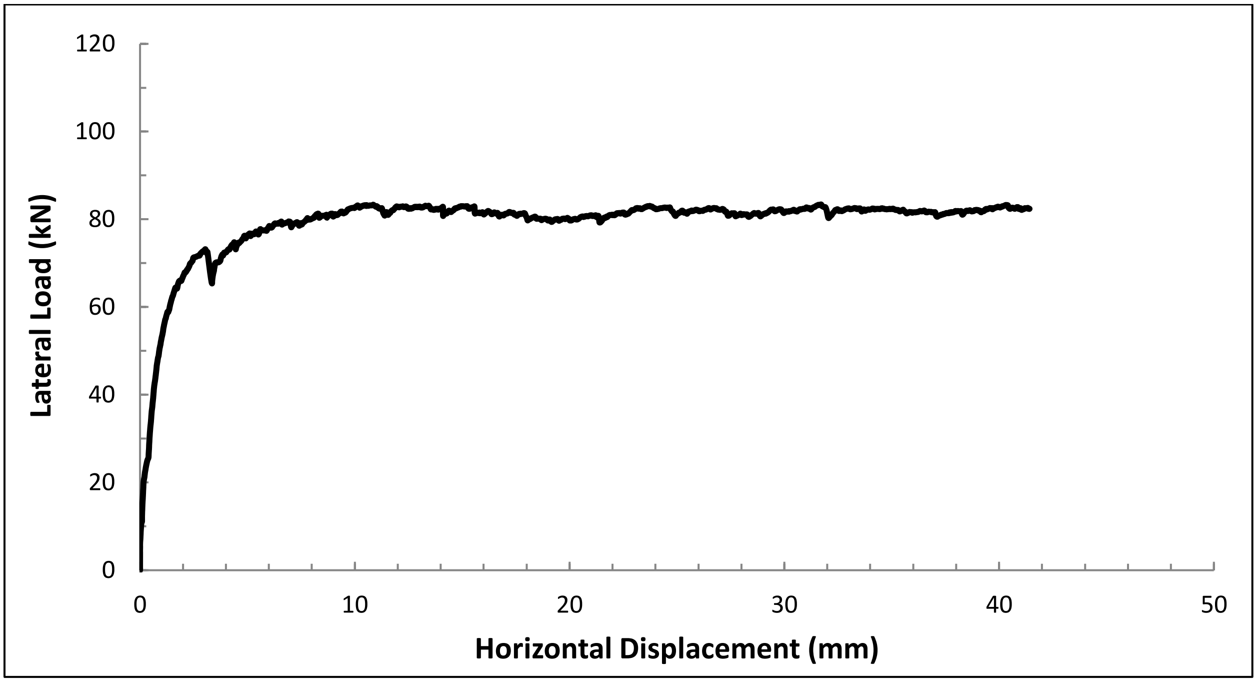

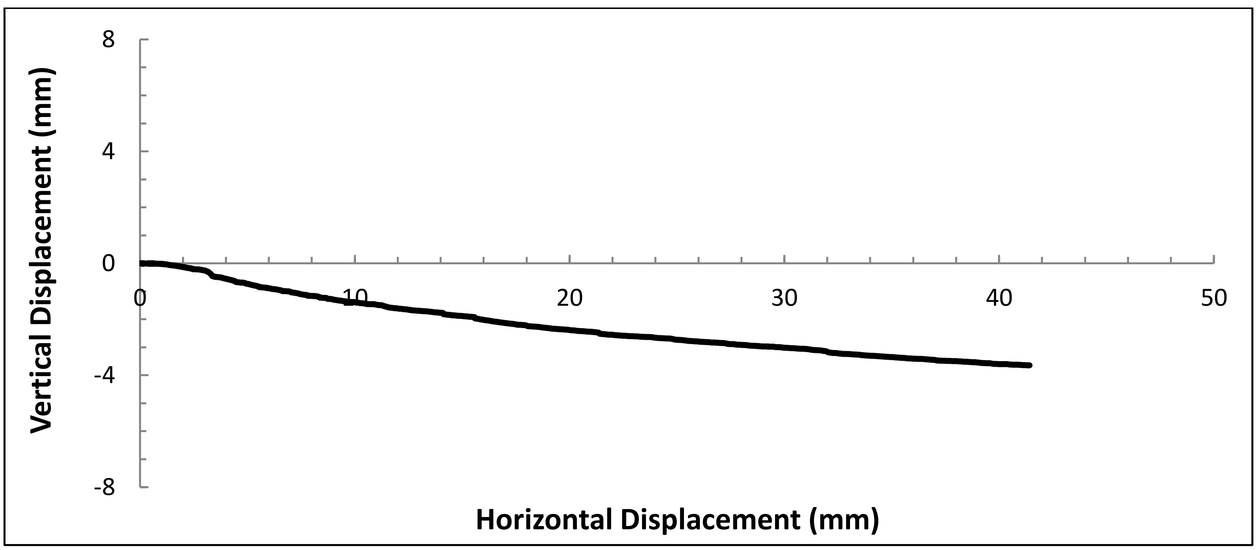

Test ID: G_4B_160

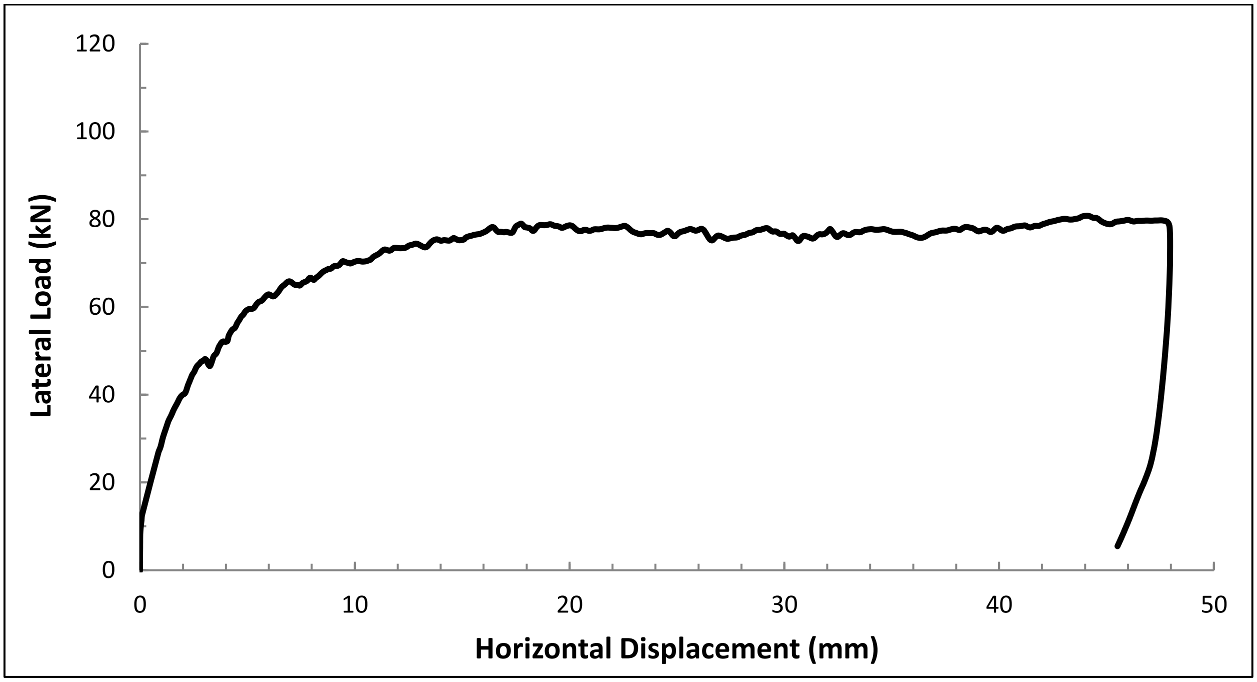

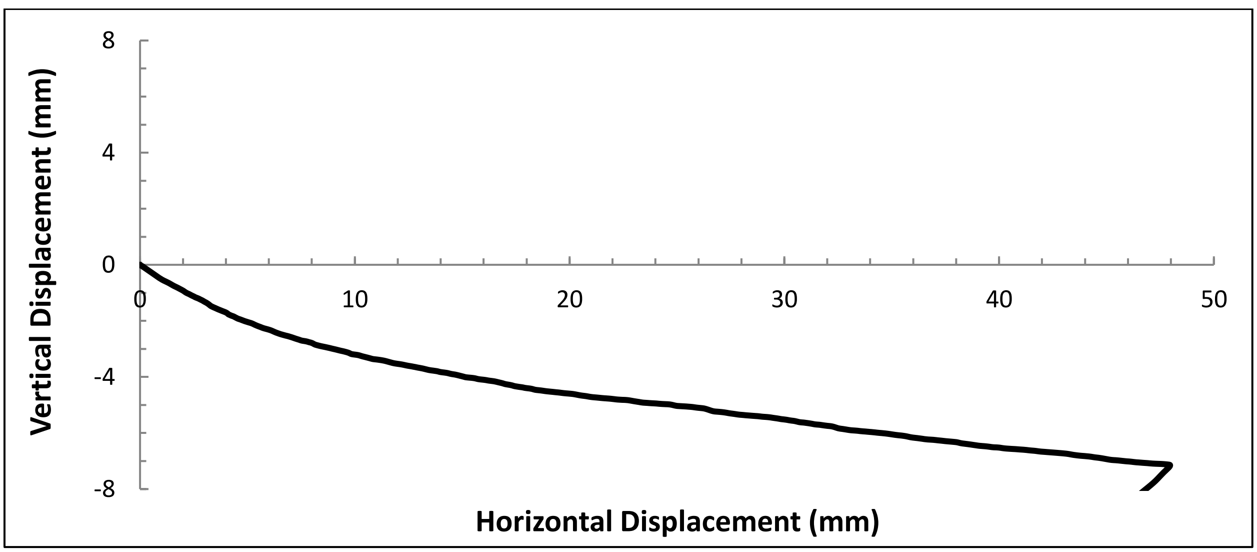

Test ID: G_4B_160 (FAST)

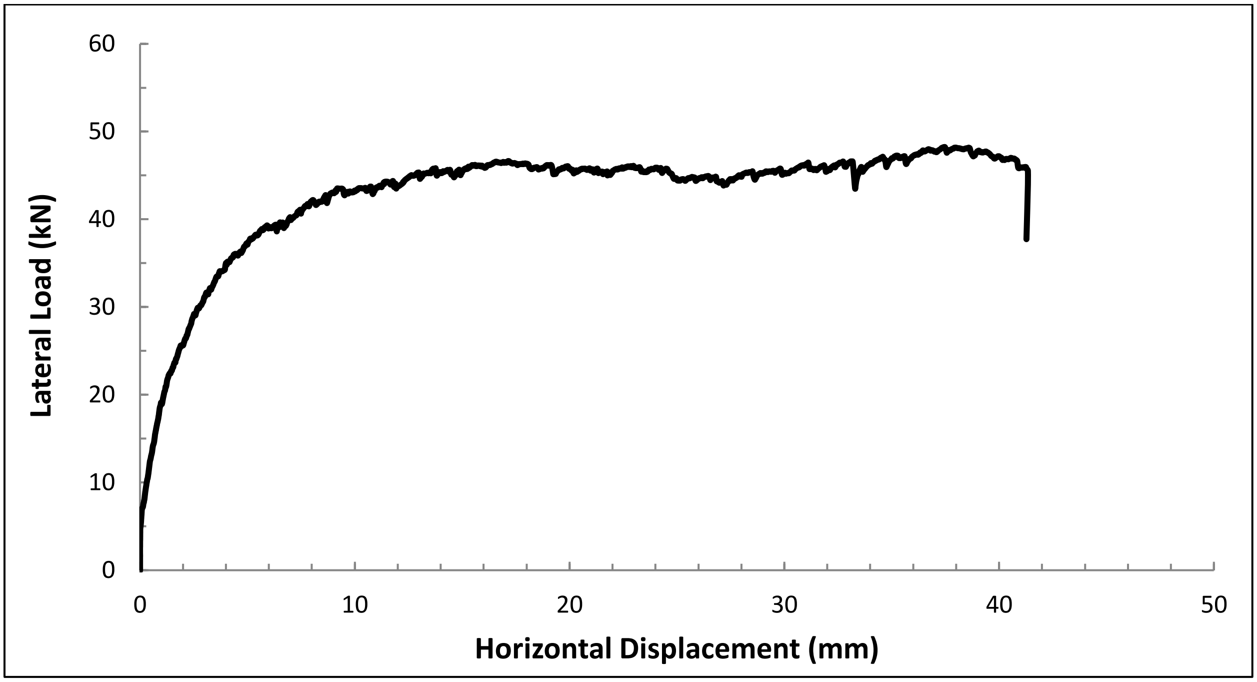

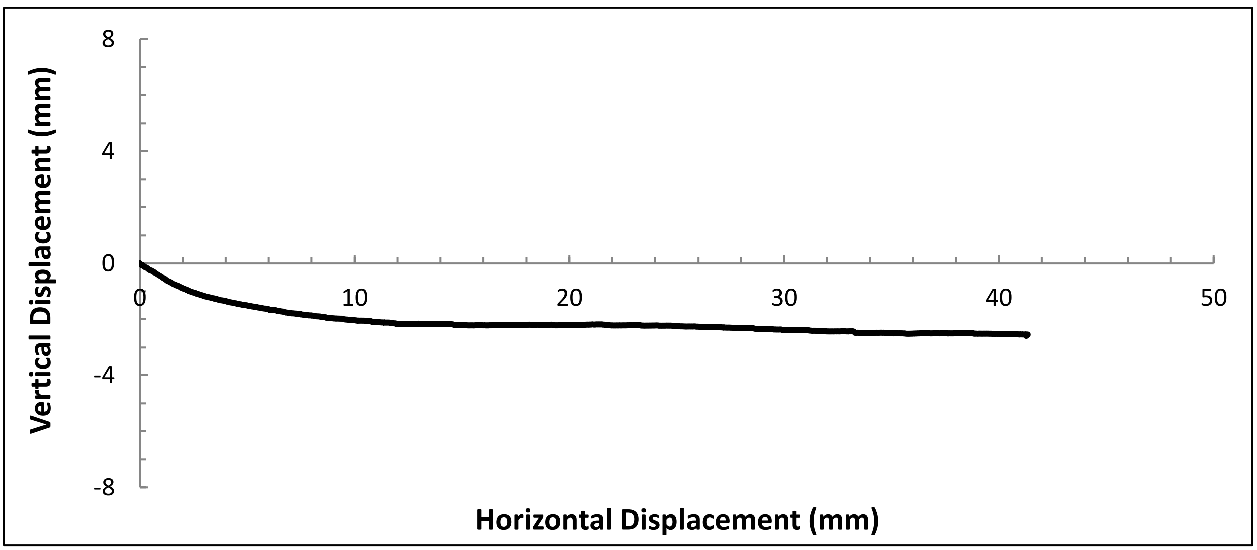

Test ID: G_4B_80

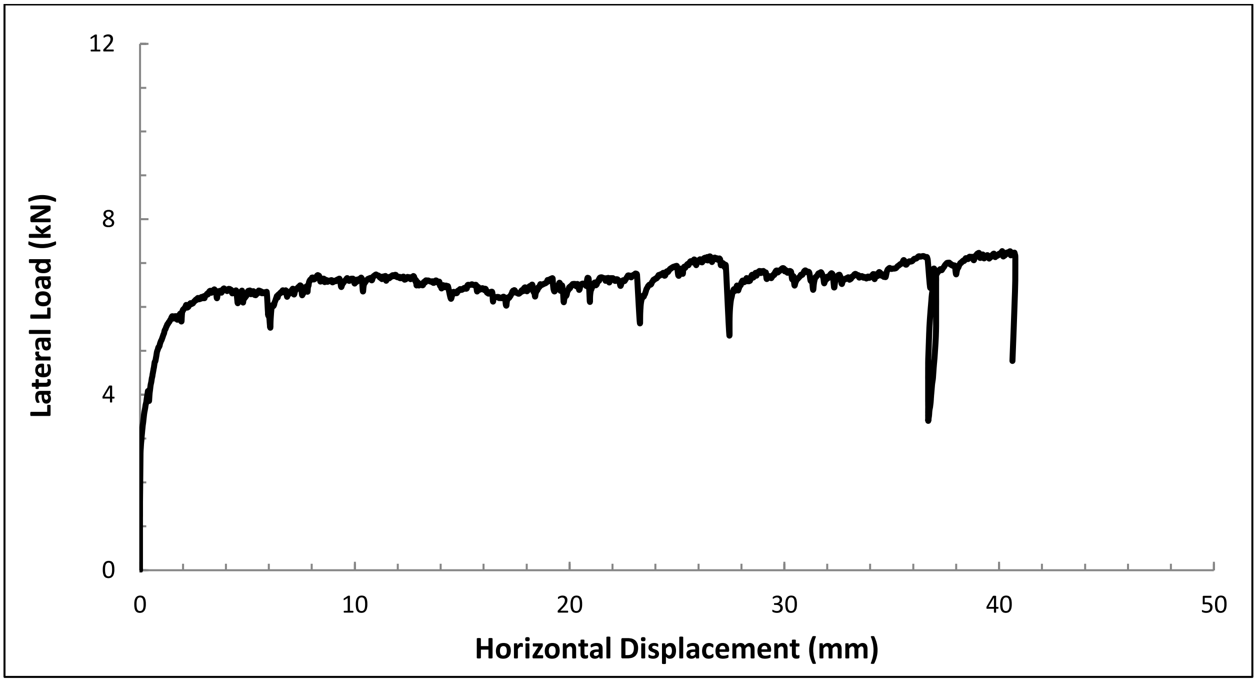

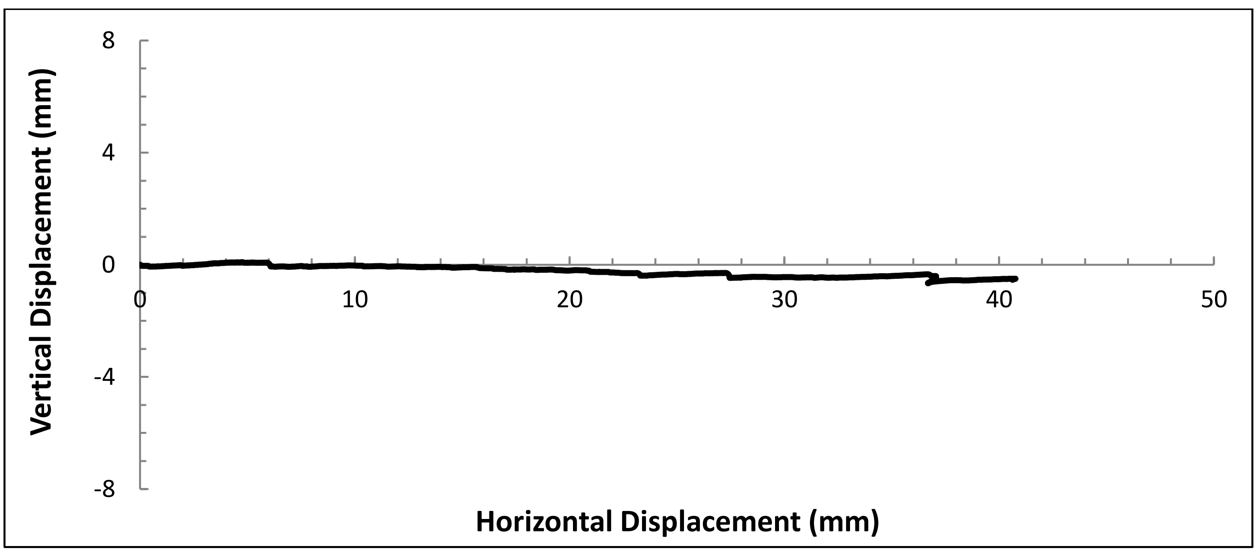

Test ID: G_4B_10

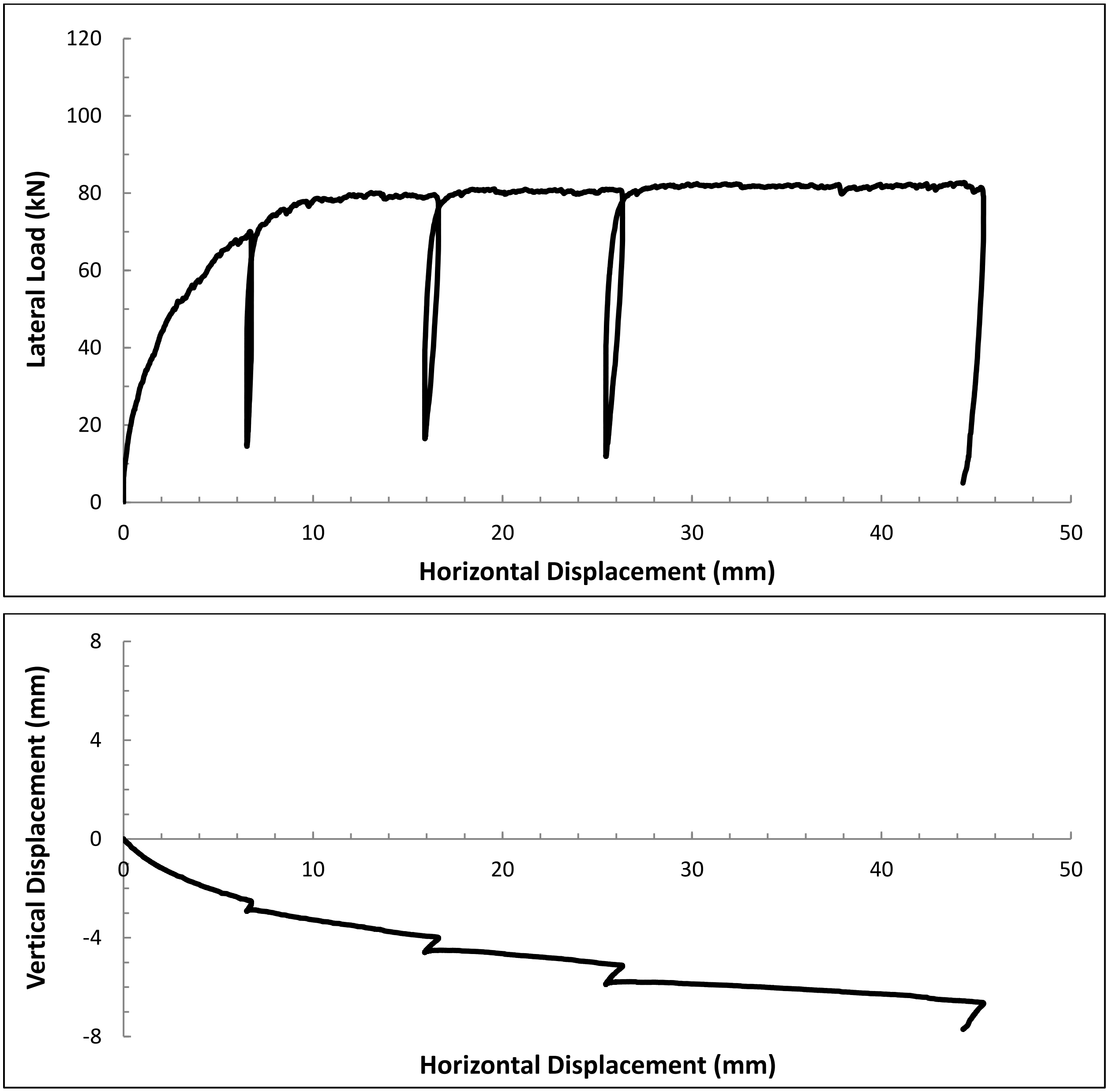

Test ID: G_4B_160 (CYCLIC)

III.3.5 Phase 2 crib test results in the Gravel Ballast

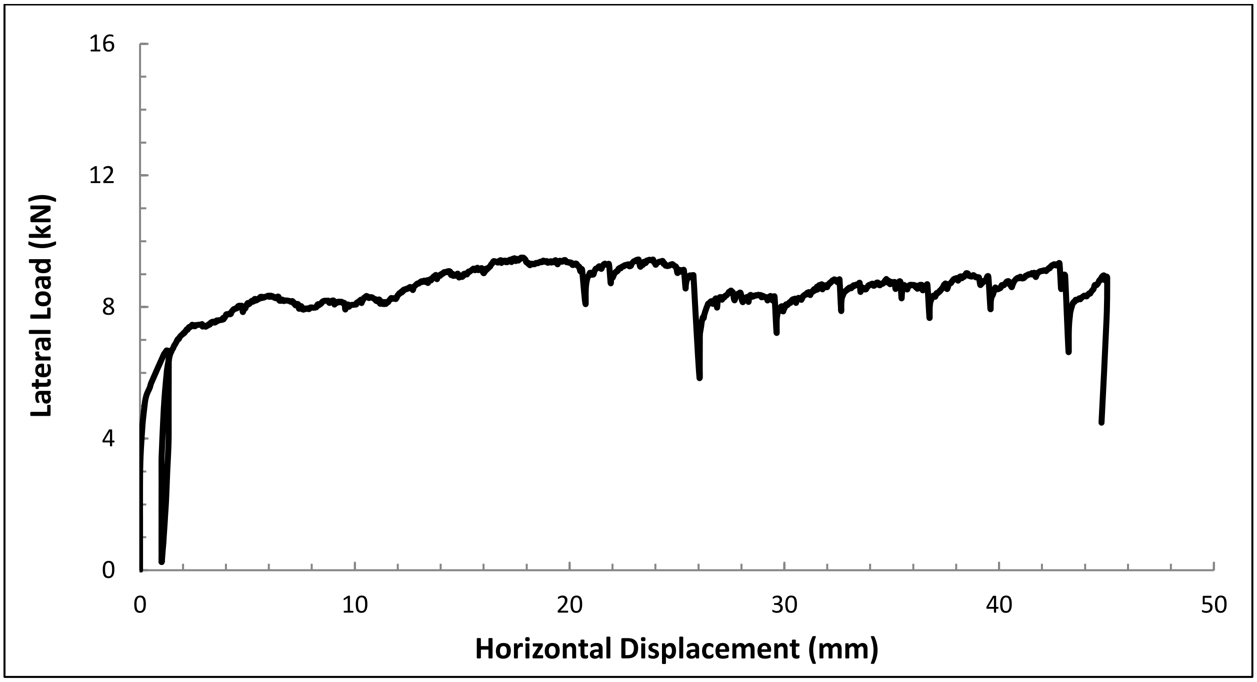

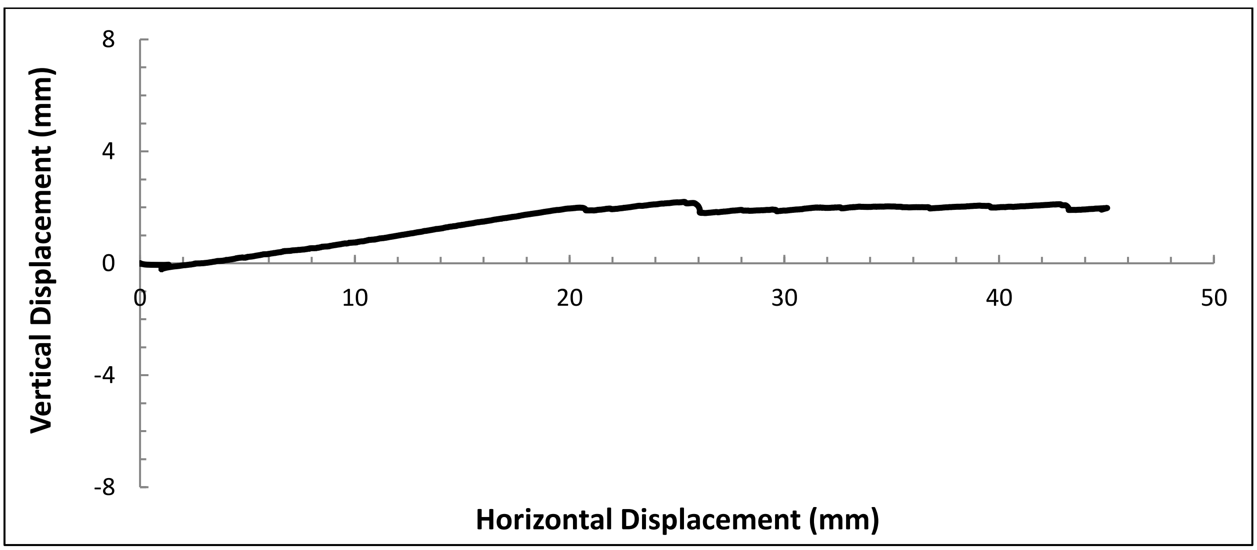

Test ID: G_6A_10

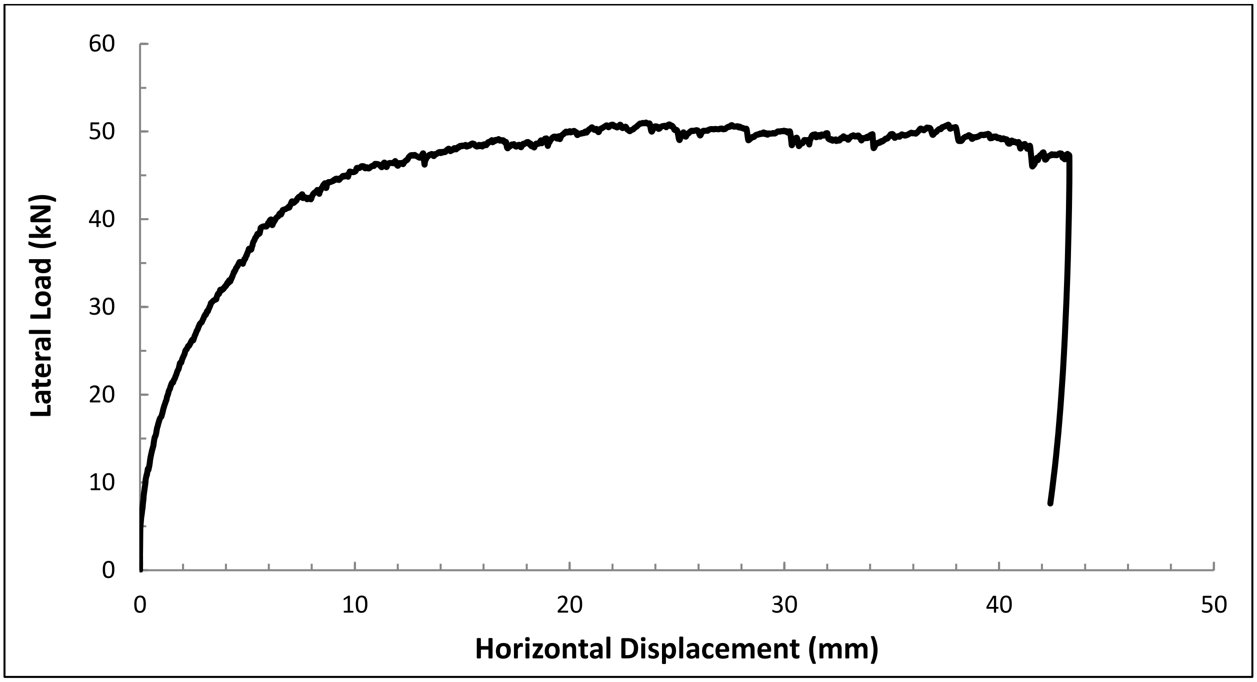

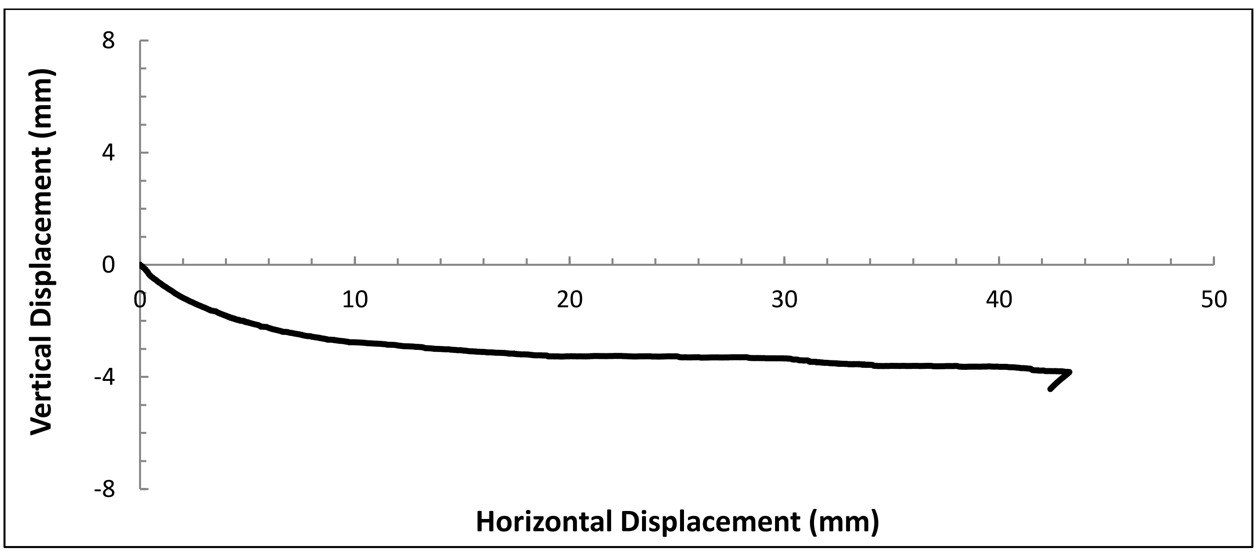

Test ID: G_6A_80

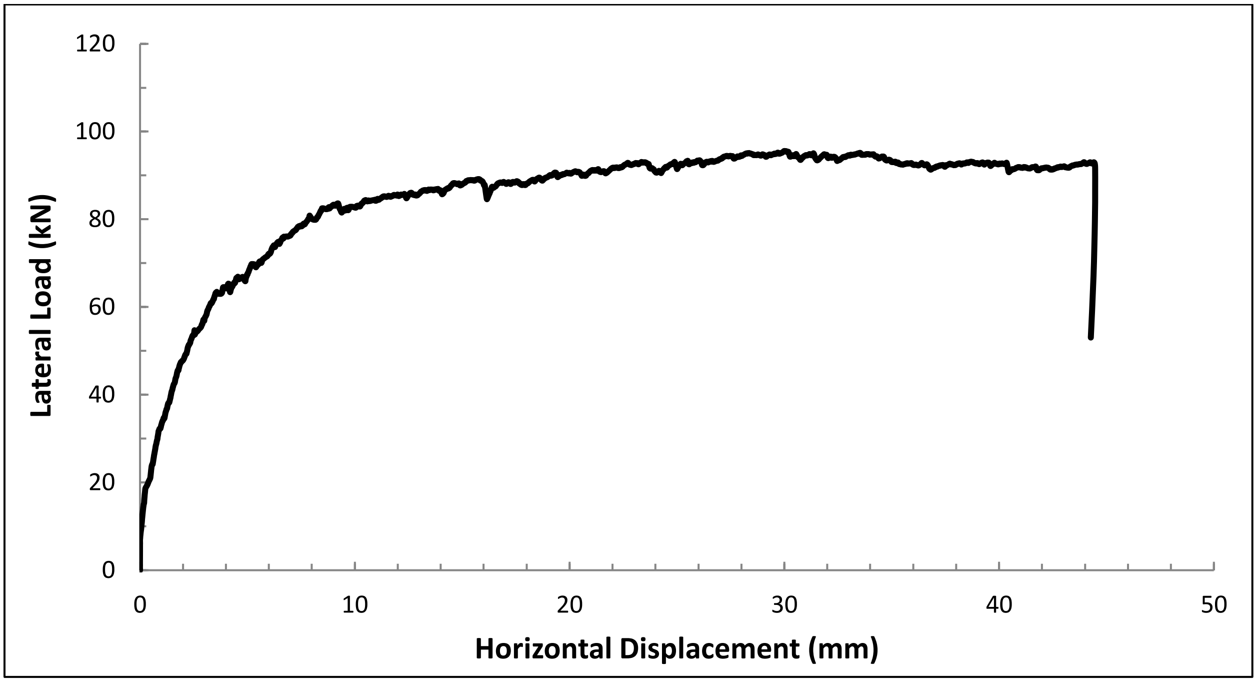

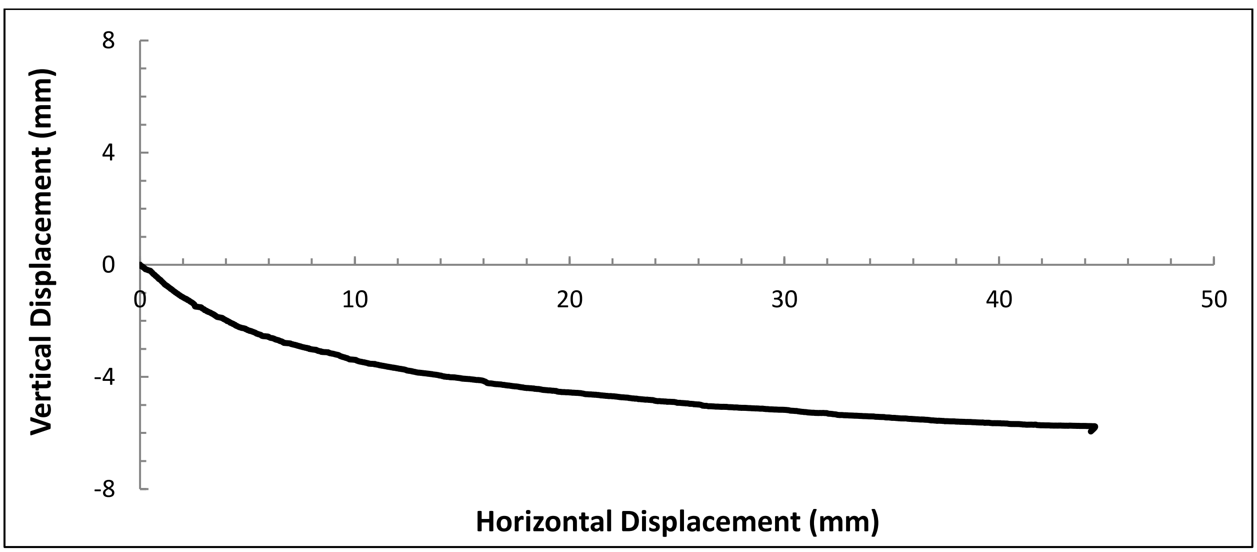

Test ID: G_6A_160

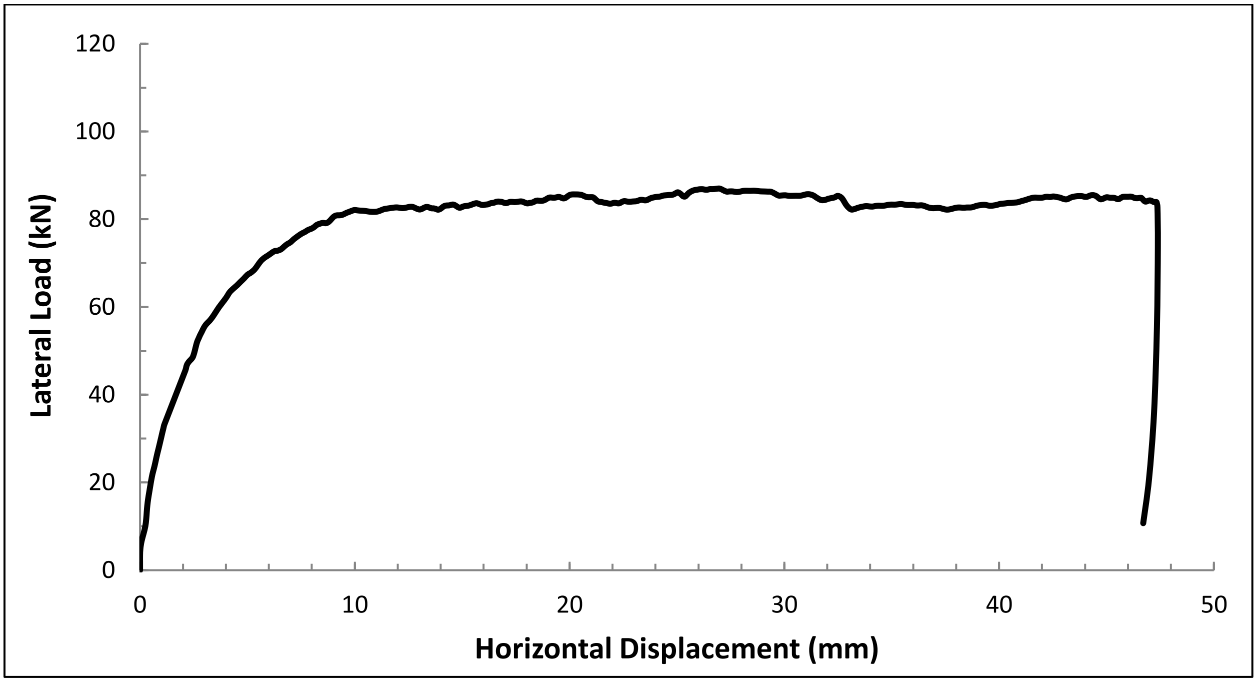

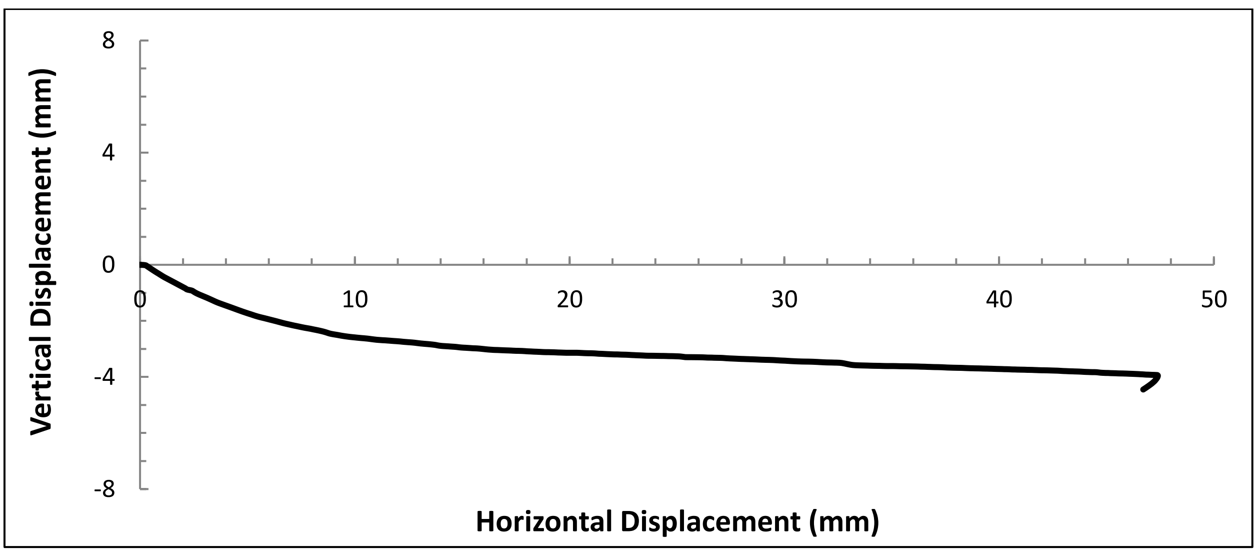

Test ID: G_6A_160 (FAST)

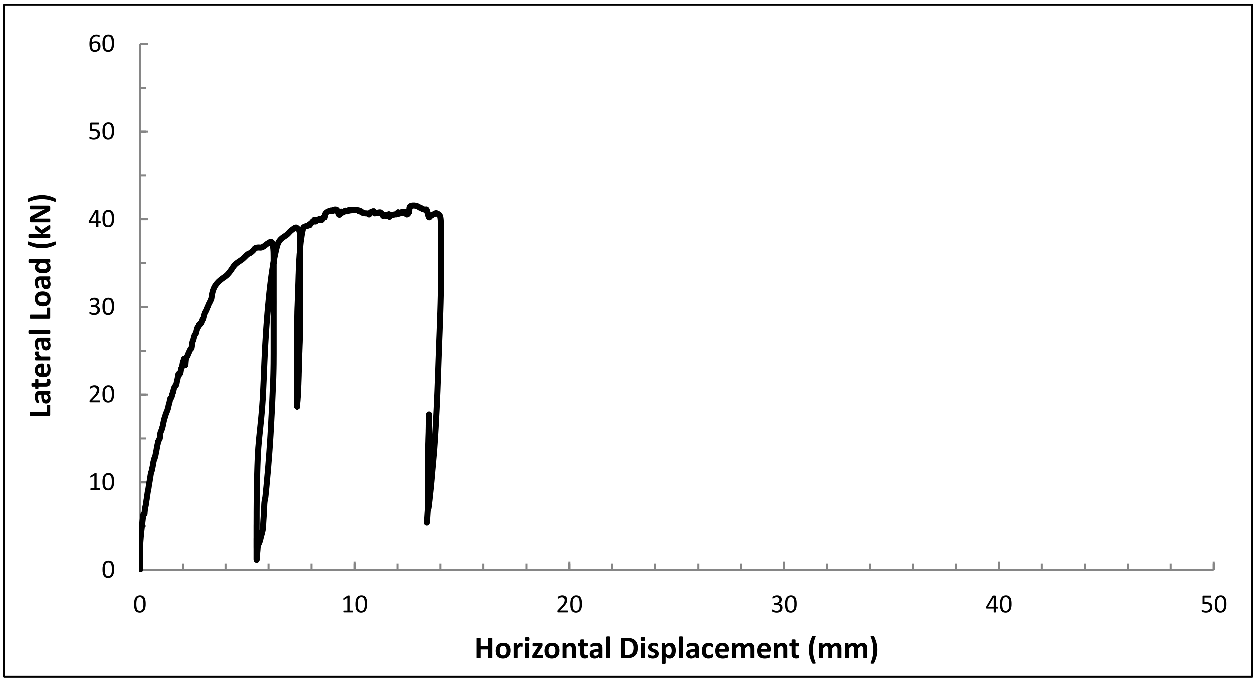

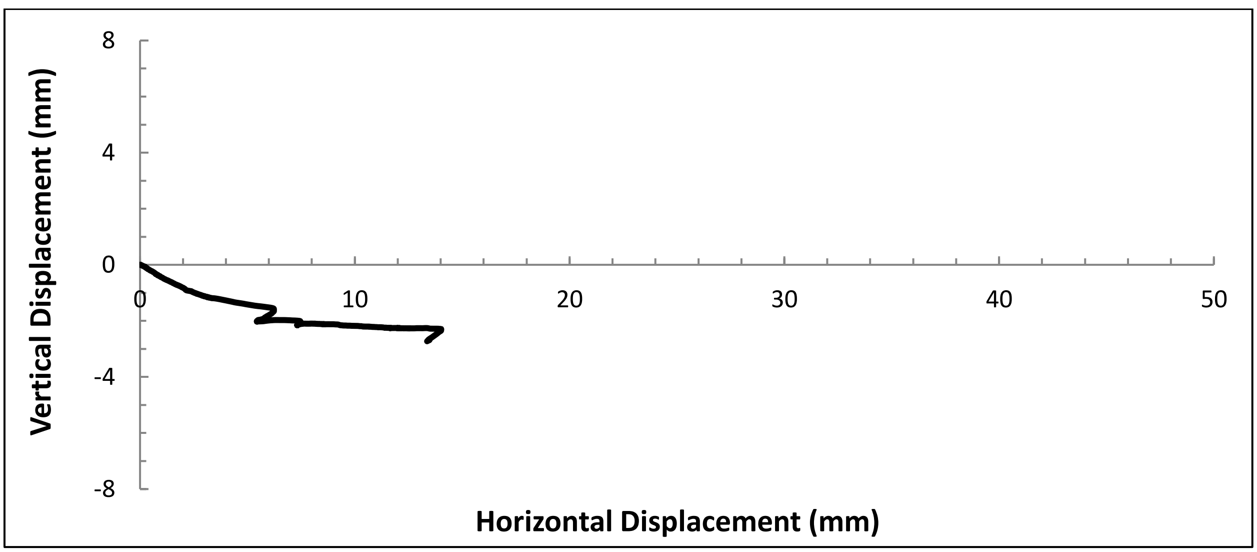

Test ID: G_6B_80 (EXLCUDED)

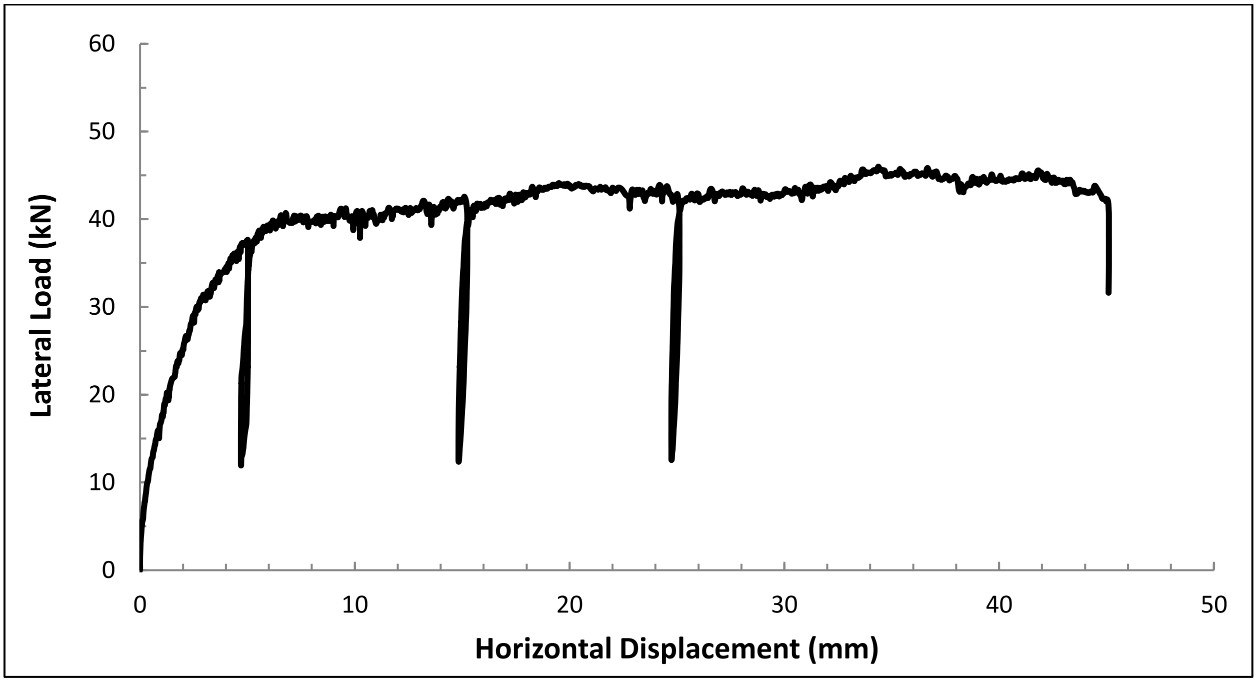

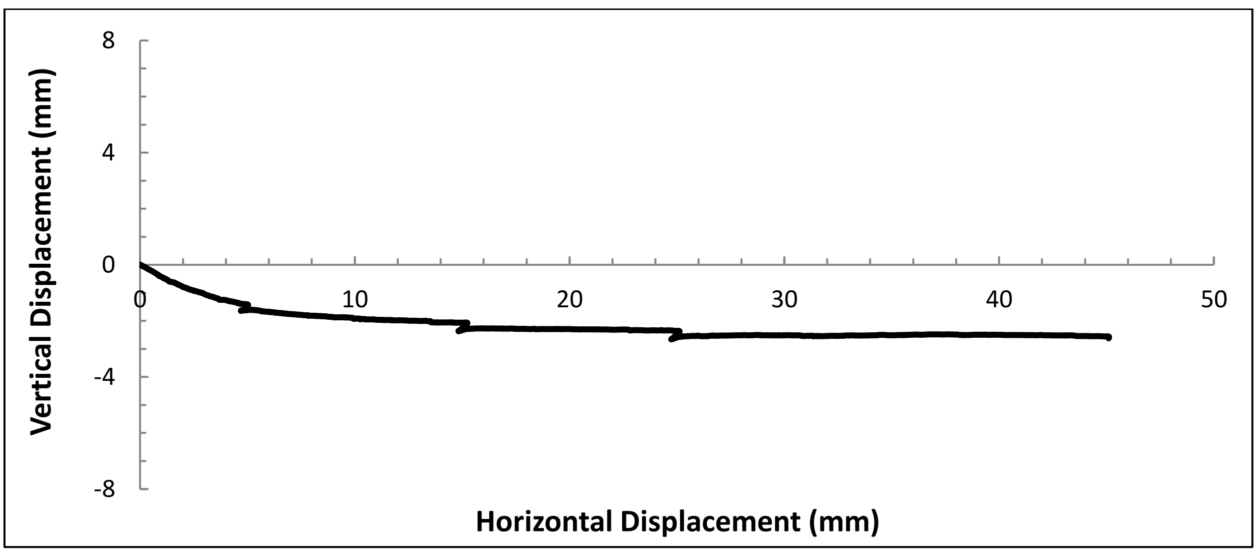

Test ID: G_6B_80 (CYCLIC)

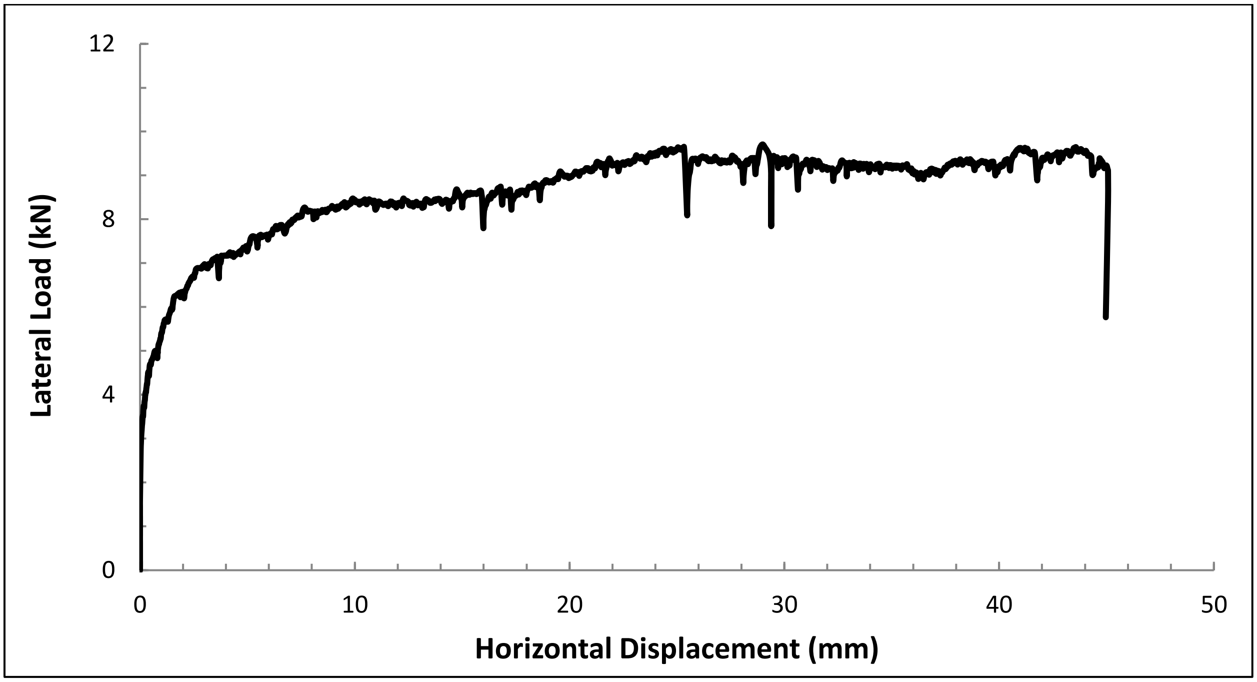

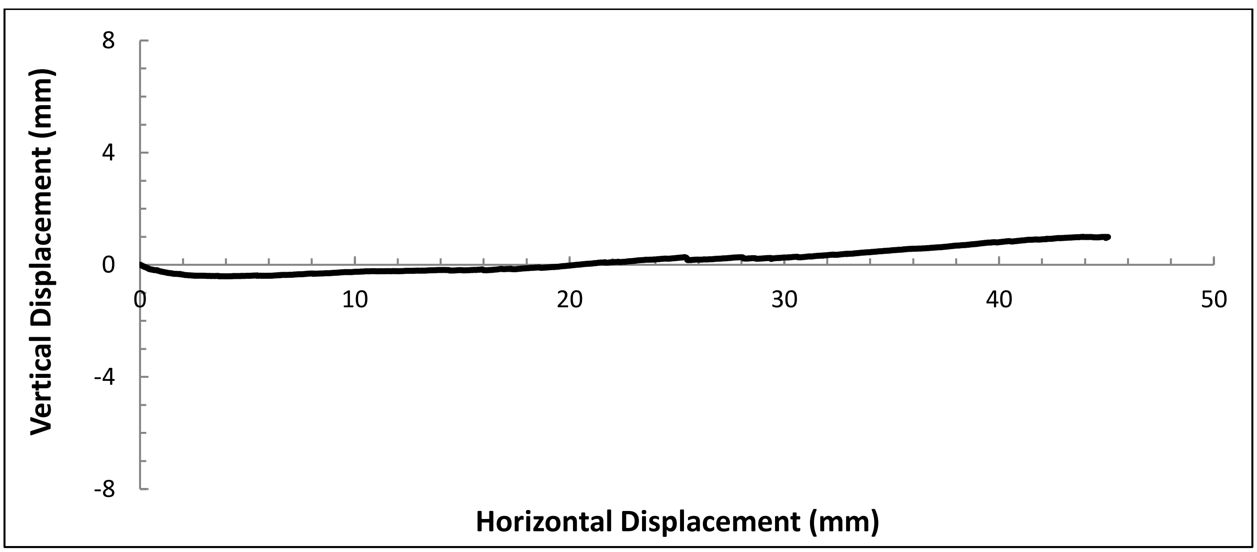

Test ID: G_6B_10

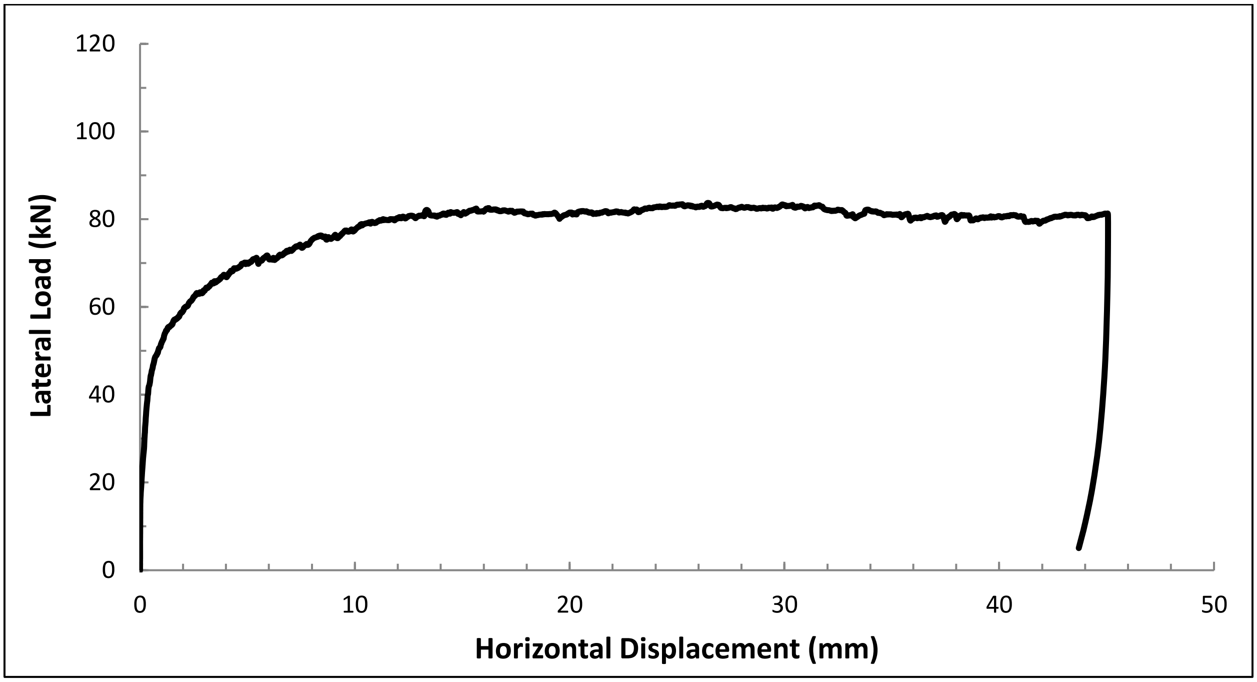

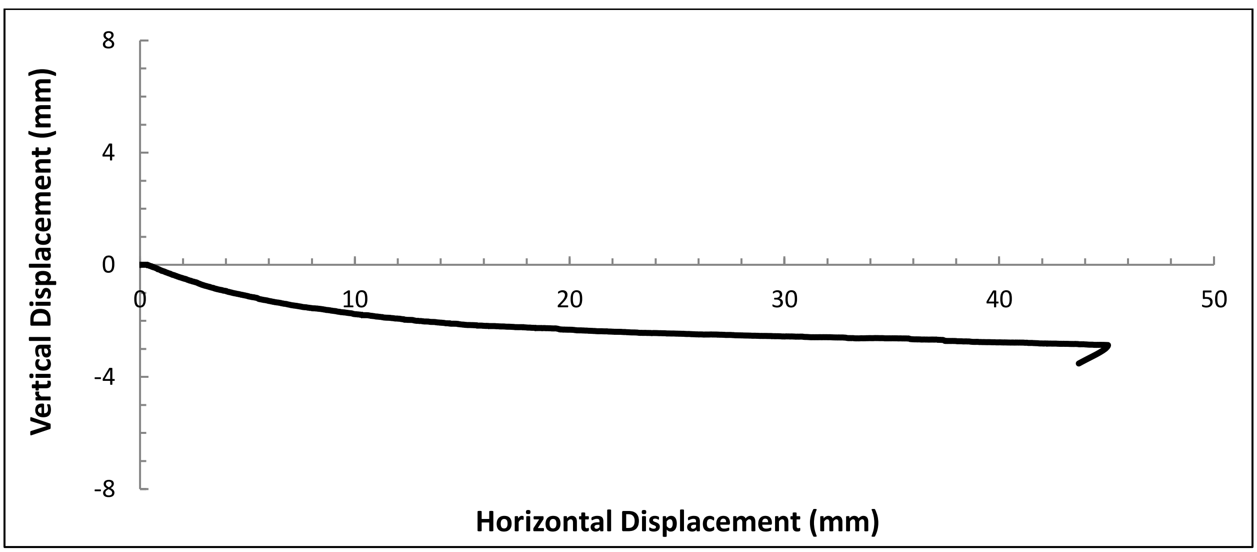

Test ID: G_6B_160

III.3.6 Phase 3 shoulder test results in the Gravel Ballast

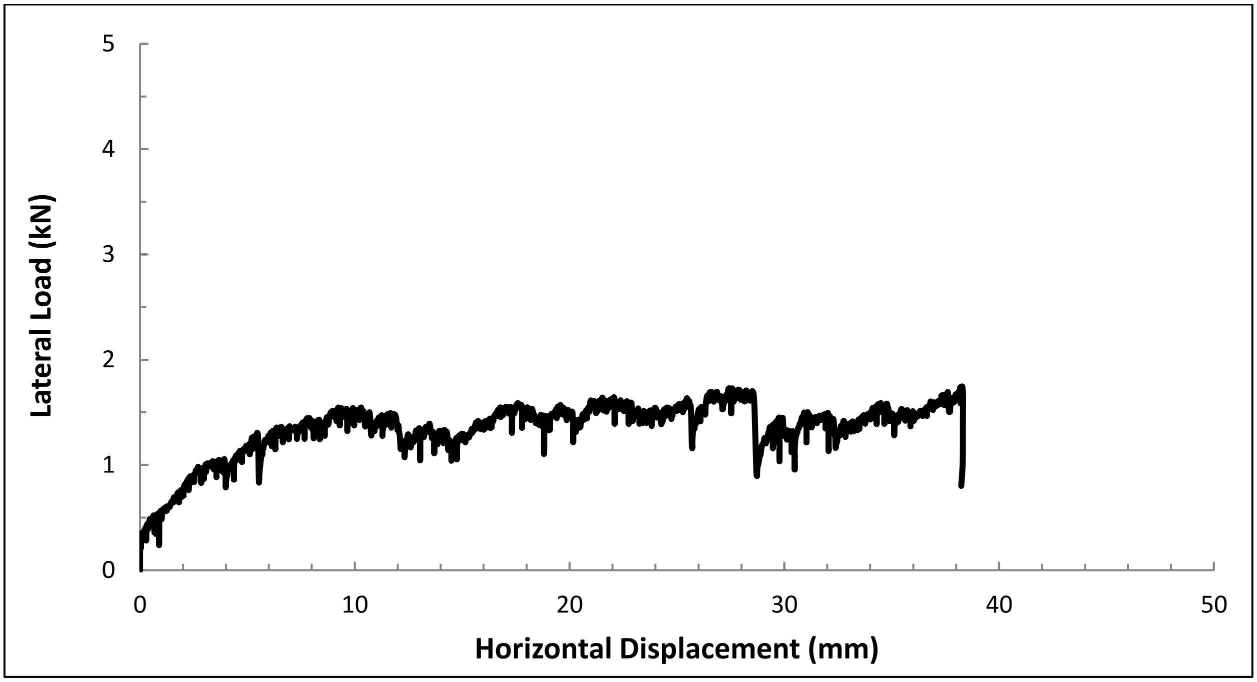

Test ID: G_7A_10

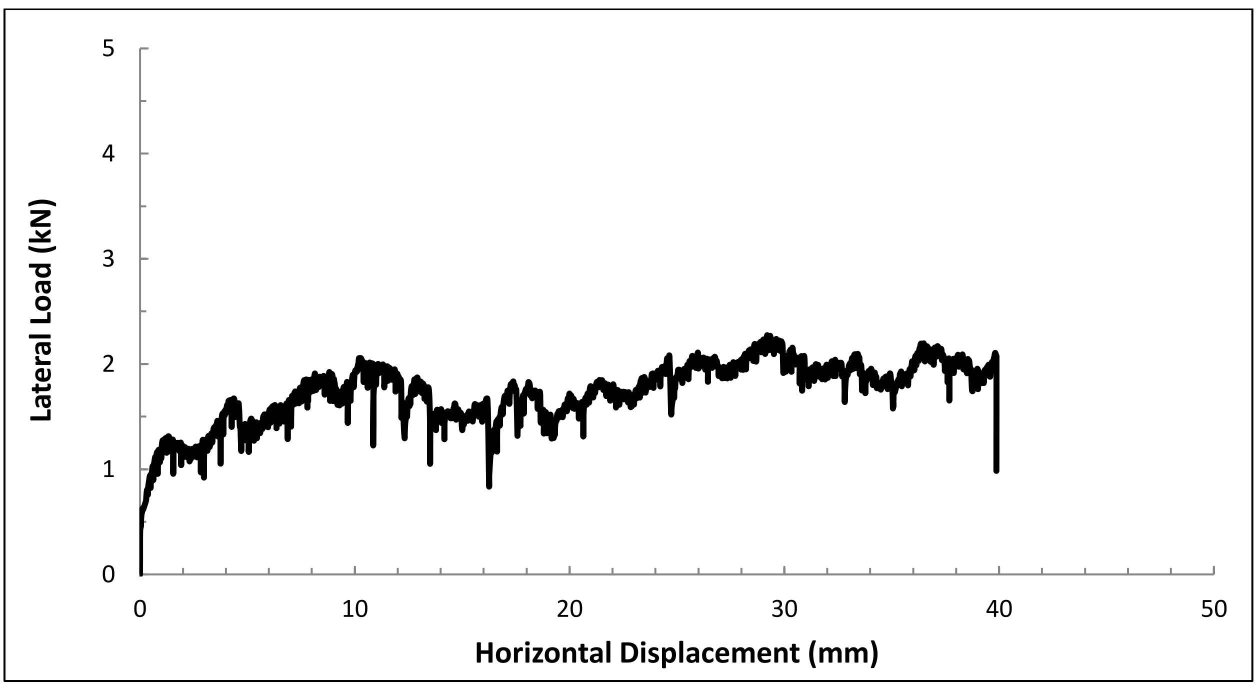

Test ID: G_7A_160

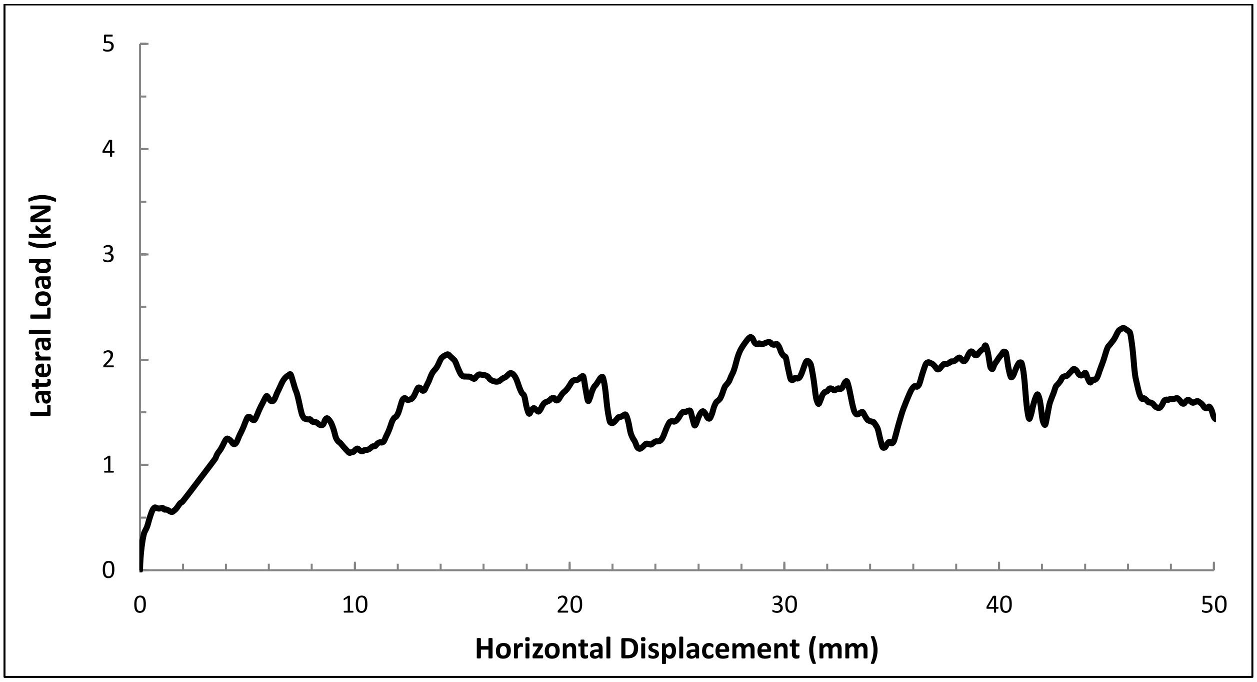

Test ID: G_7A_160 (F)

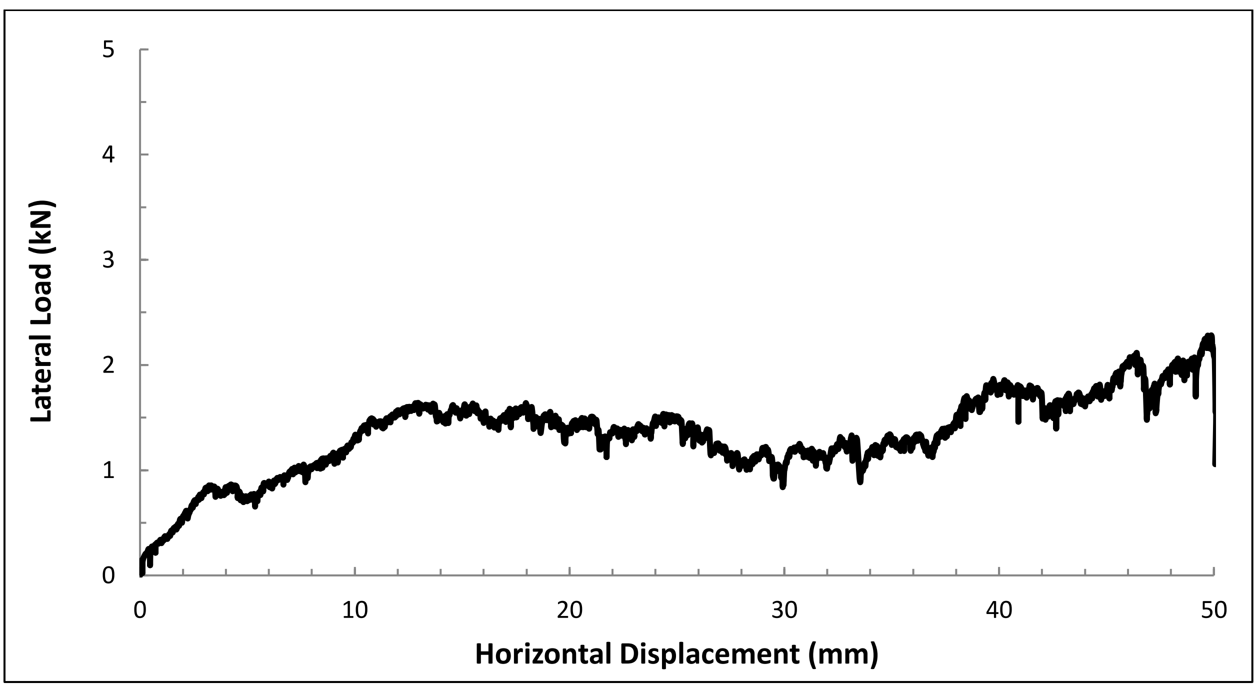

Test ID: G_7A_80

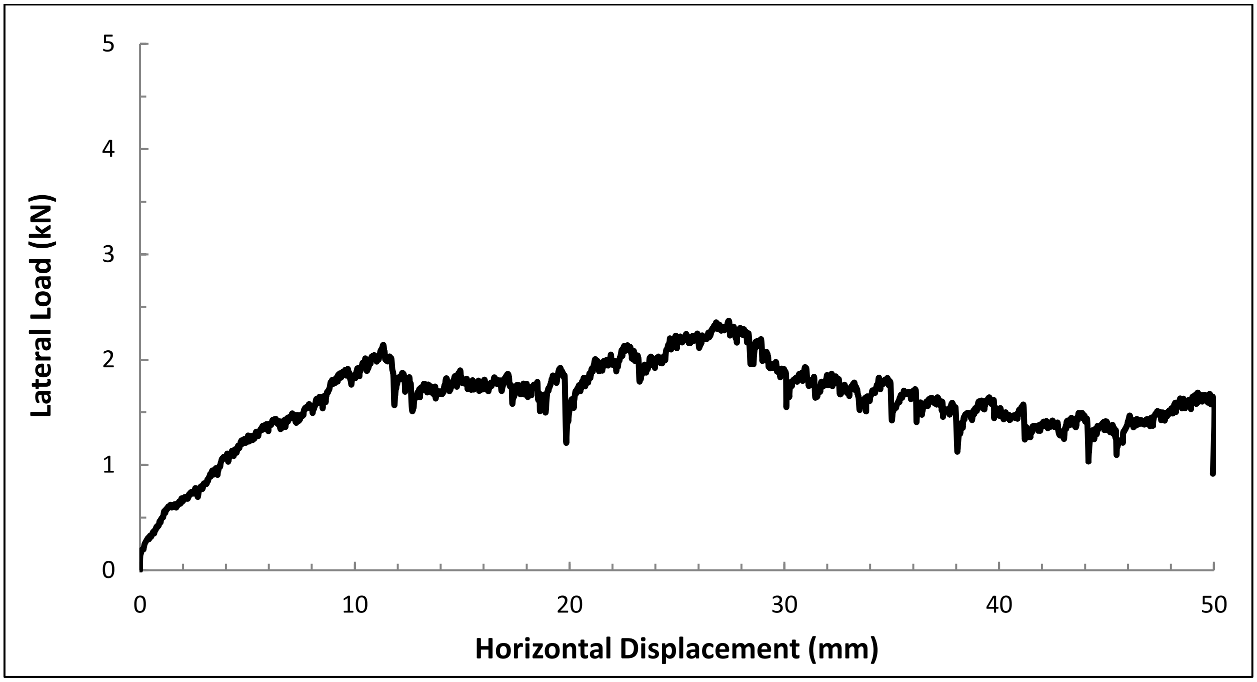

Test ID: G_7A_10 (2)

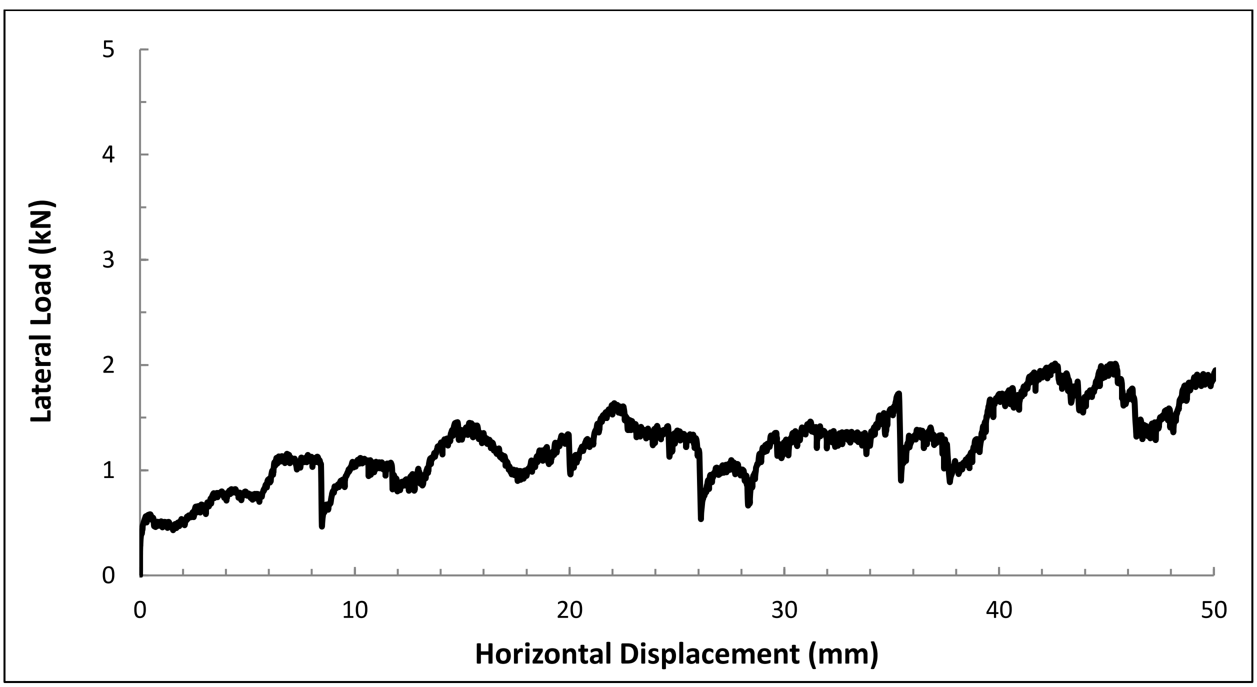

Test ID: G_7A_160 (2)

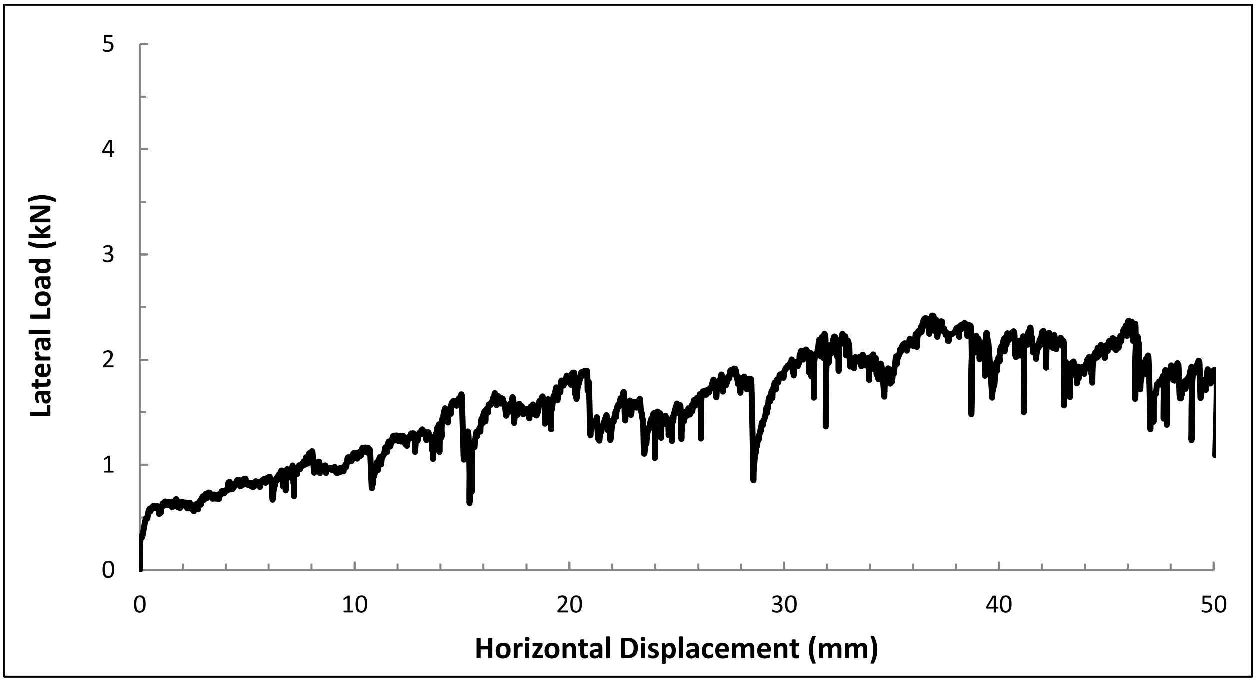

Test ID: G_7A_80 (2)

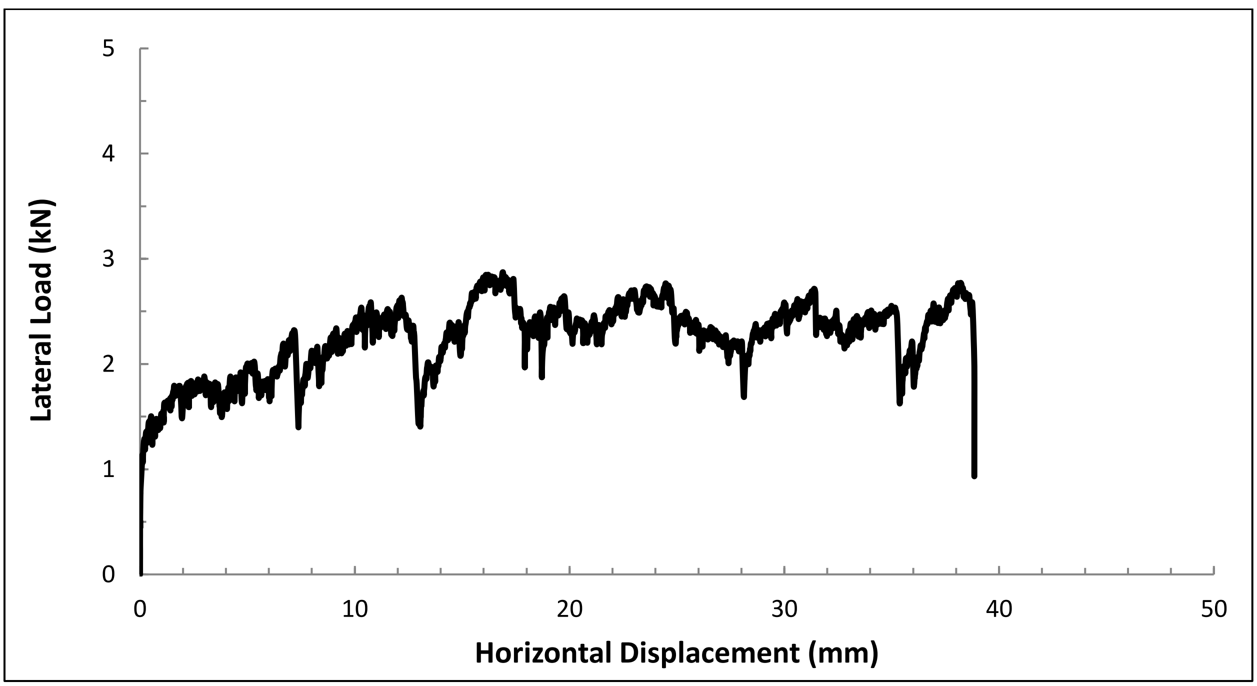

Test ID: G_7B_160

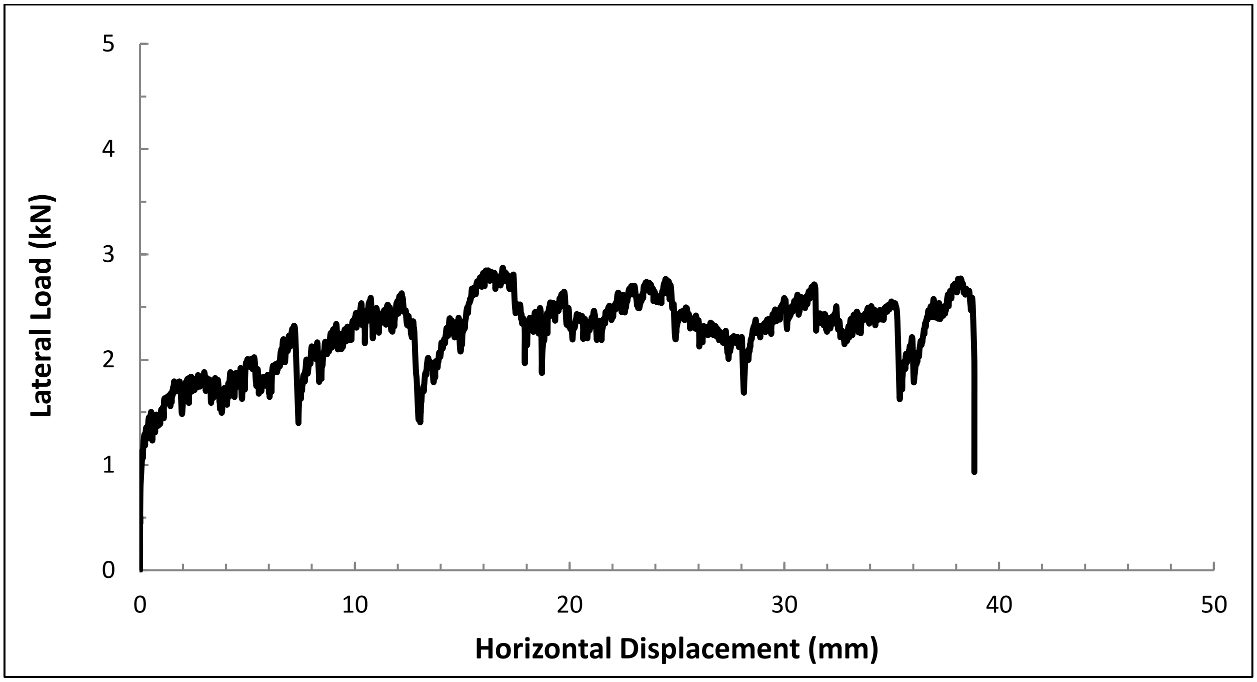

Test ID: G_7B_10

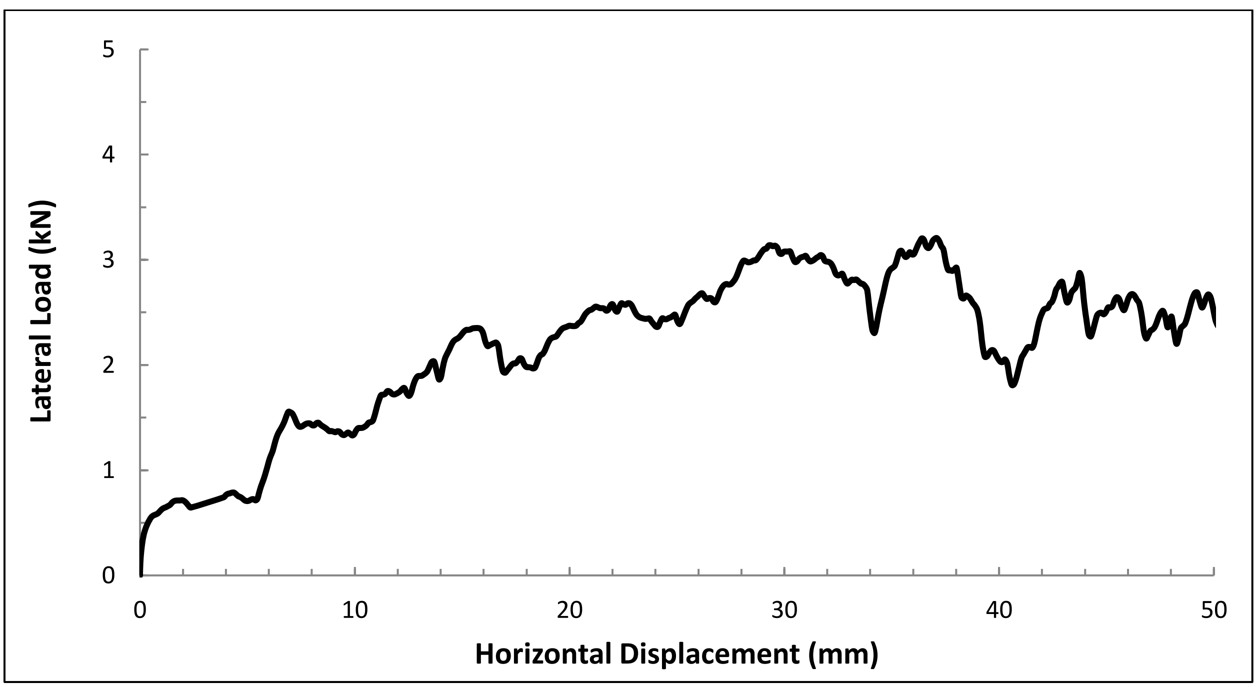

Test ID: G_7B_160 (F)

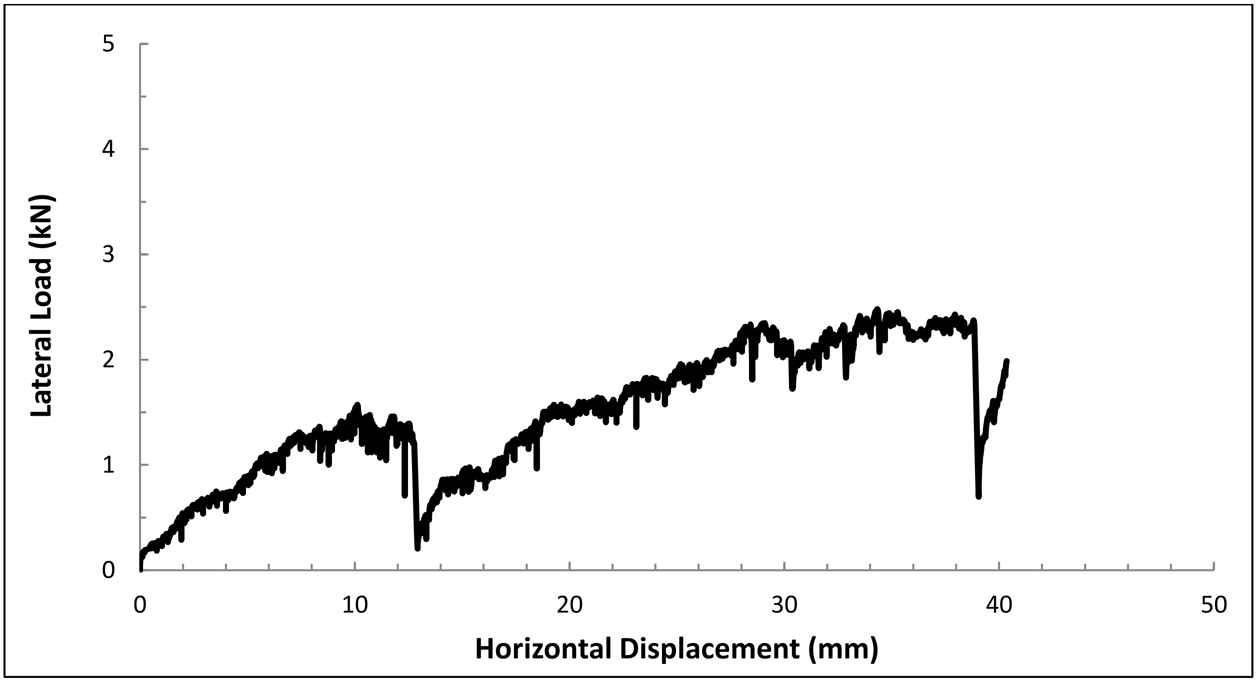

Test ID: G_7B_80

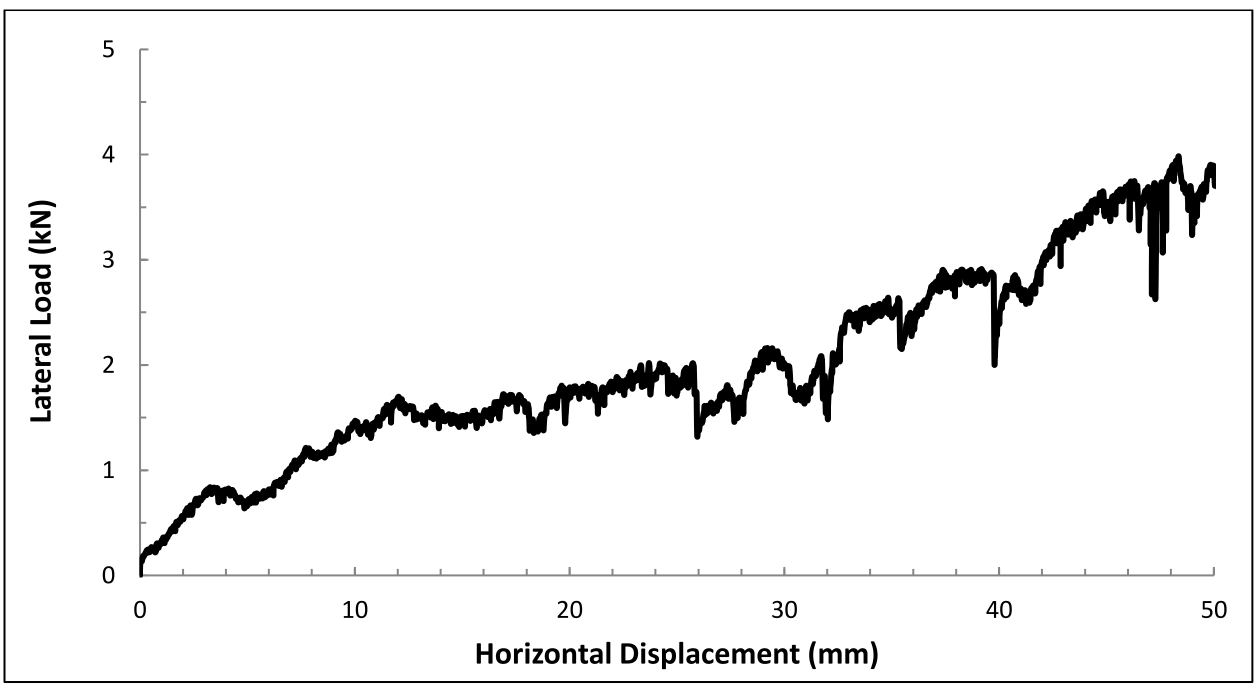

Test ID: G_7B_80 (2)

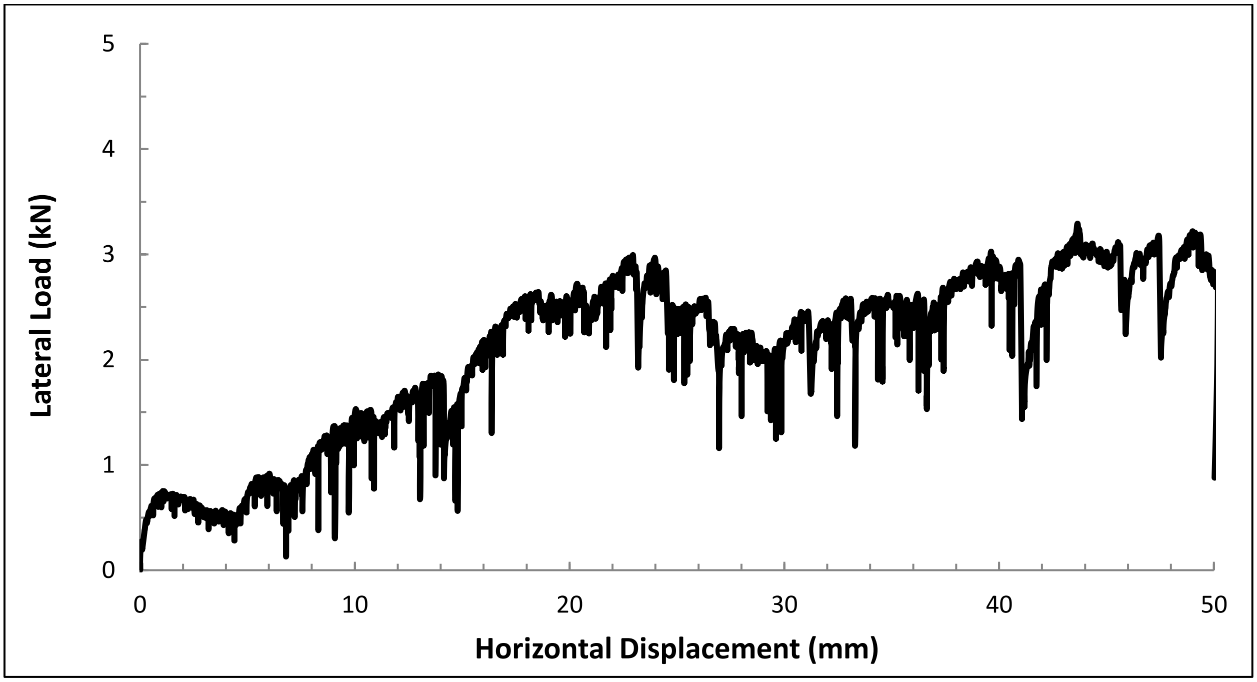

Test ID: G_7B_10 (2)

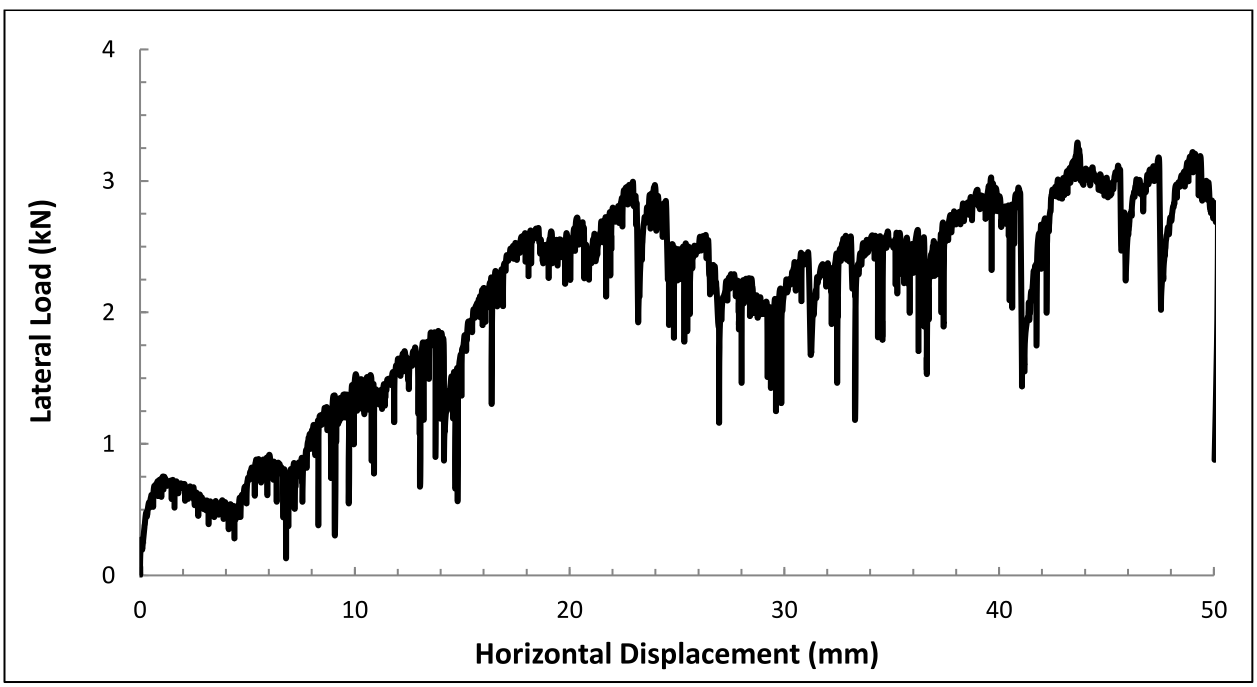

Test ID: G_7B_160 (2)